9-9-2013

Transition Metal as Tools to Probe the Electronic Properties of Porphyrinoids

Jillian Worlinsky
University of Connecticut - Storrs, jill.worlinsky@gmail.com

Transition Metals as Tools to Probe the Electronic Properties

of Porphyrinoids

Jillian Leigh Worlinsky, Ph.D.

University of Connecticut, 2013

This thesis describes in a number of separate chapters a range of studies that measure the variation of specific physical properties with structural modification of the macrocycles, with a particular focus also on using their coordinated metals as probes. Specifically, the transition metal ions are used as tools for interrogation of the electronic properties of porphyrins and pyrrole-modified porphyrins. With the aim of better understanding the electronic and structural factors that govern the optical responses, axial binding strengths, fragmentation patterns and carbonyl stretching frequencies of *meso*-tetraarylporphyrins, a rational design of pyrrole-modified metalloporphyrins with designed optical properties is derived.

Transition Metals as Tools to Probe the Electronic Properties

of Porphyrinoids

Jillian Leigh Worlinsky

B.S., Susquehanna University, 2008

A Dissertation

Submitted in Partial Fulfillment of the

Requirements for the Degree of Doctor of Philosophy

at the

University of Connecticut

2013

APPROVAL PAGE

Doctor of Philosophy Dissertation

Transition Metals as Tools to Probe the Electronic Properties

of Porphyrinoids

Presented by

Jillian Leigh Worlinsky, B.S.

Major Advisor: _____

Dr. Christian Brückner

Associate Advisor: _____

Dr. Steven Suib

Associate Advisor: _____

Dr. Edward Neth

Associate Advisor: _____

Dr. Alfredo Angeles-Boza

Associate Advisor: _____

Dr. James Bobbitt

University of Connecticut

2013

Table of Contents

Acknowledgments

First, I would like to thank my advisor Dr. Christian Brückner for his wisdom and guidance. I would like to acknowledge Dr. Neth for being a great mentor. Dr. Martha Morton for all of her advice and NMR expertise and Dr. You-Jun Fu for his Mass Spectrometry assistance.

I want to thank my family for their support and motivation. To my parents, thank you for all you love and advice along the way. I wouldn't have been able to do this without you. To my boyfriend, Paul, thank you for being completely supportive and understanding.

I would like to thank the past and present members of the Brückner group for their advice and support. Michael, thanks for the life lessons, VIP tables, and of course your awesome pitching skills. Junichi (Jay), thanks for the laughs and casino nights. Lalith, you are the most compassionate person I know and I cannot thank you enough for the guidance and wisdom you have given me. Eileen, the lab wouldn't be the same with you and our loud music and dancing, thanks for all the vent sessions. Steven, you are the best undergrad ever! Thanks for always making me laugh and your amazing membrane skills. Jenn, thanks for being my meatball, for all our Deena and Snooki nights, our gym sessions, being the best shopping buddy and most of all for always be there for me. Johanna, thanks for being an awesome friend and sharing your love of country music with me! Chris Lorenc, thanks for gracing all of us with your pong skills. Kelli and Julie, thanks for the good times and I will miss you both! Emilie, thanks for all your guidance over the years and I will definitely miss all our quality time at softball.

List of Abbreviations

aq	aqueous
^{13}C NMR	^{13}C nuclear magnetic resonance
COSY	correlation spectroscopy
conc	concentrated
CTAP	cetyltrimethylamonium permanganate
EAS	electrophilic aromatic substitution
ESI	electrospray ionization
eq	equivalence
^{1}H NMR	^{1}H nuclear magnetic resonance
HOMO	highest occupied molecular orbital
HR-MS	high-resolution mass spectrometry
IR	infrared
λ	wavelength
LR-MS	low-resolution mass spectrometry
LUMO	lowest unoccupied molecular orbital
py	pyridine
r.t.	room temperature
S_NAr	nucleophilic aromatic substitution
TLC	thin layer chromatography
TPP	*meso*-tetraphenylporphyrin
T^FPP	*meso*-tetrakis(pentafluorophenyl)porphyrin

List of Instruments

UV-visible spectroscopy	VARIAN CARY 50 SCAN
Fluorescence spectroscopy	VARIAN CARY ECLIPSE
NMR spectroscopy	BRUKER AVANCE 300 MHz (COSY, NOESY) BRUKER AVANCE III 400 MHz (^{1}H NMR, ^{13}C NMR) BRUKER AVANCE 500 MHz (^{13}C NMR, HMBC)
HR-MS	AB SCIEX Q-STAR-ELITE JEOL ACCUTOF LC-PLUS
LR-MS	WATERS QUATTRO II
IR-spectroscopy	THERMO NICOLET NEXUS 670
automated chromatography	ISCO TELEDYNE COMBIFLASH RF

List of Figures

List of Schemes

List of Tables

1. General Introduction

1.1. Porphyrins and Chlorins

Porphyrins are a class of intensely colored macrocycles. The name porphyrin is derived from the Greek word *porphura*, meaning purple.[1] Porphyrins are fully saturated macrocycles comprised of four pyrrolic subunits, each linked by methine bridges, referred to as the *meso*-positions. The peripheral pyrrolic positions are referred to as the β-positions. The numbering scheme and common nomenclature of the ring positions used to describe this class of macrocycles is described in Figure 1-1.

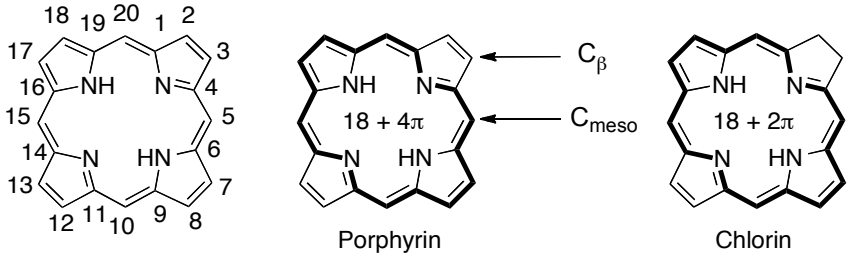

Figure 1-1. The nomenclature of a porphyrin and chlorin (the bold regions indicate the 18 π-aromatic system).

The porphyrin macrocycle contains a total of 22-conjugated π-electrons, although only 18 π-electrons are required to maintain a closed aromatic system. Therefore, the cross-conjugated β,β'-double bonds can be modified. This does not interrupt the 18 π-aromatic system but drastically alters the electronic properties of the macrocycle. The reduction product of a single β,β'-double bond is called a chlorin (Figure 1-1).

Due to their aromatic nature, porphyrins can undergo a number of chemical reactions typical of aromatic compounds at the β-positions. Examples include electrophilic aromatic substitution reactions such as formylation, nitration, and halogenations.[2] On the other hand, the

β,β'-double bonds are also referred to as "pseudo-olefinic" because they can undergo some reactions characteristic of olefins including a dehydroxylation reaction by OsO_4, which leads to the formation of a 2,3-dihydroxychlorin.[3]

1.2. Naturally Occurring Porphyrins and Chlorins

In nature, porphyrins and chlorins play a fundamental role in many biological processes. For instance, heme, the iron complex of protoporphyrin IX, is the prosthetic group in a number of hemoproteins, such as hemoglobin, myoglobin and cytochromes, whose functions range from oxygen transport and storage to electron transfer.[1,4] Chlorophyll *a*, a magnesium chlorin complex, is responsible for the green pigment in leaves and as the primary light-harvesting pigment is crucial for photosynthesis in all plants (Figure 1-2).[1,4] Many other free base or metallo-porphyrins and -chlorins (and other, related, hydroporphyrins), the so-called "pigments of life", are naturally occurring.[1]

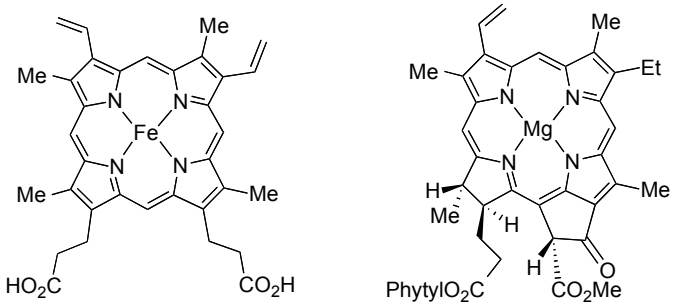

Figure 1-2. Naturally occurring porphyrin (heme) and chlorin (chlorophyll *a*).

1.3. Synthesis of Porphyrins

All naturally occurring porphyrins and chlorins are β-octaalkylated. The isolation and purification of these β-substituted porphyrins from natural sources requires difficult multi-step procedures. Therefore, synthetic porphyrins are frequently used to provide model systems. Modern methods have been developed for the synthesis of β-alkyl and *meso*-aryl porphyrins (Figure 1-3).[5] Even though *meso*-substituted porphyrins have no natural counterpart, the ease of their synthesis makes them excellent molecules for a wide range of porphyrin applications such as in the development of dye-sensitized solar cells, pressure sensitive paints and photodynamic therapy (PDT).[5-8]

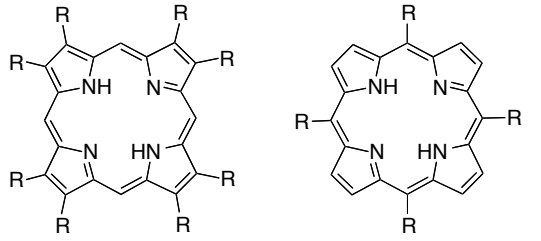

Figure 1-3. Generic β-substituted and *meso*-substituted porphyrins.

meso-Tetraarylporphyrins

meso-Tetraphenylporphyrin (TPP) **1** was first synthesized by Rothemund in 1936 through the direct condensation of benzaldehyde and pyrrole in pyridine in a sealed bomb at high temperature for 24 h.[9] This reaction was low yielding and was carried out under such harsh conditions that very few substituted benzaldehydes could be converted to the corresponding porphyrin. Adler and Longo modified this reaction in 1967 (Scheme 1-1).[10] They reacted the benzaldehyde and pyrrole in refluxing propionic acid exposed to air for 30 min, which allowed

for a wider range of benzaldehydes to be converted to the corresponding porphyrin in large scales and yields up to 20% as crystalline material. Due to its scalability, the Adler method is most suitable for the synthesis of batches of up to 20 g of porphyrin per 3 L flask.

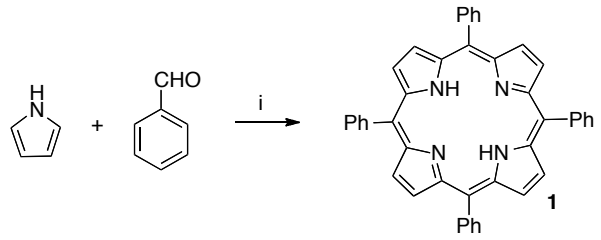

Scheme 1-1. Adler/Longo method for the synthesis of *meso*-tetraphenylporphyrin. *Reaction conditions:* i. propionic acid, reflux, air.

In 1987, Lindsey and co workers optimized the 4×4 condensation reaction and provided procedures with yields up to 60%.[11] Lindsey's method relies of the formation of a porphyrinogen under anoxic conditions as an intermediate (Scheme 1-2), which then is oxidized in a separate step to the porphyrin using an oxidant such as 2,3-dichloro-5,6-dicyanoquinone (DDQ). Although Lindsey's method is significantly higher yielding, it is only suitable for smaller scale syntheses due to the high dilution conditions employed.

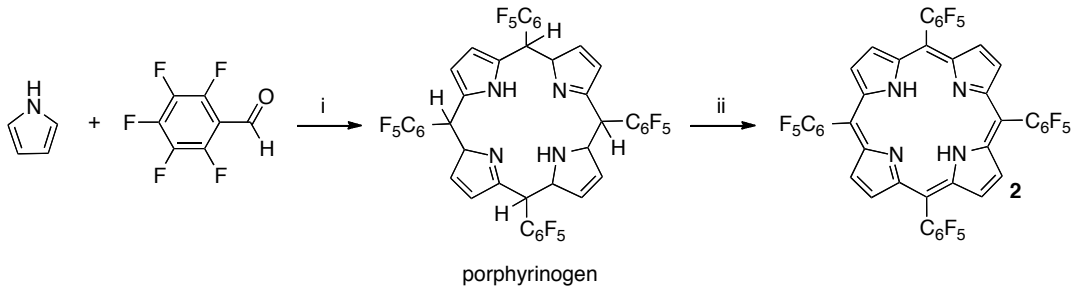

Scheme 1-2. Lindsey method for the synthesis of *meso*-tetrakis(pentafluorophenyl)porphyrin. *Reaction conditions:* i. $BF_3{\cdot}OEt_2$, CH_2Cl_2; ii. DDQ, reflux.

In 1969, Longo *et al.* reported the synthesis of *meso*-tetrakis(pentafluorophenyl)-porphyrin (T^FPP) **2** and noted the unusual spectrum due to the presence of the electron-

withdrawing fluorine groups.[12] The synthesis can also be carried out using Lindsey's method (Scheme 1-2).[11] The electronic structure of **2** was described in detail.[13]

1.4. Synthesis of Chlorins

In 1946, Calvin and co-workers identified a contaminant in the synthesis of TPP using the Rothemund-type synthesis as *meso*-tetraphenylchlorin (TPC).[14] Chlorins can also be synthesized directly by the reduction of porphyrins. In 1968, Whitlock and co-workers reported the reduction of TPP **1** by diimide (HN=NH), formed *in situ* by heating tosyl hydrazide with base, to produce chlorin **3** (Scheme 1-3).[15] One of the major drawbacks of this reaction is the susceptibility of the hydroporphyrin to oxidize back to the corresponding porphyrin. One other method to synthesize chlorins is the OsO_4-mediated dihydroxylation developed by Brückner *et al.*[3] This reaction involved the addition of OsO_4 in a solution of pyridine to the β,β'-double bond of porphyrin **1**, which formed an osmate ester chlorin. Reductive cleavage of the osmate ester chlorin afforded the corresponding dihydroxychlorin **4** (Scheme 1-3).

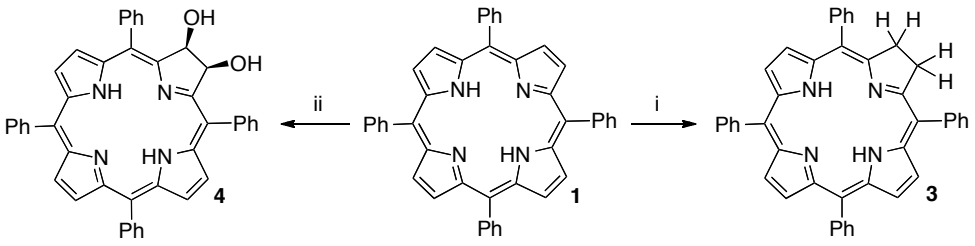

Scheme 1-3. Synthesis of *meso*-tetraphenylchlorin **3** and *meso*-tetraphenyl-2,3-dihydroxychlorin **4**. *Reaction conditions:* i. *p*-Toluenesulfonylhydrazide, K_2CO_3, pyridine; ii. 1. OsO_4, pyridine/$CHCl_3$ 2. H_2S.

1.5. Pyrrole-Modified Porphyrins

Pyrrole-modified porphyrins are porphyrinoids in which at least one of the pyrrolic subunits has been formally replaced by a non-pyrrolic heterocycle. They can be prepared by total synthesis or stepwise modification of a porphyrin. In 1984, Crossley and King reported the synthesis of pyrrole-modified porphyrins by oxidation at the β-pyrrolic position of the porphyrin macrocycle. This led to the introduction of oxygen into the β-pyrrolic position of porphyrins and the formation of *meso*-tetraphenylporpholactone (TPL) **8** (Scheme 1-4).[16]

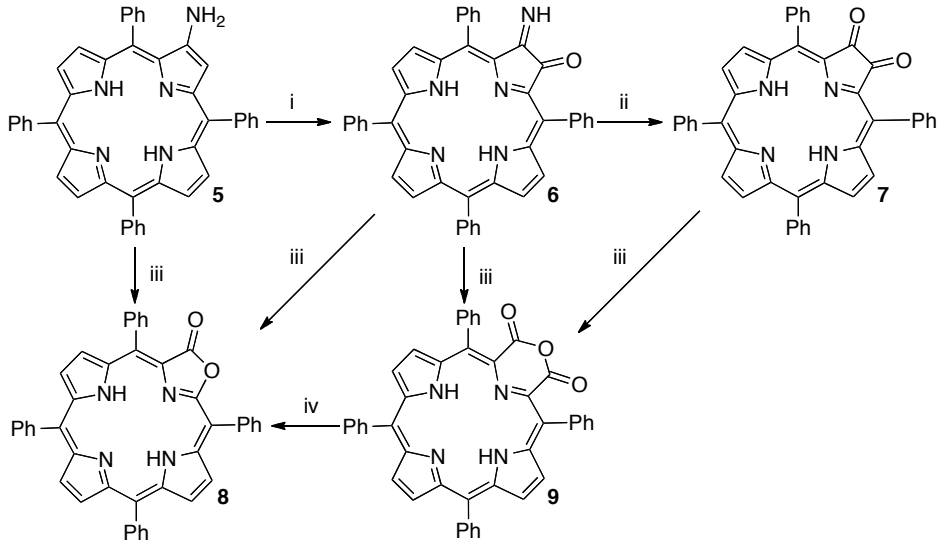

Scheme 1-4. Crossley's introduction of oxygen into the ß-pyrrolic position of porphyrins. *Reaction conditions:* i. *hv*, O_2; ii. H^+/H_2O or silica gel; iii. MCPBA; iv. NaOH, H_2O, DMF.

Starting with *meso*-tetraphenyl-2-aminoporphyrin **5**, available by reduction of the corresponding β-nitroporphyrin, Crossley and co-workers used a series of oxidative conditions for the modification of the periphery of the macrocycle.[16] One synthetic route involved the photo-oxidation of β-amioporphyrin **5** to give 2-imino-3-oxochlorin **6**, which was then hydrolyzed to the 2,3-dioxochlorin **7**. Oxidation of **6** with MCPBA under Baeyer-Villiger

conditions formed **8**. Traces of **8** are also formed by the reaction of dione **7** with MCPBA, but the main product was the pyrrole-modified porphyrin containing a six-membered ring, 2,3a-dioxo-3a-homo-2-oxachlorin **9**. Attempted base-induced ring opening of **9** failed to provide the desired dicarboxylate; instead, the lactone **8** was produced.

These reactions illustrate clearly that a number of pyrrole-modified porphyrins can be synthesized by modifications on the periphery of the macrocycle, as opposed to the total synthesis of the porphyrin. With these precedents in mind, the group of Brückner began a program to evaluate the scope and limits of the conversion of porphyrins to pyrrole-modified porphyrins using the approach they dubbed the "breaking and mending" approach (Scheme 1-5).[17] Their approach started with the conversion of *meso*-tetraarylporphyrin **10** to the corresponding diol chlorin **11** via OsO_4-mediated dihydroxylation.[18-20] The β,β'-double bond is oxidatively cleaved using $NaIO_4$ heterogenized on silica gel, initiating the "breaking" process and forming the bisaldehyde secochlorin **12**.[21] Lastly, a ring closure reaction forms a new heterocycle, such as **13-19**.[17-19,21-42]

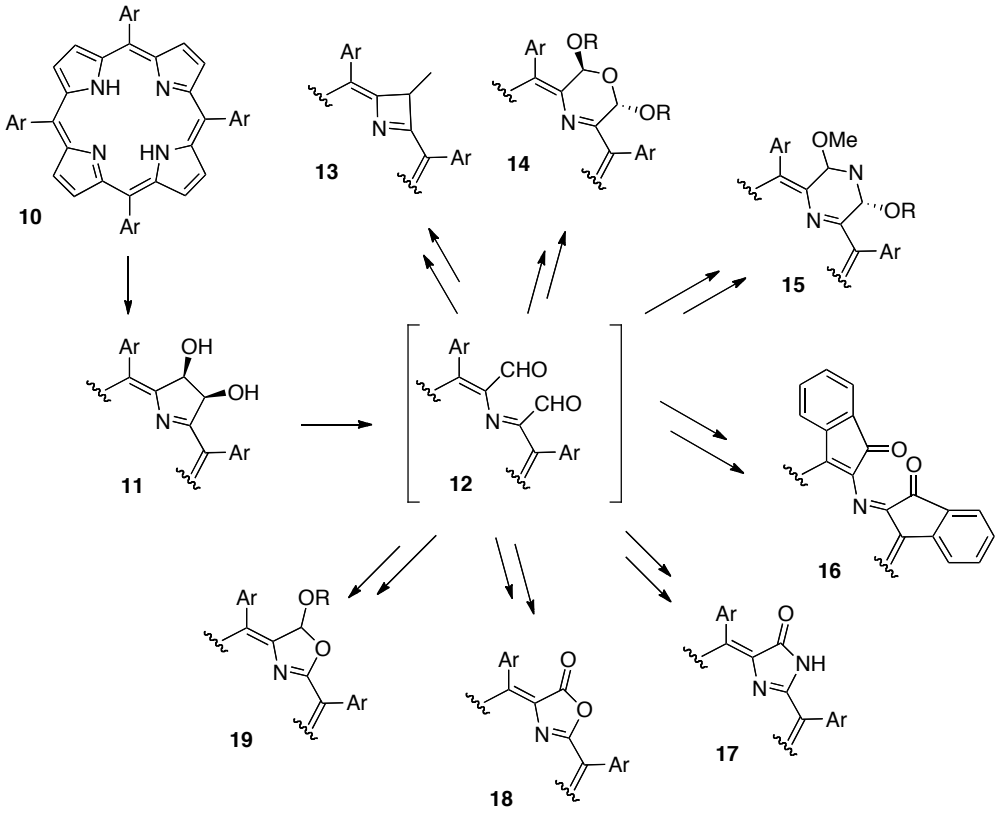

Scheme 1-5. "Breaking and Mending" approach to pyrrole-modified porphyrins.

In 1989, a direct porphyrin to pyrrole-modified porphyrin conversion was discovered by serendipity: *meso*-tetrakis(pentafluorophenyl)porpholactone (T^FPL) **20** was formed when the group of Gouterman and Khalil attempted to insert silver into the free base *meso*-tetrakis(pentafluorophenyl)porphyrin (Scheme 1-6).[43] The downfall with this synthesis is the number of side products formed, leading to difficulty in isolation of the products and low yields of the desired porpholactone. Other direct oxidations of porphyrins to porpholactones have become known.[44]

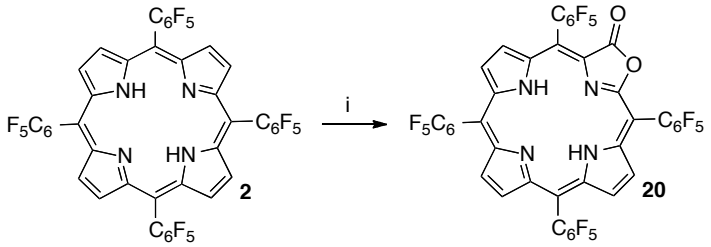

Scheme 1-6. One-step oxidation of *meso*-tetrakis(pentafluorophenyl)porphyrin to *meso*-tetrakis(pentafluorophenyl)porpholactone (T^FPL) **20**. *Reaction Conditions:* i. $AgNO_3$, acetic acid, reflux.

Porpholactone **20** can also be made using the breaking and mending approach (Scheme 1-7).[45]

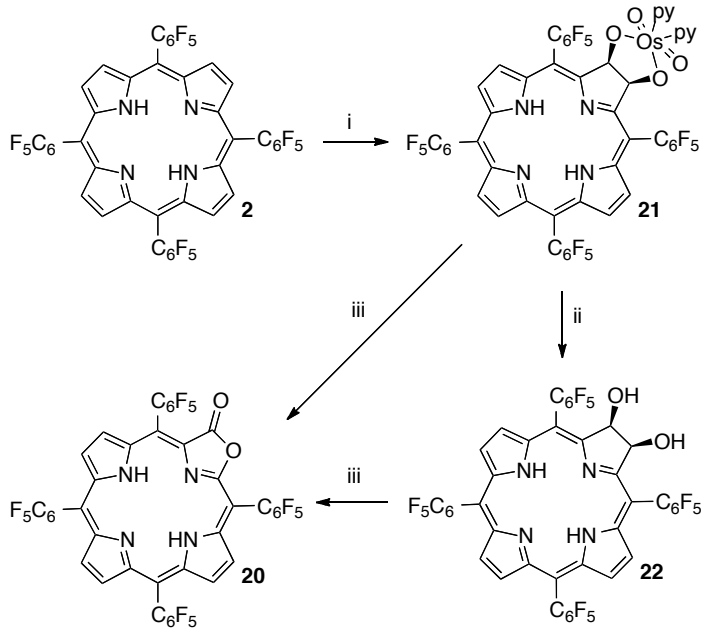

Scheme 1-7. Synthesis of T^FPL **20** using the "breaking and mending" approach. *Reaction Conditions:* i. OsO_4/py, $CHCl_3$, r.t. 2 d; ii. Sat. $NaHSO_3/H_2O$:MeOH (1:1), 30% $CHCl_3$/py; iii. CTAP.

The osmate ester is formed. The reductive cleavage of the osmate ester, however, cannot be accomplished using H_2S because of the reactivity of the C_6F_5 groups toward a nucleophilic aromatic substitution of the *p*-fluorine by the soft nucleophile SH^-. However, an aqueous sodium bisulfite solution allows the preparation of *meso*-tetrakis(pentafluorophenyl)dihydroxychlorin **22**.[35] A subsequent oxidation of the diol with MnO_4^- induces an oxidative cleavage and formation of **20** in high yields.[46]

1.6. Metalloporphyrins

Porphyrins have the ability to bind to a wide range of metal ions, including all first and second row transition metals.[47,48] A porphyrin with two central hydrogens in its inner cavity is referred to as a free base porphyrin, while the metal complexes are called metalloporphyrins. Upon complexation, the two inner pyrrole protons of the free base porphyrin are removed and the resulting porphyrin dianion coordinates to the metal ion (Scheme 1-8). This reaction is termed metallation. Depending on the metal, this process can be reversible. Demetallation can be frequently achieved by treatment with acids of various strengths.

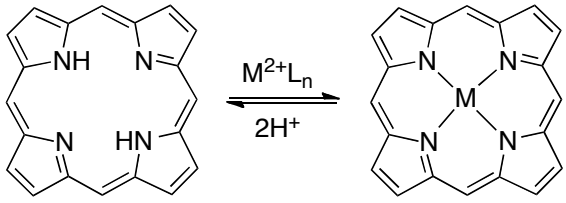

H_2(Por) M(Por)

Scheme 1-8. The reversible metathesis reaction of the porphyrin macrocycle.

A common method for metallation involves the addition of the metal acetate to a refluxing solution of porphyrin in an appropriate solvent, such as chloroform, acetic acid, pyridine, DMF or benzonitrile.[47] Other labile metal complexes, such as metal halides or acetylacetonates, are also frequently used as metal ion sources.[47] Recently, microwave heating has been found to be successful for the insertion of Group 10 metals into various porphyrinoids.[49] This drastically reduces the reaction times while obtaining high yields.

Depending upon the size and charge of the central metal, the presence of axial ligands, and preferred coordination geometry by the metal ion, a range of coordination geometries is found.[50] While the porphyrin generally acts as a square planar N_4-ligand, addition axial ligands form overall square pyramidal or octahedral complexes. Not all metals fit perfectly in the center of the porphyrin cavity, giving rise to, for instance, distorted octahedral and trigonal prismatic complexes (Figure 1-4).[47]

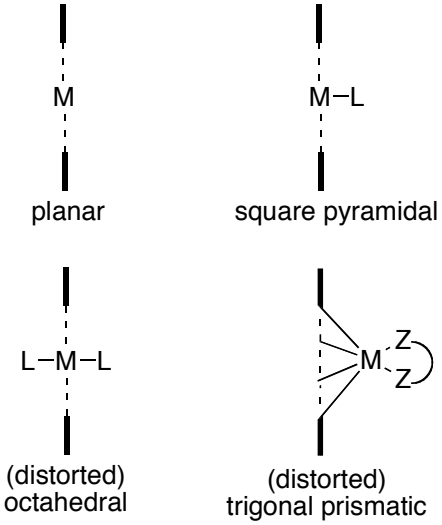

Figure 1-4. Graphics of select metalloporphyrin binding modes.[47]

1.7. Optical Properties of Porphyrinic Chromophores

Porphyrins and chlorins possess aromatic 18 π-electron systems that are responsible for their strong absorption in the UV-visible region of the electromagnetic spectrum. Generally, free-base porphyrins show four absorption bands (Q-bands) in the visible region between 500-650 nm in decreasing order of intensity with λ_{max} possessing the lowest intensity (the longest wavelength absorption) and a very intense band (Soret band), which occurs between 400-500 nm in the near ultraviolet region ($\varepsilon > 10^5\ M^{-1}cm^{-1}$) (Figure 1-5).

Free-base chlorins also possess a Soret band and four side bands, but the λ_{max} band is now the most intense Q-band (Figure 1-5). The bands are generally also broadened when compared to the corresponding bands in porphyrins, reflecting the larger conformational flexibility of this chromophore.

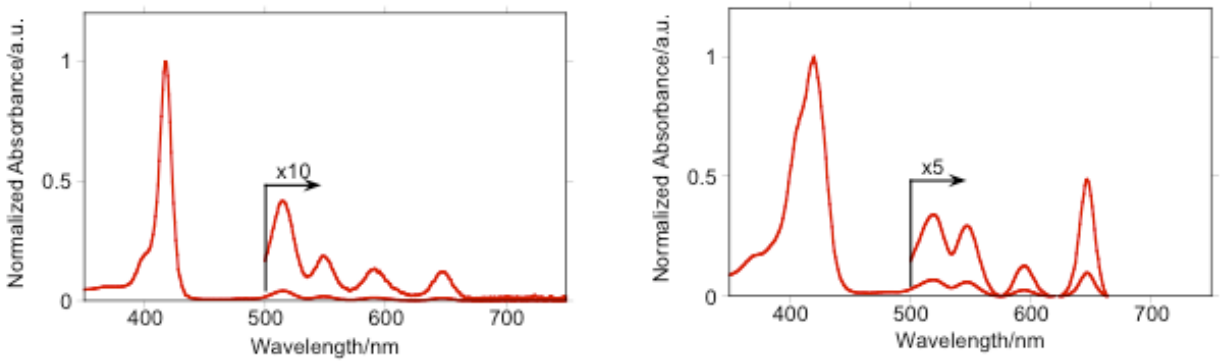

Figure 1-5. UV-vis spectra of a porphyrin (left) and a chlorin (right).

Metallation increases the symmetry of the macrocycle (ideally from two-fold symmetry to four-fold symmetry) and in turn the four side bands diminish to two Q-bands. The longest wavelengths absorption band (λ_{max}) is now hypsochromically shifted compared to the free base chromophore, whereas the Soret band remains in the usual range.[47]

Gourterman *et al.* proposed that the energies of the four frontier orbitals (HOMO and LUMO orbitals) and the corresponding HOMO-LUMO energy gaps determine the wavelengths at which the chromophore absorbs light.[51] The lowest energy electronic transitions from a ground state to an excited state occur between a single highest occupied molecular orbital (HOMO) and a single lowest unoccupied molecular orbital (LUMO) (Figure 1-6A). The Soret and Q bands both arise from π to π* transitions and can be understood by considering Gouterman's four-orbital model.[51] The relative energies of these electronic transitions are affected by the introduction of metal centers, substituents at the *meso*- or β-positions on the macrocycle ring, and the conformation of the macrocycle.[52-56]

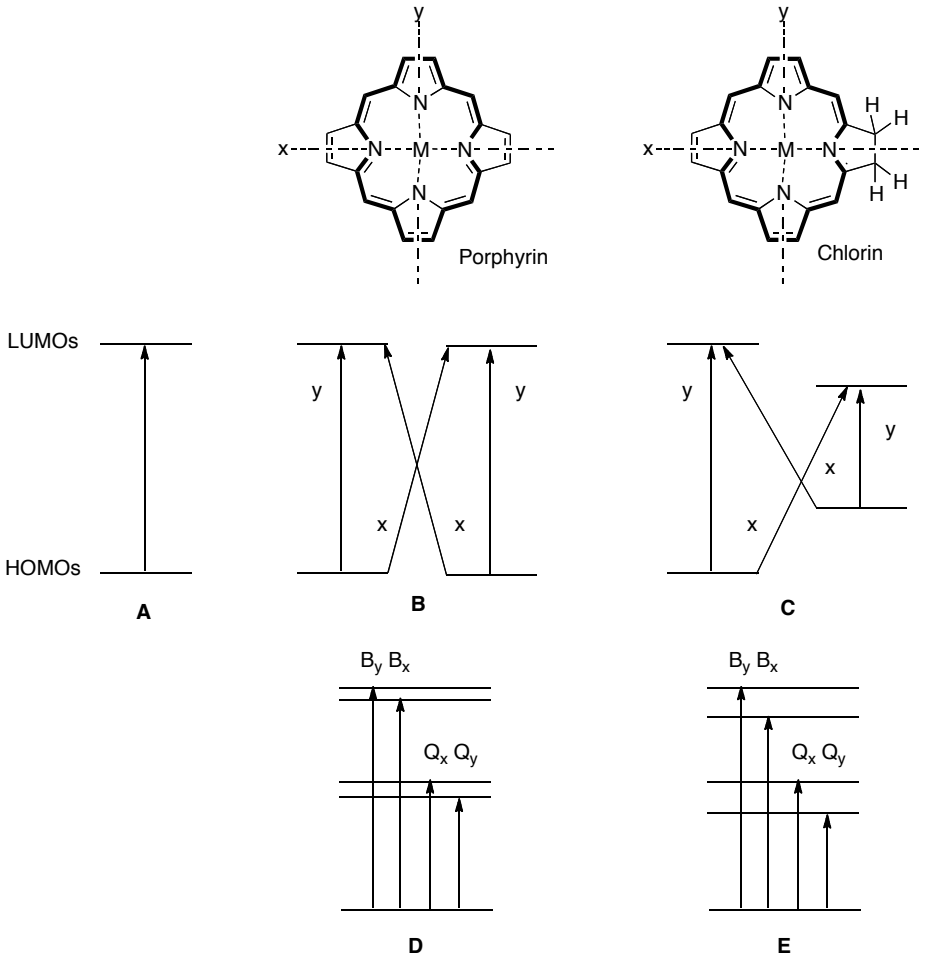

Figure 1-6. A schematic representation of the two HOMO and two LUMO orbitals (A-C) and the corresponding electrons transitions (D,E) for no degenerate species (A); porphyrins with high degeneracy (B, D) and porphyrins with lower degeneracy (C, E).

For a porphyrin with square planar, D_{4h} symmetry (i.e. a metalloporphyrin), the HOMO and LUMO orbitals are each quasi-degenerate by symmetry (Figure 1-6B). The HOMO-LUMO transitions split into two high energy, short wavelength (B_x and B_y) and two low energy, long wavelength (Q_x and Q_y) transitions (Figure 1-6D). Symmetrical porphyrins are predicted to have strongly allowed B transitions and zero probability of Q transitions.

Reduction of the porphyrin symmetry by vibrations, ring modifications or addition of substituents lifts the degeneracy and changes the HOMO-LUMO gap and increase the probability of Q transitions. (Figures 1-6C, 1-6E). For example, the reduction of one ß,ß'-double bond to form a chlorin will destabilized the π-system of a porphyrin and lifts the degeneracy of the two HOMOs and two LUMOs transitions.[57]

1.8. Applications of Metalloporphyrins

Synthetic metalloporphyrins and their analogues were utilized in to a wide range of applications, such as the photodynamic therapy treatment (PDT) of cancer,[58] pressure sensitive paints (PSP),[7,59,60] atom transfer catalysts,[61-63] and supramolecular assemblies for models of natural light-harvesting chlorophyll complexes.[64,65] The role of the metal varies in all these applications.

1.8.1. Photodynamic Therapy

Photodynamic therapy (PDT) is a non-invasive medical treatment that combines light, a photosensitizer molecule and oxygen for the destruction of cancerous or otherwise unwanted tissue.[66-68] In a whole-body applications of PDT, the photosensitizer is administered intravenously. Ideally, the sensitizer then localizes in the target tissue, which is then irradiated directly by a light source of appropriate wavelength. This generates reactive oxygen species (ROS), primarily singlet oxygen, which induces oxidative stress and ultimately lead to apoptosis, thus effectively killing the tumor cell in which the photosensitizer was localized.

The depth of penetration of light into tissue is limited by the light absorption by endogenous chromophores, mainly hemoglobin, and by optical scattering within the tissue.[69] Thus, to allow for treatment of deeper-seated tumors, the ideal photosensitizer must absorb light outside of the hemoglobin absorption range, i.e., in the red or near-IR region of the optical spectrum (Figure 1-7).[69]

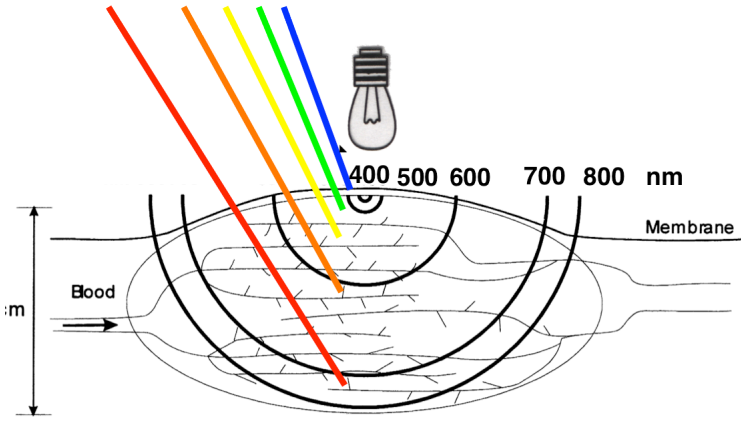

Figure 1-7. Depth of penetration of light as a function of wavelength. Figure from Ref.[69]

Upon light absorption, the singlet ground state (S_0) photosensitizer is excited into an excited singlet state (S_n) (Figure 1-8). The excited chromophore can relax back to the ground state *via* fluorescence. The $S_0 \rightarrow S_n$ and $S_n \rightarrow S_0$ transitions are quantum-chemically spin-allowed. As a consequence, excited singlet state lifetimes are very short ($\tau_{fl} = 10^{-9}$ to 10^{-6} sec). Alternatively, a number of processes can allow the electron in the excited S_n state to undergo spin inversion and to populate an excited triplet state (generally T_1). This process is referred to as intersystem crossing (ISC). Although spin inversion is spin-forbidden, excited state porphyrins are relatively efficient at undergoing ISC and consequently have high triplet state quantum yields (for a detailed description of one such process, see Section 1-7).[67,70] The excited electron can depopulate the excited triplet state (T_1) by decaying back to the ground state (S_0) *via*

phosphorescence (Figure 1-8). But since this is a spin-forbidden process, the lifetimes of phosphorescence are considerably longer (τ_P = 10^{-3} to 1 sec) compared to the fluorescence lifetimes.

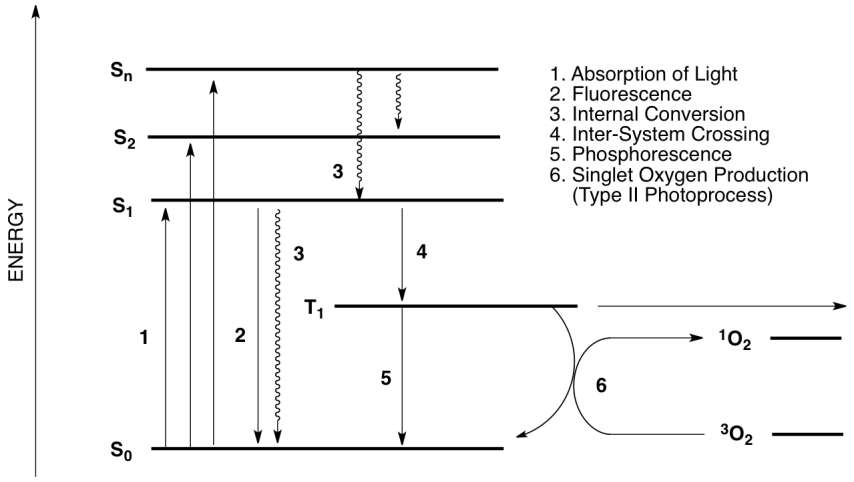

Figure 1-8. Modified Jablonski Diagram for a photosensitizer. Figure from Ref.[69]

An alternative relaxation mechanism for excited triplet-state photosensitizers exists by reactions with the environment in two ways: via a Type I or Type II process. Type I photochemical reactions involve the generation of free radicals (i.e. hydroxyl radicals ($OH^{\cdot}$), and superoxides ($O_2^{\cdot -}$) via electron transfer reactions, while Type II involves the production of singlet molecular oxygen ($^1O_2$) via an energy and spin-exchange reaction between the triplet sensitizer and ground state triplet oxygen ($^3O_2$).[67,71,72] The efficiency of Type I processes are dependent on the redox potential of the excited states while Type II processes are dependent upon the triplet state lifetime (τ_T) and the triplet quantum yield (ϕ_T) of the photosensitizer. Therefore, suitable photophysical characteristics for an ideal photosensitizer, aside from absorbing light in the red or near-IR region of the optical spectrum, are triplet state lifetime > 1 μs to allow for the bimolecular exchange reaction to take place, a high triplet state quantum yield (in the excess of 50% is excellent), and a triplet state of appropriate energy ($E_T \geq 95$ kJ mol^{-1}) to allow for

sufficient efficient energy transfer to generate singlet state oxygen.[67,68] The singlet oxygen and triplet state quantum yields and longevity of the triplet state are modulated by the substituents on the macrocycle, the macrocycle conformation and conformational flexibility, the presence of coordinated central metal ions and axial ligands attached to the metal centers.[73]

A range of synthetic metalloporphyrins have been utilized as candidates for the generation of ROS.[74] Studies have shown that the presence of the central metal cation in the porphyrin macrocycle may lead to a more efficient generation of cytotoxic products compared to the corresponding free base porphyrins.[74] This is due to the fact that the excited state deactivation and rates of ISC of the photosensitizer are strongly dependent on the metal cation. Generally, metal ions rigidify the macrocycle, shutting vibrational deactivation pathways of the sensitizer T_1 state down. Also, certain diamagnetic heavy metal ions are known to promote ISC, chief among them palladium(II) and platinum(II). The presence of atoms with a high number of d-electrons allows for rapid transitions between states with different multiplicities via spin-orbit exchange processes. The heavy metal platinum is strongly backbonded to the empty $e_g(\pi^*)$ degenerate orbitals (LUMOs), which increases the triplet state quantum yield. However, while this leads to high triplet yields, the lifetime of the triplet state may also decrease with increasing atomic number of the metal ion, thus possibly leading to an overall small singlet oxygen quantum yield.[67,75]

Complexes of metals that have completely full or completely empty d-orbitals (such as cadmium(II), magnesium(II) or zinc(II)) do not allow for any spin-orbital interaction to occur – after all, their d-electrons cannot exchange their angular momentum quantum number m_ℓ with the excited electron spin. These metalloporphyrins are therefore characterized by long T_1 lifetimes and corresponding high quantum yields of singlet oxygen.[76] Metalloporphyrins with

paramagnetic metal ions with d^6-d^9 electron configurations have partial overlap of the π-system of the porphyrin with the d orbitals of the central metal ion.[68,74,77] This leads to increased spin-orbital interactions. Thus, metalloporphyrins containing central metal ions from the first row of transition metals on the periodic table (cobalt(II), nickel(II) and copper(II) are non-emissive and are characterized by extremely short triplet state lifetimes. Relative to these radiationless species, fluorescent metalloporphyrins (containing, for instance, cadmium(II), magnesium(II) and zinc(II)) have longer triplet state lifetimes (Table 1-1).[75,76]

meso-Tetrakis(4-sulphonatophenyl)porphyrin **23** and its metal(II) complexes (Figure 1-9) have been used in human medicine for PDT. The metal complexes highlight the photophysical trends delineated above (Table 1-1 and 1-2).[75,76]

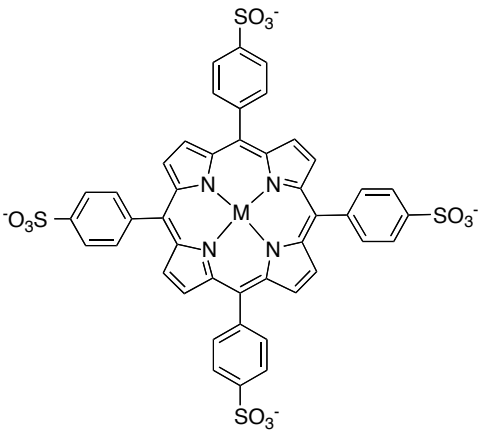

M = 2H **23**
= Ag(II) **23Ag**
= Cd(II) **23Cd**
= Co(II) **23Co**
= Cu(II) **23Cu**
= Mg(II) **23Mg**
= Ni(II) **23Ni**
= Pd(II) **23Pd**
= Pt(II) **23Pt**
= Pt(II) **23Pt**
= Zn(II) **23Zn**

Figure 1-9. Structure of *meso*-tetrakis(4-sulfonatophenyl)porphyrin **23** and its metal(II) complexes.

Table 1-1. Photophysical properties of the triplet states of metal complexes of 23: natural lifetimes τ_T and bimolecular reaction constant for oxygen quenching $k(O_2)$ in 10^{-5} M solution, Extinction coefficient of triplet state at 460 nm ε_{460}, estimated quantum yield of triplet state formation ϕ_T and fraction of triplet state quenched by oxygen which yield $^1O_2$ for all the test substances S_Δ.[75,76]

Compound	τ_T (μs)	$k(O_2) \times 10^9$ (M^{-1} s^{-1})	$\varepsilon_{460} \times 10^{-5}$ (M^{-1} cm^{-1})	ϕ_T	S_Δ
23	414	2.0 ± 0.1	1.30	0.76	0.62
23Zn	2040	1.3 ± 0.1	1.61	0.86	0.74
23Pd	268	2.2 ± 0.1	1.32	0.63	0.49
23Pt	12.7	2.9 ± 0.9	1.71	0.40	0.06
23Mg	467 (43%)				0.69
	2640 (57%)	1.2 ± 0.3	0.43	0.85	-
23Cd	149	1.4 ± 0.1	0.80	0.88	-
23Co	-	-	-	-	0
23Ni	-	-	-	-	0
23Cu	-	-	-	-	0
23Ag	301	1.8 ± 0.1	-	-	0

Table 1-2. Calculated slopes *k* (iodide method), *B* (RNO method) and quantum yields of quantum yield of $^1O_2$ obtained by the iodide method ($\phi_{\Delta\ I}$) and the RNO method ($\phi_{\Delta\ RNO}$); both relative to **23** = 0.62. [75,76]

Compound	Slope ***k*** (s^{-1}) (iodide method) $\times 10^{-5}$	$\phi_{\Delta\ I}$	Slope ***B*** (s^{-1}) (RNO method) $\times 10^{-5}$	$\phi_{\Delta\ RNO}$
23	730	0.62	13	0.62
23Zn	868	0.74	17	0.81
23Pd	580	0.49	10	0.48
23Pt	171	0.06	1.2	0.06
23Mg	812	0.69	14	0.67
	-	-	-	-
23Cd	-	-	12	-
23Co	0	0	0	0
23Ni	0	0	0	0
23Cu	0	0	0	0
23Ag	0	0	0	0

Metalloporphyrins with electronic configurations of d^0 and d^{10} (**23Mg, 23Zn** and **23Cd**) showed the longest triplet state lifetimes and therefore highest quantum yields of singlet oxygen due to the fluorescent capabilities and absence of spin-orbital interactions.

Even though the photophysical factors can sometimes be used to correctly predict the trends for the actually observed phototoxicity of a given photosensitizer, there are many other practical factors that come into consideration when the photosensitizers are being investigated for *in vivo* and *in vitro* studies. Chief among them are issues relating to the pharmacology (pharmacodynamics and pharmacokinetics) of the compounds. Solubility and lipophilicity of a compound are obvious factors that will determine whether a compound can enter a cell, for example. The presence of a metalloporphyrin with a metal carrying an inert axial ligand may bio-distribute differently compared to the same porphyrin carrying a metal with a metal absent of an axial ligand or a metal that can exchange rapidly its axial ligand(s).

Kolarova and co-workers examined the metallated *meso*-tetrakis(4-sulfonato-phenyl)porphyrin with respect to the effect of the central metal ion on cell survival. *meso*-tetrakis(4-sulfonatophenyl)porphyrin **23** and its metal(II) complexes **23Zn** and **23Pd** photosensitizers (Figure 1-9) were chosen and their phototoxicity in the G361 (human melanoma) cell line was compared.[78] The most effective sensitizer was found to be **23Zn** followed by **23Pd** and **23**.

Tin etiopurpurin **24Sn**, a chlorin photosensitizer, marketed under the trade name Purlytin by Miravant Medical Technologies (Santa Barbara, CA) (Figure 1-10), has been used in phase II/III clinical studies for photodynamic therapy for the treatment of cutaneous metastatic breast cancer. The presence of the tin causes a red-shift of approximately 20-30 nm (λ_{max} = 650 nm) compared to the free base etiopurpurin.[79,80]

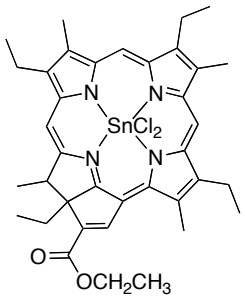

24Sn

Figure 1-10. Structure of tin etiopurpurin **24Sn**.

Morgan and co-workers evaluated benzochlorin derivatives with an iminium salt at the *meso*-position in preclinical studies for their efficacy in PDT (Figure 1-11).[81] Copper benzochlorin derivatives with iminium salts have triplet state lifetime of less than 20 ns; nonetheless, that have been shown to be useful as photosensitizers. *In vitro* and *in vivo* comparison with the photodynamic activity of the corresponding zinc salt and its free base.

However, among the three photosensitizers, the zinc derivative produced the greatest tumor regression.

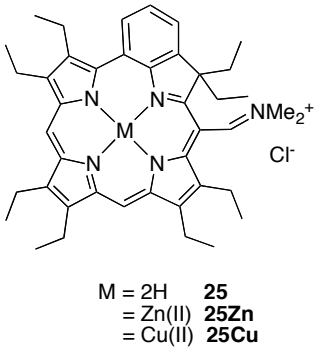

Figure 1-11. Structure of octaethylbenzochlorin iminium salt **25** and its metal(II) complexes **25Cu** and **25Zn**.

Lindsey and co-workers studied three *meso*-imidazolium-substituted metalloporphyrins: a set of net positively charged imidazolium-substituted porphyrins that contain central zinc(II), **26Zn**, palladium(II), **26Pd**, and indium(III), **26InCl**, metal ions (Figure 1-12).[70,82]

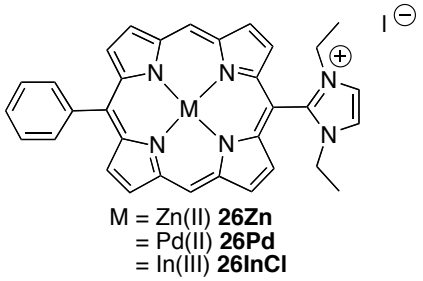

Figure 1-12. Structures of *meso*-imidazolium-substituted metalloporphyrins, **26Zn**, **26Pd**, **26InCl**.

The role of the central metal on the reactive hydroxyl radical production (Type I) of **26Zn**, **26Pd**, **26InCl**. was investigated. The *in vitro* PDT activity was studied using human (HeLa) and mouse (CT26) cancer cell lines. Predictions of the order phototoxicity were initially generated based on the lifetimes of the lowest energy singlet state (S_1) **26Pd** (0.009) < **26InCl**

(0.24) < **26Zn** (3.0). This trend reflects an increase in the yield of intersystem crossing from S_1 to the lowest energy triplet state T_1 and the order of phototoxicity: **26Pd** (> 0.99) > **26InCl** (0.98) < **26Zn** (0.80) (Table 1-3). Moreover, further experiments to determine the location of intracellular damage caused by PDT showed that the reactive oxygen species (ROS) produced was hydroxyl radicals, which is a result of a Type I process. Therefore, this trend cannot be easily explained by the comparison of the general photophysical data.

It was found that **26Pd** generated more highly toxic hydroxyl radicals as the ROS than **26InCl** and **26Zn**. Notably, palladium porphyrins have a greater ease of reduction (~0.2 eV) compared to zinc porphyrins, which is complemented by the higher energy (~0.2 eV) of the triplet excited state (T_1). This characterizes **26Pd** as a stronger electron acceptor than **26Zn.** The difference in PDT efficacy of between **26Pd** and **26Zn** can be further explained by the axial-ligation behavior of the metal ions. Palladium complexes do not coordinate axial ligands, unlike zinc complexes allowing more ligation to entities in the cellular environment causing slower diffusion to the desired location.

Table 1-3. Photophysical data of the *meso*-imidazolium-substituted metalloporphyrins **26Zn**, **26InCl** and **26Pd**: fluorescence yield ϕ_f, phosphorescence yield ϕ_p, lifetime of the lowest energy singlet excited state τ_s and lifetime of the lowest energy triplet excited state τ_T.[70]

Compound	T(K)	ϕ_f	ϕ_p	τ_s	τ_T
26Zn	295	0.015		3.0	6.1
	77		0.0021		54
26InCl	295	0.0078		0.24	
26Pd	295	0.00012		0.009	0.01
	77		0.078		2.0

Rosenfeld *et al.* investigated the in *vitro* and *in vivo* photosensitizing efficacy of metallated analogs of methyl-13^2-oxopyropheophorbide-*a* **27** (Scheme 1-9).[72] The effect of the central metal on the photochemical activity was investigated using indium(III), copper(II) and

zinc(II) and free base complexes of the pyrodione (Scheme 1-9). Among these complexes, indium(III) pyrodione **27InCl** was determined to be the most effective, followed by zinc(II), free base and copper(II). This trend can be explained by the heavy atom effect of an atom, which increases the rate of ISC and a correspondingly high singlet oxygen quantum yield. Methyl-13^2-oxopyrophenophorbide-*a* **27** was then converted into a series of 3-substituted alkyl ether analogues **28-31** to study the effect of the carbon chain length on the photochemical activity. Since, indium(III) pyrodione **27InCl** was the most effective, the 3-substituted alkyl ether analogues **28-31** were converted into the corresponding indium(III) complexes **28InCl-31InCl** (Scheme 1-10). Among the alkyl ether derivatives, the methyl 3-decyloxyethyl-3-devinyl-13^2-oxo-pyrophenophorbide-a indium(III) complex **28InCl** (ϕ_Δ = 0.72) enhanced its *in vitro* and *in vivo* photosensitizing efficacy, highlighting how the modulation of the lipophilicity of the chromophore also has major effects on the phototoxicity of a particular sensitizer.

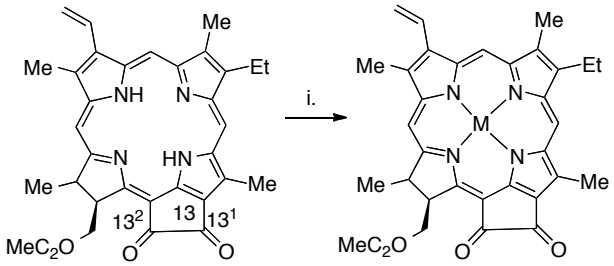

Scheme 1-9. Synthesis of metallated pyrodione **27M**. *Reaction Conditions:* i. metal insertion: $InCl_3$, $Cu(OAc)_2$ and $Zn(OAc)_2$.

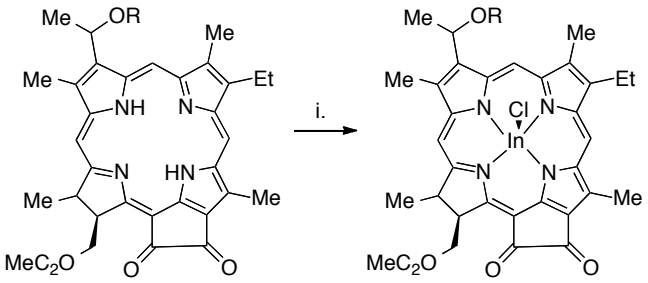

28; R=Methyl **29;** R=Pentyl
30; R=Hepty **31**; R=Decyl

28InCl; R=Methyl **29InCl**; R=Pentyl
30InCl; R=Hepty **31InCl**; R=Decyl

Scheme 1-10. Synthesis of In(III) 3-substituted alkyl ether pyrodione. (**28InCl-31InCl**).
Reaction Conditions: i. metal insertion: $InCl_3$.

Due to the fact that the photosensitizers are administered intravenously, water-soluble photosensitizers can also be used rather than using a delivery vehicle, such as liposomes. Boyle *et al*. directly attached PEG chains to photoactive, yet hydrophobic, porphyrins and metalloporphyrins in order to synthesize water-soluble photosensitizers (Scheme 1-11).[83] The phototoxicity of the PEGylated porphyrins and metalloporphyrins were investigated in human Caucasian colon adenocarcinoma (Caco 2) cells. Of interest is the effect of the coordinated metal and axial ligand on the phototoxicity of the cells.

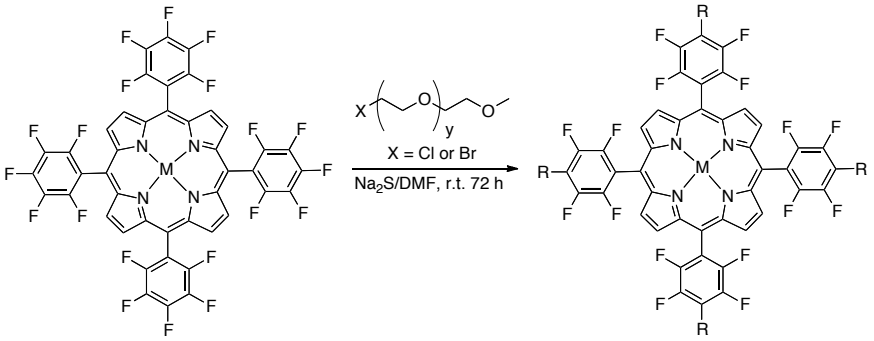

M = 2H **2**
= Ni(II) **2Ni**
= Ga(OPh)(III) **2Ga(OPh)**
= GaCl(III) **2GaCl**

R = PEG
where n = 2 (PEG), 11 (PEG_{550}), 15 (PEG_{750})

M = 2H **2-PEG, PEG_{550}** or **PEG_{750}**
= Ni(II) **2Ni-PEG, PEG_{550}** or **PEG_{750}**
= Ga(OPh)(III) **2Ga(OPh)-PEG, PEG_{550}** or **PEG_{750}**
= GaCl(III) **2GaCl-PEG, PEG_{550}** or **PEG_{750}**

Scheme 1-11. General synthetic route to PEGylated porphyrins and metalloporphyrins.

The testing of the free base PEGylated porphyrins **2-PEG** and **2-PEG$_{750}$** showed significant phototoxicity. The nickel(II) complexes **2Ni-PEG**, **2Ni-PEG$_{550}$** and **2Ni-PEG$_{750}$** showed no observable phototoxicity, while the gallium(III)OPh complexes **2Ga(OPh)-PEG**, **2Ga(OPh)-PEG$_{550}$** and **2Ga(OPh)-PEG$_{750}$** showed interesting trends. **2Ga(OPh)-PEG** failed to kill 50% of cells even at the highest concentration. However, **2Ga(OPh)-PEG$_{550}$** and **2Ga(OPh)-PEG$_{750}$** killed 90% of the cells when irradiated with red light (>600 nm). The chloride axial ligand compound showed over time a significantly increased toxicity. These results highlight the strong influence of the axial ligand and the general hydrophobicity of the sensitizer.

1.8.2. Pressure-Sensitive Paint

Pressure-sensitive paint (PSP) technology was first introduced in the 1980s and has evolved as an important tool in the measurement of surface pressure in aerodynamic testing.[84] Surface pressure measurements are important for basic fluid dynamics experiments, studying specific flow phenomena and validating computational fluid dynamic codes.

PSP is based on the oxygen-induced luminescence quenching of a coating that is painted on a model surface. The coating is comprised of a luminescent molecule (also known as a luminophor) that is dispersed in an oxygen-permeable polymer binder. When the luminophor is excited to a high-energy singlet state (S_1), the excited electrons undergo intersystem crossing to a triplet state (T_1) from which the luminophore can relax back to the ground state via phosphorescence. However, if the excited luminophore interacts with triplet oxygen, the excited state and corresponding light emission is quenched, resulting in an oxygen partial pressure dependent luminescence intensity that can be captured with digital cameras. The resulting image will be brightest in the areas of low pressure (low oxygen concentration) and less intense in the areas of high pressure (where oxygen is most abundant on the surface). Thus, PSPs can provide an image of the local pressure of oxygen over the surface during aerodynamic flow.[85]

PSPs offer a number of advantages over the pressure taps traditionally used on conventional wind tunnel models:[86,87] (i) PSPs provide pressure measurements in areas not possible with conventional pressure taps (i.e. leading and trailing edges). (ii) PSPs have the ability to capture the surface pressure distribution over an entire model with exceptional spatial resolution. (iii) PSPs allow for real time modeling and better integration of experimental and computational fluid dynamics allowing for a significant decrease in the time required for prototyping of new designs.

The performance of the PSP depends on combined characteristics of the binder and the luminophor. The binder must be permeable to oxygen while the luminophor should possess high luminescence quantum yields, long emission lifetimes, and excellent photostability. Metalloporphyrins typically exhibit triplet yields $\phi_T > 50\%$. For platinum(II) and palladium(II) porphyrins, ϕ_T is nearly 100%, they are bright luminophores. The high oxygen sensitivity of these complexes comes from the long triplet lifetimes allowing ample time for the excited state molecule to interact with oxygen.[85,88]

In the late 1980's, Gouterman and co workers utilized the oxygen quenching capability of platinum(II) octaethylporphyrin **29Pt** (Figure 1-13) and performed qualitative experiments on the first PSP for aerodynamic testing.[85] The porphyrin complex **29Pt** was selected for its large phosphorescence quantum yield (approximately 90%) and its long triplet lifetime (approximately 100 μs) and possessing a large radiative decay rate, k_p, for the phosphorescence emission.[89]

The active molecule, **29Pt**, was suspended in a silicon resin, which was painted onto the surface of interest. The paint was excited at 360 nm and **29Pt** phosphoresces at ~650 nm.[85] However, undesirable characteristics of the luminophore include a significant temperature dependence for the luminescence, photodegradation pf **29Pt** after extended exposure to UV light and lastly, a delay of 10 s for the luminescence intensity to respond fully to pressure changes.

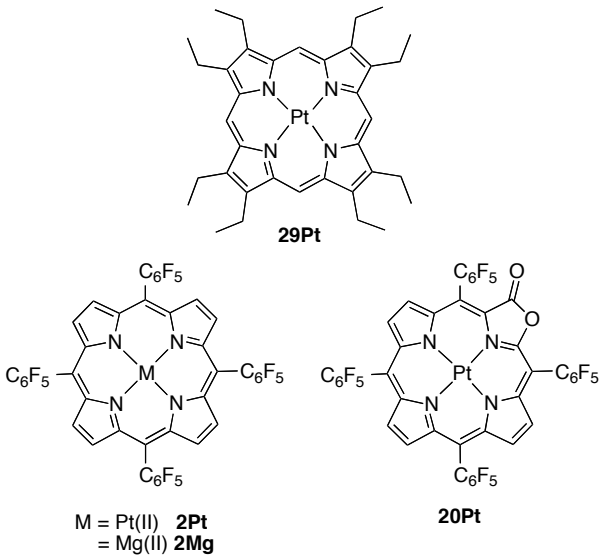

Figure 1-13. Structures of porphyrin luminophores used in oxygen sensing.

Gouterman and co-workers subsequently developed an improved PSP using a porphyrin complex, [*meso*-tetrakis(pentafluorophenyl)porphyrinato]platinum(II) **2Pt** (Figure 1-13), a fluoro-acrylic polymer (FIB) as the binder and the base coat.[90] This PSP is more photostable due to the electronegativity of the pentafluorophenyl groups, slowing photodegradation reactions. Moreover, it has a response time of less than 1 s and the dependence on pressure and temperature are nearly independent. Notably, the decrease in temperature sensitivity comes from the low activation energy involved in the FIB oxygen diffusion coefficient.

There still lies the issue that PSP data is generally derived by rationing two images of a PSP-coated wind tunnel model. One image is taken at a known "wind-off" reference pressure distribution while the other is taken at the "wind-on" pressure distribution. This calibration is necessary in order to factor out the effects of inconsistent surface illumination and paint thickness.[87,89] In order to get around the image registration problems, Gouterman and co-workers developed a dual-luminophor paint containing both a sensor and a reference luminophor, independent of pressure and FIB as the binder.[87] This dual-luminophor PSP introduced a new

oxygen-sensitive molecule, a porpholactone complex, *meso*-[tetrakis(pentafluorophenyl)porpholactonato]platinum(II) **20Pt** (Figure 1-13) with *meso*-tetrakis(pentafluorophenyl)porphyrinato]magnesium(II) **2Mg** as the reference molecule. The absorption spectra of the two luminophors do not closely overlap, **20Pt** absorbs at 395 nm, while **2Mg** absorbs at 418 nm. The emission spectrum of **20Pt** at ~740 nm is highly sensitive to oxygen and the emission spectrum of **2Mg** at 650 nm shows almost no dependence on oxygen concentration. This dual-luminophor system produced "ideal" PSP measurements with pressure sensitivity of 4.5%/psi and a temperature dependency of less than -0.1%/°C.

1.8.3. Supramolecular Assemblies

Light harvesting antenna complexes (LH-I and LH-II) in photosynthetic purple bacteria are naturally occurring porphyrin-derivative nanorings in which, respectively, 30 and 16 bacteriochlorophylls (BChls) are arranged in circular arrays. Many scientists are interested in modeling this circular structure along with its electron transfer processes and therefore try to synthesize model systems that mimic their structural and functional characteristics. Zinc porphyrins have been utilized for the formation of large nano-ring systems. These systems were either constructed with the help of, or are held together with, directed metal-ligand complementary coordination interaction. A number of examples will illustrate the structural roles of the metal in these systems.

Imidazole to zinc coordination porphyrin nanorings

Kobuke and co-workers reported on a series of macrocyclic porphyrin assemblies by complimentary coordination of [bis-imidazolylporphyrinato]zinc(II) connected by spacers such as, ferrocene,[91] *m*-phenylene and *m*-bis(ethylene)phenylene[92] and 2,5-thienylene.[65] The size of

the resulting macrocycle depends on the type of spacer in the [bisporphyrinato]zinc(II) complexes.

In the case with ferrocene, which possesses a unique rotational behavior, reorganization of the ferrocene linked dimer **30Zn** into a series of macrocycles ranging from a trimer to a decamer was observed (Scheme 1-12).[91]

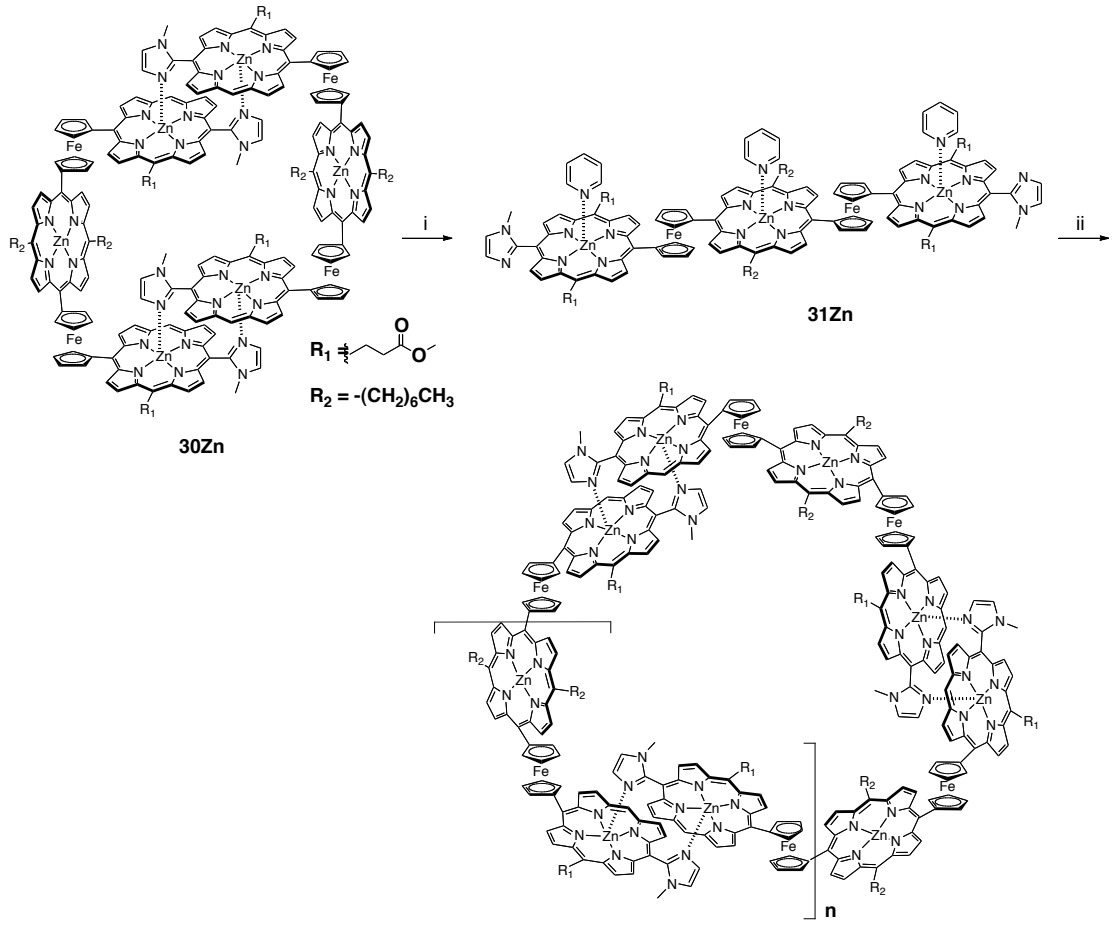

Scheme 1-12. Reorganization of ferrocene-linked trisporphyrin; Conformational structure: 2, 3, 4, 5, 6, 7, 8, 9, 10-mer; *Reaction conditions*: i. pyridine; ii. removal of pyridine, $CHCl_3$/0.5% ethanol.

After the reorganization of **30Zn** into a pyridine-coordinated monomer **31Zn** was achieved, the pyridine was evaporated to dryness and the solid sample was left standing in chloroform solution. A polymeric mixture of large molecular weights was formed in the

chloroform solution (including 0.5% of ethanol) at room temperature in the dark. A large peak with a strong tailing was observed initially at the exclusion limit in the GPC chromatographs (Figure 1-14). This broad peak shifted day by day to longer retention times and well-separated peaks of lower molecular weights and this transformation is completely reversible. This demonstrates the value of the labile nature of the coordination interaction that holds the rings together and that allows the slow sorting of the initially formed random assemblies to the thermodynamically most stable arrangements.

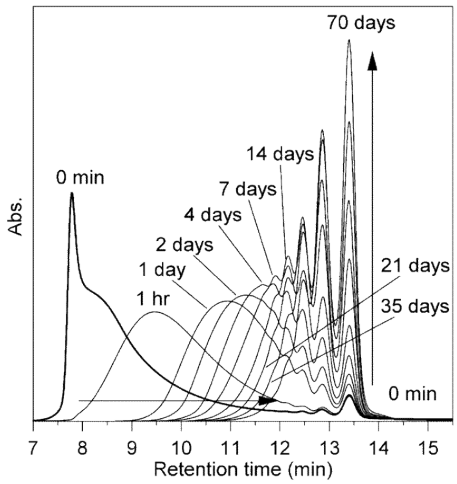

Figure 1-14. Time-dependent change of GPC chromatograms in the reorganization process of **30Zn**. [**30Zn**] = 0.4 mM. Times are 0 min (thick line) (the sample immediately after the reorganization), 1 h, 1 day, 2 days, 4 days, 7 days, 14 days, 21 days, 35 days, and 70 days. Figure from Ref.[91]

Previously, pentamer **P5** and hexamer **P6** bis(zinc-imidazolylporphyrin) macrocycle arrays linked through a *m*-phenylene moiety were reported in a 1:1 mixture (Figure 1-15). However, π-conjugation is limited due to the porphyrin and phenylene planes being orthogonal to each other. Therefore, cyclic pentamers **EP5** and hexamers **EP6** linked by a m-bis(ethylene)phenylene spacer were constructed, increasing the π-conjugation. The hexamer macrocycles showed faster excitation energy hoping (EEH) rates than the pentamer macrocycles,

which may be due to the 120° angle of the 1,3-bis(ethynl)phenylene linker being better suited for the hexagonal structure that it is fro the pentagonal structures.[92]

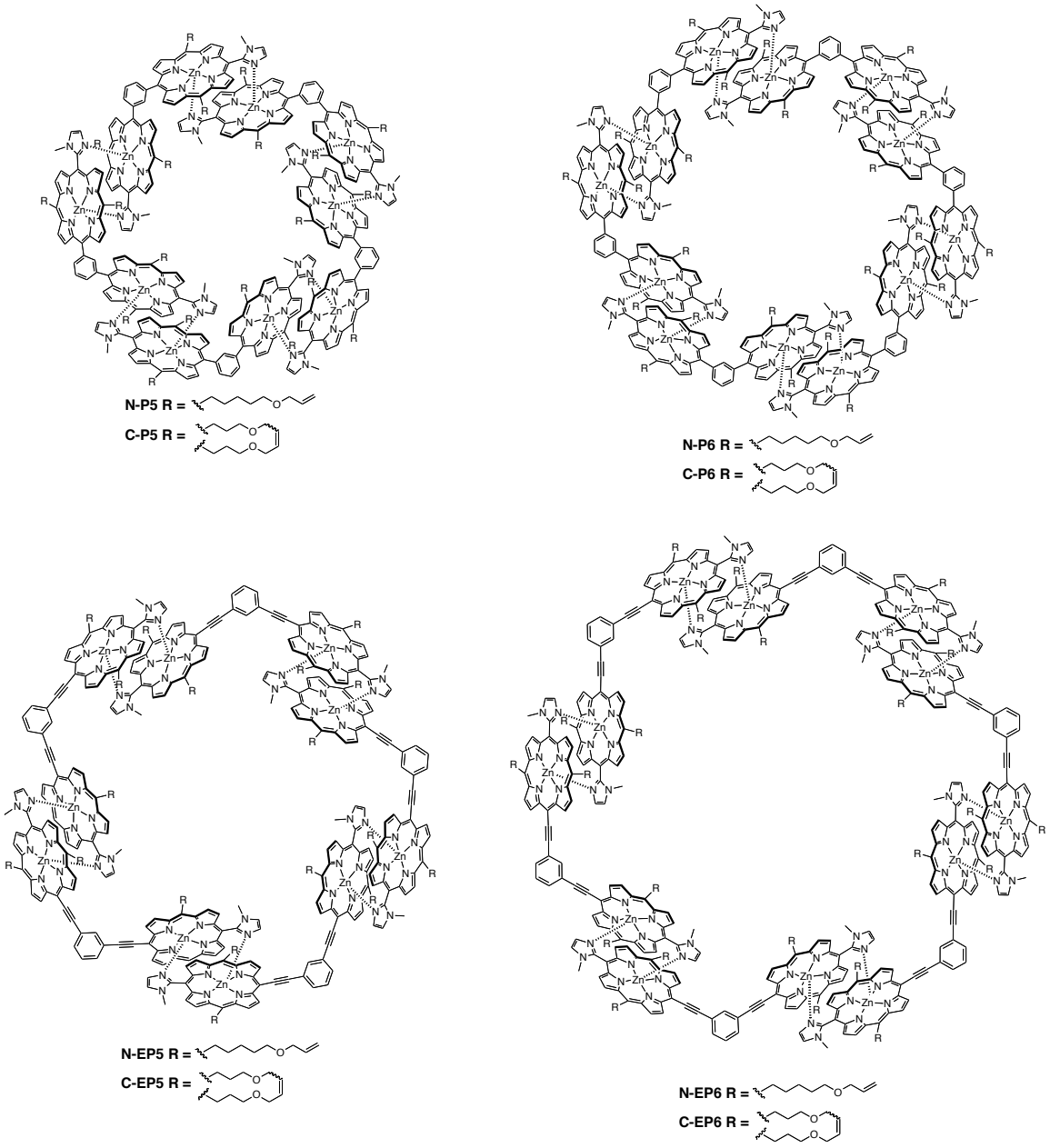

Figure 1-15. Structures of pentamer and hexamer porphyrin arrays; N = noncovalently linked; C = covalently linked.

Kobuke and co-workers explored the use of a thiophene linker between [bis(imidazolyl-porphyrinato]zinc(II) complexes with enlarged internal angles to construct even larger macrocycles (Scheme 1-13).[65]

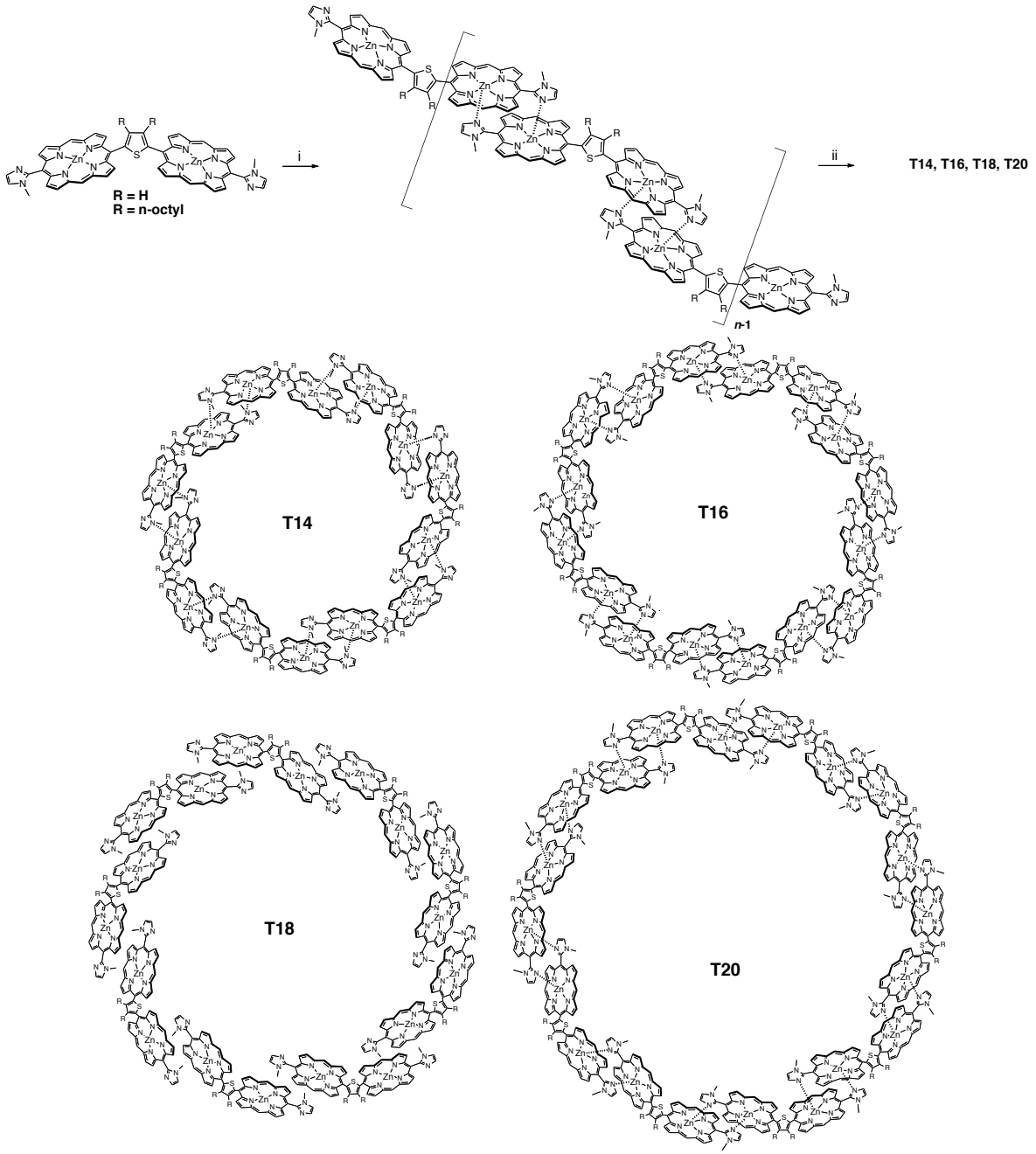

Scheme 1-13. Self assembly of thiophenylene-linked bisporphyrins **T14**, **T16**, **T18**, **T20**; *Reaction conditions*: i. wash with water, $CHCl_3$; ii. Reorganization, $CHCl_3$ or $CHCl_3$/1% MeOH (v/v).

A mixture of a heptamer **T14** to a decamer **T20** was obtained and the corresponding UV-vis spectra were red-shifted as the ring size increased, which indicates that larger macrocycles are ideal models for bacterial photosynthetic light-harvesting antennas.

Butadiyne-linked porphyrin nanorings

Anderson and co-workers developed a methodology for the synthesis of a series of fully conjugated butadiyne-linked porphyrin oligomers of defined lengths using template-directed syntheses by pyridine-zinc ligation (Figure 1-16). These complexes have very similar structural arrangements as the chlorophyll units in the LH2 light-harvesting system.

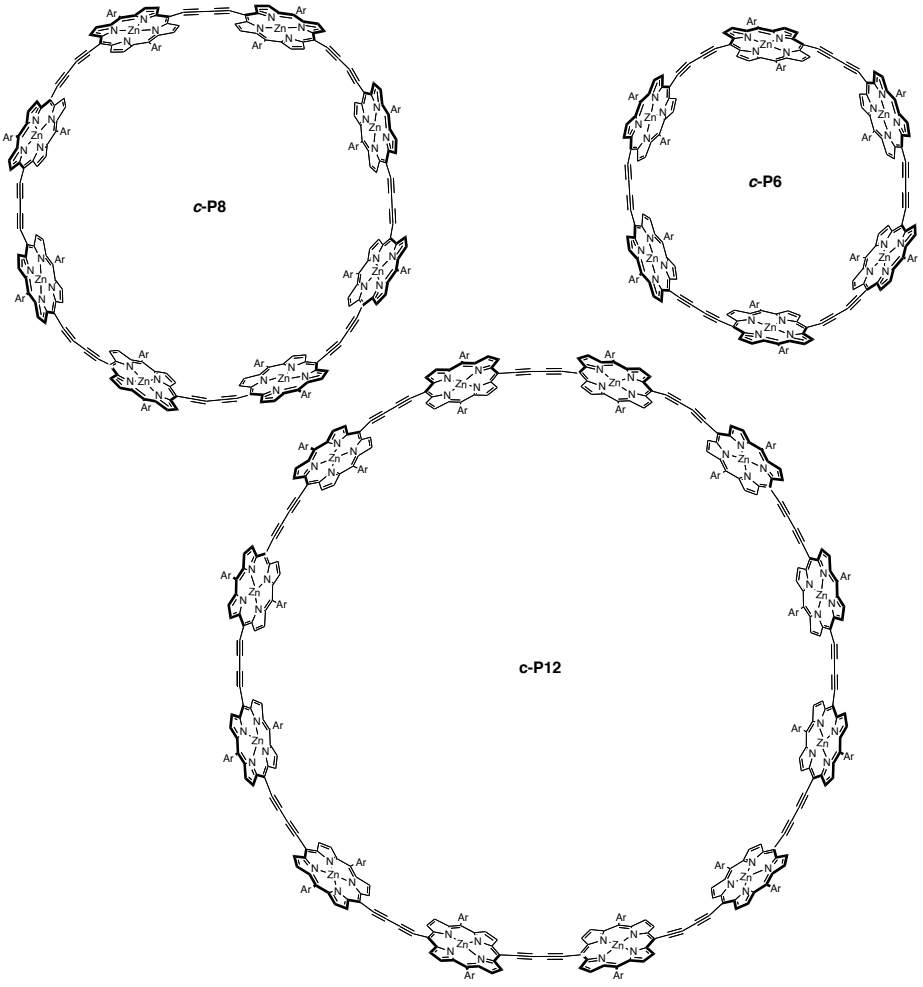

Figure 1-16. Structures of porphyrin nanorings, ***c*-P8**, ***c*-P6** and ***c*-P12**.

In 2007, they reported on a cyclic porphyrin octamer complex by 1:1 stoichiometry of linear porphyrin octamer ***l*-P8** and a complementary octadentate ligand **T8** (Scheme 1-14).[94] Oxidative coupling of ***l*-P8** and **T8** was achieved under palladium/copper catalysis, using iodine as the oxidant giving the cyclized ***c*-P8•T8** complex. Spectroscopy proved that all eight coordination sites of the template bind to the zinc centers of the linear porphyrin octamer. Treatment of this complex with excess pyridine, as a competing ligand, resulted in the quantitative conversion to the template-free cyclic octamer ***c*-P8** having a distance of 3.4 nm between the zinc metal centers of each porphyrin.

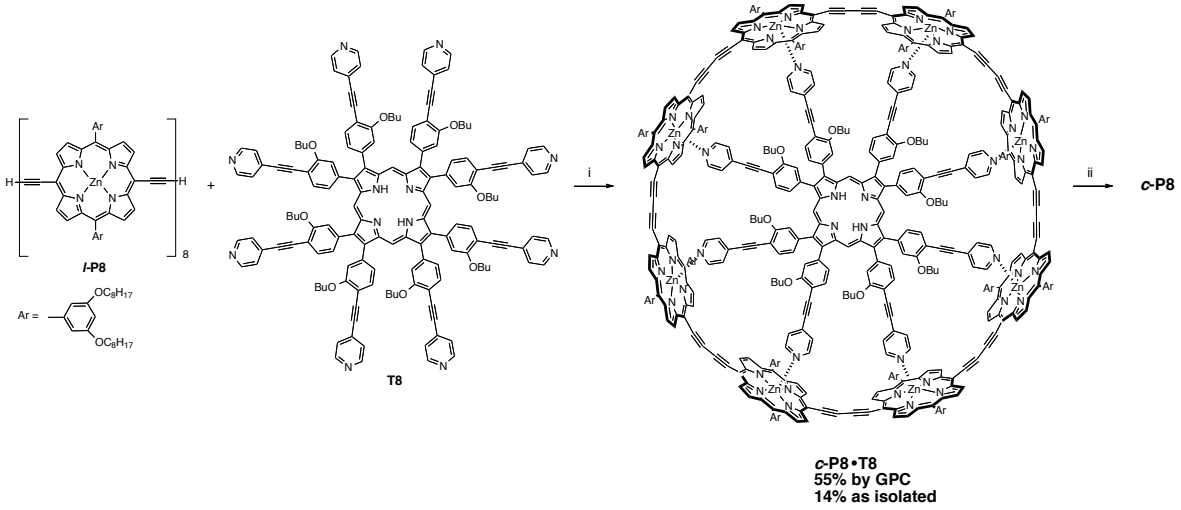

Scheme 1-14. Classical template-directed synthesis of cyclic porphyrin octamer **c-P8**; *Reaction Conditions:* i. $PdCl_2(PPh_3)_2$, CuI, iPr_2NH, I_2, air, 60°C; ii. pyridine.

The equilibrium constant, K_f, for the formation of ***c*-P8•T8** is too large to measure directly, but can be evaluated by measuring how easily pyridine displaces the template **T8** (K_b) shown in Figure 1-17, which corresponds to Equation 1, where K_{py} is the binding constant of pyridine for one zinc center of the porphyrin octamer.[94]

$$K_f = \frac{K_{py}^{\ 8}}{K_b} \qquad (1)$$

The coordination of a weak monodentate ligand, pyridine, (K_{py} = 1.9 × 10^4 M^{-1}) competing with the octadentate **T8** template ($K_f >> 10^8$ M^{-1}) seems surprising at first. However, the position of equilibrium 3 (Figure 1-17) depends on the eighth power of pyridine concentration shown in Equation 2. Therefore, the concentration of pyridine can be as high as 10 M, while the concentration of the template ([**T8**] ≈ [***c*-P8**] ≈ 10^{-6} M).[94]

$$\frac{[(c-P8)\cdot py^8]}{[c-P8 \bullet T8]} = \frac{K_b[py]^8}{[T8]} \qquad (2)$$

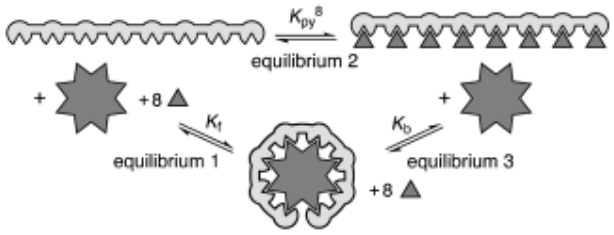

Figure 1-17. Thermodynamic cycle for binding linear porphyrin octamer ***l*-P8** (rod) to template **T8** (star) and pyridine (triangle). Figure from Ref.[94]

A cyclic hexamer porphyrin nano-ring was synthesized using a similar building principle than utilized for the cyclic octamer. The template-directed synthesis utilized a porphyrin dimer ***l*-P6** and a hexapyridyl template **T6** to form a cyclic hexamer complex ***c*-P6• T6** (Scheme 1-15).[95] Pyridine was used to remove the template from the cyclic octameric nanoring. However a more strongly coordinating amine, DABCO, was needed for the displacement of the hexadentate template **T6** from the presumably more rigid and better size-matched structure leading to extreme binding constants to give the template-free nanoring ***c*-P6**.

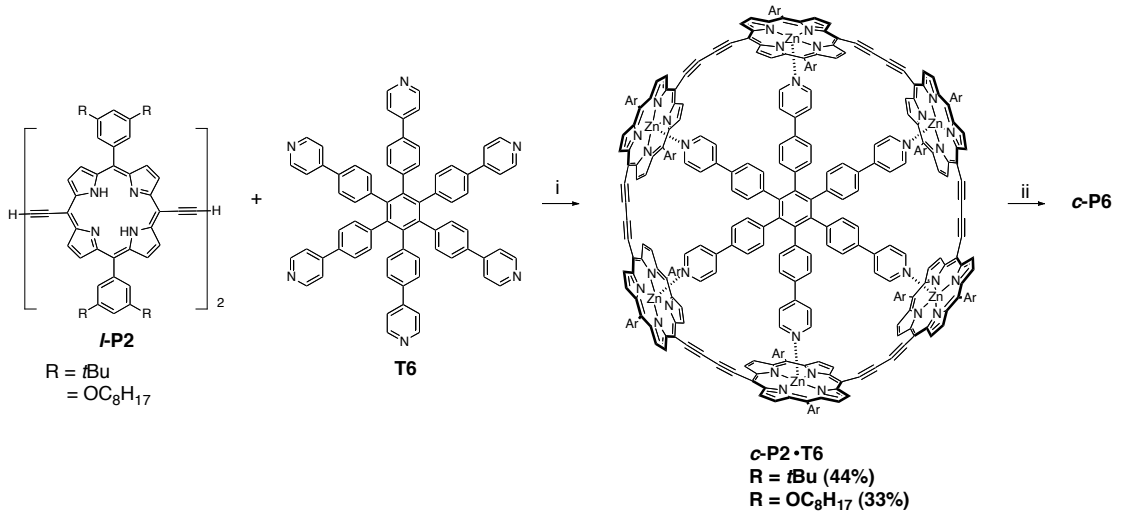

Scheme 1-15. Classical template-directed synthesis of cyclic porphyrin hexamer **c-P6**; *Reaction Conditions:* i. $PdCl_2(PPh_3)_2$, CuI, iPr_2NH, I_2, air, 60°C; ii. DABCO.

In 2011, Anderson and co workers developed a new strategy, called Vernier templating, to synthesize larger oligomers using simple templates[64]. The fundamental idea of Vernier templating involves the combination of two components with different numbers of binding sites. They demonstrated this concept by synthesizing a butadiyne-linked 12-porphyrin nano-ring ***c*-P12** (Scheme 1-16a) using a template with six binding sites **T6** and a linear porphyrin tetramer ***l*-P4** to form the Vernier complex **(*l*-P4)$_3$•(T6)$_2$**. The palladium-catalyzed oxidative coupling gave a figure-of-eight complex, ***c*-P12•(T6)$_2$** in 39% yield. The 12-porphyrin nano-ring was also synthesized by classical templating (Scheme 1-16b), which gave a ***c*-P12-T12** in 35% yield. However, the classical route has difficulty in purification of **c-P12**. Also, the **T12** template is synthesized in low yields along a ten-step synthesis, while the **T6** template is accessible in two steps from commercial materials.[95] Treatment of ***c*-P12•(T6)$_2$** and ***c*-P12-T12** with pyridine results in displacement of the template in quantitative conversion to the free macrocycle, ***c*-P12**. This 12-porphyrin nanoring is among the largest π-conjugated macrocycles reported, with a diameter of 4.7 nm.

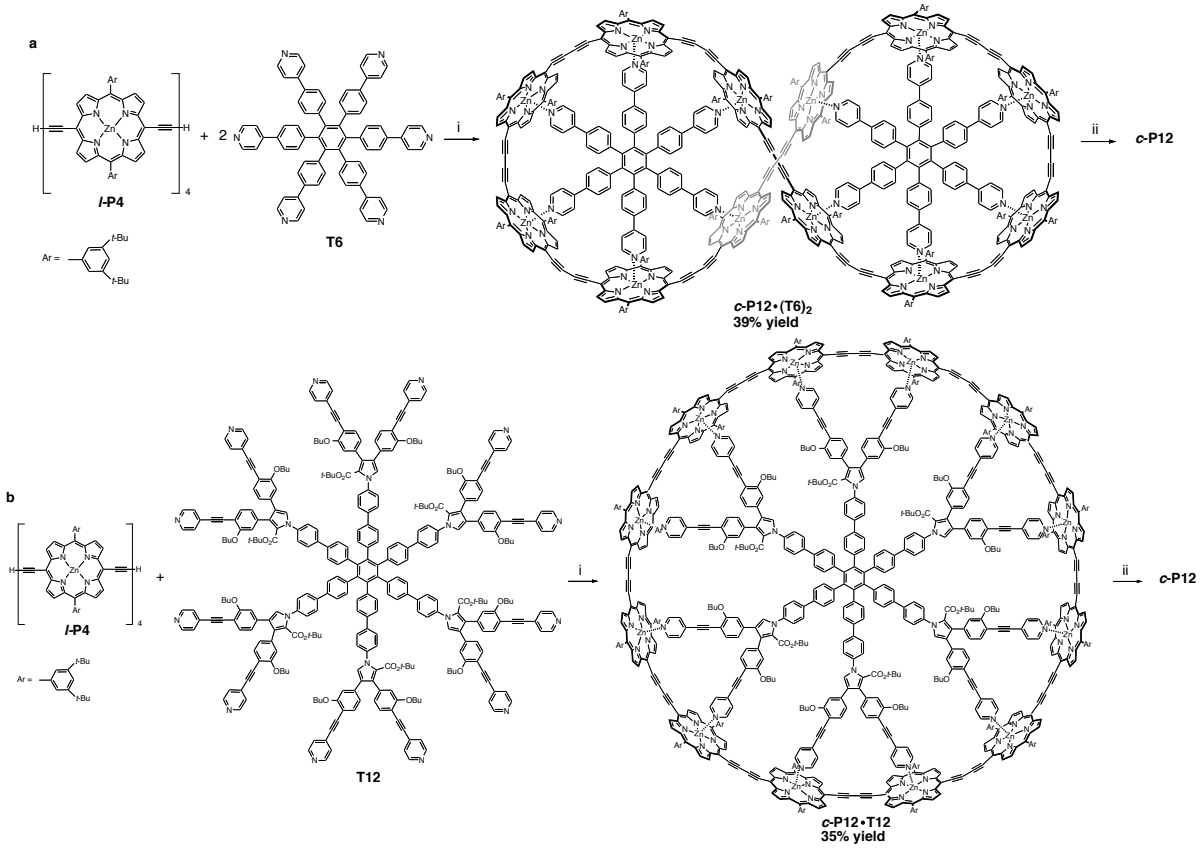

Scheme 1-16. Synthesis of 12-porphyrin nano-ring ***c*-P12**. a. Vernier template-directed synthesis; b. Classical template-directed synthesis; *Reaction Conditions:* i. $PdCl_2(PPh_3)_2$, CuI, benzoquinone, iPr_2NH; ii. pyridine.

1.9. References

(1) Milgrom, L. R. *The Colours of Life: An Introduction to the Chemistry of Porphyrins and Related Compounds*; Oxford University Press: New York, **1997**.

(2) Kadish, K. M.; Smith, K. M.; Guilard, R.; Editors *The Porphyrin Handbook: Volume 1, Synthesis and Organic Chemistry*, **2000**.

(3) Brückner, C.; Dolphin, D. *Tetrahedron Lett.* **1995**, *36*, 3295-3298.

(4) Kaim, W.; Schwederski, B. *Bioinorganic Chemistry: Inorganic Elements in the Chemistry of Life* John Wiley & Sons Ltd: West Sussex, **1994**.

(5) *The Porphyrin Handbook*; Kadish, K. M.; Smith, K. M.; Guilard, R., Eds.; Academic Press: San Diego, **2000**, **2003**; Vol. 1-20.

(6) Grätzel, M. *J. Photochem. Photobiol. C* **2003**, *4*, 145-153.

(7) Gouterman, M.; Callis, J.; Dalton, L.; Khalil, G.; Mebarki, Y.; Cooper, K. R.; Grenier, M. *Meas. Sci. Technol.* **2004**, *15*, 1986-1994.

(8) Stilts, C. E.; Nelen, M. I.; Hilmey, D. G.; Davies, S. R.; Gollnick, S. O.; Oseroff, A. R.; Gibson, S. L.; Hilf, R.; Detty, M. R. *J. Med. Chem.* **2000**, *43*, 2403-2410.

(9) Rothemund, P. *J. Am. Chem. Soc.* **1936**, *58*, 625.

(10) Adler, A. D.; Longo, F. R.; Finarelli, J. D.; Goldmacher, J.; Assour, J.; Korsakoff, L. *J. Org. Chem.* **1967**, *32*, 476.

(11) Lindsey, J. S.; Schreiman, I. C.; Hsu, H. C.; Kearney, P. C.; Marguerettaz, A. M. *J. Org. Chem.* **1987**, *52*, 827-836.

(12) Longo, F. R.; Finarelli, M. G.; Kim, J. B. *J. Heterocycl. Chem.* **1969**, *6*, 927-931.

(13) Nardi, M.; Verucchi, R.; Aversa, L.; Casarin, M.; Vittadini, A.; Mahne, N.; Giglia, A.; Nannarone, S.; Iannotta, S. *New. J. Chem.* **2013**, *37*, 1036-1045.

(14) Ball, R. H.; Dorough, G. D.; Calvin, M. *J. Am. Chem. Soc.* **1946**, *68*, 2278-2281.

(15) Whitlock Jr., H. W.; Hanauer, R.; Oester, M. Y.; Bower, B. K. *J. Am. Chem. Soc.* **1969**, *91*, 7485-7489.

(16) Crossley, M. J.; King, L. G. *J. Chem. Soc., Chem. Commun.* **1984**, 920-922.

(17) Akhigbe, J.; Peters, G.; Zeller, M.; Brückner, C. *Org. Biomol. Chem.* **2011**, *9*, 2306-2313.

(18) Brückner, C.; Rettig, S. J.; Dolphin, D. *J. Org. Chem.* **1998**, *63*, 2094-2098.

(19) McCarthy, J. R.; Jenkins, H. A.; Brückner, C. *Org. Lett.* **2003**, *5*, 19-22.

(20) Samankumara, L. P.; Zeller, M.; Krause, J. A.; Brückner, C. *Org. Biomol. Chem.* **2010**, *8*, 1951-1965.

(21) Akhigbe, J.; Ryppa, C.; Zeller, M.; Brückner, C. *J. Org. Chem.* **2009**, *74*, 4927-4933.

(22) Daniell, H. W.; Brückner, C. *Angew. Chem., Int. Ed.* **2004**, *43*, 1688-1691.

(23) McCarthy, J. R.; Hyland, M. A.; Brückner, C. *Org. Biomol. Chem.* **2004**, *2*, 1484-1491.

(24) Brückner, C.; Hyland, M. A.; Sternberg, E. D.; MacAlpine, J.; Rettig, S. J.; Patrick, B. O.; Dolphin, D. *Inorg. Chim. Acta* **2005**, *358*, 2943-2953.

(25) Lara, K. K.; Rinaldo, C. K.; Brückner, C. *Tetrahedron* **2005**, *61*, 2529-2539.

(26) Ryppa, C.; Niedzwiedzki, D.; Morozowich, N. L.; Srikanth, R.; Zeller, M.; Frank, H. A.; Brückner, C. *Chem. Eur. J.* **2009**, *15*, 5749-5762.

(27) Banerjee, S.; Hyland, M. A.; Brückner, C. *Tetrahedron Lett.* **2010**, *51*, 4505-4508.

(28) Banerjee, S.; Zeller, M.; Brückner, C. *J. Org. Chem.* **2010**, *75*, 1179-1187.

(29) Akhigbe, J.; Haskoor, J.; Zeller, M.; Brückner, C. *Chem. Commun.* **2011**, *47*, 8599–8601.

(30) Brückner, C.; Götz, D. C. G.; Fox, S. P.; Ryppa, C.; McCarthy, J. R.; Bruhn, T.; Akhigbe, J.; Banerjee, S.; Daddario, P.; Daniell, H. W.; Zeller, M.; Boyle, R. W.; Bringmann, G. *J. Am. Chem. Soc.* **2011**, *133*, 8740–8752.

(31) Ogikubo, J.; Brückner, C. *Org. Lett.* **2011**, *13*, 2380–2383.

(32) Akhigbe, J.; Samankumara, L.; Brückner, C. *Tetrahedron Lett.* **2012**, *53*, 3524-3526

(33) Banerjee, S.; Zeller, M.; Brückner, C. *J. Porphyrins Phthalocyanines* **2012**, *16*, 576–588.

(34) Brückner, C.; Ogikubo, J.; McCarthy, J. R.; Akhigbe, J.; Hyland, M. A.; Daddario, P.; Worlinsky, J. L.; Zeller, M.; Engle, J. T.; Ziegler, C. J.; Ranaghan, M. J.; Sandberg, M. N.; Birge, R. R. *J. Org. Chem.* **2012**, *77*, 6480–6494.

(35) Hyland, M. A.; Morton, M. D.; Brückner, C. *J. Org. Chem.* **2012**, *77*, 3038–3048.

(36) Ogikubo, J.; Meehan, E.; Engle, J. T.; Ziegler, C.; Brückner, C. *J. Org. Chem.* **2012**, *77*, 6199–6207.

(37) Samankumara, L. P.; Wells, S.; Zeller, M.; Acuña, A. M.; Röder, B.; Brückner, C. *Angew. Chem. Int. Ed.* **2012**, *51*, 5757–5760.

(38) Akhigbe, J.; Brückner, C. *Eur. J. Org. Chem.* **2013**, 3876–3884.

(39) Akhigbe, J.; Haskoor, J. P.; Krause, J. A.; Zeller, M.; Brückner, C. *Org. Biomol. Chem.* **2013**, *11*, 3616–3628.

(40) Ogikubo, J.; Meehan, E.; Engle, J. T.; Ziegler, C. J.; Brückner, C. *J. Org. Chem.* **2013**, *78*, 2840–2852.

(41) Ogikubo, J.; Worlinsky, J. L.; Fu, Y.-J.; Brückner, C. *Tetrahedron Lett.* **2013**, *54*, 1707-1710.

(42) Yu, Y.; Czepukojc, B.; Jacob, C.; Jiang, Y.; Zeller, M.; Brückner, C.; Zhang, J.L. *Org. Biomol. Chem.* **2013**, *11*, 4613-4621.

(43) Gouterman, M.; Hall, R. J.; Khalil, G. E.; Martin, P. C.; Shankland, E. G.; Cerny, R. L. *J. Am. Chem. Soc.* **1989**, *111*, 3702-3707.

(44) Yu, Y.; Lv, H.; Ke, X.; Yang, B.; Zhang, J. L. *Adv. Synth. Catal.* **2012**, accepted for publication.

(45) Hyland, M. A.; Morton, M. D.; Brueckner, C. *J. Org. Chem.* **2012**, *77*, 3038-3048.

(46) Khalil, G. E.; Daddario, P.; Lau, K. S. F.; Imtiaz, S.; King, M.; Gouterman, M.; Sidelev, A.; Puran, N.; Ghandehari, M.; Brückner, C. *Analyst* **2010**, *135*, 2125-2131.

(47) Buchler, J. W. In *Porphyrins*; Dolphin, D., Ed. 1978; Vol. 1, p 389-483.

(48) Buchler, J. W.; Dreher, C.; Künzel, F. M. *Struct. Bonding (Berlin)* **1995**, *84*, 1-69.

(49) Dean, M. L.; Schmink, J. R.; Leadbeater, N. E.; Brückner, C. *Dalton Trans.* **2008**, 1341-1345.

(50) *Handbook of Porphyrin Science*; Kadish, K. M.; Smith, K. M.; Guilard, R., Eds.; World Scientific Publishing Co: Singapor, **2010**; Vol. 1-15.

(51) Gouterman, M. In *The Porphyrins*; Dolphin, D., Ed.; Academic Press: New York, San Francisco, London, **1978**; Vol. 3, p 1-165.

(52) Shelnutt, J. A.; Song, X.Z.; Ma, J.-G.; Jentzen, W.; Medforth, C. J. *Chem. Soc. Rev.* **1998**, *27*, 31-41.

(53) Parusel, A. B. J.; Wondimagegn, T.; Ghosh, A. *J. Am. Chem. Soc.* **2000**, *122*, 6371-6374.

(54) Haddad, R. E.; Gazeau, S.; Pécaut, J.; Marchon, J.-C.; Medforth, C. J.; Shelnutt, J. A. *J. Am. Chem. Soc.* **2003**, *125*, 1253-1268.

(55) Song, Y.; Haddad, R. E.; Jia, S.-L.; Hok, S.; Olmstead, M. M.; Nurco, D. J.; Schore, N. E.; Zhang, J.; Ma, J.-G.; Smith, K. M.; Gazeau, S.; Pecaut, J.; Marchon, J.C.; Medforth, C. J.; Shelnutt, J. A. *J. Am. Chem. Soc.* **2005**, *127*, 1179-1192.

(56) Röder, B.; Büchner, M.; Rückmann, I.; Senge, M. O. *Photochem. Photobiol. Sci.* **2010**, *9*, 1152-1158.

(57) Brückner, C.; McCarthy, J. R.; Daniell, H. W.; Pendon, Z. D.; Ilagan, R. P.; Francis, T. M.; Ren, L.; Birge, R. R.; Frank, H. A. *Chem. Phys.* **2003**, *294*, 285-303.

(58) Kadish, K. M.; Smith, K. M.; Guilard, R.; Editors *The Porphyrin Handbook: Volume 6, Applications: Past, Present and Future*, 2000.

(59) Zelelow, B.; Khalil, G. E.; Phelan, G.; Carlson, B.; Gouterman, M.; Callis, J. B.; Dalton, L. R. *Sens. Actuators, B* **2003**, *96*, 304-314.

(60) Khalil, G. E.; Costin, C.; Crafton, J.; Jones, G.; Grenoble, S.; Gouterman, M.; Callis, J. B.; Dalton, L. R. *Sens. Actuators, B* **2004**, *97*, 13-21.

(61) Ruppel, J. V.; Fields, K. B.; Snyder, N. L.; Zhang, X. P. In *Handbook of Porphyrin Science*; Kadish, K. M., Smith, K. M., Guilard, R., Eds.; World Scientific: Hackensack, New Jersey, 2010; Vol. 10, p 1–182.

(62) Fields, K. B.; Engle, J. T.; Sripothongnak, S.; Kim, C.; Zhang, X. P.; Ziegler, C. J. *Chem. Commun.* **2011**, *47*, 749-751.

(63) Liang, L.; Lv, H.; Yu, Y.; Wang, P.; Zhang, J.-L. *Dalton Transactions* **2012**, *41*.

(64) O'Sullivan, M. C.; Sprafke, J. K.; Kondratuk, D. V.; Rinfray, C.; Claridge, T. D. W.; Saywell, A.; Blunt, M. O.; O'Shea, J. N.; Beton, P. H.; Malfois, M.; Anderson, H. L. *Nature* **2011**, *469*, 72-75.

(65) Fujisawa, K.; Satake, A.; Hirota, S.; Kobuke, Y. *Chem. Eur. J* **2008**, *14*, 10735-10744.

(66) MacDonald, I. J.; Dougherty, T. J. *J. Porphyrins Phthalocyanines* **2001**, *5*, 105-129.

(67) Josefsen, L. B.; Boyle, R. W. *Theranostics* **2012**, *2*, 916-966.

(68) DeRosa, M. C.; Crutchley, R. J. *Coord. Chem. Rev.* **2002**, *233-234*, 351-371.

(69) Sternberg, E. D.; Dolphin, D.; Bruckner, C. *Tetrahedron* **1998**, *54*, 4151-4202.

(70) Mroz, P.; Bhaumik, J.; Dogutan, D. K.; Aly, Z.; Kamal, Z.; Khalid, L.; Kee, H. L.; Bocian, D. F.; Holten, D.; Lindsey, J. S.; Hamblin, M. R. *Cancer Letters* **2009**, *282*, 63-76.

(71) Milanesio, M. E.; Alvarez, M. G.; Silber, J. J.; Rivarola, V.; Durantini, E. N. *Photochem. Photobiol. Sci* **2003**, *2*, 926-933.

(72) Rosenfeld, A.; Morgan, J.; Goswami, L. N.; Ohulchanskyy, T.; Zheng, X.; Prasad, P. N.; Oseroff, A.; Pandey, R. K. *Photochem. Photobiol.* **2006**, *82*.

(73) Redmond, R. W.; Gamlin, J. N. *Photochem. Photobiol.* **1999**, *70*, 391–475.

(74) Guldi, D. M.; Mody, T. D.; Gerasimchuk, N. N.; Magda, D.; Sessler, J. L. *J. Am. Chem. Soc.* **2000**, *122*, 8289-8298.

(75) Kubát, P.; Mosinger, J. *J Photochem. Photobiol., A* **1996**, *96*, 93-97.

(76) Mosinger, J.; Micka, Z. *J Photochem. Photobiol., A* **1997**, *107*, 77-82.

(77) Ball, D. J.; Wood, S. R.; Vernon, D. I.; Griffiths, J.; Dubbelman, T. M. A. R.; Brown, S. B. *Photochem. Photobiol. B* **1998**, *45*, 28-35.

(78) Kolarova, H.; Bajgar, R.; Tomankova, K.; Nevrelova, P.; Mosinger, J. *Toxicol. in vitro* **2007**, *21*, 1287-1291.

(79) Mang, T. S.; Allison, R.; Hewson, G.; Snider, W.; Moskowitz, R. *Cancer J. Sci. Am.* **1998**, *4*, 378-384.

(80) Josefsen, L. B.; Boyle, R. W. *Metal-Based Drugs* **2008**, *2008*, 1-24.

(81) Garbo, G. M.; I, V. H. F.; Wiemanl, T. J.; Ill, E. B. N.; Haydon, P. S.; Cerrito, P. B.; Kesse, D. H.; Morgan, A. R. *Photochem. Photobiol.* **1998**, *68*, 561-568.

(82) Bhaumik, J.; Yao, Z.; Borbas, K. E.; Taniguchi, M.; Lindsey, J. S. *J. Org. Chem.* **2006**, *71*, 8807-8817.

(83) Mewis, R. E.; Savoie, H.; Archibald, S. J.; Boyle, R. W. *Photodiagnosis and Photodynamic Therapy* **2009**, *6*, 200-206.

(84) Peterson, J. I.; Fitzgerald, R. V. *Rev. Sci. Instrum.* **1980**, *51*, 670-671.

(85) Kavandi, J.; Callis, J.; Gouterman, M.; Khalil, G.; Wright, D.; Green, E. *Rev.Sci.Instrum.* **1990**, *61*.

(86) Gouterman, M.; Callis, J.; Dalton, L.; Khalil, G.; Mebarki, Y.; Cooper, K. R.; Grenier, M. *Meas. Sci. Technol.* **2004**, *15*, 1986-1994.

(87) Khalil, G. E.; Costin, C.; Crafton, J.; Jones, G.; Grenoble, S.; Gouterman, M.; Callis, J. B.; Dalton, L. R. *Sens. Actuators, B* **2004**, *97*, 13-21.

(88) Mills, A.; Lepre, A. *Anal. Chem.* **1997**, *69*, 4653-4659.

(89) Gouterman, M. *J. Chem. Ed.* **1997**, *74*, 697-702.

(90) Puklin, E.; Carlson, B.; Gouin, S.; Costin, C.; Green, E.; Ponomarev, S.; Tanji, H.; Gouterman, M. *J. Appl. Polym. Sci.* **2000**, *77*, 2795-2804.

(91) Shoji, O.; Okada, S.; Satake, A.; Kobuke, Y. *J. Am. Chem. Soc.* **2005**, *127*, 2201-2210.

(92) Hajjaj, F.; Yoon, Z. S.; Yoon, M.-C.; Park, J.; Satake, A.; Kim, D.; Kobuke, Y. *J. Am. Chem. Soc.* **2006**, *128*, 4612-4623.

(93) Takahashi, R.; Kobuke, Y. *J. Am. Chem. Soc.* **2003**, *125*, 2372-2373.

(94) Hoffmann, M.; Wilson, C. J.; Odell, B.; Anderson, H. L. *Angew. Chem. Int. Ed.* **2007**, *46*, 3122-3125.

(95) Hoffmann, M.; Kä rnbratt, J.; Chang, M.-H.; Herz, L. M.; Albinsson, B.; Anderson, H. L. *Angew. Chem. Int. Ed.* **2008**, *47*, 4993-4996.

2. Aim and Overview of this Thesis

This thesis describes in a number of separate chapters a range of studies that measure the variation of specific physical properties with structural modification of the macrocycles, with a particular focus also on using their coordinated metals as probes. Specifically, the thesis is comprised of the following chapters:

Chapter 3:

Tuning the Dynamic High pH Sensing Range of [*meso*-tetraarylporpholactonato]M(II) Complexes by Variation of the Central metal ion, the Aryl Substituents, and Introduction of a β-nitro Group

Based on the known high pH-sensing ability of [*meso*-tetrakis(pentafluorophenyl)-porpholactonato]platinum(II), we investigated the influence of the metal (M = Zn(II), Ni(II), Cu(II), Pd(II), Ag(II), Pt(II)), the aryl group (Ar = C_6H_5, C_6F_5), and the presence of a β-NO_2 group on the pH sensing range. The UV-vis base titration midpoints for all derivatives were determined in an aqueous solution containing a surfactant, showing that the metal has the least influence, thus identifying cheaper and easier to prepare porpholactone M complex-based high pH-sensors. β-Nitration and pentafluorophenyl-substitution had additive effects.

This section of the chapter was published: Worlinsky, J. L.; Zarate, G.; Zeller, M.; Ghandehari, M.; Khalil, G.; Brückner, C. 'Tuning the Dynamic High pH Sensing Range of [*meso*-Tetraarylporpholactonato]M(II) Complexes by Variation of the Central Metal Ion, the Aryl Substituents, and Introduction of a β-Nitro Group' *J. Porphyrins Phthalocyanines* **2013**, accepted for publication (DOI: 10.1142/S1088424613500478). GZ contributed some phenyl-

substituted derivatives; MZ was the crystallographer on the project; GM and GK are engineering collaborators that seek the utilization of the sensors in the field.

A Transparent Membrane for the Optical Sensing of High Hydroxide Concentrations

The incorporation of the known optical high pH sensing chromophore, [*meso*-tetrakis(pentafluorophenyl)porpholactonato]platinum(II), derivatized at the aryl group with PEG groups for better solubility in the aqueous solutions during the preparation of a Nafion®-based membrane, is described (detection of the absorption increase at 695 nm). The immobilized sensor was shown be suitable for the rapid (response time in minutes), selective, and reversible sensing of high concentrations of hydroxides (pH 11 and above, up to 5 M NaOH concentrations). The membrane remains transparent and stable even under extended times of exposure to the very caustic environments, and no leaching of the chromophore is observed. The membrane might find use in fiber optics-based optodes suitable for the monitoring of high hydroxide environments inside chemical reactors, fuel cells.

This section of the chapter will be submitted for publication: Worlinsky, J.L.; Halepas, S.; Brückner, C. 'A Transparent Membrane for the Optical Sensing of High Hydroxide Concentrations' in preparation for submission to *Sens. Actuators B*. SH contributed to the preparation of the sensor membrane.

Chapter 4:

Optical Cyanide Sensing Using Metalloporpholactones in Aqueous Solution

The colorimetric cyanide sensing ability of a free base porpholactone, a pyrrole-modified porphyrin in which a porphyrin β,β'-double bond was replaced by a lactone functionality, and its zinc(II), platinum(II), and gallium(III) complexes in aqueous solutions is reported. The central

metal-dependent sensing mechanism (nucleophilic addition of the CN^- to the lactone or axial ligation to the central metal) was investigated. Water-solubility of the parent *meso*-pentafluorophenyl-derivatized porphyrinoid was assured by PEGylation of the *p*-position using a nucleophilic aromatic substitution reaction with thiol-terminated PEG derivatives. Cyanide addition to the novel fluorescent gallium(III) complex led to the formation of an adduct of low fluorescence intensity, prohibiting the use of this dye as a switch-on sensor. This fundamental study on the ability to utilize the once rare but now readily available class of pyrrole-modified porphyrins as chemosensors highlights the multiple ways these sensor platforms can be modified.

This chapter will be submitted for publication: Worlinsky, J.L.; Brückner, C. 'Optical Cyanide Sensing Using Metalloporpholactones in Aqueous Solution' in preparation for submission to *Sens. Actuators B.*

Chapter 5

Axial Imidazole Binding Strengths in Porphyrinoid Cobalt(III) Complexes as Studied by Tandem Mass Spectrometry

The Co(II) complexes of twelve *meso*-tetraaryl-porphyrins, -chlorins, and chlorin analogues containing non-pyrrolic heterocycles were synthesized and converted *in situ* to the corresponding Co(III) complexes coordinated to one or two imidazoles. Electrospray ionization tandem mass spectrometry (ESI-MS/MS) in conjunction with the energy-variable collision-induced dissociation (CID) technique was used to compare the relative gas-phase binding strength of the axially coordinated imidazoles to the octahedral and square planar Co(III) porphyrinoid complex ions. The observed binding energies of these ligands were rationalized in

terms of the effects of porphyrinoid core structure and *meso*-substitution on the electron density on the central Co(III) centers.

This section of the chapter was published: Mishra, E.; Worlinsky, J. L.; Gilbert, T. M.; Brückner, C.; Ryzhov, V. 'Axial Imidazole Binding Strength in Porphyrinoid Cobalt(III) Complexes as Studied by Tandem Mass Spectrometry' *J. Am. Soc. Mass. Spectrom.* **2012**, 23, 1135–1147. Erratum (correction of systemic typesetting errors): *J. Am. Soc. Mass. Spectrom.* **2012**, *23*, 1428–1439. EM and VR were the mass spectrometrists on the manuscript, TMG performed the computations, and JLW performed all syntheses.

ESI MS/MS Fragmentation Behavior Study of *meso*-Phenylporphyrinoids Containing Non-pyrrolic Heterocycles and *meso*-Thienyl-substituted Porphyrins

Using electrospray ionization tandem mass spectrometry (ESI-MS/MS), free base and cobalt(II) complexes of six *meso*-tetraphenylporphyrinoids containing non-pyrrolic heterocycles and of three *meso*-thienylporphyrins were studied. Their fragmentation was studied in a quadrupole ion trap as a function of the porphyrinoid macrocycle structure and compared to the fragmentation behavior of the benchmark compound *meso*-tetraphenylporphyrin. *In situ* oxidation of the neutral cobalt(II) complexes under ESI conditions produced singly charged cobalt(III) porphyrinoid ions; the free bases were ionized by protonation.

The section of the chapter will be submitted for publication: Mishra, E.; Worlinsky, J. L.; Brückner, C.; Ryzhov, V. '+ESI MS/MS Fragmentation Behavior Study of *meso*-Phenylporphyrinoids Containing Non-pyrrolic Heterocycles and *meso*-Thienyl-substituted Porphyrins' in preparation for submission to *J. Am. Soc. Mass. Spectrom*. EM and VR were the mass spectrometrists on the manuscript, JLW performed all syntheses.

Chapter 6:

The carbonyl complexes of [meso-tetraphenylporphyrin]ruthenium(II), Ru(TPP)(CO)(py) and its pyrrole modified derivatives have been synthesized and characterized by UV-vis, ^{1}H NMR, ^{13}C NMR and IR spectroscopy. Crystallographic results of [meso-tetraphenylporpholactonato]ruthenium(III) permits a detailed comparison to the previously published crystal structure of Ru(TPP)(CO)(py). The shifts in ν_{CO} for this series of complexes are consistent with the existence of M-CO π-back bonding and trends were explained in terms of π-acidity of the porphyrin macrocycle.

This chapter will be submitted for publication: Worlinsky, J. L.; Engle, J. T.; Brückner, C.; Ziegler, C. J. 'Trends in the CO Stretching Frequency and Bond Distance in [Porphyrinoid]Ru(py)CO Complexes as Tool to Assess Porphyrinoid Basicity' in preparation for *Inorg. Chem.*

3. General Introduction to Porpholactones as High pH Sensors

The development of optical high pH sensors for solution and optode-based measurements is desirable for a multitude of technical applications in chemistry and engineering. The standard glass electrode is widely used in the laboratory because of its wide sensing range and rapid response but exposure of the glass electrode to highly alkaline solutions (i.e., solutions above ~ pH 11) causes the so-called 'alkaline error', making them unsuitable for longer duration monitoring applications in this pH range. Because of this, optical fiber-based sensors measuring the absorbance, reflectance, fluorescence, or refractive index changes of solutions in the deeply alkaline pH range were developed as an alternative.[1-3] Optical fiber sensors offer several other practical advantages, such as not requiring a reference element, having the potential for miniaturization, low costs, and ease of long distance signal transmission. The realization of optical high pH sensing fiber sensors (optodes) requires a high pH sensing dye that can be affixed to the end of the optical fiber. In addition to this requirement, the ideal optical pH sensor needs to exhibit, *inter alia*, a rapid color change upon change of pH and high chemical stability at the extreme pH values.[1-3]

A few indicator dyes were developed that respond in the high pH regime, among them Titan Yellow **1** (also named thiazole yellow), a triazene-based sensor with a response between pH 12 and 13, and indigo carmine **2** (also called indigotine or FD&C Blue #2), a dye that is blue up to pH 11.4 and yellow at pH 13. Overall, however, only comparably few optical sensors for high pH values have been reported.[1,2,4-8] In a disadvantage for their practical uses, some sensors show considerable spectral overlap between their spectra at lower and high pH values. Some also exhibit chemical instability.[4,8]

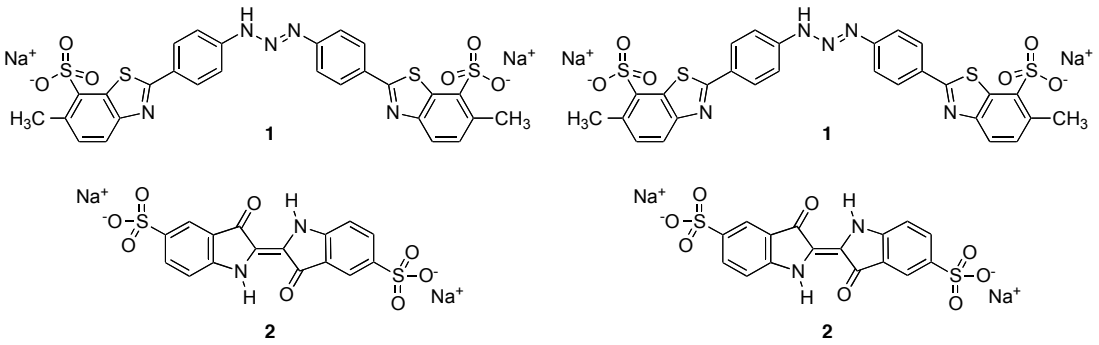

Because of the inherently high extinction coefficients, often high fluorescence yields, and chemical robustness, porphyrins are good dyes. Moreover, their inherent basicity and the basicity of a range of substituents, make them natural choices as low pH sensors.[3,9-13] Albeit more rare, high pH sensors have also become known.[3,9] For instance, the phenolic oxygens of [tetrakis(4-hydroxyphenyl)porphyrinato]cobalt(II) **3** can be sequentially deprotonated at high pH values, causing a pH shift of the optical spectrum in the unusually wide pH range between 8 and 12.[11]

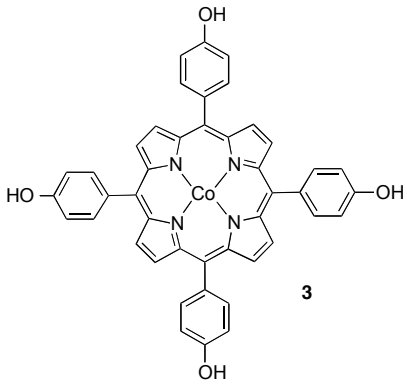

Porpholactones are oxazole-derived pyrrole-modified porphyrins in which one of the β,β′-double bonds has been replaced by a lactone moiety, thus formally substituting one of the pyrrolic subunits with an oxazolone.[13-17] A number of complementary syntheses for porpholactones are known.[14,18-24] The lactone moiety in the free base porpholactones mimics the electronic properties of the β,β'-double bond, as their UV-visible spectra are very similar to [25]like.[17,26] Porpholactones found utility as catalysts and they were used as sensor dyes in pressure-sensing paints.[19,20,23,27-30] We used porpholactones as starting materials for a range of

other porphyrinoids. For instance, we reduced or alkylated the lactone functionality to generate oxazolochlorins[17,31-33] and we converted it to a lactam group, thus generating porpholactams.[25,34] All these reactions are based on the ability to attack the lactone moiety in porpholactones in a nucleophilic fashion (with hydride, a Grignard reagent, or hydrazine). This susceptibility to nucleophilic attack also lies at the heart of the ability of porpholactones to act as high pH sensors (Scheme 3-1). As hydroxide (or alkoxides) attack the lactone and convert the sp^2-hybridized ketone carbon to an sp^3-hybridized carbon, the porphyrin-like chromophore is effectively changed into an anionic chlorin-like chromophore. This rationalizes the observed dramatic red-shift of the UV-vis spectrum of **4^{F}Pt** at high OH^- concentrations.[13] We further hypothesized that a stabilizing interaction between the negatively charged oxygen and the center of the positively polarized flanking pentafluorophenyl group contributes to the ability of **4^{F}Pt** to act as an excellent high pH sensor.[13]

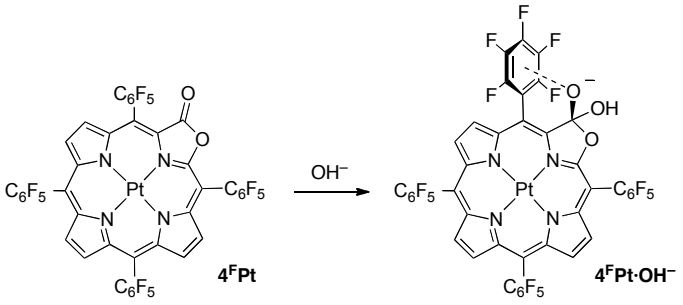

Scheme 3-1. Mode of operation of the optical high pH sensor **4^{F}Pt.**[14,17,38-40]

As the costs of the platinum complex **4^{F}Pt** are high (both the central metal and the pentafluorophenyl-porpholactone are costly; the multiple steps requiring chromatography are the major contributor to the high costs of the ligand), there exists a desire to find similarly well functioning but cheaper high pH sensors. Moreover, it is desirable to find a range of similar sensors with dynamic sensing ranges above and below the pH range for which **4^{F}Pt** is suitable.

In the chapter we will report on the evaluation of non-platinum-based porpholactones as pH sensors and an evaluation of a method to tune the dynamic pH range by modification of the ß-positions of the porpholactones.

In a second part of this chapter we will report on the incorporation of the high pH sensor **4^{F}Pt** into a membrane, thus providing the basis for the realization of a high pH-sensing optode.

3.1. Tuning the dynamic high pH sensing range of [*meso*-tetraaryl-porpholactonato]M(II) complexes by variation of the central metal ion, the aryl substituents, and introduction of a β-nitro group

Our interest in the fundamental evaluation of the factors that render the porpholactones good high pH sensors, led us to investigate the influence of the metal ion and the aryl substituent on the pH sensing range. In addition, we wanted to answer the question whether the pH range can be shifted to lower pH values by increasing the susceptibility of the lactone moiety to nucleophilic attack by establishing a strongly electron-withdrawing nitro group at the porpholactone β-position. We will detail here the results of these investigations.

3.1.1. Results and Discussion

Syntheses of metalloporpholactones 4M and 4^{F}M

A number of pathways for the synthesis of porpholactones are available.[18,20-24,26,35] We chose the porphyrin dihydroxylation-oxidation pathway previously described by us as this method is arguably the simplest pathway to allow the preparation of 500 mg or larger batches of tetraphenyl- (**4**) and tetrakis(pentafluorophenyl)-substituted (**4^{F}**) porpholactones (Scheme 3-2).[17,35-38] With the porpholactones in hand, the insertion of a range of divalent metals (Ni(II), Cu(II), Zn(II), Pd(II), Ag(II), and Pt(II)) proceeded smoothly along established metalation strategies.[39] All metalloporpholactones were previously described.[17,18,21,22,24,26,40]

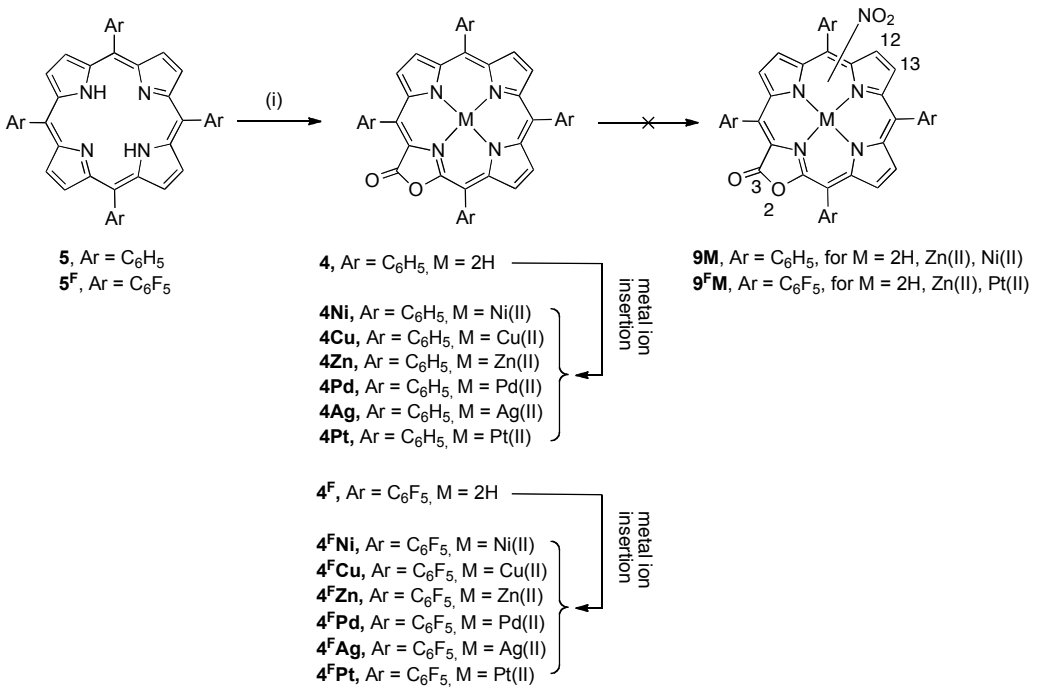

Scheme 3-2. Syntheses of metalloporpholactones 4M. *Reaction Conditions:* (i) 1. OsO_4, pyridine, r.t., up to 7 d, followed by chromatography; 2. for **5**: H_2S, for $\mathbf{5^F}$: sat. $NaHSO_3$ in MeOH:H_2O, $CHCl_3$/30% pyridine; 3. CTAP, CH_2Cl_2.

We attempted the nitration of a range of free base or metal complexes of porpholactones **4** and $\mathbf{4^F}$ using a number of different methods reported to lead to β-nitration of (metallo)porphyrins.[41,42] However, none allowed access to the target product, highlighting the electron-poor nature of the porpholactones as compared to porphyrins. This electron-poor nature was also previously demonstrated by the reduced Brønsted basicity of the porpholactones when compared to porphyrins.[13]

Syntheses of β-Nitrodiolchlorins 8 and $\mathbf{8^F}$

Since the β-nitration of *meso*-tetraphenyl- and tetrakis(pentafluorophenyl)-porphyrins is well described[41,42], we decided to attempt the dihydroxylation and oxidation of the corresponding β-nitroporphyrins to access β-nitroporpholactones. This pathway was indeed successful (Scheme 3-3).

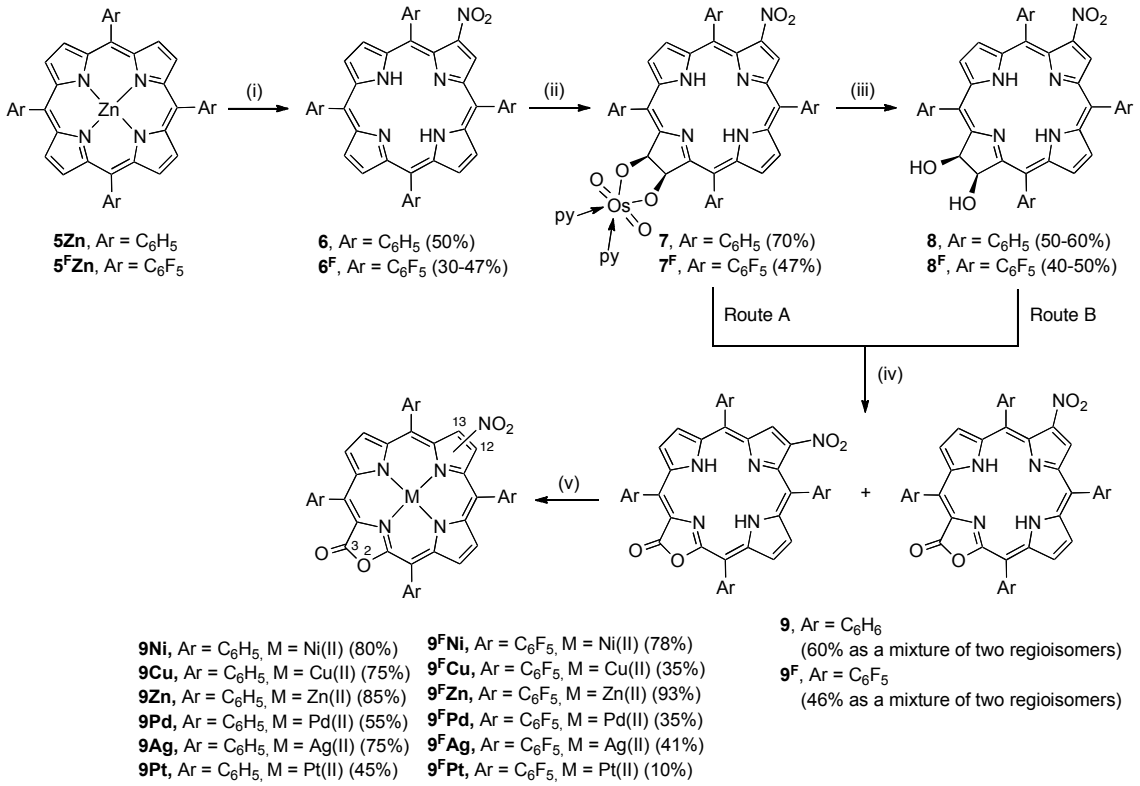

Scheme 3-3. The synthesis of β-nitroporpholactones. *Reaction Conditions:* (i) 1. $AgNO_3$, I_2, CH_2Cl_2/MeCN; 2. HCl (ii) OsO_4, pyridine, r.t., up to 10 d (iii) 8: H_2S; $\mathbf{8^F}$: sat. $NaHSO_3$ in MeOH:H_2O, $CHCl_3$/30% pyridine; (iv) CTAP, CH_2Cl_2; (v) M(II) sources, solvent, conventional or microwave heating.

Thus, [*meso*-tetraphenylporphyrinato]zinc(II) **5Zn** and its pentafluorophenyl analogue $\mathbf{5^FZn}$ were converted to the β-nitro derivatives.[41,42] Subsequent reaction of the nitroporphyrins with stoichiometric amounts of osmium tetraoxide under the usual conditions (r.t., $CHCl_3$-pyridine, up to one week reaction times) led to the formation of a single major product in acceptable yields (with the remainder recoverable porphyrin starting material). The reductive cleavage of the osmate esters $\mathbf{7/7^F}$, each using a unique methodology, proceeded also smoothly, providing compounds $\mathbf{8/8^F}$.[36,37] Both the osmate esters $\mathbf{7/7^F}$ and the diols $\mathbf{8/8^F}$ provided NMR spectra that, based on the number of peaks present, indicated the regioselective formation of a single product, but an unambiguous determination whether the nitration had taken place at the

pyrrole moiety opposite or adjacent to the dihydroxypyrroline moiety could not be derived (Figure 3-1).

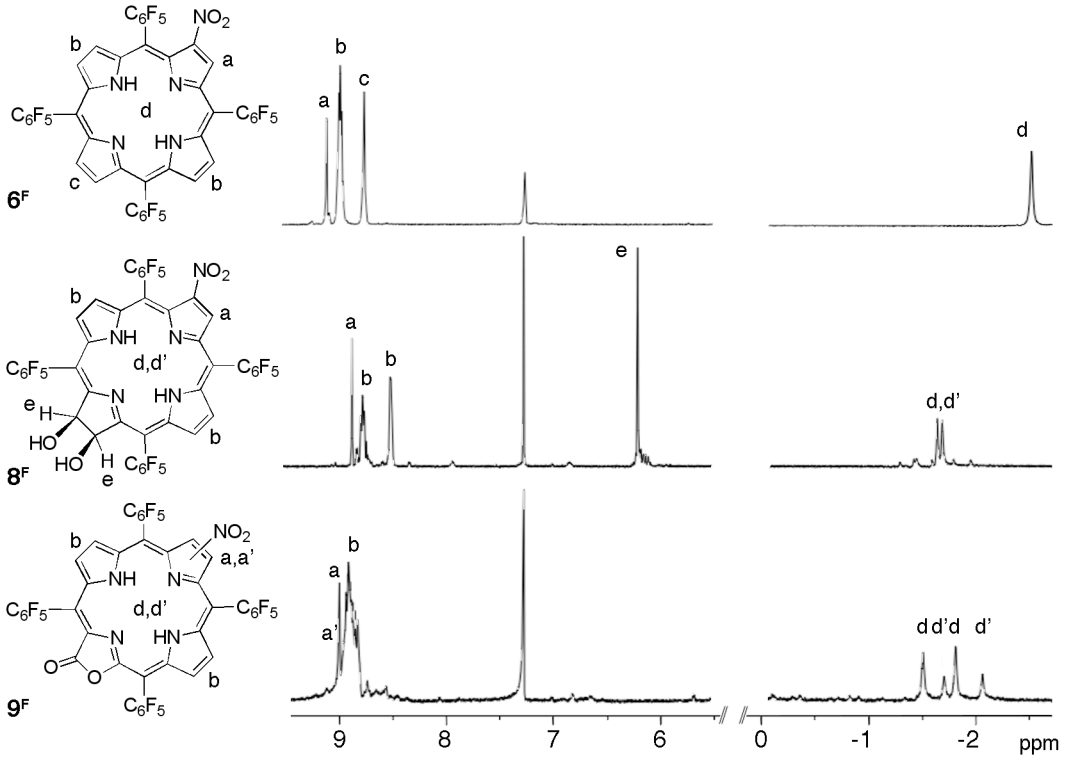

Figure 3-1. ^{1}H NMR spectra (400 MHz, $CDCl_3$) of $\mathbf{6^F}$, $\mathbf{8^F}$ and $\mathbf{9^F}$.

The UV-vis spectra of the β-nitro diolchlorins **8** and $\mathbf{8^F}$ (and of their osmate esters **7** and $\mathbf{7^F}$) are, as expected, typical chlorin-like spectra, though they are–analogously to the β-nitroporphyrin spectra–slightly distorted when compared to their non-nitrated compounds, underlining the strong electronic influence of the nitro group on the electronic structure of the chromophore.[36,37,43] Figure 3-2 demonstrates the effects on the optical spectrum upon dihydroxylation of β-nitroporphyrin $\mathbf{6^F}$ to form β-nitrochlorin $\mathbf{8^F}$. The (slightly distorted) porphyrin-like spectrum of $\mathbf{6^F}$ becomes a typical chlorin spectrum for $\mathbf{8^F}$. As is typical for dihydroxylations, the longest wavelength absorption band (λ_{max}) of the chlorin is slightly

hypsochromically shifted compared to the porphyrin band, albeit it is chlorin-like much more intense.

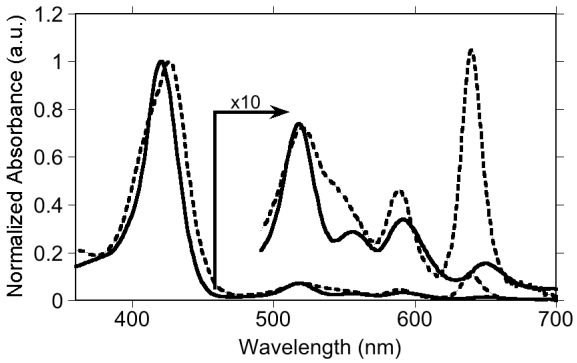

Figure 3-2. Comparison of the UV-vis spectra (CH_2Cl_2) of $\mathbf{6^F}$ (solid trace) and $\mathbf{8^F}$ (broken trace).

Single Crystal X-Ray Structure of 12/13-nitro-2,3-*vic*-dihydroxychlorin 8

The ultimate proof that the nitration had taken place at the pyrrole opposite of the pyrroline was provided by single crystal X-ray structure diffraction analysis of β-nitrodiolchlorin **8** (Figure 3-3). The solid state structure of **8** also shows that the conformation of the nitrated dihydroxychlorin is significantly more saddled (as expressed in larger rms values of the central $C_{18}N_4$ chromophore) than its non-nitrated parent diolchlorin (as its dimethyl ether), or the parent β-nitroporphyrin.[38,44,45] The distortion is likely caused by a steric interaction between the nitro-group and the adjacent *meso*-phenyl group, and the conformationally more flexible hydroporphyrin framework is evidently responding stronger to the steric interaction than a porphyrin.[46]

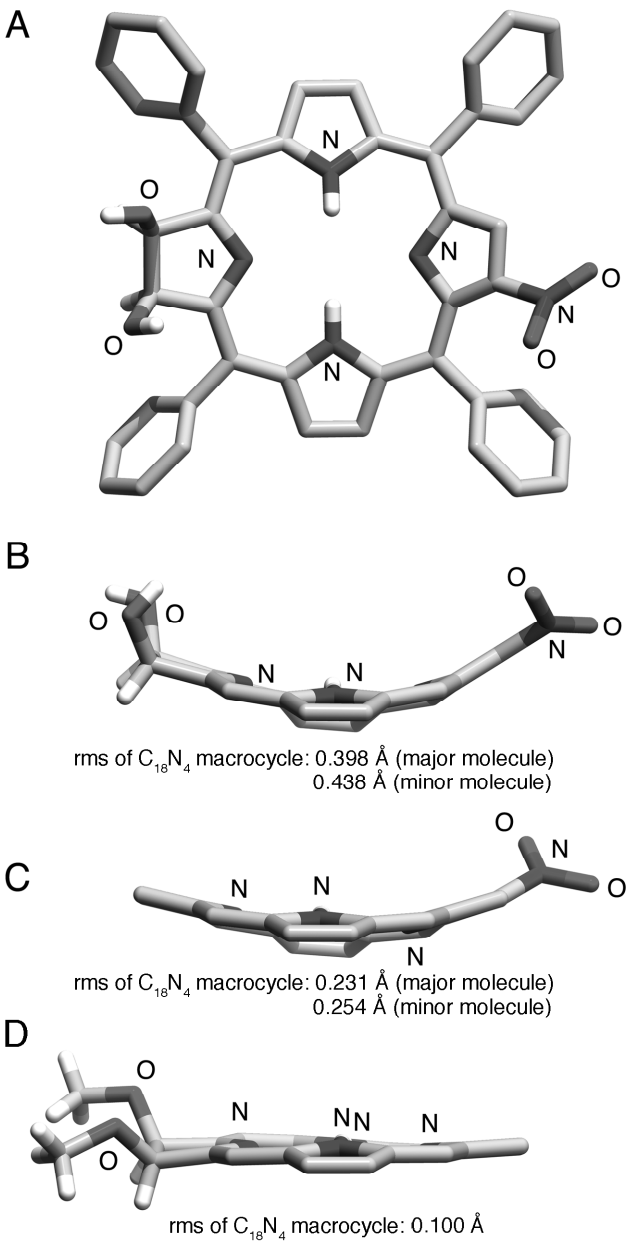

Figure 3-3. A: Stick representation of the molecular structure of **8** as determined by X-ray crystal diffratometry. Top view, sp^2 hydrogen atoms omitted for clarity; B: Side view, along one $N_{pyrrole}$-$N_{pyrrole}$ axis; *meso*-phenyl groups and sp^2 hydrogen atoms omitted for clarity. C: Side view of the crystal structure of *meso*-tetraphenyl-2-nitroporphyrin.[44] D: Side view of the crystal structure of *meso*-tetraphenyl-2,3-dimethoxychlorin.[38] In all side views, *meso*-phenyl groups and sp^2 hydrogen atoms omitted for clarity; solvent molecules and any disorder omitted for clarity in all structures. rms = root mean square deviation from planarity. The major/minor molecules refer to the two disordered molecules present in the crystal.

Syntheses of β-Nitroporpholactones

The oxidative conversion of a diolpyrroline moiety, or its osmate ester, to an oxazolone moiety using permanganate (as its organic solvent-soluble cetyltrimethylammonium salt, CTAP) was described for a number of porphyrinoids.[13,15-17,35,47-49] This reaction is also applicable to the nitrated chlorins **7**/**7**$^{\mathbf{F}}$ and **8**/**8**$^{\mathbf{F}}$ forming one major product that can be isolated in acceptable yields (Scheme 3-2). The reaction is smooth and generates few, if any, side products but the isolation of the product from the pasty manganese oxide side products poses practical challenges. This factor mainly contributes to the less than optimal yields.

The NMR spectra of the β-nitroporpholactones **9** and **9**$^{\mathbf{F}}$ show the presence of two regioisomers in a 1:1 and 1:2 ratio, respectively, as determined by the relative integration of the two high-field NH signals for each isomer (see Figure 3-1). The two regioisomers are the result of the two non-equivalent positions (β-carbons position 12 and 13) the nitro group can be found at relative to the lactone moiety (the numbering scheme used in the naming of the compounds is shown in compound **9** in Scheme 3-2).[50] The modest regioselectivity observed in the formation of **9**$^{\mathbf{F}}$ is comparable to the regioselectivity observed for diol-to-lactone conversion in bis-oxazolochlorin and –bacteriochlorin.[48] The two regioisomers could not be separated from each other. Thus, mixtures of these isomers were used in all metallation and pH titration studies.

The UV-vis spectra of the nitroporpholactones are signifcantly altered compared to the spectra of the parent porpholactones (Figure 3-4) with respect to the relative Q-band intensities and band positions, again confirming the strong electronic influence of the nitro group on the electronic structure of the chromophore.

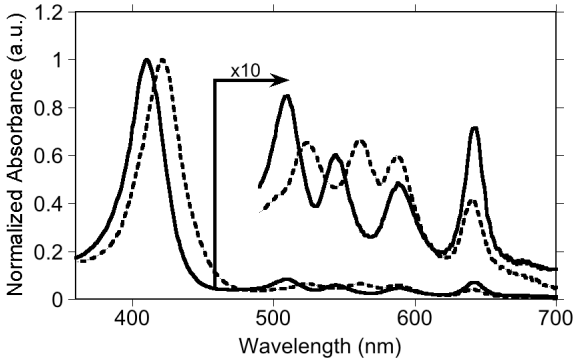

Figure 3-4. Comparison of the normalized UV-vis spectra (CH_2Cl_2) of $\mathbf{4^F}$ (solid trace) and $\mathbf{9^F}$ (broken trace).

Formation of the [β-Nitroporpholactonato]M(II) Complexes

The insertion of the divalent metals Ni(II), Cu(II), Zn(II), Pd(II), Ag(II), and Pt(II) into the porpholactones and β-nitroporpholactones was achieved using standard methods under conventional and microwave heating conditions.[39,51] Spectroscopic and analytical data confirmed the successful formation of the target metalloporphyrinoids (Figure 3-5).

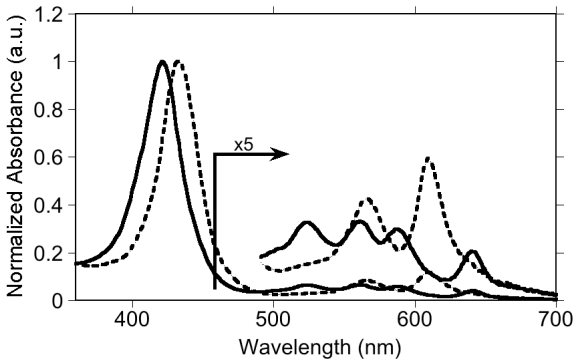

Figure 3-5. Comparison of the normalized UV-vis spectra (CH_2Cl_2) of $\mathbf{9^F}$ (solid trace) and $\mathbf{9^FZn}$ (broken trace).

The UV-vis spectrum of $\mathbf{9^F}$ in comparison to its zinc complex $\mathbf{9^FZn}$ demonstrates the successful metal insertion but, more importantly, it also shows that the

[β-nitroporpholactonato]M complexes express, like their non-nitrated parent compounds, the metallo-chlorin-like relative Q-band intensity order.[17,26]

Comparative Halochromic Responses of the Metalloporpholactones

None of the tetraarylporphyrinoids investigated are water-soluble. Thus, in order to compare the optical response curves of the porpholactones in the high pH regime in aqueous solutions, we needed to use aqueous solutions containing THF and Cremophor EL®, a synthetic, nonionic surfactant.[52] The THF brought the porphyrins into solution. A dilution of this stock solution with water/surfactant furnished fully transparent solutions that held the porphyrinoids reliably in solution for the duration of the pH titration (~15 min). We could not find any signs of porphyrin aggregrations in these solutions (broadened spectra, etc.). While this methodology allowed us to record pH titration curves, we understand that the 'pH values' cited are only idealized, at best. For one, the pH scale is not defined in partially organic solvents. Furthermore, the conventional glass electrode used to determine the pH value was at the limits of its useful operational range. Lastly, the solvent mixture proved to not be pH stable over longer periods of time. At high pH values, the presence of the surfactant slowly lowers the pH value of the solution, distorting the pH titration curves. This is because Cremophor EL® is a PEGylated castor oil and the triglyceride core structure can be saponified. Also, a minor component in this vehicle is the polyethylene glycol esters of ricinoleic acid that are also hydrolytically unstable. Over time, the appearance of turbidity indicated the degradation of the surfactant and/or the precipitation of the porphyrin, upon which the experiments were aborted and, if needed, repeated. These shortcomings demanded rapid titrations. Fortunately, the pH response of the porpholactone indicators is rapid and equilibrium is established 'instantaneously', i.e., upon mixing of the titrant into the solutions. Despite all these practical limitations and the caveat that

the pH (and pK_{OH}) values reported are not to be confused with true pH (or pK_{OH}) values, we feel confident that the comparisons of the metalloporpholactones studied under identical conditions are valid. Figure 3-6 shows a series of typical titration results, Table 1 tabulates the corresponding 'pK_{OH}' values, i.e. the pH at which half of the porpholactone was converted to its high pH species.

Addition of base to the free base *meso*-tetraphenylporpholactone **4M** or any of its metal(II) complexes (M = 2H, Cu, Ni, Zn, Pd, Ag, Pt) studied here did not result in any change of the optical spectrum of the respective species. However, substitution of the *meso*-phenyl groups by pentafluorophenyl groups (in the compounds $\mathbf{4^FM}$) resulted in a strong and fully reversible response (equivalent to that observed previously for the Pt species $\mathbf{4^FPt}$).[13] Thanks in part to well pronounced responses in the 700 nm range, generally very well-behaved UV-vis titrations with sharp isosbestic points could be obtained (with at least an 18-fold increase of the λ_{max} band at 699 nm for $\mathbf{4^FZn}$). However, only very small metal-dependencies of the pK_{OH} values became evident, and even the free base showed a good response (alas, here the response is due to the deprotonation of the inner NH).[13] All metal complexes showed an equivalent behavior: the Soret band of the neutral compound diminished as a broadened and red-shifted Soret band for the anionic complex appeared; the two side bands were replaced by a single, much red-shifted band. The zinc(II) complex $\mathbf{4^FZn}$ performed in an essentially identical fashion to the more expensive and harder to prepare compound $\mathbf{4^FPt}$.

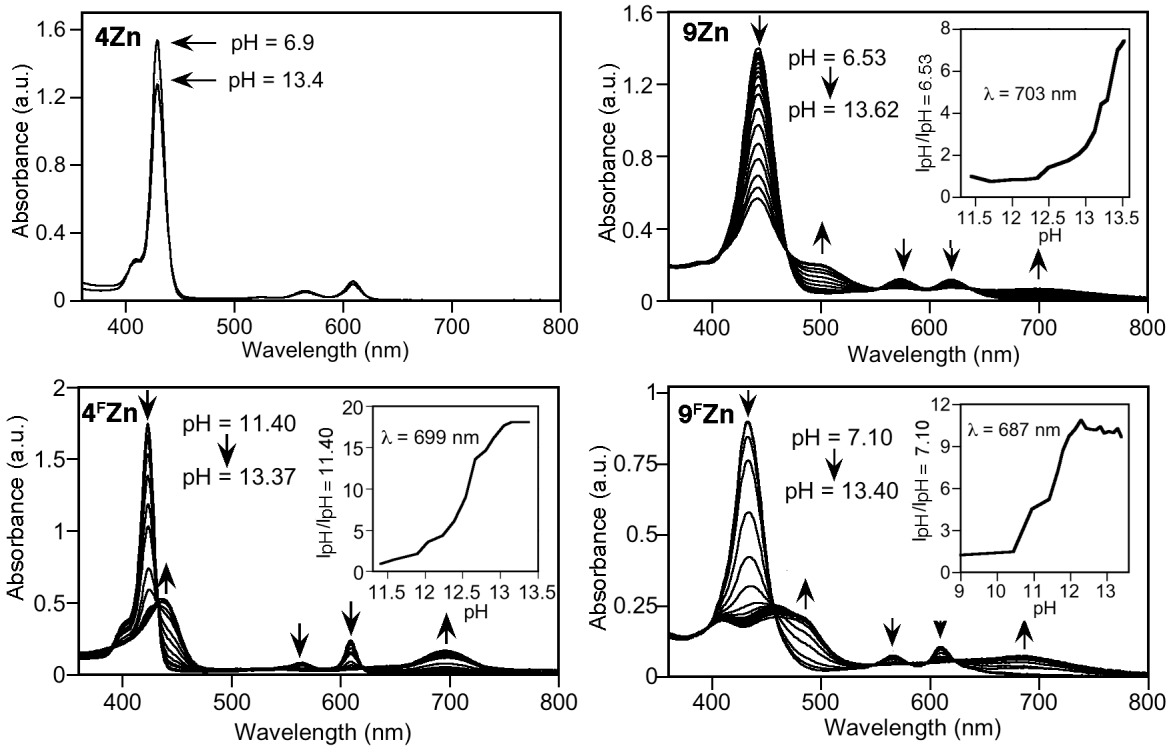

Figure 3-6. UV-vis spectra of the species indicated upon titrations with base. Inserts: titration curves at the wavelength indicated. Conditions: porphyrinoid (10^{-6} M) in 3 mL 5% Cremophor EL® in water, titrated with 0.1-5 M NaOH solution to the pH values recorded; all titrations were relatively rapid (within 5 min) to avoid excipient hydrolysis with concomitant porphyrin precipitation. Note that the change observed for **4Zn** can be solely attributed to dilution effects. For a reproduction of all titration curves, see ESI.[53]

As pointed out above, [*meso*-tetraphenylporpholactonato]zinc(II) **4Zn** (or any of the other **4M** complexes studied**)** does not show any response up to pH values well above 13. Its nitrated analogue **9Zn**, however, responds in this range, with a pK_{OH} of 13.1 (Table 3-1). Thus, the introduction of a β-nitro group to the *meso*-phenyl-substituted porpholactones evidently increased, as hypothesized, the nucleophilicity of the chromophore. Correspondingly, addition of

base to the other chromophores **9M** (M = Cu, Ni, Pd, Ag, Pt) also resulted in a profound change of their optical spectra. The base-induced changes observed for **9M** are reminiscent to that observed for $\mathbf{4^F Pt}$, and we rationalize it in an equivalent fashion.[13] When comparing the pK_{OH} values determined for *meso*-phenyl-β-nitro-porpholactone complexes **9M** and the corresponding non-nitrated *meso*-pentafluorophenyl-substituted complexes $\mathbf{4^F M}$, they vary by only about a half pK value up or down. Within the error limits of our experiment, we consider the nucleophilicity of both chromophore classes to be about equivalent.

However, one major difference is noticeable: the spectral response of the β-nitroporpholactones **9M** around 700 nm are much less well defined and pronounced (with only a 7 to 8-fold increase of the λ_{max} band at 703 nm for **9Zn**). Two reasons might be attributable to this. One, compounds **9M** are mixtures of two regioisomer and both regioisomers likely have slightly different optical spectra (at least we know that the regioisomers of the bis-oxazolobacteriochlorins possess different optical spectra).[54] The presence of a compound mixture is also likely broadening and 'washing out' the titration spectra (the absence of sharp isosbestic points is another indication for the presence of multiple compounds). Second, we believe that the intramolecular anion-aromatic interaction with the neighboring pentafluorophenyl groups shown in Scheme 1 stabilizes the anionic base form of the chromophores. The missing corresponding stabilizing interaction in **9M** is likely also affecting the electronic structure of the anion. Thus, while the β-nitro group and the *meso*-pentafluorophenyl group have roughly equivalent effects on the nucleophilicity of the lactone carbonyl group, the electronic structure and regioisomeric purity of $\mathbf{4^F M}$ results in better optical responses upon titration with base. Again, there are only minor differences between the different metal complexes.

Compounds **9^{F}M** combine the features of the β-nitroporphyrin **9M** with those of **4^{F}M**. In fact, the effects of the β-nitro group and the *meso*-pentaflurophenyl group on the nucleophilicity of the lactone carbonyl are additive, as the pK_{OH} values determined for **9^{F}M** (M = 2H, Cu, Ni, Zn, Pd, Ag, Pt) are all significantly lower than for either **9M** or **4^{F}M**. Further cementing the trend already established, the differences between the various metal complexes are small. The metal complex with the lowest pK_{OH} value (**9^{F}Zn**) is not the metal species of the lowest pK_{OH} value in the other chromophores. The intensity of the response in the NIR region of the spectra (an 11-fold increase of the λ_{max} band at 687 nm for **9^{F}Zn**) is in between those of **9Zn** and **4^{F}Zn**, as one might have expected. Again, the zinc complex appears to be a functionally very good and much cheaper alternative to the hard to prepare platinum and palladium complexes.

Table 3-1. Apparent pK_{OH-} values computed for each sensor.

Compound	pK_{OH}[b]	Compound	pK_{OH}[b]	Compound	pK_{OH}[b]	Compound	pK_{OH}[b]
4	–[a]	**9**	12.9	**4^{F}**	12.6	**9^{F}**	11.8
4Zn	–[a]	**9Zn**	13.1	**4^{F}Zn**	12.5	**9^{F}Zn**	11.1
4Ni	–[a]	**9Ni**	12.5	**4^{F}Ni**	12.6	**9^{F}Ni**	11.6
4Cu	–[a]	**9Cu**	12.6	**4^{F}Cu**	13.0	**9^{F}Cu**	11.4
4Pd	–[a]	**9Pd**	12.7	**4^{F}Pd**	12.5	**9^{F}Pd**	11.6
4Ag	–[a]	**9Ag**	12.3	**4^{F}Ag**	13.0	**9^{F}Ag**	11.3
4Pt	–[a]	**9Pt**	12.8	**4^{F}Pt**	12.4	**9^{F}Pt**	11.7

[a] No halochromic response in the pH range measured.

[b] Apparent pK_{OH}, i.e., the pH recorded by glass electrode at which 50% of the porpholactone was converted to the high pH species, as measured by UV-vis spectroscopy. For the spectra and titration conditions used, see Figure 3-6 and the ESI.[53]

3.1.2. Conclusion

In conclusion, we have shown the preparation of porpholactone derivatives that are β-nitrated at the pyrrole moiety opposite to the oxazolone moiety. We demonstrated that a range of divalent metal analogs (M = Cu, Ni, Zn, Pd, Ag) to [*meso*-tetrakis(pentafluorophenyl)-porpholactonato]Pt(II) (**4^{F}Pt**), the known optical high pH sensor, are also suitable for high pH sensing, whereby the influence of the metal type on the pH sensing profile was minor. β-Nitration was also shown as an effective means of increasing the nucleophilicity of the lactone moiety of *meso*-tetraphenylporpholactone as well as *meso*-tetrakis(pentafluorophenyl)-porpholactone metal complexes **9M** and **9^{F}M** (M = Cu, Ni, Zn, Pd, Ag, Pt), respectively. This gave rise to the lowering of the useful pH sensing range for this sensor class down to about pH 10. However, the optical response of both nitrated porpholactones is inferior compared to that of those of the corresponding (pentafluorophenyl)porpholactonato complexes.

This work further bolsters the proposed mechanism of action of the porpholactone-based sensors (nucleophilic attack of the hydroxide onto the lactone carbonyl, with formation of a stabilizing intramolecular interaction between the alkoholate oxygen and the flanking pentafluorophenyl group). This work has practical value as it identifies the cheaper and easier prepared zinc, copper and silver complexes **4^{F}Zn**, **4^{F}Cu**, and **4^{F}Ag**, respectively, as excellent alternatives to **4^{F}Pt**, at least as long as no (time-resolved) luminescence-based pH assays are desired.[55]

3.2. A Transparent Membrane for the Optical Sensing of High Hydroxide Concentrations

There are multiple reports about the immobilization of colorimetric molecules onto various films and membranes for the construction of optical pH sensors.[1-3,6,7,9-13,56-58] Among these reports, however, the construction of optical pH sensors for high pH (pH > 10) values are limited.[1,2,6,7,11,13] None are capable of sensing the differences between extremely high hydroxide concentrations, such as 1 M and 3 M aqueous NaOH. Many of the sensors developed show significant overlap between their spectra over a range of low to high pH values, have insufficient chemical stability of the chromophore at high pH values, or are characterized by nonhomogenous distribution of the immobilized dye on the support.[1] Thus, simple, sensitive and stable devices for the optical measurements of high pH values or high hydroxide concentrations above the pH scale still need to be explored.

We demonstrated that a class of pyrrole-modified porphyrins, the *meso*-tetraarylporpholactones, are suitable as optical high pH sensors.[13] Porpholactones are porphyrin analogues in which a ß,ß'-double bond of a porphyrin was replaced by a lactone moiety. They are prepared along a number of alternative oxidation procedures from the corresponding tetraarylporphyrins.

One particular porpholactone metal complex, [*meso*-tetrakis(pentafluorophenyl)porpholactonato]platinum(II) **4^{F}Pt** showed, among a number of different metal complexes of variously aryl- and ß-nitrated *meso*-tetrakis(pentaaryl)porpholactones, particularly favorable sensing properties. The sensing mechanism relies on a nucleophilic attack of OH^- (or alkoxides) on the lactone moiety, forming a chlorin-like species. Moreover, the pentafluorophenyl groups can be used as a synthetic handle to generate water-soluble derivatives using a PEGylation strategy,

utilizing the ability of the pentafluorophenyl groups to undergo a nucleophilic aromatic substitution at the *p*-aryl position (Scheme 3-4).[54]

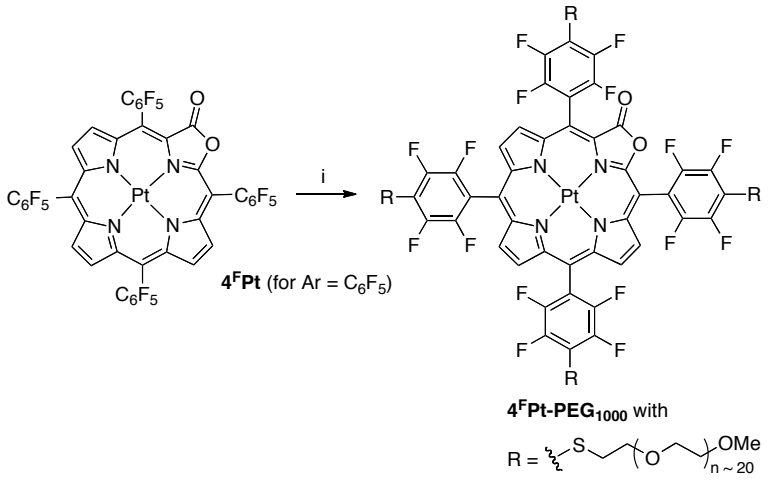

Scheme 3-4. Synthesis of **4^{F}Pt-PEG$_{1000}$**; *Reaction Conditions:* (i) DMF, NEt_3, reflux, 3 h.

Nafion® membranes were previously reported as a carrier for optical chemosensors.[57-59] A number of physical and chemical properties make this material particularly suitable for use in harsh environments. Nafion® is a chemically, fairly inert ion exchange polymer, most commonly used in fuel cell applications. A fluorocarbon chain forms the backbone of the membrane, lending its exceptional chemical, thermal and mechanical stability (Figure 3-7). It is also sulfonated. This functionality lends it its hydrophilic and ion exchange properties and results in the formation of an anionic backbone.

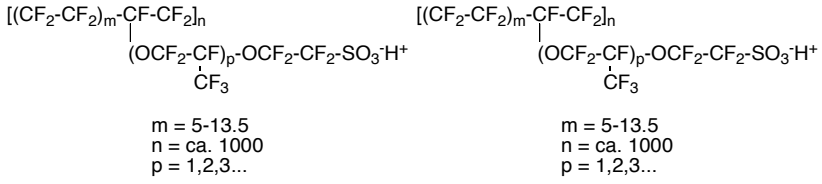

Figure 3-7. Backbone structure of Nafion®

We will report here the fabrication and evaluation of an optically transparent high hydroxide concentration Nafion®-based sensor membrane into which a metalloporpholactone-type known high pH sensor was embedded during membrane manufacture. The resulting halochromic sensor membrane was evaluated with respect to its dynamic sensing range, response time, reversibility, and long-term stability.

3.2.1. Results and Discussion

Metalloporpholactone-based high pH sensors 4^FPt and 4^FPt-PEG_{1000}

The known metalloporpholactone-based high pH sensor **4^FPt** was synthesized by oxidation of *meso*-tetrakis(pentafluorophenyl)porphyrin (using the OsO_4-mediated dihydroxylation, permanganate oxidation route).[13] As this molecule is soluble in DMF, we attempted to incorporate this molecule into a Nafion® membrane (for its preparation, see below). However, we failed to accomplish a homogenous distribution of the sensor, even when we attempted the membrane preparation in the presence of the surfactant Cremophore® (that was shown to result in good water-solubility of the sensor). Thus, we resorted to the freely water-soluble derivative **4^FPt-PEG_{1000}** that recently had become available (Scheme 3-1). This derivative allowed the homogenous distribution of the sensor into a Nafion® membrane (see also below, Figure 3-8).

Fabrication of the sensor membrane

We prepared a Nafion® membrane by casting an aqueous/DMF solution of Nafion® onto both sides of a Teflon sheet using established protocols,[60,61,62] with the exception that we embedded the high pH sensor molecule **4^FPt-PEG_{1000}** by simple addition of this sensor to the Nafion® solution (8.4 μmol sensor/cm^2 final membrane). Visual inspection of the final membrane (of

17.8–38.1 µm thickness) indicated a homogenous distribution of the pink-red dye (Figure 3-8) in a membrane of excellent transparency.

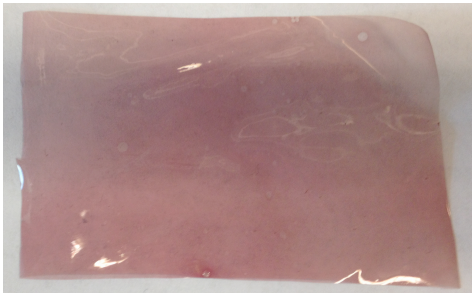

Figure 3-8. Photograph of a Nafion® membrane containing **4^{F}Pt-PEG$_{1000}$** (~2.8 × 10^{-7} M/cm^2).

The metallochlorin-like UV-vis spectrum of **4^{F}Pt-PEG$_{1000}$** in aqueous solution is near-identical to that of **4^{F}Pt-PEG$_{1000}$** embedded in a Nafion® membrane (Figure 3-9). This proves the presence of the unaltered chromophore in the film and also indicates that the sensor is not significantly stacked or in an environment that otherwise changed its optical properties.

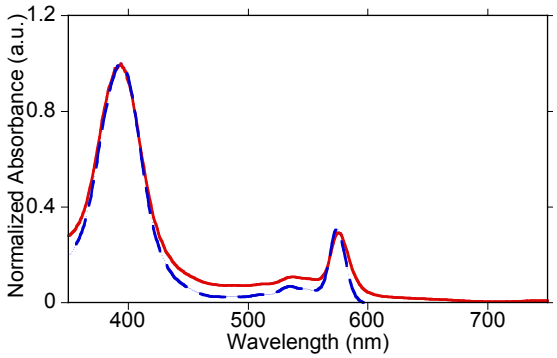

Figure 3-9. Normalized UV-vis spectrum of **4^{F}Pt-PEG$_{1000}$** in water (solid trace) and the Nafion® membrane containing **4^{F}Pt-PEG$_{1000}$** (broken trace).

Colorimetric base sensing of the sensor membrane

Upon exposure to strongly basic solutions (above pH 11.5), the sensor membrane turns green. The resulting spectrum is qualitatively equivalent to that of the sensor in aqueous

solution,[13] notably the appearance of the diagnostic new band at 695 nm, except for two major quantitative differences (Figure 3-10). Free sensor **4^{F}Pt-PEG$_{1000}$** exposed to an aqueous solution of pH 12.8, essentially quantitatively converts to the base-form of the sensor (Figure 3-11). On the other hand, when **4^{F}Pt-PEG$_{1000}$** embedded in the Nafion® membrane is exposed to a 5 M NaOH solution it is not fully in the base form, as indicated by the presence of a strong residual Soret peak for the neutral form of the sensor (Figure 3-10). The nature of the Nafion® matrix is likely responsible for this: The membrane matrix may embed some sensor chromophores deeply enough so as not to be accessible by hydroxide; moreover, the Nafion® backbone is anionic, thus representing an electrostatic barrier toward hydroxide diffusion.

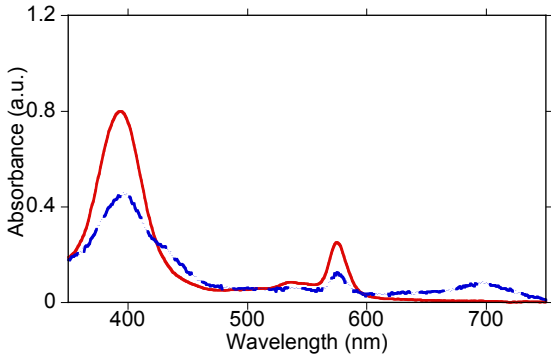

Figure 3-10. UV-vis spectrum of the Nafion® membrane containing **4^{F}Pt-PEG$_{1000}$** before (solid trace) and after (dotted trace) exposure to pH above 14 (5.0 M aq NaOH).

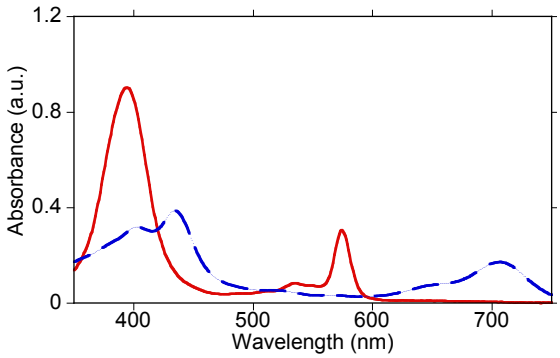

Figure 3-11. UV-vis spectrum of free sensor **4^{F}Pt-PEG$_{1000}$** before (solid trace) and after (dotted trace) exposure to pH 12.8.

A pH titration of the sensor membrane can be seen in Figure 3-12. An increase in the absorbance at 695 nm is visible in the pH range from 11 to above 14. An optical response becomes visible upon addition of a pH 12 solution.

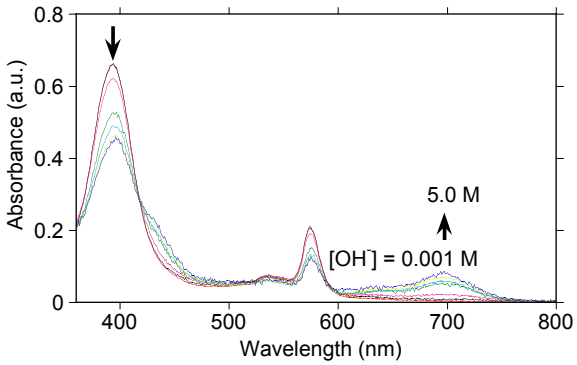

Figure 3-12. UV-vis spectrum of the Nafion® membrane containing **4^{F}Pt-PEG$_{1000}$** upon titration with aq. NaOH solutions (0.001-5 M) to the pH range 11 to above 14.

The diffusion-limited response of the sensor membrane is nonetheless rapid and within 4 min upon exposure to a 1 M aq NaOH solution, 68% of the maximum absorption value at 695 nm is reached (Figure 3-13). In comparison, the sensor molecule in solution shows an 'instantaneous' response, i.e., the response is completed after mixing. Importantly, the hydroxide-dependent response of the membrane is fully reversible within 4 min (Figure 3-13). Thus, repeated exposure to a solution at pH 14 for 28 min, followed by a pH 7 buffer, shows that the membrane response remains the same (Figure 3-14).

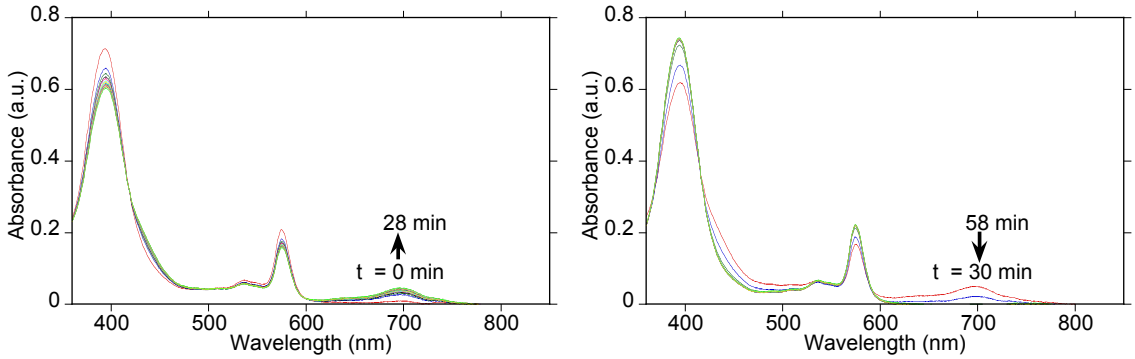

Figure 3-13. UV-vis spectra of the Nafion® membrane containing **4^{F}Pt-PEG$_{1000}$** after exposure to pH 14 for 28 min (left) and after exposure to pH 7 for 28 min (right).

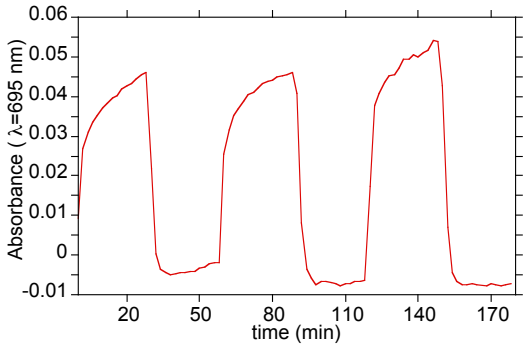

Figure 3-14. Absorbance versus time graph of the Nafion® membrane containing **4^{F}Pt-PEG$_{1000}$** after repeated exposure to pH 14 and pH 7 Buffer for 180 min.

3.2.2. Conclusion

In conclusion, we presented the fabrication of a Nafion®-based high pH optical sensing membrane with an excellent 695 nm on/off signal separation, high absorption coefficients, good chemical and physical stability, and reproducibility. The membrane features the well-described platinum porpholactone-based high pH sensing chromophore that, however, was derivatized to assure solubility in the Nafion® matrix. In contrast to the free sensor in aqueous solution, the sensor embedded in the anionic Nafion® matrix responded to high pH solutions a bit slower and with significantly lower sensitivity. This property can be utilized for the determination of the

concentration of high concentration of hydroxide (up to 5 M). Many applications in industry use highly concentrated hydroxide solutions. As the membrane is potentially suitable for the preparation of high hydroxide solution-sensing optodes, this will provide a possibility for simple optical measurements of these solutions.

3.3. Experimental Section

3.3.1. Materials

All solvents and reagents (Aldrich, Acros) were used as received. Cremophor EL® was purchased from Acros. Osmium tetroxide was purchased from Pressure Chemical Co, Pittsburgh, PA and used neat or as a solution in pyridine (typically 1 g OsO_4 in 50 mL pyridine; CAUTION! Well ventilating fume hood, gloves and goggles needed to protect against the toxic and volatile reagent! Consult corresponding material safety data sheets for further safety measures!). Cetyltrimethylammonium permanganate (CTAP) was prepared as described.[63,64] *meso*-Tetraphenylporphyrin **5** was prepared according to the method of Adler.[65] *meso*-Tetrakis(pentafluorophenyl)porphyrin $\mathbf{5^F}$ was either synthesized as described in the literature or purchased from Huhu Technology, Inc., San Diego, CA.[66] Porpholactones **4** were prepared as described previously.[17,35] Metalloporpholactones **4M** were prepared by metal insertion into the free base or the oxidation of the corresponding metallodihydroxychlorin, also according to the literature.[14,17,51] Nitroporphyrins **6** and $\mathbf{6^F}$ were prepared as described.[41] *meso*-tetraphenyl-porpholactone and its metal complexes were synthesized and characterized by Gloria Zarate. 5% Nafion® solution (1100EW) was purchased from Ion Power, Inc. (Newcastle, DE, USA). Teflon film (5.5" × 5.5" sheets, 0.7 mils thickness) was purchased from Tetratek (Pasadena, CA, USA). The PEGylated derivative of tetrakis(pentafluorophenyl)porpholactonato]platinum(II) $\mathbf{4^FPt\text{-}PEG_{1000}}$ was prepared as described previously.[54] Analytical (aluminum backed, silica gel 60, 250 μm thickness) and preparative (20 × 20 cm, glass backed, silica gel 60, 500 or 1000 μm thickness) TLC plates and the flash column silica gel (premium grade, 60 Å, 32-63 μm) used were provided by Sorbent Technologies, Atlanta, GA.

3.3.2. Instruments

UV-vis spectra were recorded on a Cary 50 spectrophotometer, Varian Inc. ^{1}H and ^{13}C NMR spectra were recorded on Bruker Avance 300 or Avance II 400 instruments in the solvents indicated. IR spectra were recorded on a Thermo Nicolet Nexus 670 FTIR spectrometer using an ATR attachment. High and low resolution mass spectra were provided by the Mass Spectrometry Facilities at the Department of Chemistry, University of Connecticut.

3.3.3. Preparation and Characterization

***meso*-Tetrakis(pentafluorophenyl)-2-nitroporphyrin (6^{F}).** *meso*-Tetrakis(pentafluoro-phenyl)-2-nitroporphyrin $\mathbf{6^{F}}$ was prepared from $\mathbf{6^{F}Zn}$ in 96% yield (452 mg, 4.18×10^{-4} mol).[41] R_f (silica, CH_2Cl_2/50% petroleum ether 30-60) = 0.72. UV-vis ($CHCl_2$) (log ε): λ_{max}, nm 420 (5.70), 518 (4.57), 555 (4.16), 592 (4.43), 650 (3.89). ^{1}H NMR (300 MHz, $CDCl_3$, Me_4Si): δ, ppm 9.20 (s, 1H), 9.08-9.04 (m, 4H), 8.84 (s, 2H), 2.76 (s, 2H). ^{13}C NMR (75 MHz, $CDCl_3$, Me_4Si): δ, ppm 157.0, 153.9, 147.93, 147.89, 146.1, 145.5, 145.43, 145.41, 142.9, 140.8, 139.76, 139.75, 139.2, 139.14, 139.10, 138.41, 138.39, 136.7, 136.5, 135.6, 131.4, 130.4, 129.9, 129.1, 128.7, 115.2, 114.9, 113.6, 106.6, 104.7, 104.4, 103.5. HR-MS (ESI+, 100 % CH_3CN) *m/z* 1020.05482 (calculated for $C_{44}H_{10}N_5F_{20}O_2$ [MH^+] 1020.0515).

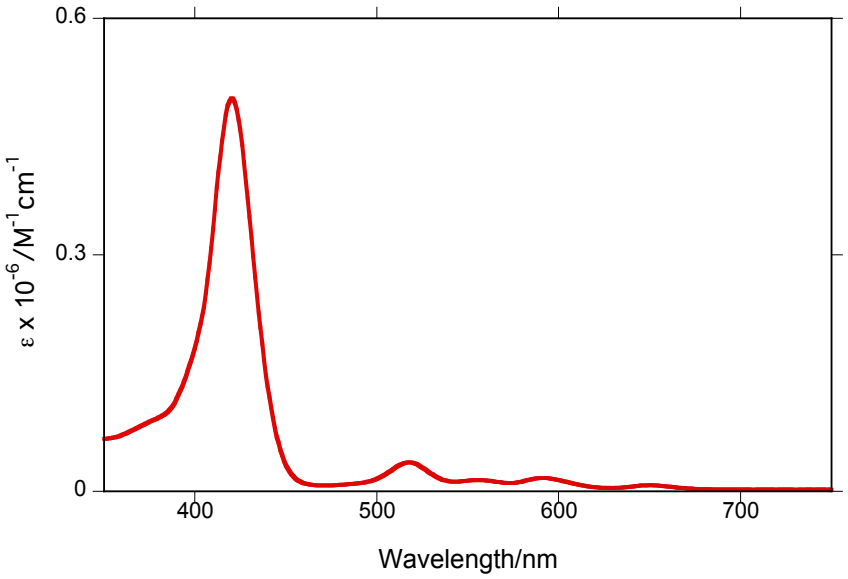

Figure 3-15. UV-vis spectrum (CH_2Cl_2) of $\mathbf{6^F}$.

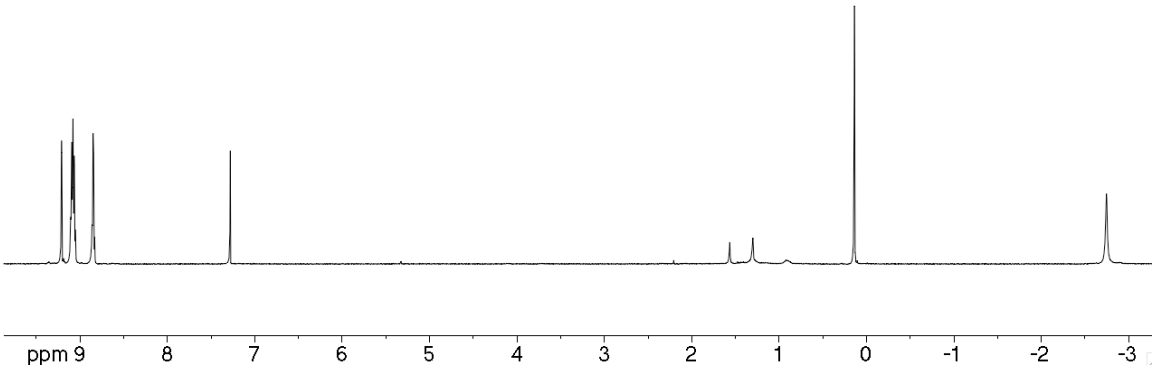

Figure 3-16. ^{1}H NMR spectrum (300 MHz, $CDCl_3$) of $\mathbf{6^F}$.

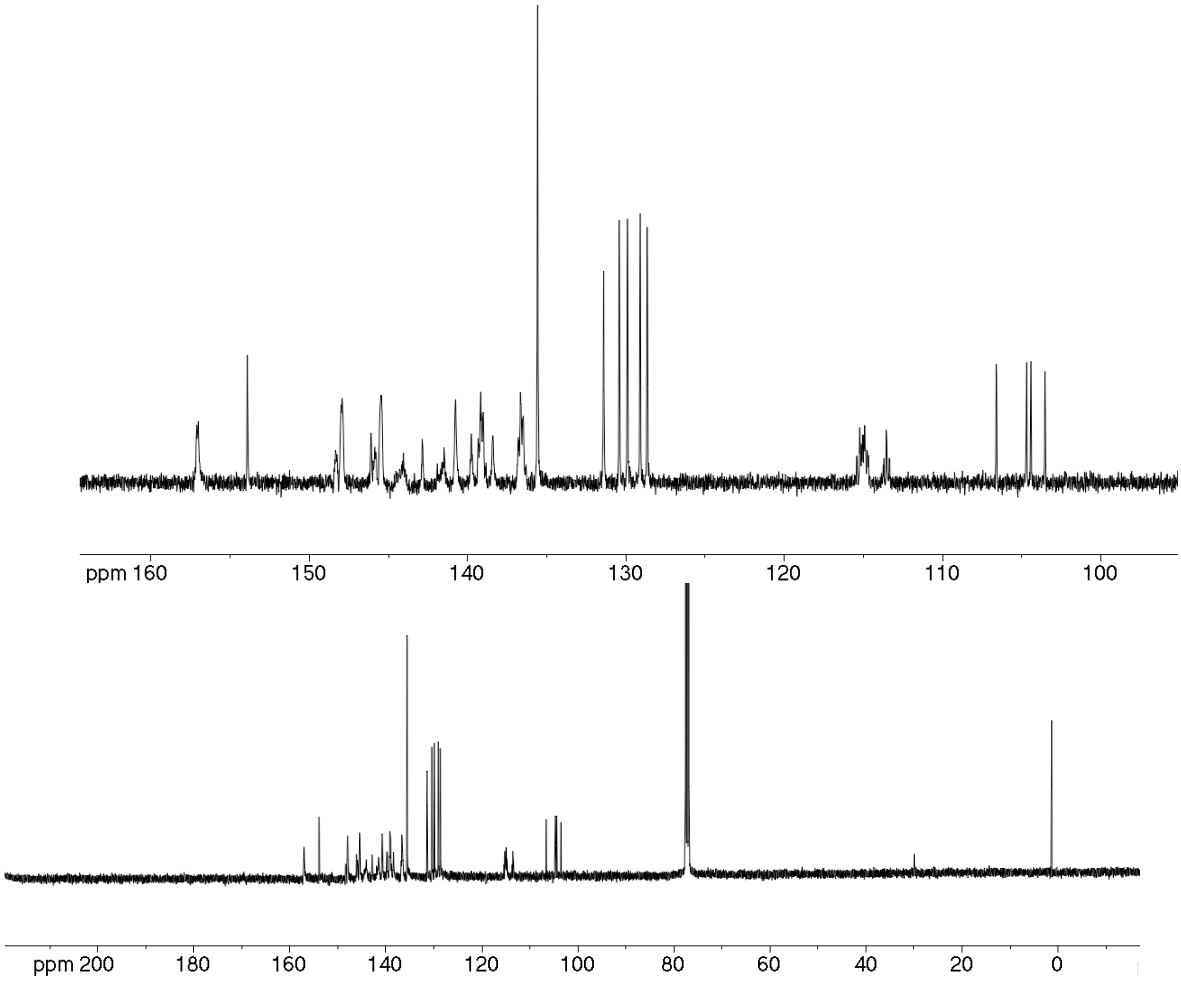

Figure 3-17. ^{13}C NMR spectrum (100 MHz, $CDCl_3$) of $\mathbf{6^F}$.

***meso*-Tetrakis(pentafluorophenyl)-2,3-*vic*-dihydroxy-12-nitrochlorin osmate ester bipyridine adduct (7^F)**. Osmate ester $\mathbf{7}^F$ was prepared from *meso*-tetrakis(pentafluorophenyl)-2-nitroporphyrin $\mathbf{6}^F$ (116 mg, 1.14×10^{-4} mol) and OsO_4 (44 mg, 1.5 equiv) in pyridine (2.2 mL) in 47% yield (77 mg) according to the procedure described for **7**. R_f (silica, CH_2Cl_2/3% MeOH) = 0.67. UV-vis (CH_2Cl_2) (log ε): λ_{max}, nm 431 (5.39), 523 (4.29), 590 (4.24), 640 (4.43). ^{1}H NMR (400 MHz, $CDCl_3$, Me_4Si): δ, ppm 8.94 (s, 1H), 8.78 (s, 2H), 8.59 (d, ^3J = 5.2 Hz, 4H, py-CH(2)), 8.52 (d, ^3J = 4.4 Hz, 2H), 7.90 (t, ^3J = 7.6 Hz, 2H, py-CH(4)), 7.44 (t, ^3J = 6.8 Hz, 4H, py-CH(3)), -1.48 (s, 1H), -1.52 (s, 1H). The osmate ester is not susceptible to analysis by MS.

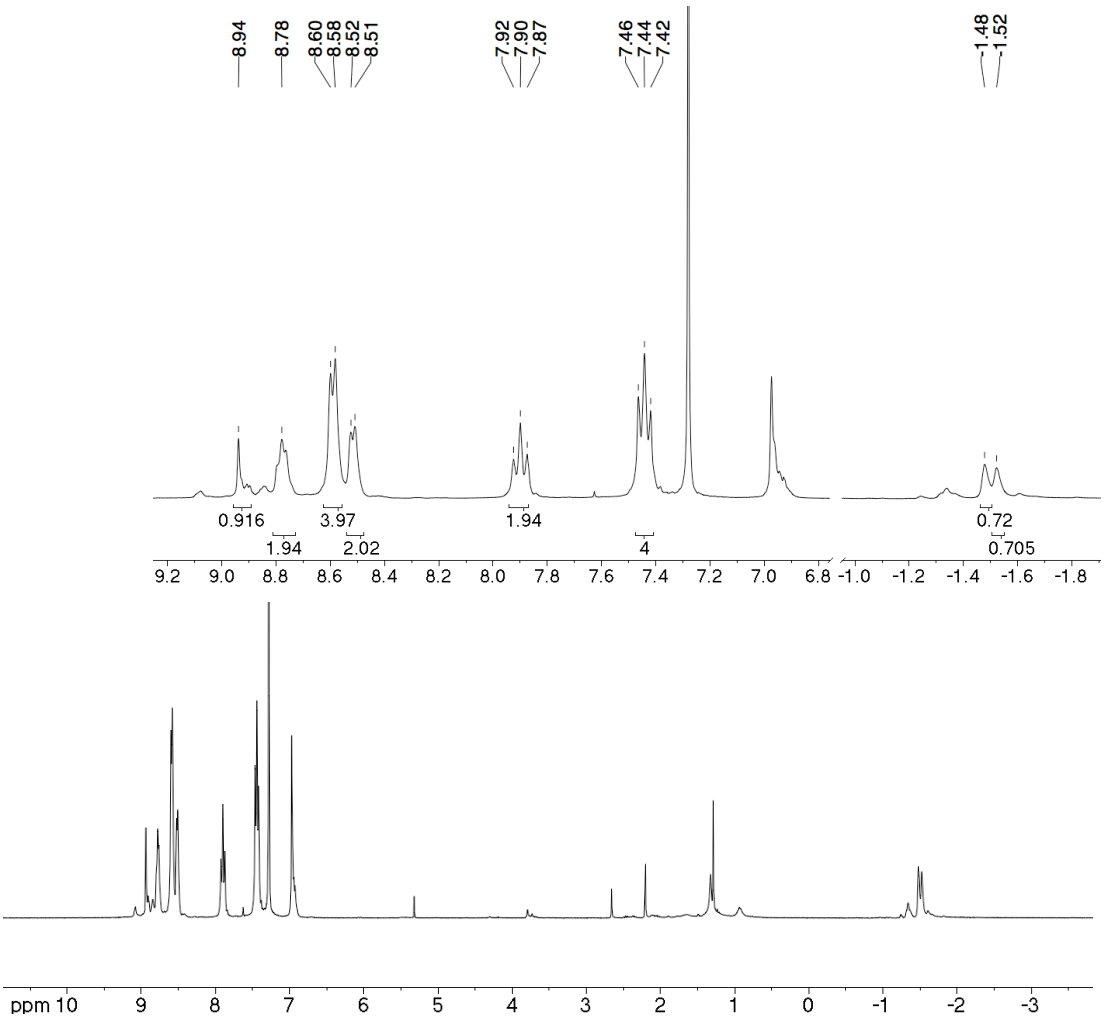

Figure 3-18. ^{1}H NMR spectrum (300 MHz, $CDCl_3$) of $\mathbf{7}^F$.

***meso*-Tetrakis(pentafluorophenyl)-2,3-*vic*-dihydroxy-12-nitrochlorin (8^F).** *meso*-Tetrakis(pentafluorophenyl)-2,3-*vic*-dihydroxy-12-nitrochlorin osmate ester 7^F (305 mg, 2.13×10^{-5} mol) was dissolved in freshly distilled, ethanol-stabilized $CHCl_3$/30% pyridine (50 mL) (or the crude reaction mixture resulting from the preparation of 7^F as described above was used). To this mixture, a saturated solution of $NaHSO_3$ in MeOH:H_2O (1:1, v/v, 90 mL) was added. The flask was stoppered, shielded from ambient light with aluminum foil, and the biphasic solution was vigorously stirred at room temperature for 5 d. Once TLC control indicated the desired degree of conversion, the reaction mixture was transferred into a 125 mL separatory funnel. The organic fraction was extracted with CH_2Cl_2. The crude product was dried by rotary evaporation and purified by column chromatography (silica, CH_2Cl_2). The crude product was purified by flash column chromatography (silica, CH_2Cl_2/1% MeOH) to provide 8^F in 41% yield. R_f (silica, CH_2Cl_2/1% MeOH) = 0.55. UV-vis (CH_2Cl_2) (log ε): λ_{max}, nm 426 (5.14), 520 (4.01), 588 (3.85), 640.01 (3.61), 647 (4.54). ^{1}H NMR (400 MHz, $CDCl_3$, Me_4Si): δ, ppm 8.88 (s, 1H), 8.80-8.75 (m, 2H), 6.22 (d, 2H), 3.37 (t, 2H), -1.61 (s, 1H), -1.66 (s, 1H).

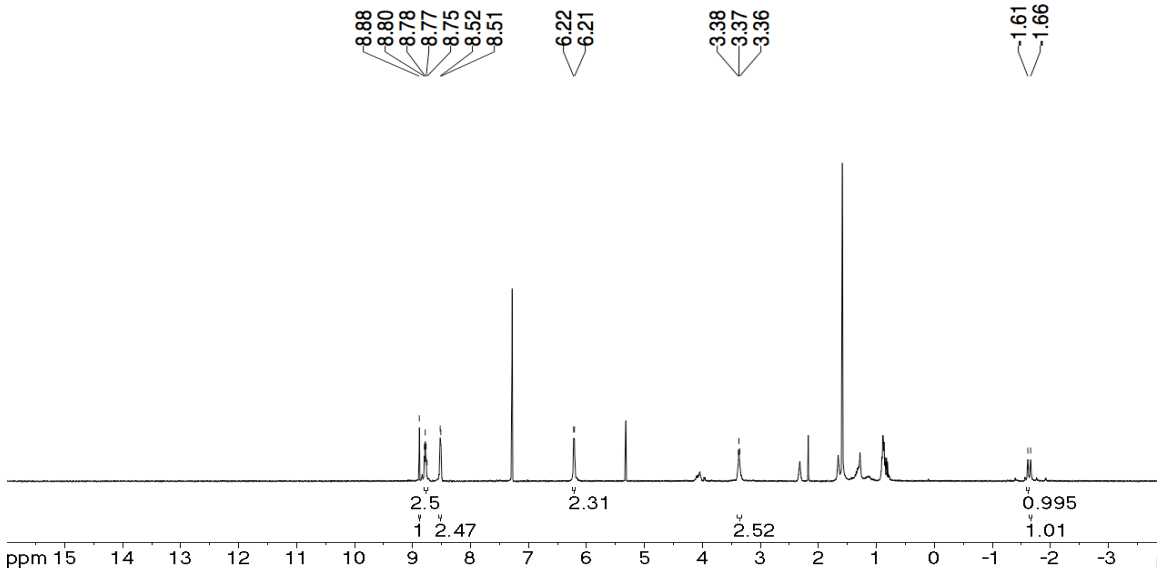

Figure 3-19. ^{1}H NMR spectrum (300 MHz, $CDCl_3$) of 8^F.

***meso*-Tetrakis(pentafluorophenyl)-12/13-nitroporpholactone (9^F).** Prepared in 46% yield (25 mg) from 7^F (70 mg, 4.90×10^{-5} mol) dissolved in $CHCl_3$ (100 mL) and CTAP (66 mg, 3 equiv) according to the procedure for **9**. R_f (silica, CH_2Cl_2/25% petroleum ether 30-60) = 0.81. UV-vis (CH_2Cl_2) (log ε): λ_{max}, nm 419 (5.24), 524 (4.00), 564 (4.01), 589 (4.00), 642 (3.81). ^{1}H NMR (300 MHz, $CDCl_3$, Me_4Si): δ, ppm 9.00 (s, 1H), 8.94-8.85 (m, 4H), -1.51 (s, 1H), -1.70 (s, 1H), -1.81 (s, 1H), -2.06 (s, 1H). ^{13}C NMR (75 MHz, $CDCl_3$, Me_4Si): δ, ppm 165.3, 165.2, 156.4, 156.2, 153.5, 153.3, 148.2, 147.7, 145.7, 145.2, 144.8, 144.4, 143.4, 143.0, 142.3, 141.9, 141.2, 140.1, 139.7, 139.1, 138.7, 137.6, 137.2, 136.6, 136.4, 134.2, 134.1, 132.1, 132.0, 131.6, 131.4, 130.8, 130.6, 130.1, 130.0, 128.8, 128.4, 127.1, 126.9, 126.6, 126.4, 125.7, 114.1, 113.9, 112.7, 112.2, 110.6, 110.4, 109.0, 107.6, 104.8, 103.2, 102.8. For its ^{19}F NMR spectrum, see ESI. IR (ATR): υ, cm^{-1} 1773.8 ($\upsilon_{C=O}$), 1518.3, 1498.8 (υ_{NO_2}). HR-MS (ESI+, 100 % CH_3CN) *m/z* 1037.0332 (calculated for $C_{44}H_7F_{20}N_5O_4$ [M^+] 1038.0257).

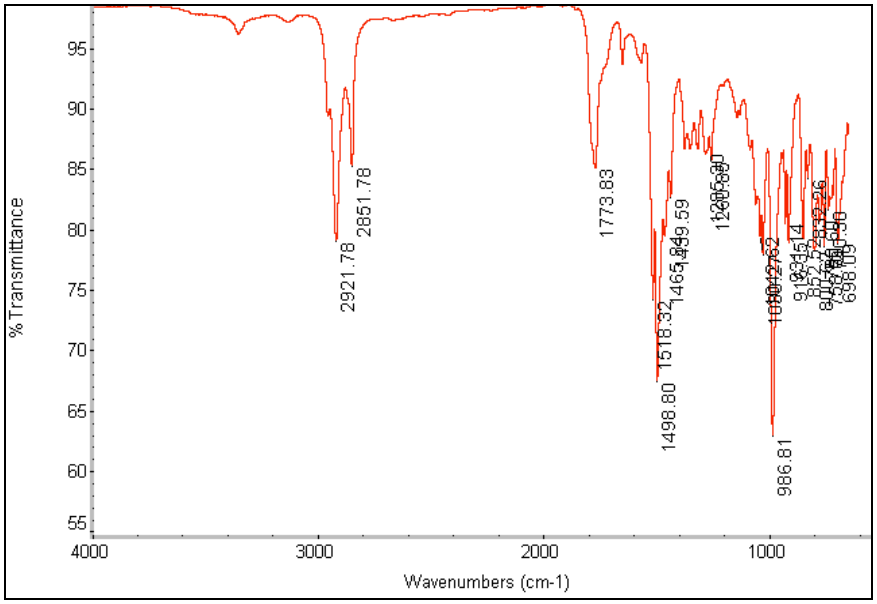

Figure 3-20. FT-IR spectrum (neat, diffuse reflectance) of 9^F.

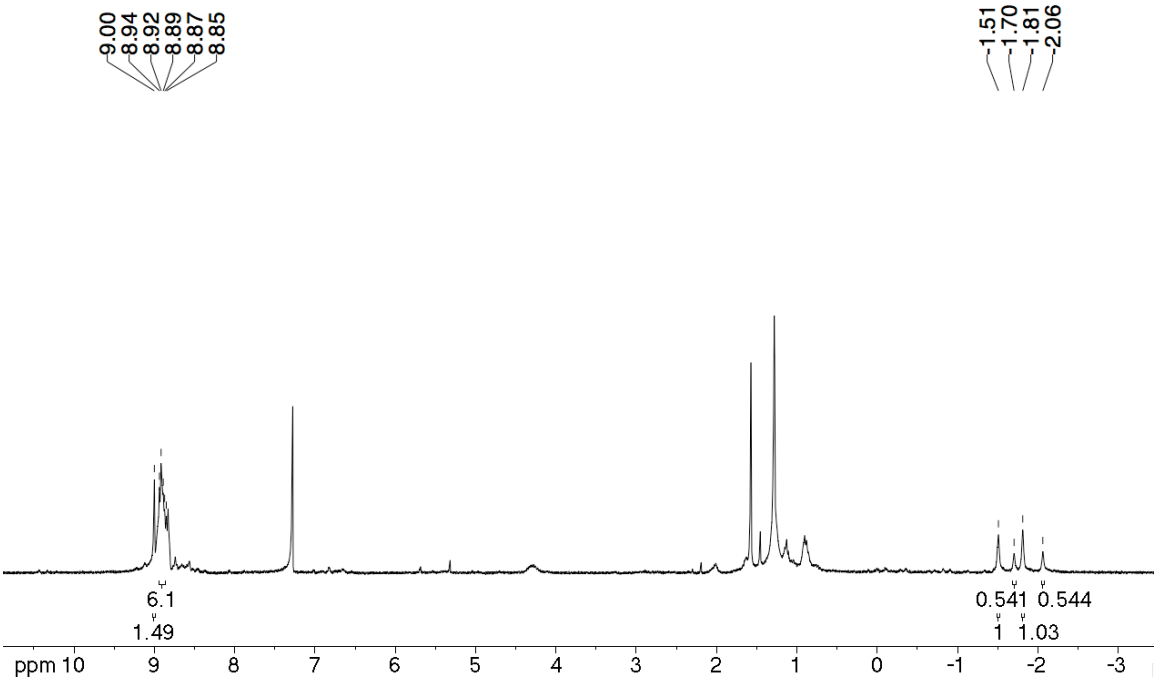

Figure 3-21. ^{1}H NMR spectrum (300 MHz, $CDCl_3$) of $\mathbf{9^F}$.

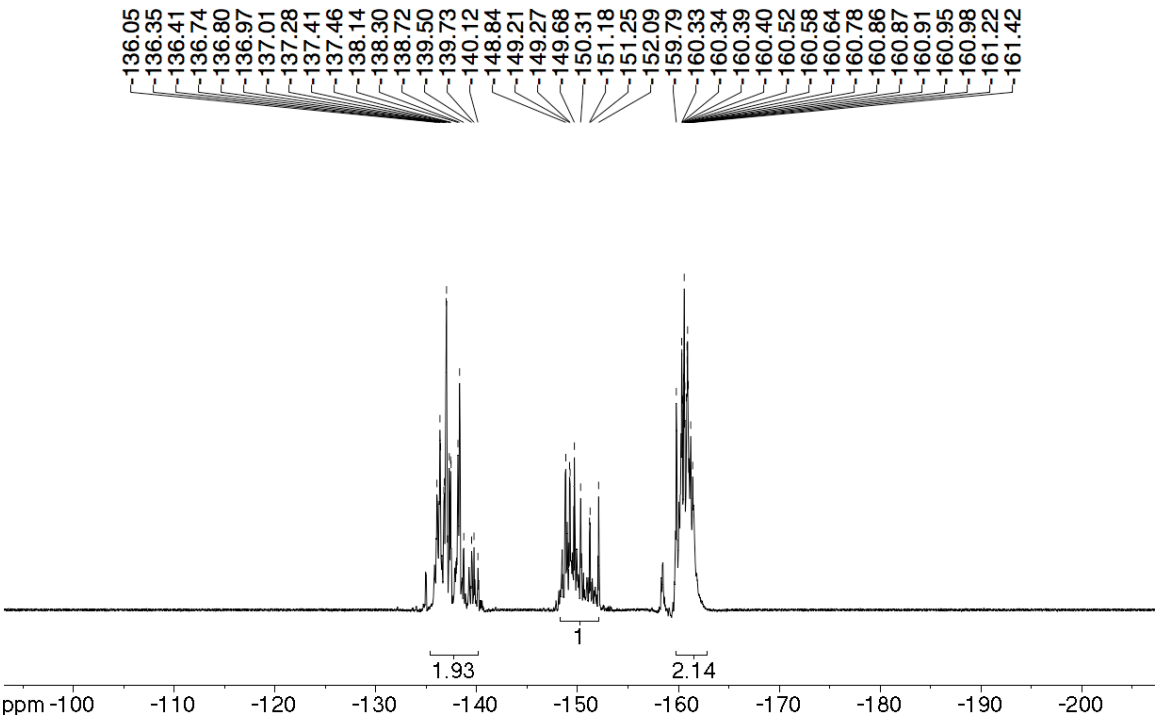

Figure 3-22. ^{19}F NMR spectrum (376 MHz, $CDCl_3$) of $\mathbf{9^F}$.

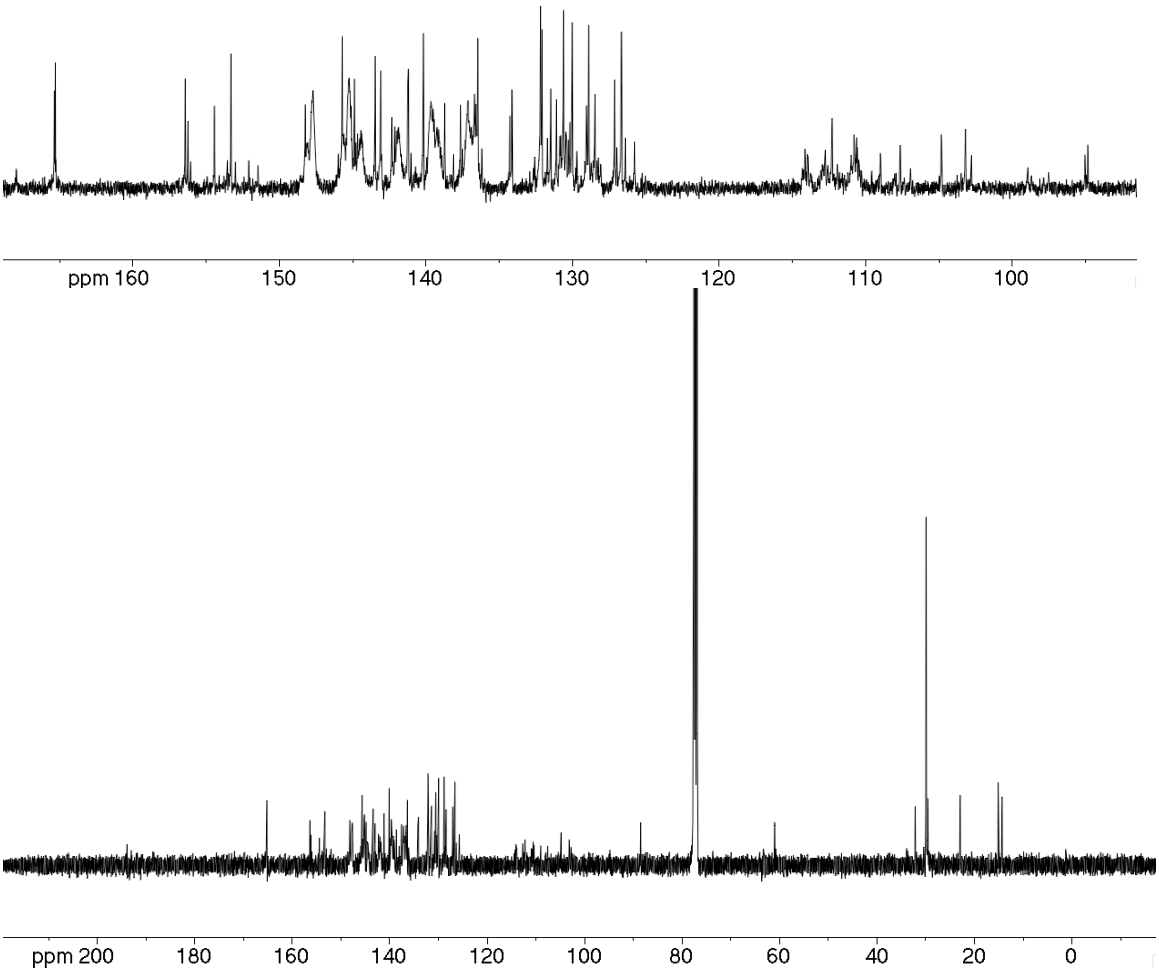

Figure 3-23. ^{13}C NMR spectrum (100 MHz, $CDCl_3$) of $\mathbf{9^F}$.

[*meso*-Tetrakis(pentafluorophenyl)-12/13-nitroporpholactonato]nickel(II) ($\mathbf{9^FNi}$). *meso*-Tetrakis(pentafluorophenyl)-12/13-nitroporpholactone $\mathbf{9^F}$ (39 mg, 3.76×10^{-5} mol) was dissolved in glacial acetic acid (15 mL) and the solution was stirred for 10 min. $Ni(OAc)_2 \cdot 4H_2O$ (37 mg, 4 equiv) was added and the solution was heated to reflux. After 10 h, the reaction reached the desired conversion (as per TLC and UV-vis spectroscopy). The solution was reduced to dryness using rotary evaporation and the residue purified by column chromatography (silica, CH_2Cl_2/50% petroleum ether 30-60) to provide $\mathbf{9^FNi}$ in 78% yield (32 mg). R_f (silica, CH_2Cl_2/50% petroleum ether) = 0.80. UV-vis ($CHCl_2$) (rel. I): λ_{max}, nm 414 (1.00), 551 (0.78),

591 (0.19). ^{1}H NMR (300 MHz, $CDCl_3$, Me_4Si): δ, ppm 8.96 (s, 1H), 8.70-8.60 (m, 4H), 8.88 (s, 1H), 8.63-8.58 (m, 2H), 8.52-8.52 (m, 2H). IR (ATR): υ, cm^{-1} 1779.3 ($\upsilon_{C=O}$), 1520.2, 1496.8 (υ_{NO_2}). HR-MS (ESI+, 100 % CH_3CN) *m/z* 1093.9132 (calculated for $C_{43}H_6F_{20}N_5NiO_4$ [MH^+] 1093.9454).

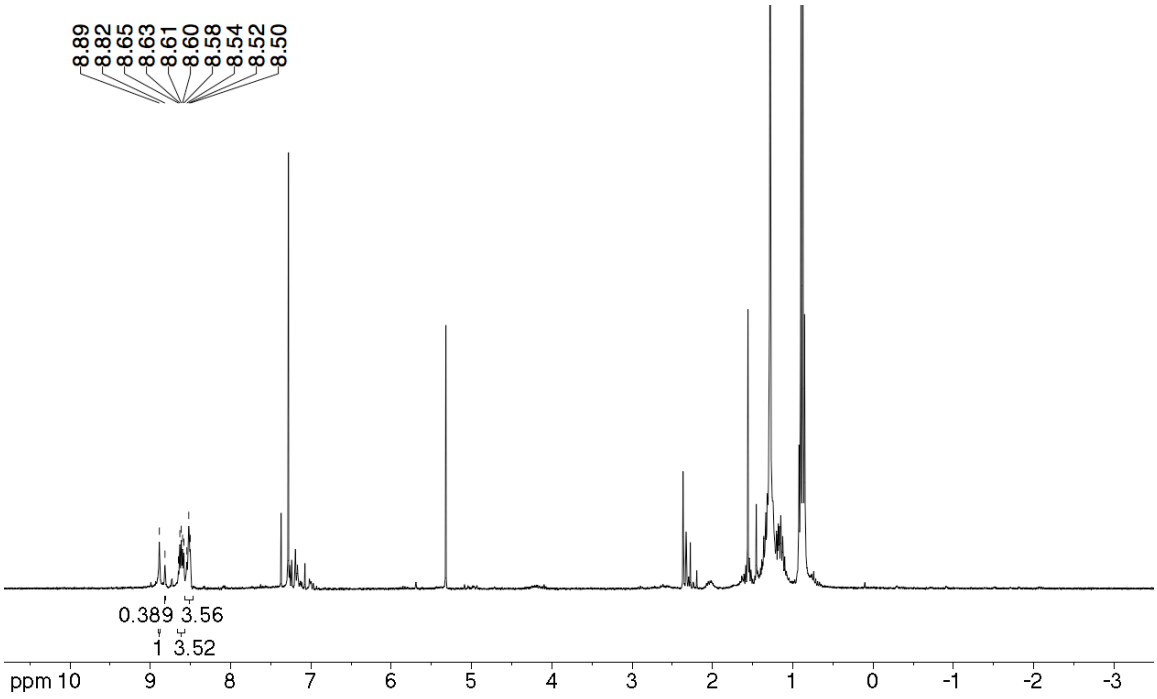

Figure 3-24. ^{1}H NMR spectrum (300 MHz, $CDCl_3$) of **9^{F}Ni**.

[*meso*-Tetrakis(pentafluorophenyl)-12/13-nitroporpholactonato]copper(II) (9^{F}Cu). *meso*-Tetrakis(pentafluorophenyl)-12/13-nitroporpholactone **9^F** (11 mg, 1.01×10^{-5} mol) and $Cu(OAc)_2 \cdot H_2O$ (10.8 mg, 5 equiv) were added to a solution of DMF (5 mL) and heated to reflux until TLC and UV-vis spectrocopy indicated a completion of the reaction (~45 min). The solution was reduced to dryness using rotary evaporation and the residue was purified on a preparative plate (silica, CH_2Cl_2/50% hexane) to provide **9^{F}Cu** in 35% yield (4.0 mg). R_f (silica, CH_2Cl_2/50% hexane) = 0.47. UV-vis ($CHCl_2$) (rel. I): λ_{max}, nm 414 (1.00), 551 (0.78), 591

(0.19). IR (ATR): υ, cm^{-1} 1789.0 ($\upsilon_{C=O}$), 1520.1. 1494.7 (υ_{NO_2}). HR-MS (ESI+, 100 % CH_3CN) *m/z* 1098.9049 (calculated for $C_{43}H_6F_{20}CuN_5O_4$ [MH^+] 1098.9396).

[*meso*-Tetrakis(pentafluorophenyl)-12/13-nitroporpholactonato]zinc(II) (9^FZn). *meso*-Tetrakis(pentafluorophenyl)-12/13-nitroporpholactone **9^F** (10 mg, 9.46×10^{-6} mol) was dissolved in $CHCl_3$ (6 mL) and the solution was heated to reflux. $Zn(OAc)_2 \cdot 2H_2O$ (20 mg, 10 equiv) dissolved in MeOH (4 mL) was added and the mixture heated to reflux for 30 min. The solution was reduced to dryness using rotary evaporation and the residue was purified by column chromatography (silica, CH_2Cl_2/2% MeOH) to provide **9^FZn** in 90% yield. R_f (silica, CH_2Cl_2/2% MeOH) = 0.78. UV-vis ($CHCl_2$) (rel. I): λ_{max}, nm 430 (1.00), 563 (0.07), 981 (0.11). ^1H NMR (300 MHz, $CDCl_3$, Me_4Si): δ, ppm 8.96 (s, 1H), 8.89 (s 1H), 8.75-8.59 (m, 8H). IR (ATR): υ, cm^{-1} 1779.8 ($\upsilon_{C=O}$), 1520.5, 1498.0 (υ_{NO_2}). HR-MS (ESI+, 100 % CH_3CN) *m/z* 1099.9078 (calculated for $C_{43}H_6F_{20}AgN_5O_4$ [MH^+] 1099.9392).

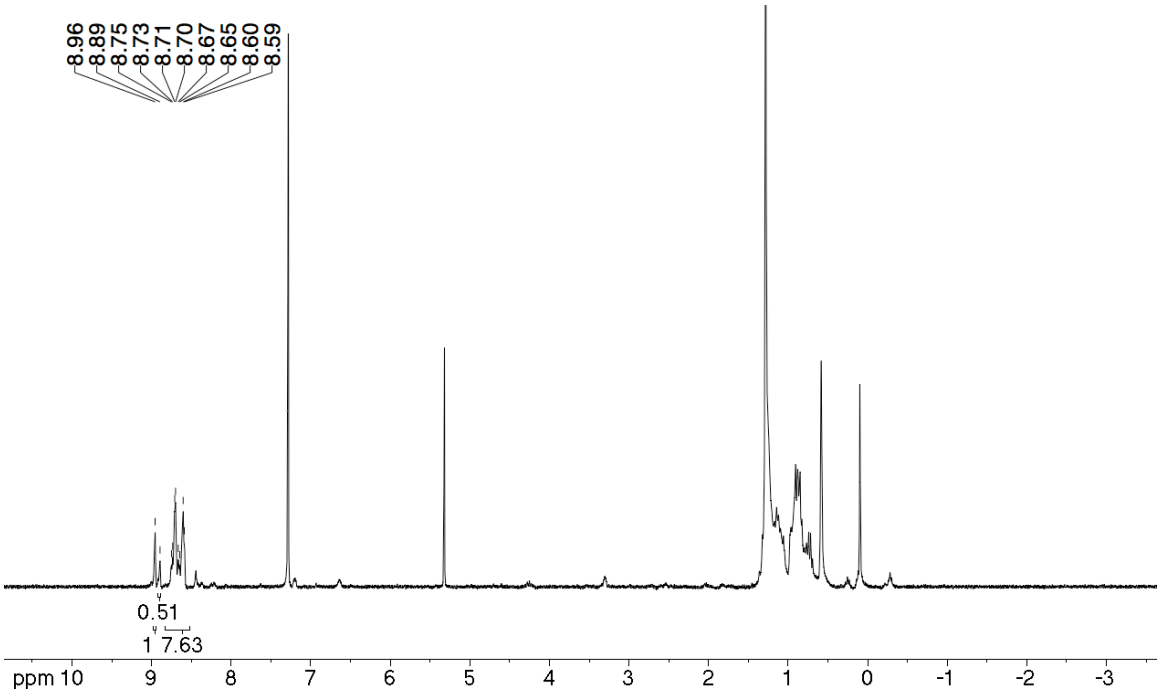

Figure 3-25. ^1H NMR spectrum (300 MHz, $CDCl_3$) of **9^FZn**.

[*meso*-Tetrakis(pentafluorophenyl)-12/13-nitroporpholactonato]palladium(II) (9^FPd). In a 10 mL thick-walled tube containing a stir bar were placed *meso*-tetrakis(pentafluorophenyl)-12/13-nitroporpholactone $\mathbf{9^F}$ (25 mg, 2.41×10^{-5} mol), $Pd(AcO)_2$ (16 mg, 3 equiv), and benzonitrile (3 mL). The vessel was sealed with a septum and placed in a microwave cavity. Using an initial microwave power of 200 W, the reaction mixture was heated from ambient temperature to 250°C and held at that temperature for 20 min, then cooled to 25°C. The reaction mixture was evaporated to dryness using rotary evaporation and the resulting crude product was purified on a preparative TLC plate (silica, CH_2Cl_2/50% hexane) to give $\mathbf{9^F}$**Pd** (10 mg) in 35% yield. R_f (silica, CH_2Cl_2/50% hexane) = 0.48. UV-vis ($CHCl_2$) (rel. I): λ_{max}, nm 415 (1.00), 540 (0.098), 580 (0.23). ^{1}H NMR (300 MHz, $CDCl_3$, Me_4Si): δ, ppm 8.89 (s, 1H), 8.82 (s 1H), 8.65-8.58 (m, 4H), 8.54-8.50 (m, 4H). IR (ATR): υ, cm^{-1} 1796.2 ($\upsilon_{C=O}$), 1517.9, 1495.3 (υ_{NO_2}). HR-MS (ESI+, 100 % CH_3CN) *m/z* 1141.8771 (calculated for $C_{43}H_6F_{20}N_5O_4Pd$ [MH^+] 1141.9150).

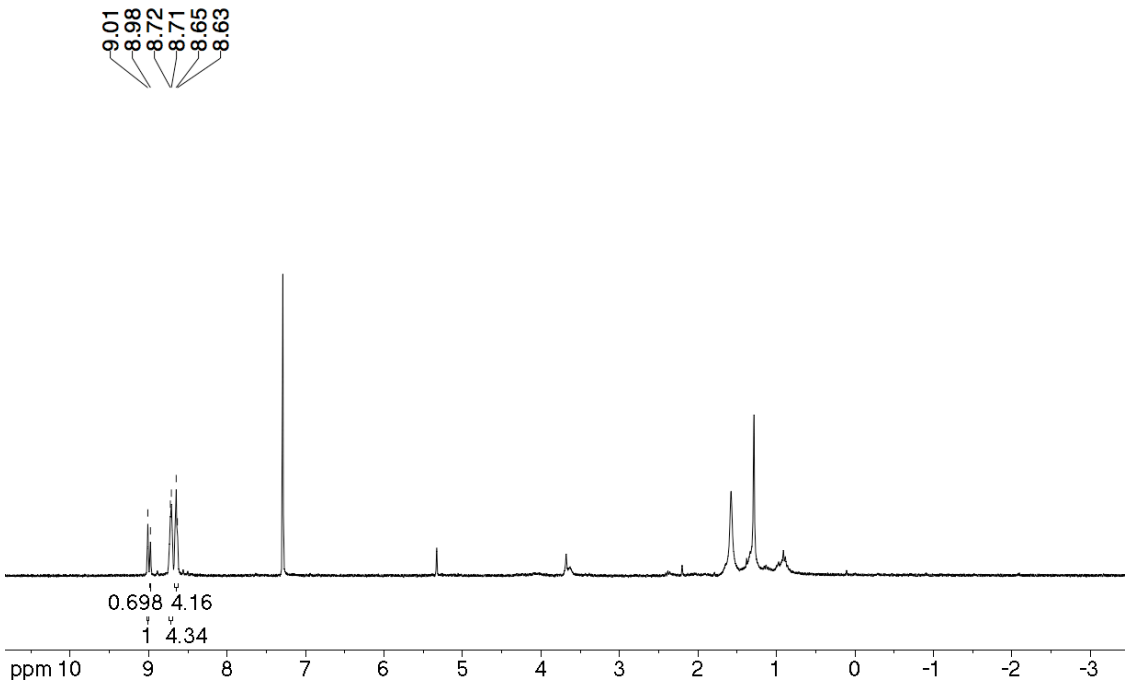

Figure 3-26. ^{1}H NMR spectrum (300 MHz, $CDCl_3$) of $\mathbf{9^F}$**Pd**.

[*meso*-Tetrakis(pentafluorophenyl)-12/13-nitroporpholactonato]silver(II) (9^FAg). Glacial acetic acid (20 mL) was warmed and *meso*-tetrakis(pentafluorophenyl)-12/13-nitroporpholactone $\mathbf{9^F}$ (42 mg, 4.02×10^{-5} mol) was dissolved. Then, $AgNO_3$ (68 mg, 4.02×10^{-3} mol) and $NaOAc{\cdot}3H_2O$ (35 mg, 4.27×10^{-4} mol) were added and the solution was heated to reflux for 3 h. The reaction mixture was cooled to ambient temperature and transferred to a separatory funnel. CH_2Cl_2 (50 mL) was used to extract the product. The organic layer was washed with water (3 × 50 mL), followed by a saturated aq. Na_2CO_3 solution (3 × 50 mL). The solution was reduced to dryness using rotary evaporation and purified by column chromatography (silica, CH_2Cl_2/50% petroleum ether 30-60) to provide $\mathbf{9^F Ag}$ (19 mg) in 41% yield. R_f (silica, CH_2Cl_2/50% petroleum ether 30-60) = 0.75. UV-vis ($CHCl_2$) (rel. I): λ_{max}, nm 433 (1.00), 563 (0.059), 606 (0.096). IR (ATR): υ, cm^{-1} 1772.4 ($\upsilon_{C=O}$), 1440.2 (υ_{NO_2}). HR-MS (ESI+, 100 % CH_3CN) *m/z* 1142.9440 (calculated for $C_{43}H_6F_{20}AgN_5O_4$ [MH^+] 1142.9151).

[*meso*-Tetrakis(pentafluorophenyl)-12/13-nitroporpholactonato]platinum(II) (9^FPt). Prepared in 10% yield (1.20 mg) from *meso*-tetrakis(pentafluorophenyl)-12/13-nitroporpholactone $\mathbf{9^F}$ (15 mg, 4.29×10^{-5} mol) and $Pt(acac)_2$ (17 mg, 3 equiv) in benzonitrile (3 mL) using the microwave heating method described for $\mathbf{9^F Pd}$. R_f (silica, toluene/50% hexane) = 0.50. UV-vis ($CHCl_2$) (rel. I): λ_{max}, nm 409 (1.00), 510 (0.05), 555 (0.07), 571 (0.12), 659 (0.03), 675 (0.027). IR (ATR): υ, cm^{-1} 1770.2 ($\upsilon_{C=O}$), 1518.0, 1498.0 (υ_{NO_2}). HR-MS (ESI+, 100 % CH_3CN) *m/z* 1230.9086 (calculated for $C_{43}H_6F_{20}N_5O_4Pt$ [MH^+] 1230.9751).

3.3.4. X-Ray Diffractometry

Diffraction data for **8** were collected on a Bruker AXS SMART APEX CCD diffractometer at 100 K using monochromatic Mo Kα radiation with the omega scan technique. Data were collected, unit cells determined, and the data integrated and corrected for absorption

and other systematic errors using the Apex2 suite of programs.[67] The structures were solved by direct methods in the monoclinic space group P^1 and refined by full matrix least squares against F^2 with all reflections using SHELXTL.[67] All non hydrogen atoms were refined anisotropically. Hydrogen atoms were placed in calculated positions and refined as riding.

The nitro group in β-nitro-chlorin **8** is disordered over two chemically equivalent positions in a ratio of 0.832(2) to 0.168(2). Associated with this disorder is the presence of a solvate ethanol molecule (major moiety) or of three solvate water molecules (minor moiety). The geometry of the minor moiety nitropyrrole unit was restrained to be the same as that of the major moiety. The pyrrole and the nitro N atoms were restrained to be planar for both moieties. Pairs of atoms close by to each other (C13 and C13b, C12 and C12b, O3 and O7b, and O9b and C48) were each constrained.

3.3.5. Base Sensing in Aqueous Systems

The porphyrinoids were dissolved in a few drops of THF. This concentrated stock solution was added to a solution of 5% Cremophor in water (3 mL) for a final concentration of the porphyrinoid of ~10^{-6} M. Sodium hydroxide stock solutions (0.1-0.5 M) were added per Eppendorf pipette to the desired pH value, for a maximum total addition of 350-500 μL. The use of larger quantities of porphyrinoid solutions and the intermittent transfer of aliquots of this solution to flow-through UV-vis cuvettes via syringe/Teflon tubing were also found to be beneficial. A micro-pH electrode (Fisher AB15) was used to monitor the pH value.

3.3.6. Preparation of the sensor membrane

Step 1. A Tetratek Teflon film was gently stretched over a clean 5" × 5" glass plate edges to produce a smooth surface with no visible wrinkles. To accomplish this, one side of the film was anchored by pressing it firmly around the top edge of the glass plate. The remaining three

sides were anchored (one at a time), working the wrinkles from the inside out. The film should extend at least ¼" beyond all edges. Starting in the center of the Teflon-covered glass plate, ~½ the surface of the Tetratek film was wetted with ethanol using an artist's brush. Starting from the center of the glass, any air bubbles were pushed out using firm strokes going radially outward. The Tetratek film covered glass plate was placed onto a level granite plate. A home-made Plexiglas/cardboard enclosure was constructed to shield the plate from drafts and dust while still allowing the evaporation of solvent from within the enclosure.

Step 2. **4^{F}Pt-EG_{1000}** (7.3 mg, 1.43×10^{-5} mol) was added to a 100 mL beaker containing 5% wt Nafion® solution (13 g) and a stir bar. The beaker was covered (with Parafilm) and the solution was magnetically stirred for 15 min to allow full homogenization. DMF (2.75 mL) and ethanol (11 mL) were then added to the now pink solution. The beaker was again covered with parafilm and stirred for 15 min.

Step 3. The Nafion/sensor/DMF/ethanol solution (15 mL) was cast onto the dry Tetratek film-coated and leveled glass plate by pipette. The entire surface should be evenly cast to within about ¼" of the each edge. After 10-15 min the membrane was examined for bubbles. If bubbles were present, a glass pipette (without a bulb attached) was used to remove the bubbles via capillary action. The coated plate was covered by the enclosure and not disturbed for 10 h at room temperature.

Step 4. The membrane must be flipped over so to cast the second side: To do this one edge of the cast membrane was gently lifted (with an exacto knife) to a depth of ~1/8" down its entire length. A few drops of DI water were added between the film and the glass to help lift the corner of the membrane. The glass was then placed on a bench and using a dropper, ~25 drops of DI water were added to the center of the cast membrane and a second 5" × 5" glass plate was

placed directly on top (creating a glass/membrane/DI water/glass sandwich). The second glass plate was pushed down to wet the entire glass surface. The transfer of the membrane from one glass plate to the other is then aided by peeling the overhanging Tetratek film edges from the first glass plate and anchoring them around the edge of the second plate. The 'sandwhich" was then flipped on its side and a few drops of DI water were added to the small gap (caused by ~1/8" peel) between the first plate and the membrane. The first glass plate was then gently slid past the second without any lifting action. This accomplished the membrane transfer.

Step 5. The flipped membrane on the second glass plate was placed level on the granite plate and Step 3 was repeated with the remaining 15 mL Nafion/sensor solution.

Step 6. After the second membrane side had become solid, the membrane (still attached to the glass) was baked at 150°C in a vacuum oven (Isotemp Vacuum Oven 280A) for 3 h (to remove the excess DMF). A corner of the membrane was then gently peeled off the glass. A few drops of DI water were added at the exposed membrane/glass interface and the membrane was then gently pulled off the glass.

3.3.7. Spectroscopic measurements

The setup for UV-vis measurements is shown in Figure 3-27. Two 1.5 cm diameter stainless steel washers were soldered parallel to each other (hard braise) to the ends of a pair of stainless steel curved tweezers. A ~1.6 mm diameter piece of the sensor membrane was held taught between the washers and the tweezers were held clamped using a metal binder clip. The washers holding the membrane were submersed in a 4.8 × 4.7 × 0.2 cm^3 glass cuvette containing the desired aqueous solution, with the 1 cm path length of the cuvette perpendicular to the washer and the hole in the washer carefully placed into the center of the beam of the UV-vis spectrometer. The Nafion® membrane containing **4^FPt-PEG$_{1000}$** was thus exposed to 0.001-5 M

aqueous NaOH solutions (pH 11 to above 14). The optical response was recorded under conditions indicated in the captions of the response curves.

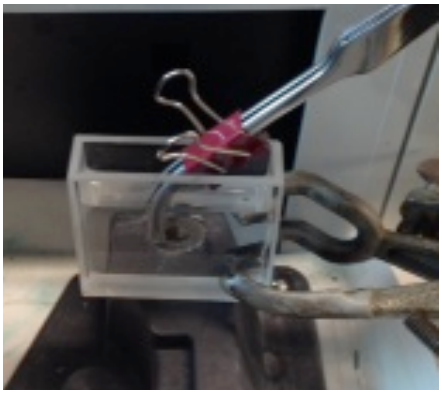

Figure 3-27. Set up for the UV-vis measurements of the Nafion®-**4^{F}Pt-PEG$_{1000}$** membrane containing.

3.4. References

(1) Werner, T.; Wolfbeis, O. S. *Fresenius J. Anal. Chem.* **1993**, *346*, 564-568.

(2) Safavi, A.; Abdollahi, H. *Anal. Chim. Acta* **1998**, *367*, 167-173.

(3) Niu, C.G.; Gui, X.Q.; Zeng, G.M.; Yuan, X.Z. *Analyst* **2005**, *130*, 1551-1556.

(4) Koncki, R.; Wolfbeis, O. S. *Anal. Chem.* **1998**, *70*, 2544-2550.

(5) Derinkuyu, S.; Ertekin, K.; Oter, O.; Denizalti, S.; Cetinkaya, E. *Anal. Chim. Acta* **2007**, *588*, 42-49.

(6) Safavi, A.; Banazadeh, A. R. *Anal. Chim. Acta* **2007**, *583*, 326-331.

(7) Ensafi, A. A.; Kazemzadeh, A. *Microchem. J.* **1999**, *63*, 381-388.

(8) Dong, S.; Luo, M.; Peng, G.; Cheng, W. *Sens. Actuators, B* **2008**, *129*, 94-98.

(9) Igarashi, S.; Kuwae, K.; Yotsuyanagi, T. *Anal. Sci.* **1994**, *10*, 821-822.

(10) Li, C.Y.; Zhang, X. B.; Han, Z. X.; Akermark, B.; Sun, L.; Shen, G. L.; Yu, R. Q. *Analyst* **2006**, *131*, 388-393.

(11) Blair, T. L.; Allen, J. R.; Daunert, S.; Bachas, L. G. *Anal. Chem.* **1993**, *65*, 2155-2158.

(12) Gulino, A.; Mineo, P.; Bazzano, S.; Vitalini, D.; Fragala, I. *Chem. Mater.* **2005**, *17*, 4043-4045.

(13) Khalil, G. E.; Daddario, P.; Lau, K. S. F.; Imtiaz, S.; King, M.; Gouterman, M.; Sidelev, A.; Puran, N.; Ghandehari, M.; Brückner, C. *Analyst* **2010**, *135*, 2125-2131.

(14) McCarthy, J. R.; Melfi, P. J.; Capetta, S. H.; Brückner, C. *Tetrahedron* **2003**, *59*, 9137-9146.

(15) Lara, K. K.; Rinaldo, C. K.; Brückner, C. *Tetrahedron* **2005**, *61*, 2529-2539.

(16) Banerjee, S.; Zeller, M.; Brückner, C. *J. Org. Chem.* **2010**, *75*, 1179-1187.

(17) Brückner, C.; Ogikubo, J.; McCarthy, J. R.; Akhigbe, J.; Hyland, M. A.; Daddario, P.; Worlinsky, J. L.; Zeller, M.; Engle, J. T.; Ziegler, C. J.; Ranaghan, M. J.; Sandberg, M. N.; Birge, R. R. *J. Org. Chem.* **2012**, *77*, 6480–6494.

(18) Crossley, M. J.; King, L. G. *J. Chem. Soc., Chem. Commun.* **1984**, 920-922.

(19) Gouterman, M.; Callis, J.; Dalton, L.; Khalil, G.; Mebarki, Y.; Cooper, K. R.; Grenier, M. *Meas. Sci. Technol.* **2004**, *15*, 1986-1994.

(20) Khalil, G.; Gouterman, M.; Ching, S.; Costin, C.; Coyle, L.; Gouin, S.; Green, E.; Sadilek, M.; Wan, R.; Yearyean, J.; Zelelow, B. *J. Porphyrins Phthalocyanines* **2002**, *6*, 135-145.

(21) Köpke, T.; Pink, M.; Zaleski, J. M. *Chem. Commun.* **2006**, 4940-4942.

(22) Jayaraj, K.; Gold, A.; Austin, R. N.; Ball, L. M.; Terner, J.; Mandon, D.; Weiss, R.; Fischer, J.; DeCian, A.; Bill, E.; Müther, M.; Schünemann, V.; Trautwein, A. X. *Inorg. Chem.* **1997**, *36*, 4555-4566.

(23) Liang, L.; Lv, H.; Yu, Y.; Wang, P.; Zhang, J.-L. *Dalton Trans.* **2012**, *41*, 1457-1460.

(24) Yu, Y.; Lv, H.; Ke, X.; Yang, B.; Zhang, J.-L. *Adv. Synth. Catal.* **2012**, *354*, 3509–3516.

(25) Akhigbe, J.; Haskoor, J.; Zeller, M.; Brückner, C. *Chem. Commun.* **2011**, *47*, 8599–8601.

(26) Gouterman, M.; Hall, R. J.; Khalil, G. E.; Martin, P. C.; Shankland, E. G.; Cerny, R. L. *J. Am. Chem. Soc.* **1989**, *111*, 3702-3707.

(27) Cetin, A.; Ziegler, C. J. *Dalton Trans.* **2005**, 25-26.

(28) Rahimi, R.; Tehrani, A. A.; Fard, M. A.; Sadegh, B. M. M.; Khavasi, H. R. *Catal. Commun.* **2009**, *11*, 232-235.

(29) Khalil, G. E.; Costin, C.; Crafton, J.; Jones, G.; Grenoble, S.; Gouterman, M.; Callis, J. B.; Dalton, L. R. *Sens. Actuators, B* **2004**, *97*, 13-21.

(30) Lau, K. S. F., Ph.D. thesis, University of Washington, **2006**.

(31) Brückner, C.; McCarthy, J. R.; Daniell, H. W.; Pendon, Z. D.; Ilagan, R. P.; Francis, T. M.; Ren, L.; Birge, R. R.; Frank, H. A. *Chem. Phys.* **2003**, *294*, 285-303.

(32) McCarthy, J. R.; Perez, M. J.; Brückner, C.; Weissleder, R. *Nano Lett.* **2005**, *5*, 2552-2556.

(33) Ogikubo, J.; Meehan, E.; Engle, J. T.; Ziegler, C.; Brückner, C. *J. Org. Chem.* **2012**, *77*, 6199–6207.

(34) Akhigbe, J.; Haskoor, J. P.; Krause, J. A.; Zeller, M.; Brückner, C. *Org. Biomol. Chem.* **2013**, *11*, 3616–3628.

(35) McCarthy, J. R.; Jenkins, H. A.; Brückner, C. *Org. Lett.* **2003**, *5*, 19-22.

(36) Brückner, C.; Rettig, S. J.; Dolphin, D. *J. Org. Chem.* **1998**, *63*, 2094-2098.

(37) Hyland, M. A.; Morton, M. D.; Brückner, C. *J. Org. Chem.* **2012**, *77*, 3038–3048.

(38) Samankumara, L. P.; Zeller, M.; Krause, J. A.; Brückner, C. *Org. Biomol. Chem.* **2010**, *8*, 1951-1965.

(39) Buchler, J. W. In *Porphyrins*; Dolphin, D., Ed. 1978; Vol. 1, p 389-483.

(40) Kalish, H.; Camp, J. E.; Stepien, M.; Latos-Grazynski, L.; Olmstead, M. M.; Balch, A. L. *Inorg. Chem.* **2002**, *41*, 989-997.

(41) Annoni, E.; Pizzotti, M.; Ugo, R.; Quici, S.; Morotti, T.; Bruschi, M.; Mussini, P. *Eur. J. Inorg. Chem.* **2005**, 3857-3874.

(42) Sen, A.; Krishhnan *Tetrahedron Lett.* **1996**, *37*, 5421-5424.

(43) Brückner, C.; Dolphin, D. *Tetrahedron Lett.* **1995**, *36*, 3295-3298.

(44) Akhigbe, J.; Peters, G.; Zeller, M.; Brückner, C. *Org. Biomol. Chem.* **2011**, *9*, 2306-2313.

(45) M. O. Senge, Acta Cryst. C, 1998, C54, iIUC9800022 (CSD code of the crystal structure: NOZKUI).

(46) Kratky, C.; Waditschatka, R.; Angst, C.; Johansen, J. E.; Plaquevent, J. C.; Schreiber, J.; Eschenmoser, A. *Helv. Chim. Acta* **1985**, *68*, 1313-1337.

(47) Ogikubo, J.; Brückner, C. *Org. Lett.* **2011**, *13*, 2380–2383.

(48) Ogikubo, J.; Meehan, E.; Engle, J. T.; Ziegler, C. J.; Brückner, C. *J. Org. Chem.* **2013**, *78*, 2840-2852.

(49) Lara, K. K.; Rinaldo, C. R.; Brückner, C. *Tetrahedron Lett.* **2003**, *44*, 7793-7797.

(50) The numbering scheme is not following IUPAC nomenclature, cf. G. P. Moss, Eur. J. Biochem. 1988; 178: 277–328. (http://www.chem.qmw.ac.uk/iupac/tetrapyrrole) rules, but a simplified and much more intuitive scheme.

(51) Dean, M. L.; Schmink, J. R.; Leadbeater, N. E.; Brückner, C. *Dalton Trans.* **2008**, 1341-1345.

(52) Cremophore EL (BASF) is a polyethoxylated castor oil with excellent surfactant qualities that is an FDA-approved excipient for hydrophilic drugs.

(53) Worlinsky, J. L.; Zarate, G.; Zeller, M.; Ghandehari, M.; Khalil, G.; Brückner, C. *J. Porphyrins Phthalocyanines* **2013**, accepted for publication (DOI: 10.1142/S1088424613500478).

(54) Ogikubo, J.; Worlinsky, J. L.; Fu, Y.-J.; Brückner, C. *Tetrahedron Lett.* **2013**, *54*, 1707-1710.

(55) For an overview over the current state of the art in fluorescence imaging with chemical sensors, see: Schäfer M Angew. Chem. Int. Ed. **2012**, *51*, 3532-3554.

(56) Safavi, A.; Bagheri, M. *Sens. Actuators, B* **2003**, *90*, 143-150.

(57) Misra, V.; Mishra, H.; Joshi, H. C.; Pant, T. C. *Sens. Actuators B* **2002**, *82*, 133-141.

(58) Castriciano, M. A.; Carbone, A.; Sacca, A.; Donato, M. G.; Micali, N.; Romeo, A.; De Luca, G.; Scolaro, L. M. *J. Mater. Chem.* **2010**, *20*, 2882-2886.

(59) Sendhil, K.; Vijayan, C.; Kothiyal, M. P. *Opt. Mater.* **2005**, *27*, 1606-1609.

(60) Fenton, J.M.; Kunz, H.R.; Lin, J.C. University of Connecticut, "Membrane Electrde Assemblies Using Ionic Composite Membranes", U.S. Patent No. 6,638,659 B1, Filed Sept 12, 2000; Date of Patent October 28, 2003.

(61) Fenton, J.M.; Kunz, H.R.; Cutlip, M.B. Lin, J.C. University of Connecticut, "Membranes, Membrane Electrode Assemblies, and Fuel Cells Employing Same, and Process for Preparing", United States Patent No. US 6,465,136 Bl, October 15, 2002: ELECTROCHEMICAL CITATIONS.

(62) Lin, J.C.; Kunz, H.R.; Cutlip, M.B.; Fenton, J.M. University of Connecticut, "Preparation of High Temperature Composite Membranes for Hydrogen Proton Exchange Membrane Fuel Cells", Proceedings of the Hazardous & Industrial Wastes-31st Mid-Atlantic Industrial & Hazardous Wastes Conference, pp. 656 **1999**.

(63) Lee DG. Phase Transfer Assisted Permanganate Oxidations. In: Trahanovsky WS, editor: AP, **1982**.

(64) Furniss BS, Hannaford AJ, Smith PWG, Tatchell AR. Vogel's Textbook of Practical Organic Chemistry. New York: Longman Scientific & Technical / Wiley, **1989**.

(65) Adler, A. D.; Longo, F. R.; Finarelli, J. D.; Goldmacher, J.; Assour, J.; Korsakoff, L. *J. Org. Chem.* **1967**, *32*, 476.

(66) Spellane, P. J.; Gouterman, M.; Antipas, A.; Kim, S.; Liu, Y. C. *Inorg. Chem.* **1980**, *19*, 386-391.

(67) (a) SHELXTL (Version 6.14), 2000-2003, Bruker Advanced X-ray Solutions, Bruker AXS Inc., Madison, WI, USA. (b) Apex2 v2009.7-0, 2005, Bruker Advanced X-ray Solutions, Bruker AXS Inc., Madison, WI, USA.

4. Optical Cyanide Sensing Using Metalloporpholactones in Aqueous Solution

4.1. Introduction

Because of the high toxicity of cyanide (CN^-) in physiological and environmental contexts, combined with its widespread technical use, its detection attracted significant interest.[1] The primary toxic effect of cyanide lies in the ability to impair crucial enzyme functions due to the strong affinity of cyanide for transition metals, such as the iron in heme proteins.[2] The crucial target of cyanide in the mammalian body is cytochrome c oxidase, thus inhibiting cellular respiration.[2] As little as 0.5-3.5 mg cyanide per kg of body weight are lethal to humans.[2,3]

Small amounts of cyanides are found widespread in nature. They are found in certain seeds and fruit stones, such as those of apple, mango, peach, and bitter almonds. Very large quantities of cyanides found used in industry such as for the synthesis of fibers, plastics, inks, fertilizers, nylon, in fishing, precious metal mining, for case hardening of steel, and metal electroplating processes.[4-7] Its wide-spread use raises the risk for accidental (or intentional) release into the water stream.[2,4,7]

Therefore, considerable effort has been invested in developing probes toward the selective sensing of cyanide using colorimetric and fluorometric methods. Some of the detection methods rely on hydrogen bonding interactions but they frequently suffer from poor selectivity with respect to other anions.[4,5,8,9] Reaction-based receptors take advantage of the nucleophilic and strongly metal-binding character of cyanide.[5,7-11] The formation of cyanide adducts/complexes with dipyrrins,[9] triarylboranes,[12] benzo[*f*]chromenes,[11] oxazines,[2,3] diphenylamino stilbenes,[4] and metal complexes[13] were reported. Most sensors require the use of organic solvents, or a mixture of an organic solvent and water.[2-4,9,11,12] In 2012, Li and co-

workers reported the first cyanide sensor operating in pure water, a hybrid material composed of an iridium complex and a lanthanide-doped up-conversion nanophosphor.[13]

Some metalloporphyrins have been utilized for the detection of cyanide.[14-18] Metalloporphyrins are useful as cyanide sensors because of the affinity of cyanide for some central metals, such as zinc, rhodium, copper, silver and gold, and the strong color of the porphyrin.[16] One approach investigated utilized a two-point recognition of sodium or potassium cyanide by a zinc porphyrin crown ether conjugate (Figure 1).[17,18] Other porphyrins such as a zinc porphyrin-crown ether conjugate (**1Zn**)[17], [*meso*-tetraphenylporphyrinato]zinc(II)[15] [*meso*-tetrakis(4-carboxyphenyl)porphyrinato]copper(II)[16] (**2Cu**) [*meso*-tetrakis(4-sulfonatophenyl)porphyrinato]rhodium(III)[14] (**3Rh**) have also been used for the detection of cyanide. However, the coordination of the cyanide to the central metal elicits only modest optical changes and the UV-vis spectra of the cyanide-free and cyanide-bound species largely overlap.

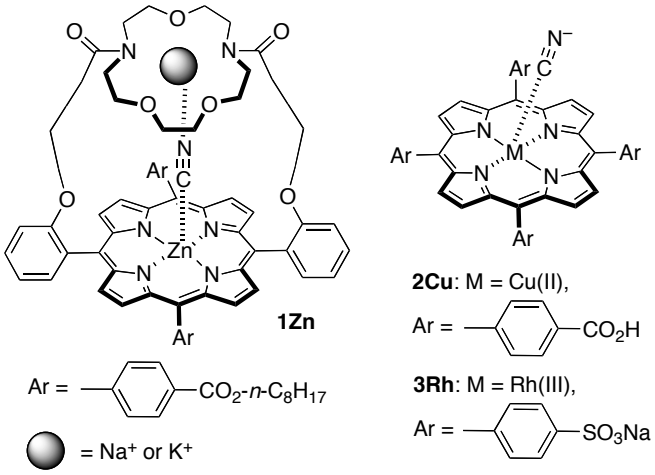

Porpholactones are derived from porphyrins by replacement of a *β,β'*-double bond by a lactone functionality; in effect, a pyrrole moiety was replaced by a oxazolone (Scheme 4-1).[19-21] Known for some time, only more recently they have become readily available along two complementary routes: a one-step Ru-catalyzed direct oxidation of a porphyrin[9] and using a two-

step route involving the OsO_4-mediated dihydroxylation of a porphyrin, followed by MnO_4^--oxidation of the dihydroxypyrroline moiety. [22]

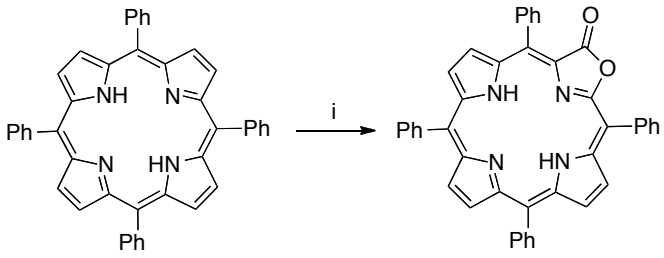

4 **5**

Scheme 4-1. Synthesis of *meso*-tetraphenylporpholactone (TPL) 5. *Reaction conditions:* 1. OsO_4, pyridine, r.t., up to 7 d, followed by chromatography; 2. H_2S 3. CTAP, CH_2Cl_2.

With their availability, their utility as starting materials for other pyrrole-modified porphyrins was discovered.[23] Selected metalloporpholactones proved also to be good catalysts in atom transfer reactions,[24-26] and the [porpholactonato]platinum(II) complex **6Pt** proved to be a particularly effective oxygen-sensing dye in pressure-sensing paints.[20,27-29] The oxygen partial pressure sensing mechanism (phosphorescence quenching of the excited triplet state of **6Pt** by triplet oxygen)[30] is only indirectly affected by the presence of the lactone moiety. This moiety is, however, the key functionality in the use of **6Pt** as a high pH indicator. The base attacks the lactone carbonyl group, causing a sp^2-to-sp^3-conversion of a β-carbon that causes a ~100 nm red-shift of the chromophore.[31] This conversion that is analogous to a porphyrin-to-chlorin conversion generally has large effects on the chromophore. The lactone-to-thionolactone conversion (and its reverse) was the basis for the use of porpholactone derivatives as chemidosimeter for hypochlorite.[32]

The accessibility of porpholactones and their functionality at the periphery of the macrocycle that is strongly electronically coupled to the chromophore make porpholactones an excellent sensor platform. Herein we report the use of a number of metalloporpholactone

derivatives as optical (colorimetric as well as fluorimetric) cyanide sensors, whereby we can directly compare the effectiveness of the sensing of cyanide by coordination to a central metal or by addition to the lactone moiety. The particular porpholactone ligand used, *meso*-tetrakis(penta-fluorophenyl)porpholactone, is also readily susceptible to conversion to water-soluble derivatives. Thus, we report also on the selective and sensitive detection of cyanide in pure water.

4.2. Results and Discussion

4.2.1. Synthesis of metalloporpholactones 6M

The metalloporpholactones, known **6Zn**, **6Pt** and novel derivative **6Ga** were synthesized my metalation of free base **1** using standard reaction conditions (in case of **6Ga**, microwave heating) (Scheme 4-2). The gallium(III) complex showed all the expected spectroscopic and analytical properties (for details, see experimental section; for the description of its optical spectra, see below). It was prepared as the square pyramidal complex carrying an axial chloride.

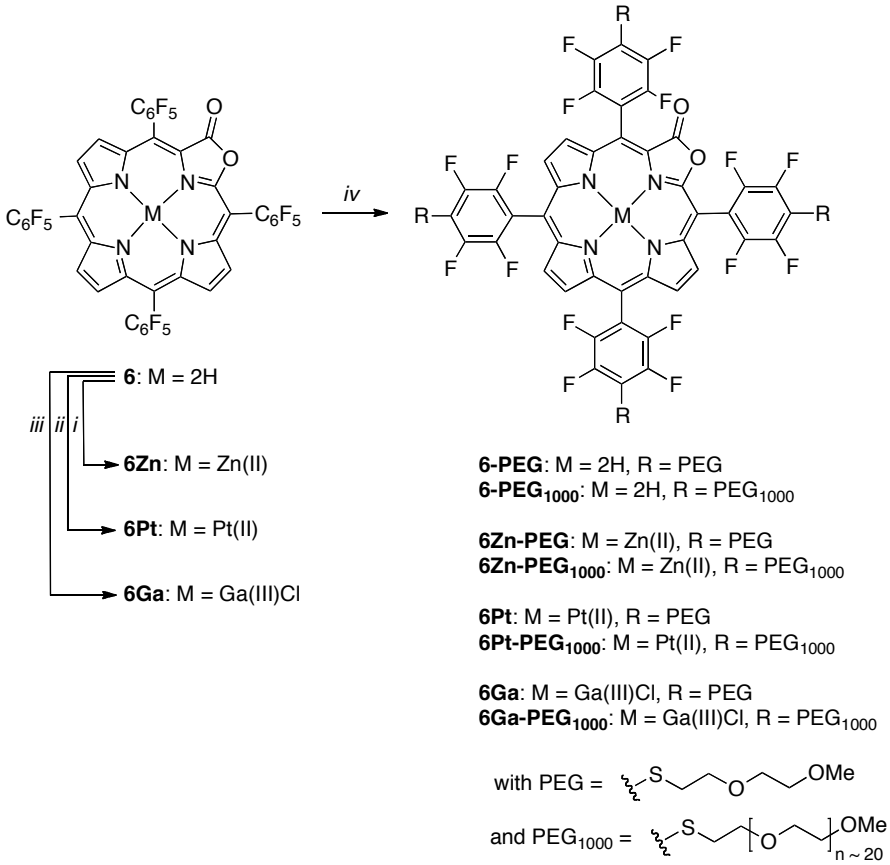

Scheme 4-2. *Reaction conditions:* i. $Zn(OAc)_2$/MeOH, $CHCl_3$, reflux; ii. $Pt(acac)_2$, PhCN, reflux; iii. $GaCl_3$, $NaOAc{\cdot}3H_2O$, CH_3COOH, MW; iv. H-PEG or H-PEG_{1000}, DMF, NEt_3, reflux.

4.2.2. Synthesis of PEGylated metalloporpholactones 6M-PEG/6M-PEG$_{1000}$

meso-Pentafluorophenyl-substituted porphyrins (and also other compounds) are susceptible to a nucleophilic aromatic substitution of the *p*-F atom with soft nucleophiles, such as sulfides.[33] This reaction was frequently used to functionalize porphyrins. We have also shown that oxazolochlorins are susceptible to this reaction, allowing the preparation of water-soluble derivatives when using thiol-terminated PEG chains as nucleophiles. Not surprisingly, the related pyrrole-modified metalloporpholactones **6M** are also susceptible to this reaction. Thus, reaction of **6M** with at least a 4-fold molar excess of 2-(2-methoxyethoxy)ethane thiol (PEG) under basic conditions (33% NEt_3 in DMF) provided **6M-PEG** (Scheme 4-2). The clean and diagnostic ^{1}H NMR spectra of these compounds confirmed the presence of four short PEG chains. However, full water-solubility could not be achieved with the short chains. We therefore reacted **6M** with a longer thiol-terminated PEG (PEG_{1000}). The molecular weight heterogeneity of the longer PEG allowed only the detection of peak clusters around a mass that suggested tetra-substitution had taken place and the ^{1}H NMR of the compounds was much obscured by the large number of methylene protons. On the other hand, the products **6M-PEG$_{1000}$** proved to be freely water-soluble. In the sensing experiments described below, we use only the PEG_{1000} derivatives in pure water as the solvent.

4.2.3. Colorimetric cyanide sensing

As described before, the UV-vis spectrum of free base porpholactones in organic solvents is porphyrin-like, and that of their metal complexes has some metallochlorin characteristics.ref The UV-vis spectrum of **6-PEG$_{1000}$** is also porphyrin-like with a weak longest wavelength absorbance band (λ_{max}) at 708 nm, i.e., substitution and solvochromic effects did not

significantly change the spectrum of the parent compound **6** in CH_2Cl_2 (Figure 4-1A and ESI). Likewise, the metallochlorin-like spectra of the PEGylated metallocomplexes are as previously described for the zinc and platinum complexes, respectively (Figures 4-1B and 4-1C). The spectrum of the gallium complex resembles that of the zinc complex (Figure 4-1D). Again this porphyrin is as expected.[34]

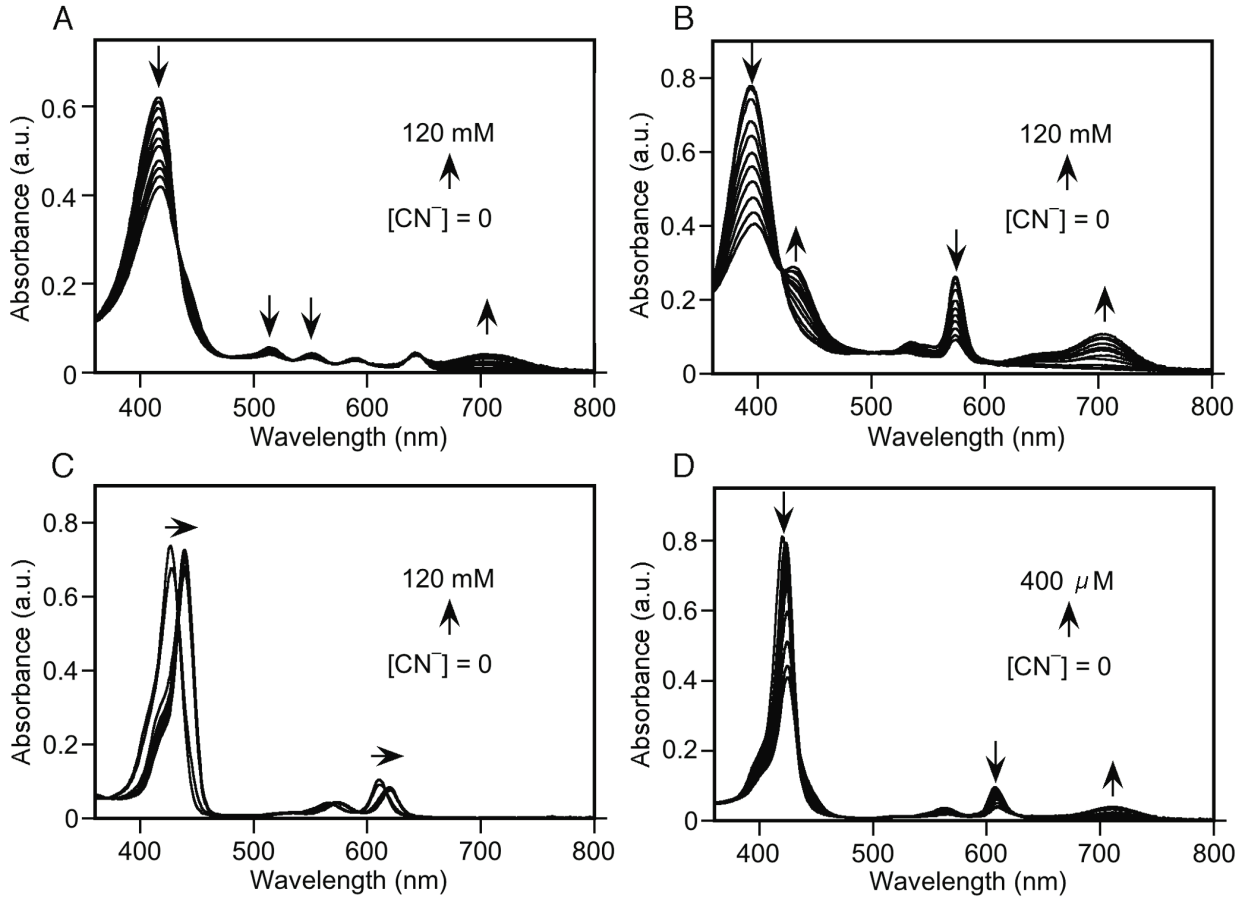

Figure 4-1. Spectrophotometric CN^- titration of the PEGylated porpholactones investigated, all in H_2O and CN^- in the form of NaCN; any dilution effects < 3%. A: **2-PEG$_{1000}$** (6.06×10^{-6} M). B: **2Pt-PEG$_{1000}$** (3.97×10^{-6}M). C: **2Zn-PEG$_{1000}$** (4.48×10^{-6} M). D: **2GaCl-PEG$_{1000}$** (5.10×10^{-6} M).

All compounds showed an optical response upon addition of cyanide (CN^-, in the form of an aqueous solution of NaCN) but their response profiles vary from each other (Figures 4-1A through 4-1D). Addition of CN^- to **6-PEG$_{1000}$** and **6Pt-PEG$_{1000}$** led to a decrease of the Soret band, the regular side bands diminished in intensity and a single new, broad, and much red-shifted band appeared (λ_{max} above 700 nm). This optical response was also observed for **2Pt** when exposed to high pH values (above 11.5).[31] The shift was deduced to be caused by a nucleophilic attack of the nucleophile OH^- (or alkoxides) to the lactone carbonyl group. Thus, we conclude that the response of **6Pt-PEG$_{1000}$** to CN^- can also be attributed to a similar attack that converts the sp^2-derivatized lactone carbonyl to a sp^3-hybridized cyanohydrin-like carbon (Scheme 4-2). Chemical reduction of the lactone also led to large optical changes in the resulting chromophore.[35] The anionic charge is likely also stabilized by interaction with the adjacent pentafluorophenyl moiety. The design of multiple other CN^- sensors also relied on the ability of CN^- to attack carbonyl groups, which is stabilized by an intramolecular hydrogen bond.[8,9]

Exposure of free base porpholactone **5** to strong base did not cause a nucleophilic attack but deprotonated the inner nitrogen. The much weaker base and stronger nucleophile CN^-, on the other hand, is also believed to add to the carbonyl functionality (Scheme 4-3). The sensitivity of the platinum complex toward CN^- is, however, much higher than that of the free base.

The optical response of the zinc complex **6Zn-PEG$_{1000}$** to CN^- differs fundamentally from that of the free base or platinum complex (and the gallium complex, see below). Addition of CN^- causes only a modest (~10 nm) bathochromic shift of the Soret and Q bands (Figure 1C). This response is similar to **1Zn** and can be attributed to the axial ligation of the CN^- to the central metal (Scheme 4-3).[17] The formation of square pyramidal complexes for the zinc

porphyrinoids is well known. Evidently, the association constant for this process is significantly higher than for the nucleophilic attack of CN^- to the lactone moiety of **6Zn-PEG$_{1000}$** for which we find no evidence.

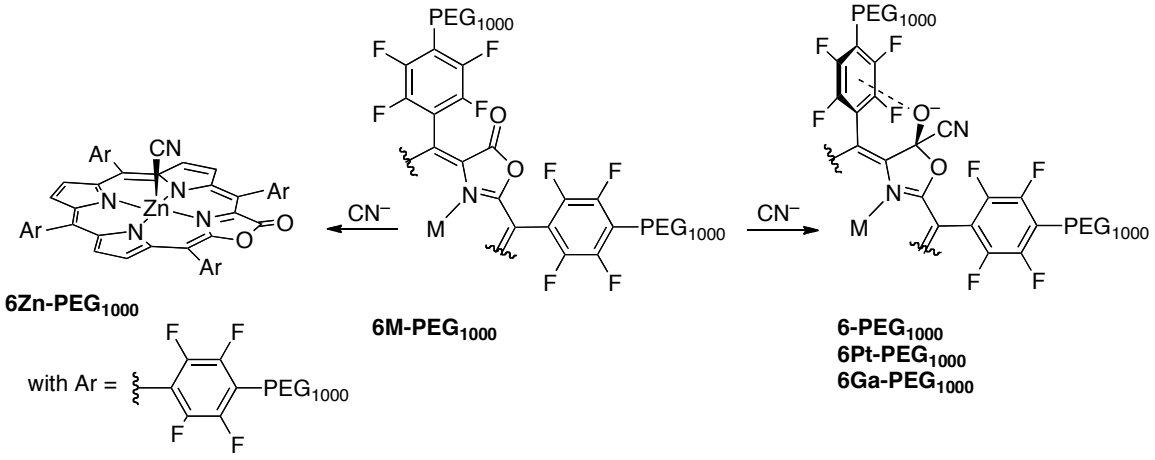

Scheme 4-3. Proposed cyanide sensing mechanism of **6M-PEG$_{1000}$**.

The response profile of the gallium complex to CN^- is similar to that of the platinum complex, suggestive of a nucleophilic attack onto the lactone, but significantly more sensitive, possibly a reflection of the higher charge of the central metal. We could not find any indication that the hard gallium(III) center has any affinity for cyanide as an axial ligand.

Thus, from a practical colorimetric assay point of view, the platinum and gallium complexes are thus the best sensors. The platinum complex **6Pt-PEG$_{1000}$** possesses a larger colorimetric response while the gallium complex **6Ga-PEG$_{1000}$** possesses the highest sensitivity. Particularly the ~100 nm peak separation between the spectra of the 'off' and 'on' stages of the sensor are particularly attractive.

4.2.4. Fluorimetric cyanide sensing

Fluorimetric sensing modes are generally more sensitive than comparable colorimetric modes.[36] The porpholactone zinc complex **6Zn-PEG$_{1000}$** is, like most zinc porphyrins, highly

fluorescent but this compound was deemed not to possess a large enough signal separation to be an attractive cyanide sensor (*cf.* Figure 4-1). Porphyrin platinum complexes are strongly luminescent but this luminescence is strongly partial oxygen pressure-dependent – platinum porphyrinoids, including **6Pt**, are therefore used as optical oxygen sensors.[29,30] We thus also did not deem this compound to be a practical sensor for CN^-. Gallium porphyrin complexes are chemically robust with respect to metal oxidation state and their resistance toward demetalation and they are fluorescent.[37] This provided the initial impetuous to prepare the gallium(III) complex **6Ga** and its corresponding PEGylated derivatives **6Ga-PEG** and **6Ga-PEG$_{1000}$**.

Indeed, **6Ga-PEG$_{1000}$** is fluorescent. The two-band emission spectrum is, mirroring the Q-band in its UV-vis spectrum, broad and featureless (Figure 4-1). A relatively low fluorescence yield of 0.7% was determined. More damaging to the utility of **6Ga-PEG$_{1000}$** as a (switch-on) fluorescence CN^- sensor, however, its cyanide-adduct is only very weakly fluorescing (ϕ was estimated to be well below 0.1%). (Figure 4-2). We suspect that the cyanohydrin anion species (cf. Scheme 4-2) is susceptible to a PET-quenching mechanism.

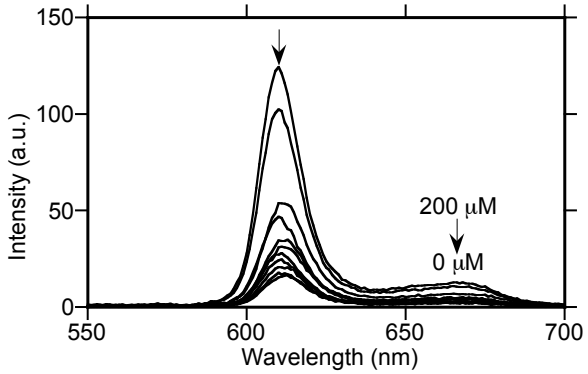

Figure 4-2. Fluorescence spectrum of **6Ga-PEG$_{1000}$** (5.10×10^{-7} M) in H_2O with 0-30 μL aq. NaCN (1.0×10^{-2} M) (λ_{em} = 418 nm).

4.2.5. Selectivity of the CN^- sensing in aqueous solutions

In the pH range between 5 and 9, the selectivity of the response for CN^- in water is excellent. No other commonly occurring anion (F^-, Cl^-, Br^-, I^-, AcO^-, ClO_4^-, NO_3^-, NO_2^-, $H_2PO_4^-$ and N_3^-, applied as their Na^+ salts) elicited a colorimetric response with **6-PEG$_{1000}$** and **6Ga-PEG$_{1000}$** even in the presence of large (50 molar equiv) excesses of the anions (Figure 4-3). Alas, at very low pH values, the free base porphyrin will become protonated and change its UV-vis spectrum dramatically; at very high pH values, the platinum complex can act, as described previously, as a high pH sensor.[31] The addition of CN^- to the aqueous solution of **6-PEG$_{1000}$** caused a color change from orange to yellow; the green color of **6Ga-PEG$_{1000}$** switched to yellow upon CN^- addition. The color change is 'instantaneous', i.e., completed upon mixing of the analyte and the sensor dye.

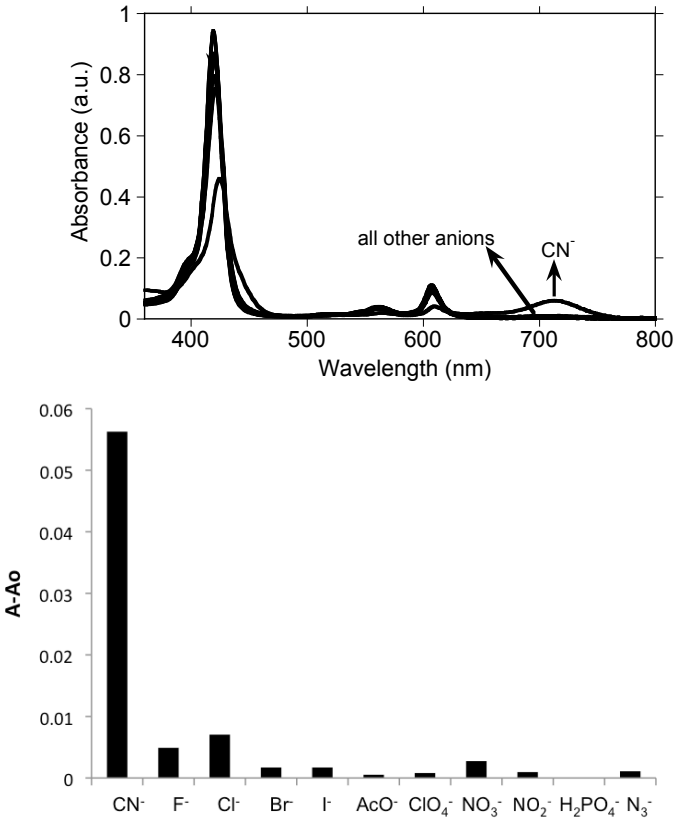

Figure 4-3. Absorbance intensity ratio ($A-A_o$) response of **6Ga-PEG$_{1000}$** upon the addition of various anions (50 equiv) in water: CN^-, F^-, Cl^-, Br^-, I^-, AcO^-, ClO_4^-, NO_3^-, NO_2^-, $H_2PO_4^-$, N_3^-.

4.3. Conclusions

We have shown that a class of pyrrole-modified porphyrins carrying a lactone functionality at the chromophore periphery can be utilized as an optical CN^- sensor. The porphyrinoids were made water-soluble through PEGylation for sensing in pure aqueous solutions. The sensing mechanism relies on a nucleophilic attack of the CN^- onto the lactone moiety, changing the hybridization of the carbonyl carbon. This results in the appearance of a dramatic (~100 nm) red-shifted band. We further showed the influence of the presence and nature of the central metal on the sensing profile. While the platinum complex exhibits excellent

CN^- sensing capabilities, the central metal is costly. Moreover, the sensor cannot be used as a fluorescent sensor in oxygenated environments. We thus tested the gallium(III) derivative. While it is highly fluorescent and highly specific in its response to CN^-, the CN^- addition product is very weakly fluorescing.

The value of this work lies in the demonstration that suitably chromophore-modified porphyrinoids can make excellent sensors. Furthermore, the variability of their central metals introduces a chance to widely tune the response of the sensor. Lastly, synthetic manipulations of the *meso*-aryl substituents allow the tuning of the solubility of the dyes. Once rarities, pyrrole-modified porphyrins, like the porpholactones investigated here, have recently become much more readily accessible.[20,31,38] We hope this study of this versatile class of dyes will inspire the further optimization of these chromophores as chemosensors for a variety of species.

4.4. Experimental

4.4.1. Materials and Instruments.

All solvents and reagents (Aldrich, Acros) were used as received. Flash column silica gel (premium grade, 60 Å, 32-63 μm) used was provided by Sorbent Technologies, Atlanta, GA. Porpholactone **6** and metalloporpholactone **6M** were prepared as described previously. The fluorescence quantum yield(ϕ) of 6Ga-PEG_{1000} was determined relative to those of *meso*-tetraphenylporphyrin (ϕ = 0.11 in benzene, calculated to be 0.09 in CH_2Cl_2); $\lambda_{excitiation} = \lambda_{Soret}$. ^1H and ^{13}C NMR spectra were recorded on Bruker Avance 300 or Avance II 400 instruments in the solvents indicated. UV-vis spectra were recorded on a Cary 50 spectrophotometer, fluorescence spectra on a Cary Eclipse, both Varian Inc. High and low resolution mass spectra were provided by the Mass Spectrometry Facilities at the Department of Chemistry, University of Connecticut.

4.4.2. UV-Vis and fluorescence spectroscopic titrations

All titrations were carried out in standard methacrylate cuvettes in H_2O at 25°C. The PEGylated dyes **6-PEG$_{1000}$, 6Pt-PEG$_{1000}$** and **6Zn-PEG$_{1000}$** were dissolved in H_2O and diluted to 10^{-6} M concentrations. A sodium cyanide (NaCN) stock solution of 5.0 M in H_2O was used as the source of CN^-. The absorbance was measured as aqueous CN^- solution were added by micropipette to 3 mL of the sensor dyes (additions ranged typically from 0 to 72 μL), **6Ga-PEG$_{1000}$** was dissolved in H_2O and diluted to 5.10×10^{-6} M. A sodium cyanide stock solution of 1.0×10^{-2} M was used as the source of CN^-. The absorbance was measured as aqueous CN^- solution was added by micropipette to 3 mL of the sensor dyes (additions ranged typically from 0 to 120 μL). All spectra are uncorrected.

In the fluorescence experiments, **6Ga-PEG$_{1000}$** was used because **6-PEG$_{1000}$, 6Pt-PEG$_{1000}$** are not fluorescent and although **6Zn-PEG$_{1000}$** is fluorescent it is not susceptible to nucleophilic attack of CN^-. The emission of **6Ga-PEG$_{1000}$** was measured from 450-880 nm as aqueous cyanide solution was added to 1.5 mL of **6Ga-PEG$_{1000}$** (5.10×10^{-7}M) in H_2O in portions (total volume: 0, 2, 4, 6, 8, 10, 12, 16, 20, 24, 30 μL of 1.0×10^{-2} M NaCN (Figure 2).

4.4.3. Synthesis of PEGylated metalloporpholactones

meso-Tetrakis(4-[2-(2-methoxyethoxy)ethane]thioxytetrafluorophenyl)porpholactone (6-PEG). Free base porpholactone **1** (20 mg, 2.0×10^{-5} mol) was dissolved in DMF:NEt_3 (2:1) (10.5 mL). 2-(2-methoxyethoxy)ethane (4 equiv, 11 μL) was added and the solution was heated to reflux for 1 h. The resulting solution was evaporated to dryness by rotary evaporation and purified by column chromatography (silica, CH_2Cl_2/5% MeOH) to provide **6-PEG** in near-quantitative yield (29 mg). ^{1}H NMR (400 MHz, $CDCl_3$, δ): 8.98-8.97 (m, 1H), 8.92 (d, J = 5.4 Hz, 2H), 8.85-8.84 (m, 1H), 8.85-8.80 (m, 1H), 8.72 (t, J = 4.7 Hz, 1H), 8.64 (d,

J = 4.7 Hz, 1H), 3.93-3.86 (m, 7H), 3.77 (dd, J = 8.2, 4.5 Hz, 1H), 3.70-3.66 (m, 7H) 3.54 (td, J = 5.9, 3.3 Hz, 8H), 3.46-3.41 (m, 9H), 3.31-3.30 (m, 14H), 3.10 (t, J = 3.0 Hz, 1H), 3.07-3.02 (m, 2H), 2.89 (q, J = 5.7 Hz, 1H), -1.73 (s, 1H), -2.03 (s, 1H) ppm; UV-vis λ_{max} (CH_2Cl_2) (Rel. Int.): 408 (1.0), 502 (0.05), 538 (0.04), 596 (0.05), 634 (0.05) nm; HR-MS (ESI+) calculated for $C_{63}H_{52}F_{16}N_4O_{10}S_4$: calc. 1457.2389, obs. 1457.2427.

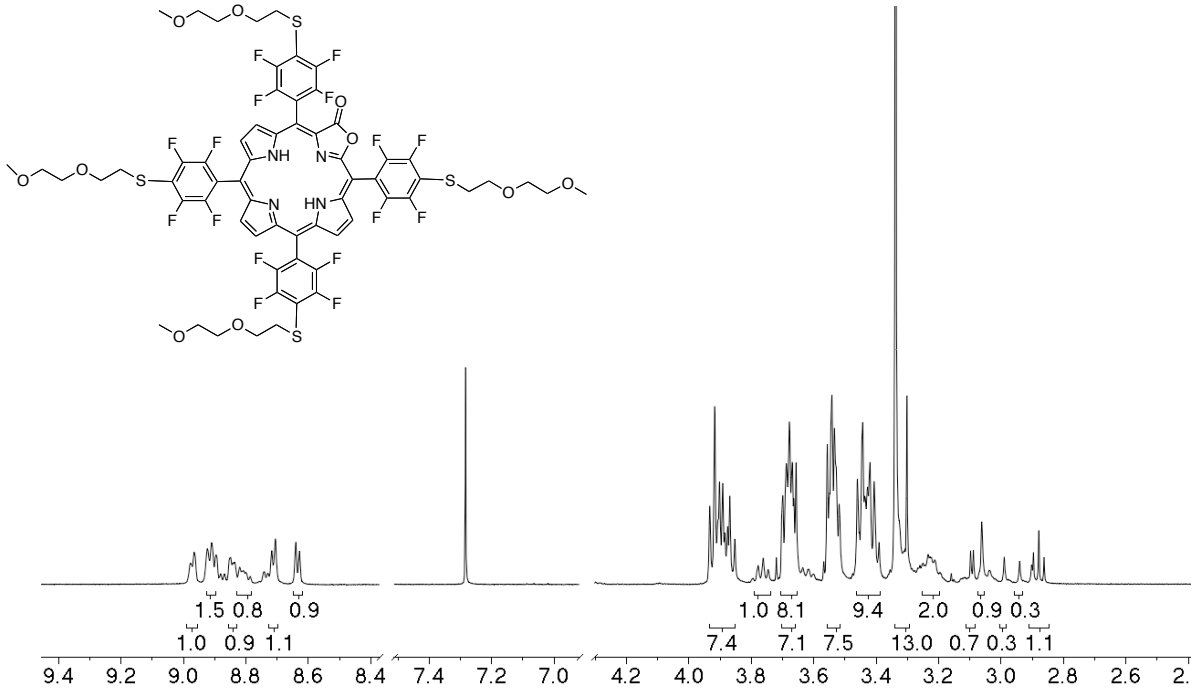

Figure 4-4. ^{1}H NMR spectrum (400 MHz, $CDCl_3$) of **6-PEG**.

***meso*-Tetrakis(4-PEG$_{1000}$thioxytetrafluorophenyl)porpholactone (6-PEG$_{1000}$).** This compound was synthesized using **1** (50 mg, 5.0×10^{-5} mol) and poly(ethylene glycol) methyl ether thiol (average M_n ~ 1,000) (~4 equiv, 202 mg) as described for the synthesis of 6-PEG. ^{1}H NMR (400 MHz, $CDCl_3$, δ): 8.96-8.93 (m, 1H), 8.90-8.87 (m, 2H), 8.83-8.78 (m, 1H), 8.69-8.68 (m, 1H), 8.62-8.60 (m, 1H), 3.94-3.37 (m, >400 H), -1.77 (s, 1H), -2.08 (s, 1H) ppm.

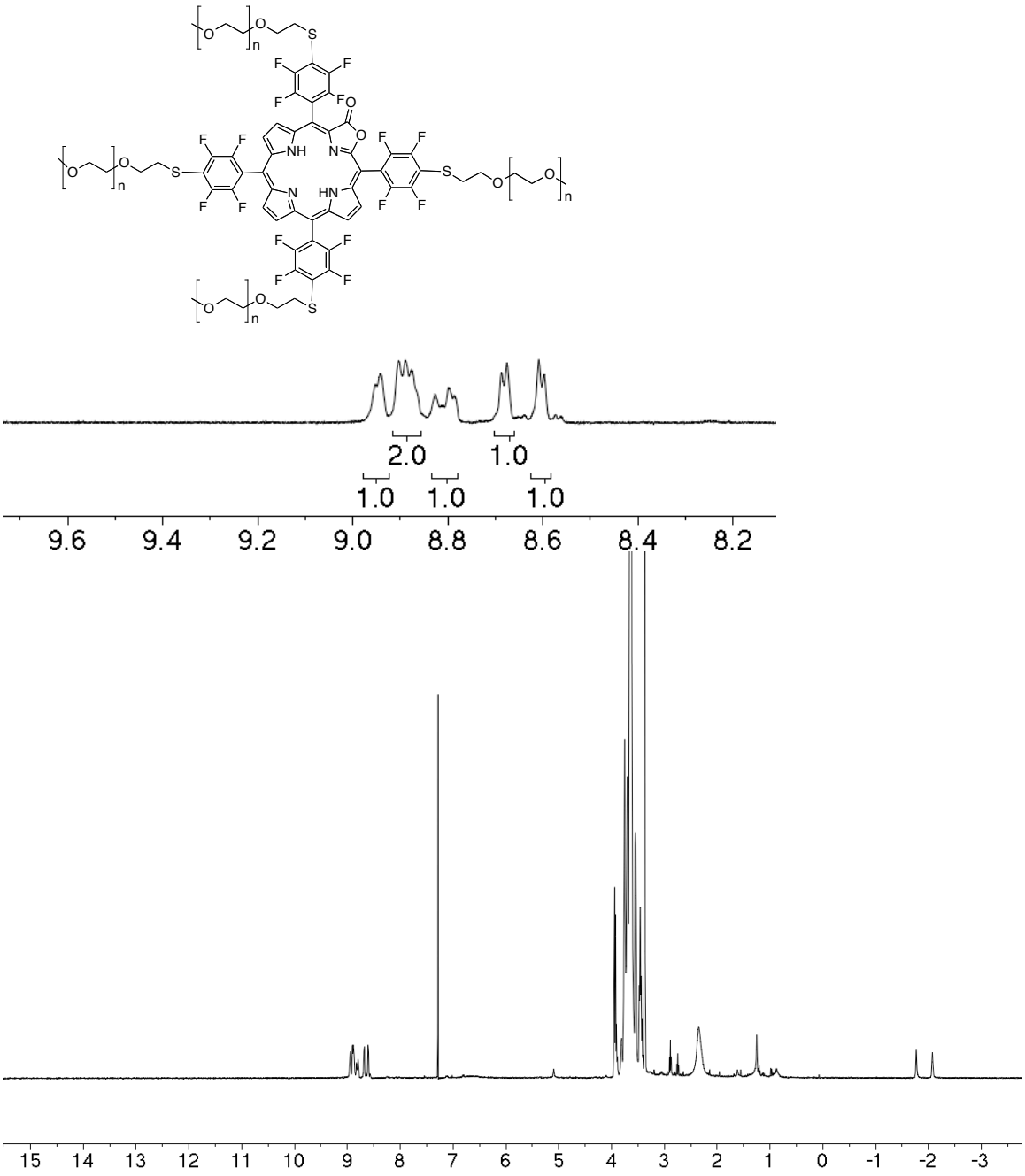

Figure 4-5. ^{1}H NMR spectrum (400 MHz, $CDCl_3$) of **6-PEG$_{1000}$** (n ~ 20).

[*meso*-Tetrakis(4-[2-(2-methoxyethoxy)ethane]thioxytetrafluorophenyl)-porpholactonato]platinum(II) (6Pt-PEG). This complex was prepared from **6Pt** (25 mg, 2.1 × 10^{-5} mol) was dissolved in DMF:Et_3N (2:1) (10.5 mL). 2-(2-methoxyethoxy)ethane (4 equiv,

12 μL,) was added and the solution was heated to reflux for 3 h. The resulting solution was evaporated to dryness by rotary evaporation and purified by column chromatography (silica, CH_2Cl_2/3% MeOH) to provide 6Pt-PEG in near-quantitative yield (31 mg). ^{1}H NMR (400 MHz, $CDCl_3$, δ): 8.78 (t, J = 2.5 Hz, 2H), 8.75 (s, 4H), 3.97-3.90 (m, 8H), 3.76-3.75 (m, 7H), 3.66-3.65 (m, 7H), 3.59-3.56 (m, 1H), 3.48-3.41 (m, 20H), 2.92 (t, J = 6.8 Hz, 1H) ppm; UV-vis (CH_2Cl_2) (Rel. Int.): 396 (1.0), 533 (0.07), 573 (0.32) nm; HR-MS (ESI+) calculated for $C_{63}H_{50}F_{16}N_4O_{10}S_4Pt$: $[M+H_2O]+$, calc. 1667.1908, obs. 1667.3102.

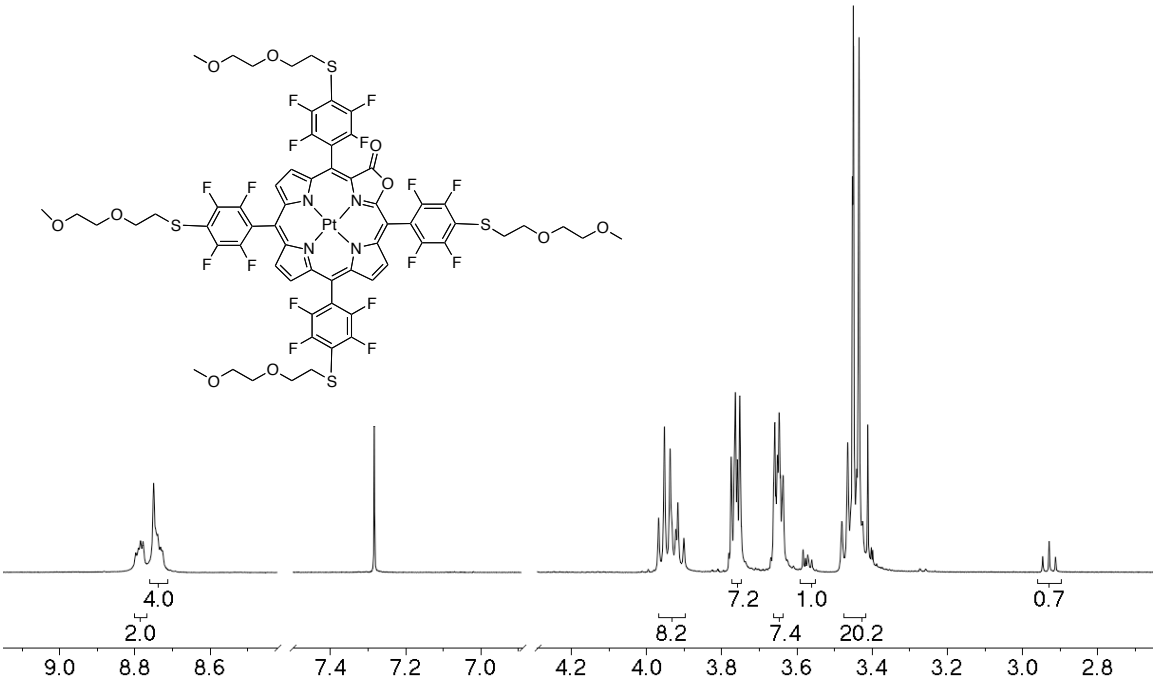

Figure 4-6. ^{1}H NMR spectrum (400 MHz, $CDCl_3$) of **6Pt-PEG**.

[*meso*-Tetrakis(4-PEG$_{1000}$thioxytetrafluorophenyl)porpholactonato]platinum(II) (6Pt-PEG$_{1000}$). This complex was prepared from **6Pt** (50 mg, 4.2×10^{-5} mol), poly(ethylene glycol) methyl ether thiol (average M_n ~ 1,000) (~4 equiv, 169 mg) in DMF:Et_3N (2:1)

(19.5 mL) as described for the synthesis of **6Pt-PEG**. ^{1}H NMR (400 MHz, CDCl3, δ): 8.76-8.66 (m, 6H) 3.91-3.35 (m, >400 H) ppm.

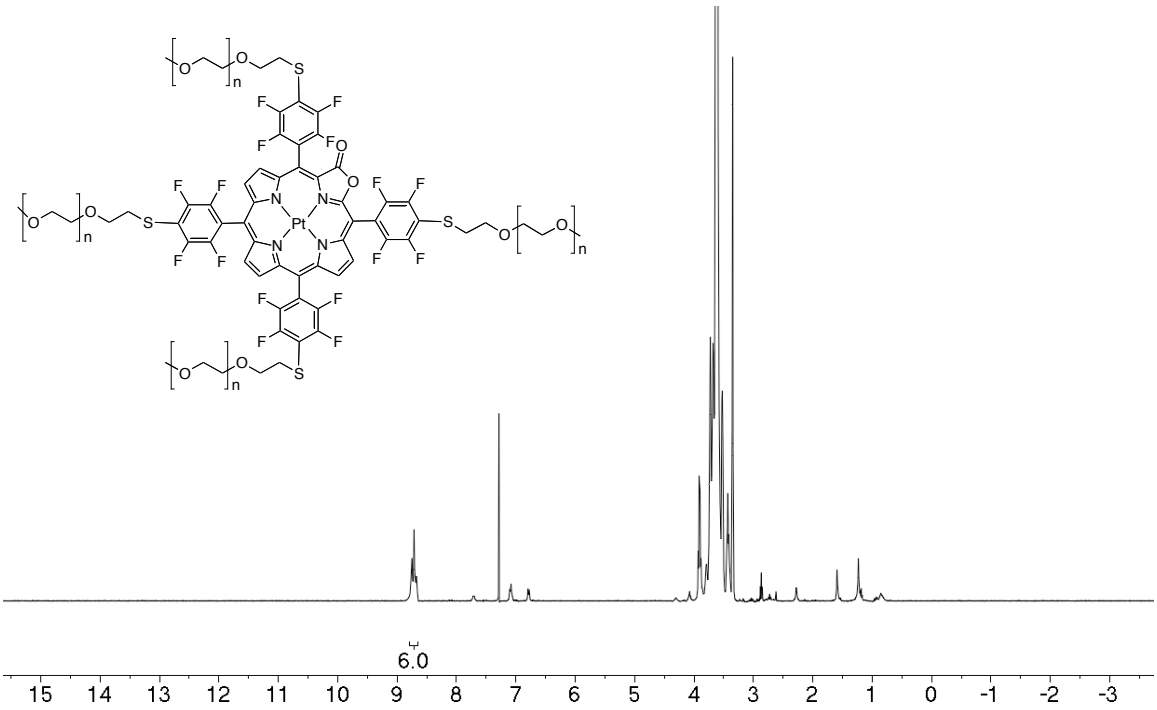

Figure 4-7. ^{1}H NMR spectrum (400 MHz, $CDCl_3$) of **6Pt-PEG$_{1000}$** (M_n ~ 1000).

[*meso*-Tetrakis(4-PEG$_{1000}$thioxytetrafluorophenyl)porpholactonato]zinc(II) (6Zn-PEG$_{1000}$). This complex was prepared from the zinc complex **6Zn** (30 mg, 2.8 × 10^{-5} mol), poly(ethylene glycol) methyl ether thiol (average M_n ~ 1,000) (~4 equiv, 114 mg) in DMF:Et_3N (2:1) (10.5 mL) as described for the synthesis of **6Pt-PEG**. UV-vis (CH_2Cl_2) (Rel. Int.): 426 (1.0), 565 (0.09), 610 (0.17) nm; ^{1}H NMR (400 MHz, $CDCl_3$, δ): 8.78-8.75 (m, 1H), 8.72-8.67 (m, 3H), 8.66-8.58 (m, 2H) 3.72-3.32 (m, >400 H), ppm

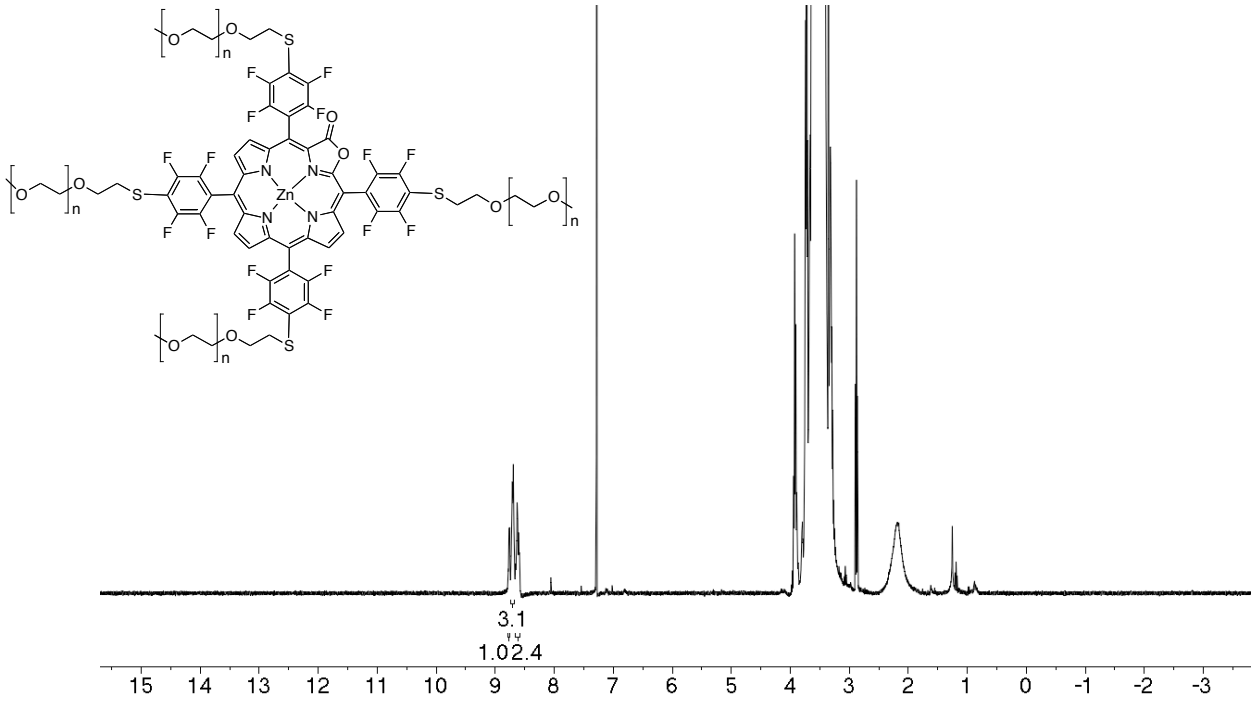

Figure 4-8. ^{1}H NMR spectrum (400 MHz, $CDCl_3$) of **6Zn-PEG$_{1000}$**.

Chloro-[*meso*-tetrakis(pentafluorophenyl)porpholactonato]gallium(III) (6Ga). In a 10 mL thick-walled tube containing a stir bar were placed free base *meso*-tetrakis(pentafluorophenyl)porpholactone **6** (50 mg, 5.04×10^{-4} mol), $GaCl_3$ (44 mg, 5 equiv.), sodium acetate trihydrate (45 mg, 3.14×10^{-4} mol) and acetic acid (5 mL). The vessel was sealed with a septum and placed in a microwave cavity. Using an initial microwave power of 200 W, the reaction mixture was heated from ambient temperature to 180°C and held at that temperature for 20 min, then cooled to 25°C. The reaction mixture was evaporated to dryness using rotary evaporation and the resulting crude product was purified by column chromatography (silica, CH_2Cl_2/50% hexane) to give **6Ga** (22 mg) in 40% yield with 55% recovery of **6**. R_f (silica, CH_2Cl_2/50% hexane) = 0.39. UV-vis λ_{max} ($CHCl_2$) (log ε): 418 (5.25), 564 (3.80), 611 (4.42) nm; IR: υ = 1782.6 (C=0) cm; Fluorescence (CH_2Cl_2, λ_{ex} = 418) (Rel. Int.) 614, 673 nm, ϕ = 0.0077; ^{1}H NMR (400 MHz, $CDCl_3$, δ): 9.00 (t, *J* = 5.3 Hz, 1H), 8.93 (dq, *J* = 16, 4.3 Hz, 3H), 8.9 (dt, *J* =

8.9, 4.6 Hz, 2H), 1H) ppm; ^{13}C NMR (100 MHz, CDCl3, δ): 170.9, 1687.9, 163.2, 154.1, 153.1, 150.9, 150.5, 150.0,147.2, 147.1, 145.1, 144.2, 141.7, 139.7, 139.53, 139.51, 137.2, 137.1, 137.0, 136.9, 134.8, 133.0, 132.9, 131.8, 131.2, 131.1, 130.1, 129.1, 126.3, 114.3, 111.0, 110.4, 106.6, 104.4, 86.91, 66.47, 66.15, 64.59, 56.14, 53.67, 32.19, 31.12, 29.9, 24.0, 22.8, 20.5, 14.4 ppm. HR-MS (ESI+ of MH+, 100% CH_3CN, TOF): m/z calculated for $C_{43}H_6ClF_{20}GaN_4O_2$: [M-Cl]+, calc. 1058.9427, obs. 1058.9401, [M-Cl+H_2O]+, calc. 1076.9533, obs. 1076.9499.

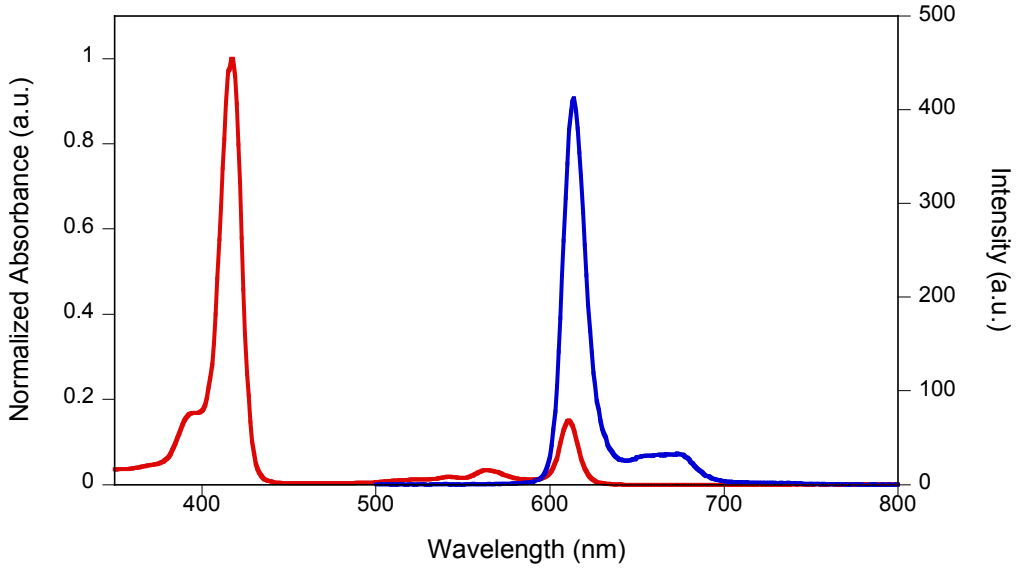

Figure 4-9. UV-vis and fluorescence spectrum (CH_2Cl_2) of **6Ga**.

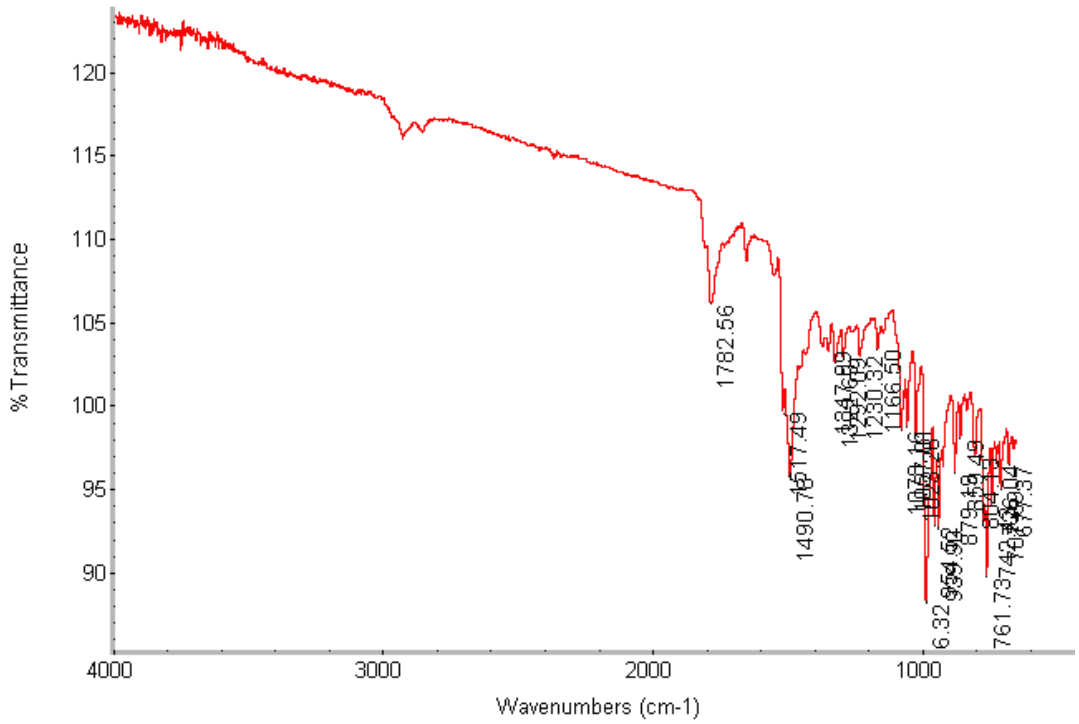

Figure 4-10. FT-IR spectrum (neat, diffuse reflectance) of **6Ga**.

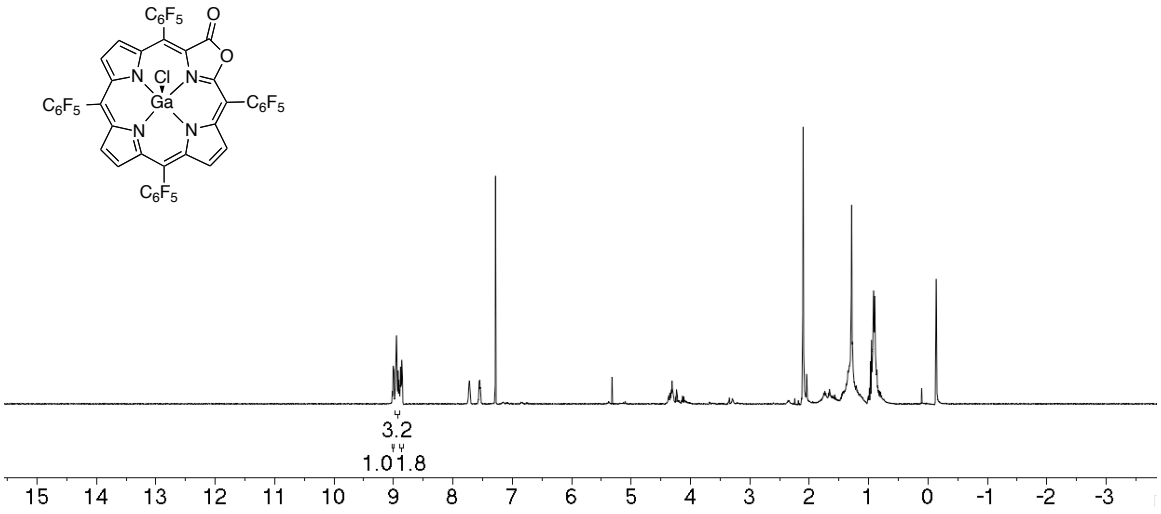

Figure 4-11. ^{1}H NMR spectrum (400 MHz, $CDCl_3$) of **6Ga**.

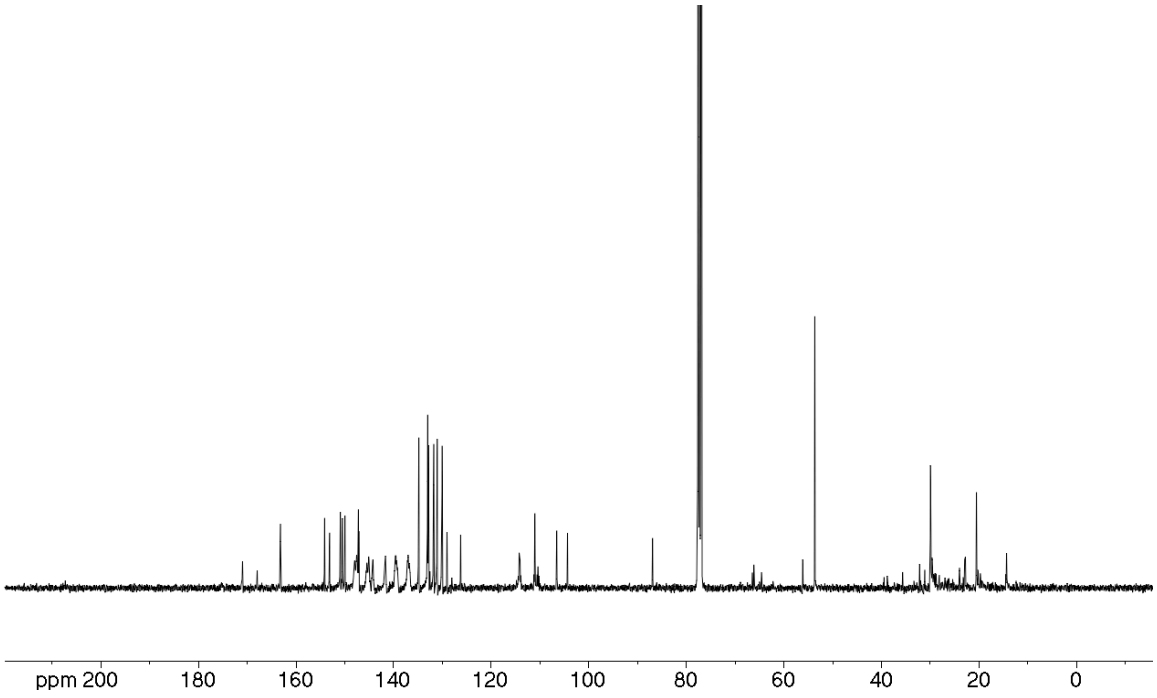

Figure 4-12. ^{13}C NMR spectrum (100 MHz, $CDCl_3$) of **6Ga**.

Chloro-[*meso*-tetrakis(4-[2-(2-methoxyethoxy)ethane]thioxytetrafluorophenyl)porpholactonato]gallium(III) (2Ga-PEG). The gallium complex **6Ga** (22 mg, 2.0×10^{-5} mol) was dissolved in DMF:Et_3N (2:1) (10.5 mL), 2-(2-ethoxyethoxy)ethane (4 equiv, 11μL,) was added and the solution was heated to reflux for 3 h. The resulting solution was evaporated to dryness by rotary evaporation and purified by column chromatography (silica, CH_2Cl_2/3% MeOH) to provide **6Ga-PEG** in near-quantitative yield (29 mg). ^1H NMR (400 MHz, CDCl3, δ): 9.04-8.84 (m, 6H), 3.99-3.90 (m, 8H), 3.78-3.75 (m, 7H), 3.65 (d, J = 3.2 Hz, 7H), 3.49-3.39 (m, 22H) ppm.

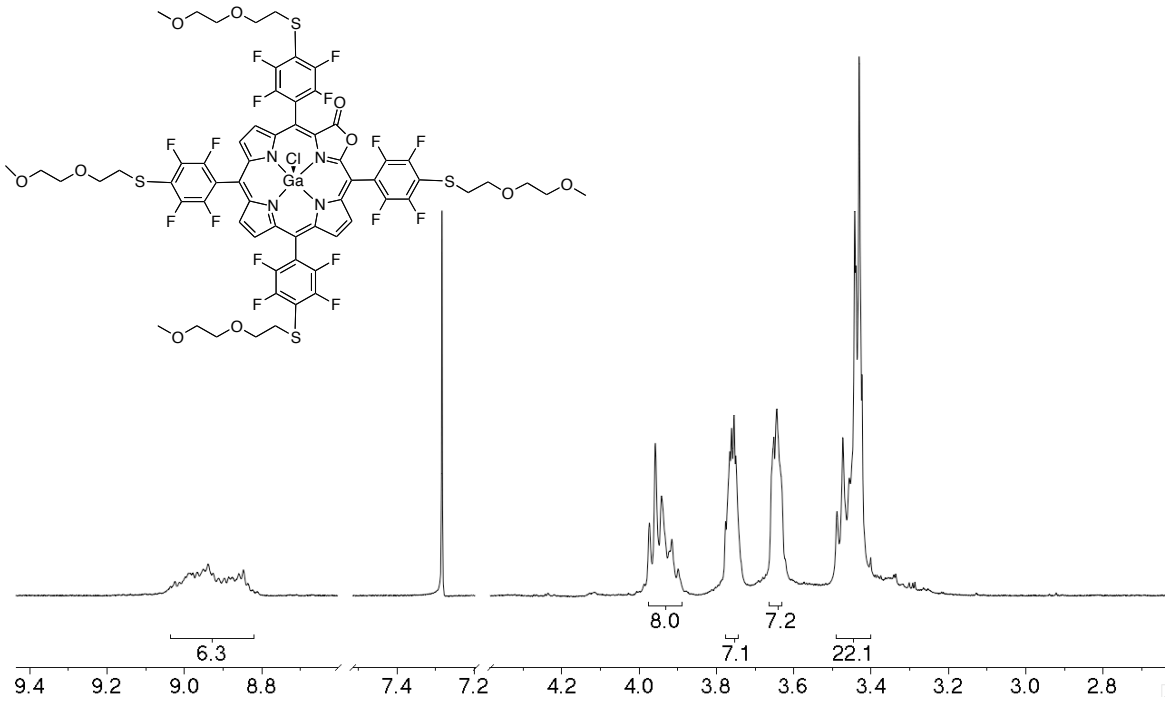

Figure 4-13. ^{1}H NMR spectrum (400 MHz, $CDCl_3$) of **6Ga-PEG**.

Chloro-[*meso*-tetrakis(4-PEG$_{1000}$thioxytetrafluorophenyl)porpholactonato]gallium(III) (6Ga-PEG$_{1000}$). This compound was prepared from the gallium complex **6Ga** (20 mg, 1.8×10^{-5} mol), poly(ethylene glycol) methyl ether thiol (average M_n 1,000) (4 equiv., 73 mg) in DMF:Et_3N (2:1) (10.5 mL) as described for the synthesis of **6Ga-PEG**. ^{1}H NMR (400 MHz, $CDCl_3$, δ): 9.01-8.79 (m, 6H) 3.75-3.38 (m, >400 H), ppm.

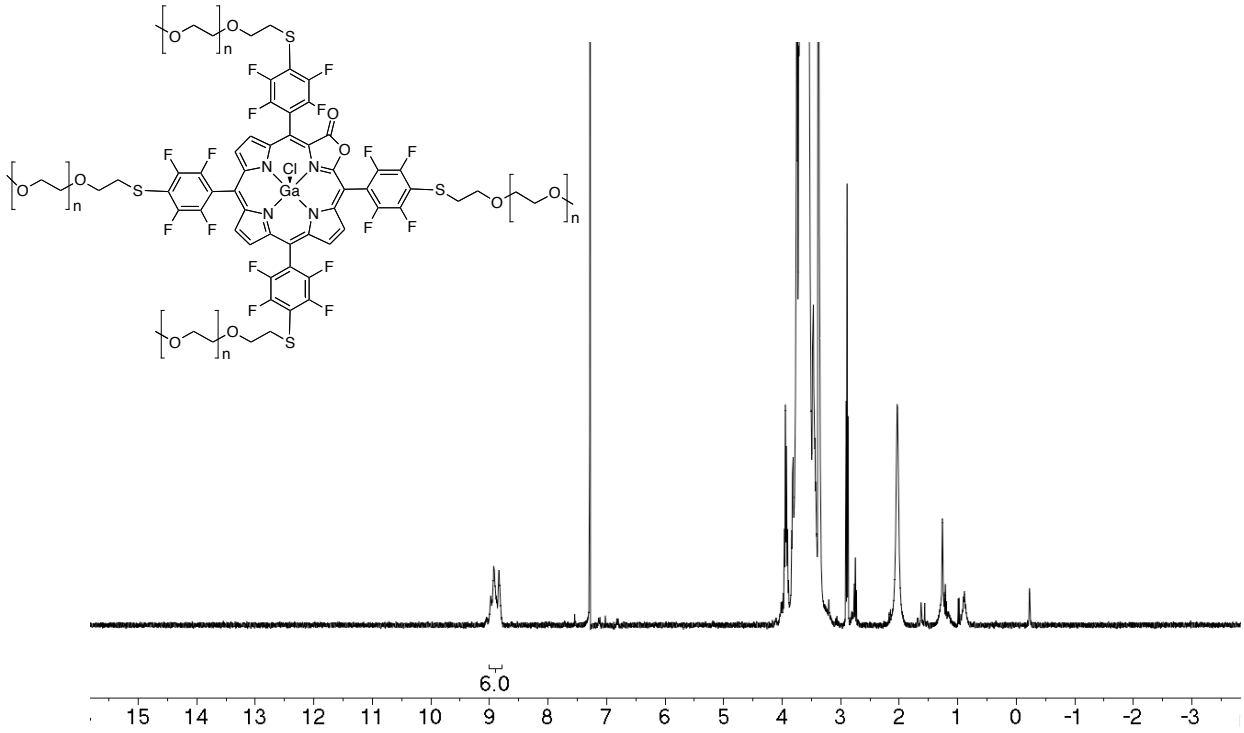

Figure 4-14. ^{1}H NMR spectrum (400 MHz, $CDCl_3$) of **6Ga-PEG$_{1000}$**.

4.5. References

(1) Xu, Z.; Chen, X.; Kim, H. N.; Yoon, J. *Chem. Soc. Rev.*, *39*, 127-137.

(2) Tomasulo, M.; Sortino, S.; White, A. J. P.; Raymo, F. M. *J. Org. Chem.* **2006**, *71*, 744-753.

(3) Tomasulo, M.; Raymo, F. M. *Org. Lett.* **2005**, *7*, 4633-4636.

(4) Lin, Y.-D.; Peng, Y.-S.; Su, W.; Tu, C.-H.; Sun, C.-H.; Chow, T. J. *Tetrahedron* **2012**, *68*, 2523-2526.

(5) Sun, Y.; Liu, Y.; Chen, M.; Guo, W. *Talanta* **2009**, *80*, 996-1000.

(6) Gotor, R.; Costero, A. M.; Gil, S.; Parra, M.; Martınez-Manez, R.; Sancenonacd, F.; Gavina, P. *Chem. Commun.* **2013**, *49*, 5669-5671.

(7) Afkhami, A.; Sarlak, N. *Sens. Actuators, B* **2007**, *122*, 437-441.

(8) Kim, D.-S.; Chung, Y.-M.; Jun, M.; Ahn, K. H. *J. Org. Chem.* **2009**, *74*, 4849-4854.

(9) Ding, Y.; Li, T.; Zhu, W.; Xie, Y. *Org. Biomol. Chem.* **2012**, *10*, 4201-4207.

(10) Sun, Y.; Liu, Y.; Chen, M.; Guo, W. *Talanta* **2009**, *80*, 996-1000.

(11) Lee, H.; Kim, H.-J. *Tetrahedron Lett.* **2012**, *53*, 5455-5457.

(12) Song, K. C.; Lee, K. M.; Nghia, N. V.; Sung, W. Y.; Do, Y.; Lee, M. H. *Organometallics* **2013**, *32*, 817-823.

(13) Yao, L.; Zhou, J.; Liu, J.; Feng, W.; Li, F. *Adv. Funct. Mater.* **2012**, *22*, 2667-2672.

(14) Hambright, P.; Langley, R. *Inorg. Chim. Acta* **1987**, *137*, 209-212.

(15) Chen, L. D.; Zou, X. U.; Buhlmann, P. *Anal. Chem.* **2012**, *84*, 9192-9198.

(16) Legako, J. A.; White, B. J.; Harmon, H. J. *Sens. Actuators, B* **2003**, *91*, 128-132.

(17) Liu, H.; Shao, X.B.; Jia, M.X.; Jiang, X.K.; Lia, Z.T.; Chen, G.J. *Tetrahedron* **2005**, *61*, 8095-8100.

(18) Kim, Y.-H.; Hong, J.-I. *Chem. Commun.* **2002**, 512-513.

(19) Crossley, M. J.; King, L. G. *J. Chem. Soc., Chem. Commun.* **1984**, 920-922.

(20) Gouterman, M.; Hall, R. J.; Khalil, G. E.; Martin, P. C.; Shankland, E. G.; Cerny, R. L. *J. Am. Chem. Soc.* **1989**, *111*, 3702-3707.

(21) Khalil, G.; Gouterman, M.; Ching, S.; Costin, C.; Coyle, L.; Gouin, S.; Green, E.; Sadilek, M.; Wan, R.; Yearyean, J.; Zelelow, B. *J. Porphyrins Phthalocyanines* **2002**, *6*, 135-145.

(22) McCarthy, J. R.; Melfi, P. J.; Capetta, S. H.; Brückner, C. *Tetrahedron* **2003**, *59*, 9137-9146.

(23) Brückner, C.; Akhigbe, J.; Samankumara, L. In *Handbook of Porphyrin Science*; Kadish, K. M., Smith, K. M., Guilard, R., Eds.; World Scientific: River Edge, NY, **2013**, accepted for publication.

(24) Cetin, A.; Ziegler, C. J. *Dalton Trans.* **2005**, 25-26.

(25) Rahimi, R.; Tehrani, A. A.; Fard, M. A.; Sadegh, B. M. M.; Khavasi, H. R. *Catal. Commun.* **2009**, *11*, 232-235.

(26) Liang, L.; Lv, H.; Yu, Y.; Wang, P.; Zhang, J.L. *Dalton Trans.* **2012**, *41*, 1457-1460.

(27) Gouterman, M.; Callis, J.; Dalton, L.; Khalil, G.; Mebarki, Y.; Cooper, K. R.; Grenier, M. *Meas. Sci. Technol.* **2004**, *15*, 1986-1994.

(28) Khalil, G. E.; Costin, C.; Crafton, J.; Jones, G.; Grenoble, S.; Gouterman, M.; Callis, J. B.; Dalton, L. R. *Sens. Actuators, B* **2004**, *97*, 13-21.

(29) Zelelow, B.; Khalil, G. E.; Phelan, G.; Carlson, B.; Gouterman, M.; Callis, J. B.; Dalton, L. R. *Sens. Actuators, B* **2003**, *96*, 304-314.

(30) Gouterman, M. *J. Chem. Educ.* **1997**, *74*, 697-702.

(31) Khalil, G. E.; Daddario, P.; Lau, K. S. F.; Imtiaz, S.; King, M.; Gouterman, M.; Sidelev, A.; Puran, N.; Ghandehari, M.; Brückner, C. *Analyst* **2010**, *135*, 2125-2131.

(32) Yu, Y.; Czepukojc, B.; Jacob, C.; Jiang, Y.; Zeller, M.; Brückner, C.; Zhang, J.L. *Org. Biomol. Chem.* **2013**, *11*, 4613-4621.

(33) Battioni, P.; Brigaud, O.; Desvaux, H.; Mansuy, D.; Traylor, T. G. *Tetrahedron Lett.* **1991**, *32*, 2893-2896.

(34) Coutsolelos, A.; Guilard, R.; Bayeul, D.; Lecomte, C. *Polyhedron* **1986**, *5*, 1157-1164.

(35) McCarthy, J. R.; Jenkins, H. A.; Brückner, C. *Org. Lett.* **2003**, *5*, 19-22.

(36) Fu, G.-L.; Zhao, C.-H. *Tetrahedron* **2013**, *69*, 1700-1704.

(37) *The Porphyrin Handbook*; Kadish, K. M.; Smith, K. M.; Guilard, R., Eds.; Academic Press: San Diego, 2000, 2003; Vol. 1-20.

(38) Yu, Y.; Lv, H.; Ke, X.; Yang, B.; Zhang, J. L. *Adv. Synth. Catal.* **2012**, *354*, 3509-3516.

5. General Introduction to Tandem Mass Spectrometric Investigations of Free Base Porphyrinoids and their Cobalt(III) Complexes

Many of the applications of porphyrins require chromophores with adjustable electronic (optical) properties. Thus, a significant body of work in contemporary porphyrin chemistry is devoted to the synthesis of porphyrin analogues, i.e., porphyrinoids with more than four pyrroles, derivatives in which a pyrrole within the ring was 'confused' (i.e., 2,4-linked instead of the regular 2,5-linkage), or altogether replaced with a non-pyrrolic heterocycle.[1-5] The group of Brückner is particularly interested in studying the latter class of compounds, whereby their primary synthetic methodology toward these systems is based on the step-wise functionalization of a regular synthetic porphyrin, such as *meso*-tetraphenylporphyrin.

In this chapter we will utilize electrospray ionization mass spectrometry (ESI-MS) as an instrument to investigate two aspects of the chemistry of a number of pyrrole-modified porphyrins and their cobalt(III) complexes. ESI-MS has been previously used in the analysis and characterization of metalloporphyrin axial ligand interactions. For instance, the loss of heme from hemoglobin and myoglobin was probed by collision-induced dissociation (CID).[6,7] We will investigate the energy of the interaction of axially bound imidazole ligands to twelve *meso*-aryl substituted porphyrinoid cobalt(II) complexes porphyrinoids. Secondly, we will compare the fragmentation patters observed for six free base *meso*-tetraphenyl-substituted porphyrinoids and their cobalt (II) complexes with each other. Lastly, we will investigate how the nature of the *meso*-aryl group affects the fragmentation behavior of porphyrins.

All of the pyrrole-modified porphyrins investigated were made by oxidative transformations of chlorin diol **4**, followed by subsequent reactions (Scheme 5-1).[8-13] An oxidation of diol **4** with DDQ generates the corresponding dione **7**,[14] a compound that was used,

for instance, in the synthesis of pyrrole-modified porphyrins and porphyrin oligomers.[15,16] Alternative syntheses for porpholactone **2**,[17-20] oxazolochlorin **6**[21-23]and dione **7**.[17,24,25] The Co(II) complexes were synthesized by metal insertion of the corresponding free base and selective UV-Vis spectra can been seen in Figure 5-1.

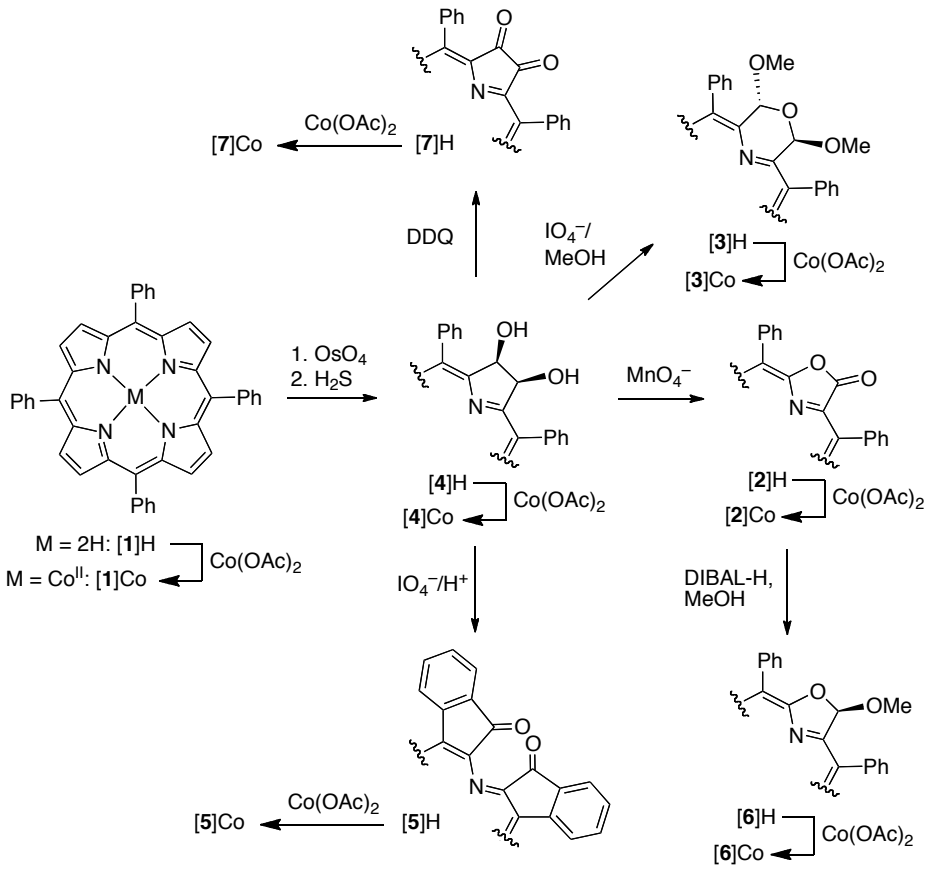

Scheme 5-1. Synthetic approach used to generate some of the porphyrinoids used in this study.

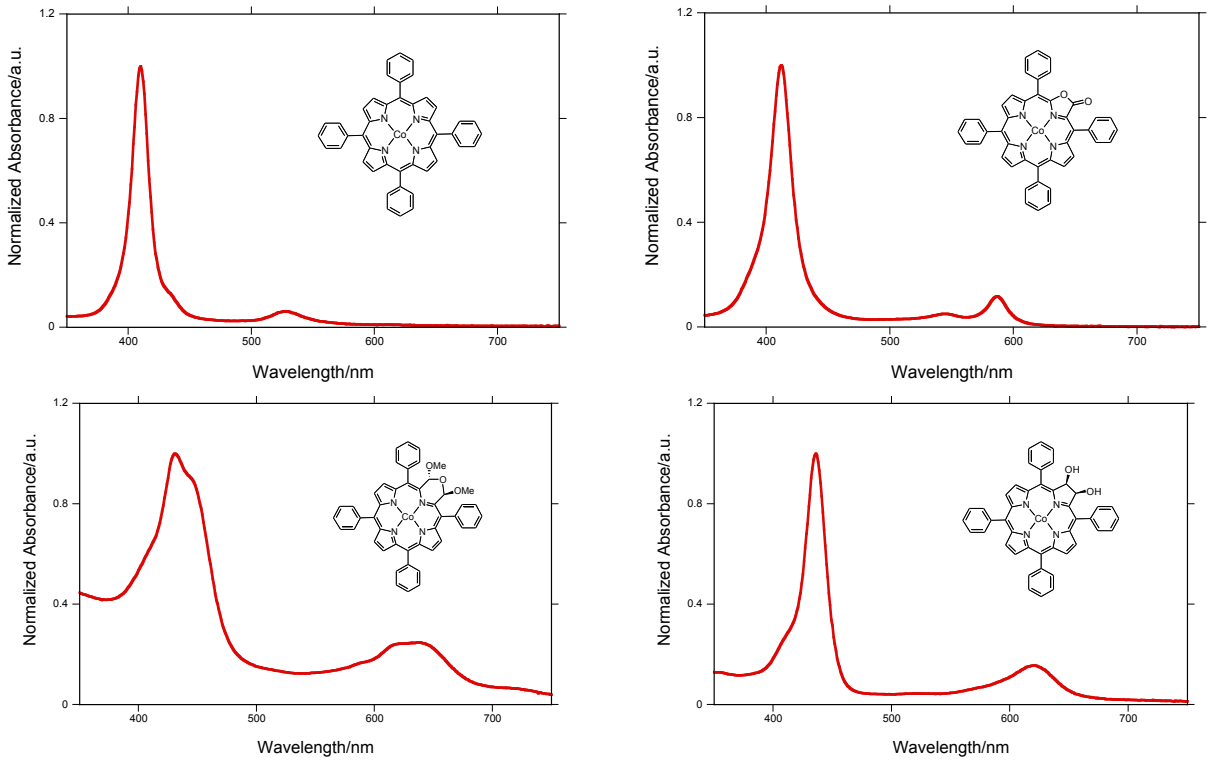

Figure 5-1. UV-vis spectra (CH_2Cl_2) of **1Co-4Co**.

5.1. Axial Imidazole Binding Strengths in Porphyrinoid Cobalt(III) Complexes as Studied by Tandem Mass Spectrometry

Most reactions of naturally occurring and synthetic metalloporphyrins involve non-covalent interactions between the metalloporphyrins and various axial ligands.[26,27] The presence of one or two axial ligands (L) expands the square planar N_4-donor set of the dianionic porphyrin ligand to form square pyramidal N_4L or octahedral N_4L_2 coordination spheres around the central metal, respectively (Figure 5-2).[28] In nature, the axial ligands are frequently imidazoles from His protein side chains.[27]The strength of this interaction is governed by the intrinsic strength of the σ-donor interaction of the nitrogen lone pair on the imidazole with the central metal. In proteins,

the imidazole is generally held in place by the protein, thereby greatly increasing its binding strength.

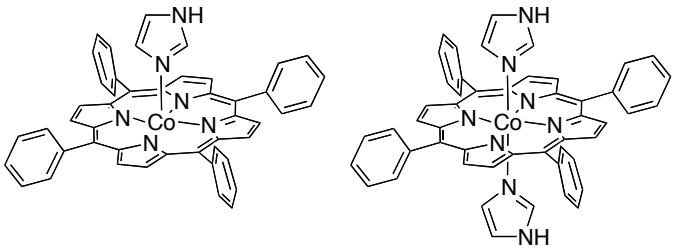

N_4L - square pyramidal
[**1**(Imi)]Co

N_4L_2 - octahedral
[**1**$(Imi)_2$]Co

Figure 5-2. Structures of **[1(Imi)]Co** and **[1(Imi)$_2$]Co** as representative for the two principle types of imidazole-metalloporphyrin complexes investigated.

Multiple studies have been performed to probe the interaction of metalloporphyrins with a variety of ligands and the binding constants derived were tabulated.[29,30] However, due to the limited water-solubility of many metalloporphyrins, it is difficult to study the macrocycle structure-dependence of these processes in aqueous media. To separate out solvent effects altogether, metal-ligand complexes have become the subject of gas-phase thermochemical studies.

Relative binding energies of non-covalent interactions can also be probed using conventional CID.[31] Energy-variable CID experiments using quadrupole ion traps to estimate the energetics of non-covalent binding parameters were popularized by the groups of McLuckey and Brodbelt.[32,33] This technique probes the kinetic stability of ions leading to thermodynamic estimates. While it is mostly used for the relative comparisons between similar complexes, a correlation between the energy-variable CID results and absolute dissociation energy was established, allowing the comparison of dissimilar systems.[34-37]

Several studies reported the use of energy-variable CID to obtain the relative binding order of various ligands to metalloporphyrins. The ligands probed included His-containing

peptides, other peptides, nitrogen bases and malaria drugs and their model compounds.[34-37] Those studies involved varying the ligands in complexes of a single metalloporphyrin, such as the Fe(III), Mn(III), and Co(III) complexes of *meso*-tetraphenylporphyrin **1**.[34]

We study here the effect of the porphyrin macrocycle structure on the axial ligand binding of their cobalt complexes, whereby we vary systematically only the structure of the porphyrinoid macrocycle, including a variation of the *meso*-substituents. This is the first study that compares the coordination properties of a range of pyrrole-modified porphyrins. As in previous work, we chose Co(III) as the central metal and imidazole as the axial ligand.[34,36] While the electronic structure of porphyrin cobalt complexes, the influence of halogen substitution on the porphyrins, and the influence of axial ligands has been thoroughly studied using experimental and computational methods, we are not aware of comparable investigations that studied the electronic structures of chlorin cobalt complexes.[38]

The porphyrins selected are the benchmark porphyrin [*meso*-tetraphenyl-porphyrinato]cobalt(II) **1Co** and its more electron-rich 3,4,5-trimethoxy derivative **9Co** (Figure 5-3). The optical properties of **1Co** and **9Co** are only very little different, highlighting the small interaction between the two essentially perpendicular π-systems on the *meso*-aryl rings and the porphyrinoid chromophore. The smaller *meso*-2-thienyl substituents (in **10Co** and **11Co**) can assume a much more co-planar conformation, enabling a much stronger interaction with the porphyrinic chromophore, while the sterically more demanding 3-thienyl substituent takes up an intermediate position between **10Co** and **1Co**.[11,39-41] Presumably the trend seen in the optical properties will also be reflected in the coordination properties of the central metal, a hypothesis as yet untested.

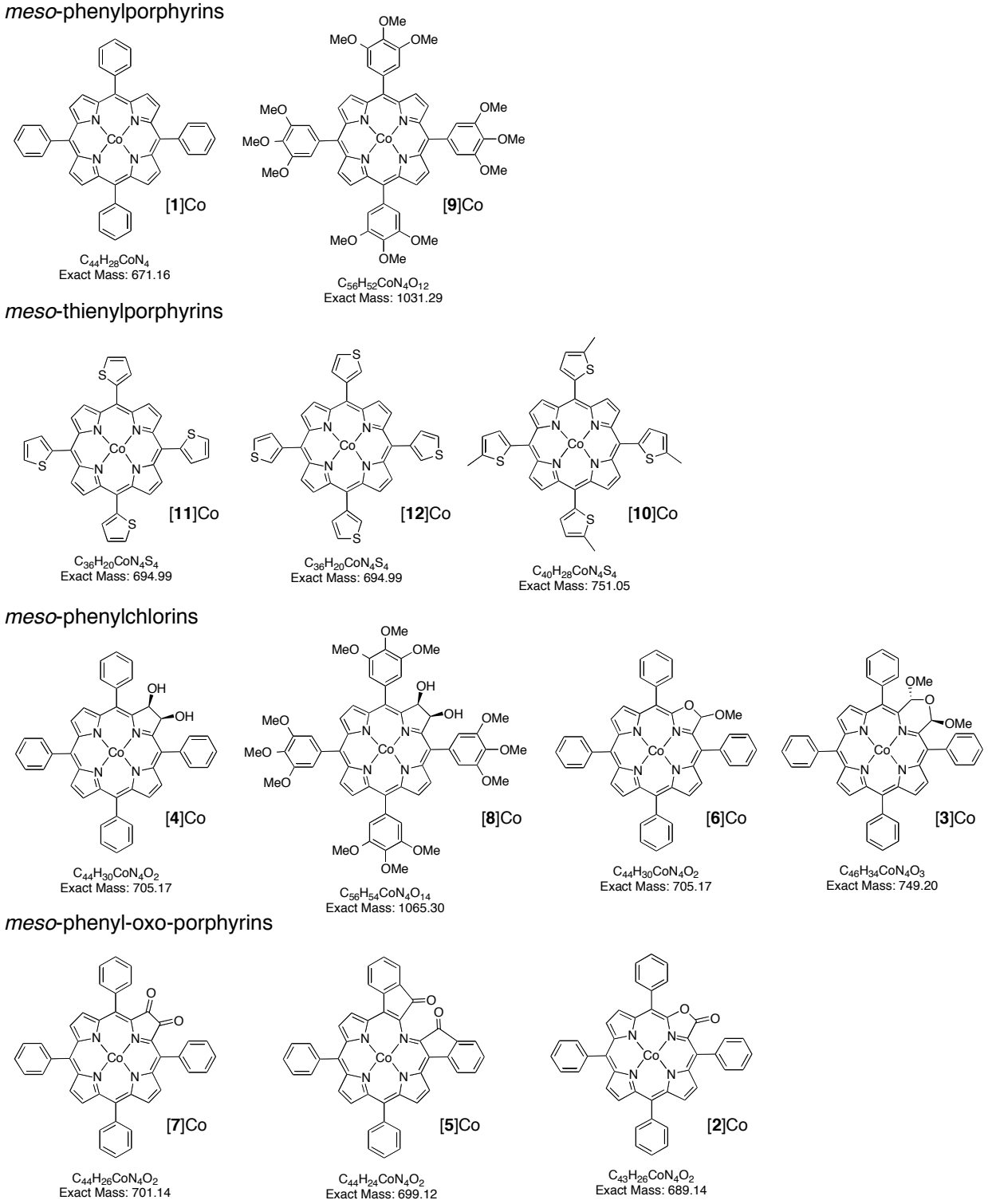

Figure 5-3. Structures of the twelve cobalt(II) porphyrinoid complexes investigated.

Metallochlorins **4Co** and **8Co** are the 2,3-dihydroxychlorin analogues to porphyrins **1Co** and **9Co**, respectively.[8] Owing to their nature as reduced porphyrins, they possess higher HOMO levels compared to porphyrins.[42] Thus, they may be considered more electron-rich (better e^--donors) than porphyrins. However, the parent *meso*-tetraphenylchlorin (*meso*-tetraphenyldihydroporphyrin) is reportedly less Brønsted-basic than the corresponding porphyrin and the pyrrolidine-M bonds in metallochlorin complexes are generally longer than the corresponding pyrrole-M bonds in porphyrins, suggesting that they are worse σ-donors.[39] The UV-Vis spectra of **4** and **4Co** are, as a result of the hydroxy substitution at the benzylic positions, not bathochromically shifted compared to those of porphyrins **1** and **1Co**, respectively, indicating that all three chromophores have very similar HOMO-LUMO gaps.[40] The inclusion of chlorins into this study will reveal to which extent their electronic structure will influence the binding of imidazole to their Co(III) complexes. A comparison of tetraphenyl-substituted tetra(3,4,5-trimethoxy)phenyl-substituted complex **4Co** and **9Co** will mirror the influence of the *meso*-aryl group that is observed between **1Co** and **9Co**, if any exists.

2,3-Dioxoporphyrin complex **7Co** is the oxidized version of chlorin **4Co** and porphyrin **1Co**.[14] As such, it is expected to be significantly less electron-rich. Porpholactone **2Co** is technically also an oxidized porphyrin.[9,41] The formal replacement of the pyrrole moiety in a porphyrin by an oxazolone moiety was shown to be barely reflected in the UV-Vis spectrum of the free base compound but to result in a metallochlorin-type spectrum of the metal complexes.[41] This is also the case for the **2Co** complex studied here. Its inclusion into the ligand binding study will reveal if it behaves more like a metalloporphyrin (**1Co**), a metallochlorin (**4Co**), or a metallodioxoporphyrin (**7Co**).

Reduction of porpholactone **2Co** generates a chlorin-like chromophore, a so called oxazolochlorin **6Co** (here in the form of its more tractable and stable methyl acetal).[21] As judged by its optical properties, its coordination properties are expected to be much more similar to those of diolchlorin complex **4Co** than those of porpholactone **2Co**. We also included two pyrrole-modified porphyrins, morpholinochlorin **3Co** and indaphyrin **5Co** in our study.[9,12] While free base morpholinochlorin **3** incorporating a six-membered ring in the macrocycle structure is nearly as planar as a porphyrin/chlorin and it possesses chlorin-like optical properties, its coordination properties may be significantly different than those of porphyrins or chlorins.[9] This is because this morpholinochlorin possesses a much-increased conformational flexibility than the parent porphyrin or chlorin.[43] Indaphyrin **5Co** is a severely non-planar porphyrinoid with an optical spectrum unlike that of any other porphyrin or chlorin.[11,12] Nonetheless, there are structural similarities to dioxoporphyrin **7Co** as both contain carbonyl groups at the (former) pyrrole β-positions.

5.1.1. Result and Discussion

Complex Ion Formation and Analysis

Singly charged [porphyrinato]Co(III)-imidazole complexes $[(Por)(Imi)]Co^{III}]^+$ and $[(Por)(Imi)_2]Co^{III}]^+$ were formed by injection of a mixture of acetonitrile solutions of imidazole and the porphyrinoid Co(II) complexes **1Co** through **12Co** into the ESI source. Ionization was brought about by a single electron oxidation in the source, a commonly observed phenomenon for Ni(II), Ag(II), Mn(II), Fe(II) or Co(II) porphyrins upon analysis by ESI-MS in the positive ion mode.[21,36]

All compounds under study formed complexes with one and two molecules of imidazole ($[(Por)(Imi)]Co^{III}]^+$ and $[(Por)(Imi)_2]Co^{III}]^+$, respectively). In CID experiments of both types of complex ions, the lowest energy dissociation process observed involved the loss of a single imidazole, resulting in the formation of the square pyramidal complex $[(Por)(Imi)]Co^{III}]^+$ in the case of dissociation of the octahedral complex $[(Por)(Imi)_2]Co^{III}]^+$ (Eq. 3), and the formation of the square planar complex $[(Por)Co^{III}]^+$ when the dissociation of $[(Por)(Imi)]Co^{III}]^+$ is considered (Eq. 4).

$$[(Por)(Imi)_2]Co^{III}]^+ \rightarrow [(Por)(Imi)]Co^{III}]^+ + Imi \qquad \text{(Eq. 3)}$$

$$[(Por)(Imi)]Co^{III}]^+ \rightarrow [(Por)]Co^{III}]^+ + Imi \qquad \text{(Eq. 4)}$$

The relative dissociation energies of the non-covalent complexes were obtained by energy-variable CID. Representative CID spectra for the dissociation of the $[(\mathbf{1})(Imi)]Co^{III}]^+$ and $[(\mathbf{1})(Imi)_2]Co^{III}]^+$ are shown in Figure 5-4, and a typical energy-variable CID curve (for the dissociation of the $[(\mathbf{1})(Imi)]Co^{III}]^+$) is shown in Figure 5-5. From these curves, the relative $E_{1/2}$ values for all mono- and bis-imidazole complexes were extracted (Tables 5-1 and 5-2).

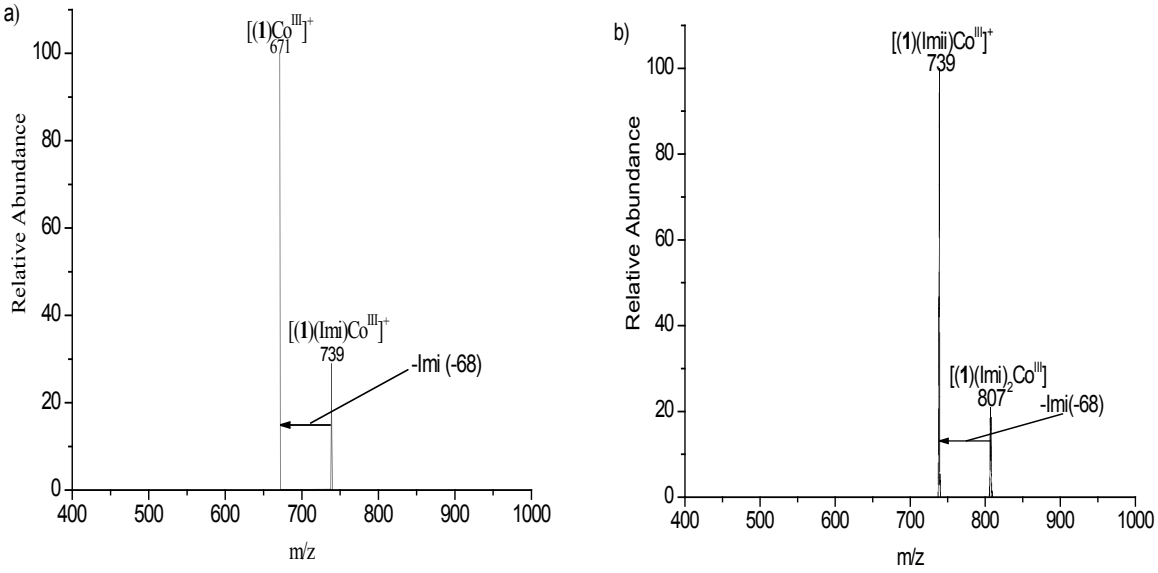

Figure 5-4. CID spectrum of complex of [**1Co**]$^+$ in the presence of imidazole. (a) CID of [(**1**)(Imi)]Co^{III}]$^+$ complex showing the loss of a single imidazole forming (**1**)Co^{III}]$^+$ (cf. to Eq. 3). (b) CID of [(**1**)(Imi)$_2$]Co^{III}]$^+$ complex showing the loss of a single axial imidazole forming [(**1**)(Imi)]Co^{III}]$^+$ (cf. to Eq. 4).

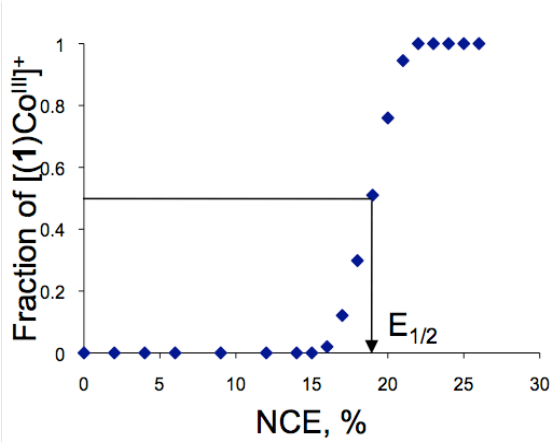

Figure 5-5. Energy-variable CID curve for [(**1**)(Imi)]Co^{III}]$^+$.

Brodbelt and co-workers showed that relative metal-ligand binding in systems of similar chemical character can be quickly screened by normalizing the $E_{1/2}$ values of the complexes with

respect to the number of DOF of all ligands coordinated to the central metal, here the DOF of the porphyrinoid and the axial imidazoles.[44] The systems in this study are quite comparable: they all possess identical axial ligand(s) and central metal and all are coordinated to a similar square planar dianionic porphyrinoid N_4 donor set. Thus, their similarity makes them excellent candidates for this approach. The resulting $E_{1/2}$' values representing the binding strength per DOF. The $E_{1/2}$' values allow a comparison of the relative binding energies. The higher the binding energy for a given dissociation process, the stronger the complex.

Relative binding strength of a single axial imidazole in the octahedral complexes $[(Por)(Imi)_2]Co^{III}]^+$

The $E_{1/2}$' values for the CID of bis-imidazole complexes of type $[(Por)(Imi)_2]Co^{III}]^+$ loosing a single imidazole (according to Eq. 3) vary between the twelve porphyrinoids investigated, with values range from 1.88 mV for the loss of a single imidazole from the chlorin complex $[(\mathbf{8})(Imi)_2]Co^{III}]^+$ to 3.12 mV for the corresponding process in the *meso*-thienylporphyrin complex $[(\mathbf{11})(Imi)_2]Co^{III}]^+$ (Table 5-1, Column D). But rather than analyzing this data in absolute terms, it might be more illustrative to compare the data trends expressed in terms of %change relative to the corresponding process in the benchmark tetraphenylporphyrin system $[(\mathbf{1})(Imi)_2]Co^{III}]^+$ ($E_{1/2}$' value of 2.55 mV). The relative change is listed in Table 5-1, Column E.

Table 5-1. Relative imidazole binding energies recorded for the dissociation of one imidazole ligand from $[(Por)(Imi)_2]Co^{III}]^+$ (Eq. 3).

Processes:		**A**	**B**	**C**	**D**	**E**
$[(\mathbf{Por})(Imi)_2]Co^{III}]^+ \rightarrow [(\mathbf{Por})(Imi)]Co^{III}]^+ + Imi$ (Eq. 3)		**$E_{1/2}$ (%NCE)**	**$E_{1/2}$ (V)**	**DOF (3N-6)**	**$E_{1/2}'$ (mV)**	**% Δ of $E_{1/2}'$ [Por]Co relative to $E_{1/2}'$ 1Co**
Porphyrins	**1Co**	17.4	0.711	279	2.55	–
	9Co	18.3	0.966	423	2.28	–11
Porpholactone	**2Co**	19.5	0.809	276	2.93	15
Chlorins	**4Co**	18.5	0.777	291	2.67	5
	8Co	15.2	0.819	435	1.88	–26
	3Co	19.5	0.804	312	2.58	1
	6Co	18.3	0.769	291	2.64	4
Oxoporphyrins	**5Co**	19.5	0.815	273	2.99	17
	7Co	18.3	0.766	279	2.75	8
meso-Thienylporphyrins	**10Co**	19.4	0.844	279	3.03	19
	11Co	18.2	0.759	243	3.12	22
	12Co	16.9	0.704	243	2.90	14

The data show some expected and some surprising trends, not all of which will find simple explanations. For instance, making the complex more electron-rich by means of decorating the *meso*-aryl groups with a total of 12 methoxy groups as in $[(\mathbf{9})(Imi)_2]Co^{III}]^+$, increases the electron density of the porphyrin donor set. In turn, this makes the cobalt center more electron-rich and, consequently, this reduction in Lewis acidity weakens the bond to the

axial imidazole by 11%. in part unexpected, the $E_{1/2}$' values measured for most chlorin complexes are only 1-5% elevated compared to the corresponding value of the benchmark porphyrin complex, except when the chlorin is combined with the electron-rich trimethoxyphenyl group. Thus, in complex $[(\mathbf{8})(Imi)_2]Co^{III}]^+$ the $E_{1/2}$' value is reduced by 26%, to 1.88 mV. On the other hand, the electron-poor, oxidized porphyrinoids porpholactone **2**, indaphyrin **5**, and dione **7**, all show 8 to 17% increased $E_{1/2}$' values, as could be expected based on the increased Lewis acidity of the central metal when coordinated to an electron-poor ligand.

The three thienylporphyrin complexes $[(\mathbf{10})(Imi)_2]Co^{III}]^+$ through $[(\mathbf{12})(Imi)_2]Co^{III}]^+$ show higher $E_{1/2}$' values than measured for a regular or even oxidized porphyrins (19%, 22%, and 14% higher than the benchmark porphyrin). This is surprising as the red-shifted optical spectra of the thienylporphyrins and their cobalt complexes suggested the presence of an electron-rich ligand. This is even though a red-shifted optical spectrum does only indicate a reduced HOMO-LUMO gap. In porphyrins, however, this is frequently achieved by the raising of the HOMO level by introducing electron-donating substituents to the chromophore.

The electronic structure of the octahedral d^6-complexes are similar in that all are singlet state compounds. Steric effects potentially also play a role in the modulation of the ligand binding strength but the immediate binding hemispheres around the central metals are believed to be very comparable across all complexes as none of the porphyrinoids investigated possess *ortho*-substituents on the *meso*-aryl groups. Before we interpret the finding any further, it is helpful to consider the trends measured for the $E_{1/2}$' values for the loss of the second imidazole from the square pyramidal complexes.

Relative binding strength of the axial imidazole in the square pyramidal complexes[(Por)(Imi)]Co^{III}]$^{+}$

The $E_{1/2}$' values for the CID of mono-imidazole complexes of type [(Por)(Imi)]Co^{III}]$^{+}$ loosing the lone imidazole to form the square planar complex [(Por)]Co^{III}]$^{+}$ (Eq. 4) vary substantially between the twelve porphyrinoids investigated, with values range from 1.50 to 3.50 mV (Table 5-2, Column D). This reflects the sum of the electronic effects of the various *meso*-substituents and porphyrinoid cores on the central Co(III) atom. Again, the $E_{1/2}$' values are best compared against that measured for the benchmark metalloporphyrin-imidazole complex [(**1**)(Imi)]Co^{III}]$^{+}$ (2.82 mV) (Table 5-2, Column E).

Table 5-2. Relative imidazole binding energies recorded for the dissociation of imidazole ligand from [(Por)(Imi)]Co^{III}]$^+$ (Eq. 4).

Processes:		**A**	**B**	**C**	**D**	**E**
[(**Por**)(Imi)]Co^{III}]$^+$ → [**Por**]Co^{III}]$^+$ + Imi (Eq. 4)		**$E_{1/2}$ (%NCE)**	**$E_{1/2}$ (V)**	**DOF (3N-6)**	**$E_{1/2}$' (mV)**	**% Δ of $E_{1/2}$' [Por]Co relative to $E_{1/2}$' 1Co**
Porphyrins	**1Co**	18.4	0.711	252	2.82	_
	9Co	18.5	0.935	396	2.36	–16
Porpholactone	**2Co**	15.4	0.600	249	2.41	–15
Chlorins	**4Co**	15.9	0.632	264	2.39	–15
	8Co	11.9	0.615	408	1.51	–46
	3Co	12.9	0.532	285	1.87	–34
	6Co	12.6	0.501	264	1.90	–33
Oxoporphyrins	**5Co**	17.5	0.692	246	2.81	0
	7Co	17.7	0.702	252	2.79	1
meso-Thienylporphyrins	**10Co**	19.2	0.793	252	3.15	12
	11Co	18.9	0.745	216	3.45	22
	12Co	17.5	0.690	216	3.19	13

Some trends mirror those found in the octahedral complexes, some are even more pronounced, but some cannot be gleaned from the octahedral complexes. For instance, making the complex more electron-rich, as in [(**9**)(Imi)]Co^{III}]$^+$, increases the electron density of the porphyrin donor set. In turn, this makes the cobalt center more electron-rich, reduces the Lewis acidity and thus weakens the bond to the imidazole donor. This is reflected in the reduction of the $E_{1/2}$' value by 16%, to 2.36 mV. Chlorin complex [(**4**)(Imi)]Co^{III}]$^+$ has a similarly reduced

$E_{1/2}$' value (-15%), to 2.39 mV, as is expected based on the elevated HOMO level of a chlorin compared to that of a porphyrin. Replacement of the *meso*-phenyl groups in this chlorin by the 3,4,5-trimethoxyphenyl groups reduces the $E_{1/2}$' value even further (by 46%) to the lowest value measured among all porphyrinoid complexes, 1.51 mV.

The other chlorin-type complexes, oxazolochlorin [(**6**)(Imi)]Co^{III}]$^+$ and morpholinochlorin [(**3**)(Imi)]Co^{III}]$^+$ possess near-identical $E_{1/2}$' values (1.87 and 1.90 mV) that are much below those of the chlorin complex [(**4**)(Imi)]Co^{III}]$^+$. Similarly, the $E_{1/2}$' values for the octahedral complexes did not differentiate the chlorins in that dramatic fashion, which may point, for instance, at spin state differences of the complexes of chlorin **4** vs. chlorins **3** and **6** that will inhibit the kinetics of the ligand loss.

Inversely, the two oxidized porphyrins, dioxochlorin [(**7**)(Imi)]Co^{III}]$^+$ and indaphyrin [(**5**)(Imi)]Co^{III}]$^+$ have, compared to the chlorins, identical and elevated $E_{1/2}$' values (2.79 and 2.81 mV), but they are essentially identical to $E_{1/2}$' value of the parent porphyrin complex [(**1**)(Imi)]Co^{III}]$^+$, and not above it. Despite the presence of the lactone carbonyl group, porpholactone complex [(**2**)(Imi)]Co^{III}]$^+$ is, with an $E_{1/2}$' value of 2.41 mV, in the range of an electron-rich porphyrin (such as [(**9**)(Imi)]Co^{III}]$^+$), but not as low as a chlorin. This may be an accurate reflection of its dual nature. In the free base form, porpholactones possess porphyrin-like optical spectra whereas in its metal complexes it is more chlorin-like, even though it lacks the chlorin-typical sp^3-carbons at the ß-position. The Brønsted basicity of the free base chromophore was also shown to be an order of magnitude lower than that of the corresponding porphyrin.

The three thienylporphyrin complexes [(**10**)(Imi)]Co^{III}]$^+$ through [(**12**)(Imi)]Co^{III}]$^+$ are characterized by similar and significantly higher $E_{1/2}$' values than measured for a regular (12%,

22%, and 13% higher than the benchmark porphyrin) or oxidized (electron-poor) porphyrins. This parallels the findings for the loss of the first imidazole from the octahedral complexes. It is well established that thienyl groups play a much stronger role in the electronic structure of the porphyrin than the phenyl ring.[45] Our gas-phase findings, in fact, correlate well with the solution data. Bhyrappa and Bhavana found that the first imidazole molecule binds 96% more strongly to [2-thienylporphyrinato]Zn(II) (the Zn analog of [(**11**)Co]) and 15% more strongly than to [tetraphenylporphyrinato]Zn(II) (Zn analog of [(**1**)Co]).[46] The same trend was reported for many other nitrogen bases and was explained by the greater inductive effect of the sulfur in 2-thienylporphyrins. Thus, the general trends within the gas phase binding data for the single imidazole in square pyramidal porphyrinoid Co(III) complexes are explained in a rather straightforward fashion while mostly fulfilling expectations based on established porphyrin chemistry principles.

The dissociation energy for the loss of one imidazole from the octahedral complex is, for example for the regular and thienylporphyrins, lower than the loss of the second imidazole. This surprises from a basic coordination chemistry point of view. The loss in ligand field stabilization energy accompanying the loss of one ligand is expected to be much larger than the increase in metal Lewis acidity caused by the loss of a donor atom. Thus, the loss of the first imidazole was expected to be associated with a significantly higher energy than the loss of the second imidazole. On the other hand, the chlorin complexes show the expected trend.

The explanation may lie in the technique used or it may point at fundamental electronic differences between square pyramidal Co(III) complexes of porphyrins and chlorin. Although it is tempting to directly compare the experimental relative binding energies of one and two imidazoles, one should exercise caution when using data derived from the energy-variable CID

experiments. Even though this technique has been routinely used to compare relative binding strengths of various non-covalent complexes, the premise for a valid comparison between two systems lies in similar vibrational properties of the two systems. [34-37,44] This is often satisfied by chemical similarities.[37] However, the vibrational properties of square pyramidal and octahedral complexes are substantially different from each other such that a direct comparison may lead to overreaching conclusions.

5.1.2. Conclusions

Energy-variable CID was used to determine the relative gas-phase binding strength of square pyramidal and octahedral Co(III) complexes of porphyrins, chlorins, and porphyrin-analogues to the first and second axially bound imidazoles. The loss of the imidazole from the octahedral complex largely follows expectations as the ligands dissociate the more readily the more electron-rich the porphyrin is believed to be. The relative energies required to dissociate the second imidazole from the square pyramidal complex also shows the influence of the macrocycle structure, but in a surprising fashion. While the chlorins show the trends that can be expected based on ligand field stabilization trends, namely that the loss of the last imidazole is per complex more readily accomplished than the loss of the first, the porphyrins and oxoporphyrins show the opposite trend. Here, the loss of the last imidazole is a higher energy process than the loss of the first. This finding points at a change of the electronic structure of the porphyrin cobalt complexes as compared to the chlorin cobalt complexes, and may also show the limits of the comparability of CID data for different species.

5.2. MS/MS Fragmentation Behavior Study of *meso*-Phenylporphyrinoids Containing Non-pyrrolic Heterocycles

The fragmentation pattern of *meso*-tetraphenylporphyrin **1** is known to involve, as expected, the loss of the phenyl groups while no significant fragmentation of the *meso*-phenyl groups attached to the porphyrin was observed.[47] Thus, as these compounds have become important in our work, and that of others, a better understanding of their MS fragmentation patterns became desirable. This provided for the impetus of the study presented here.

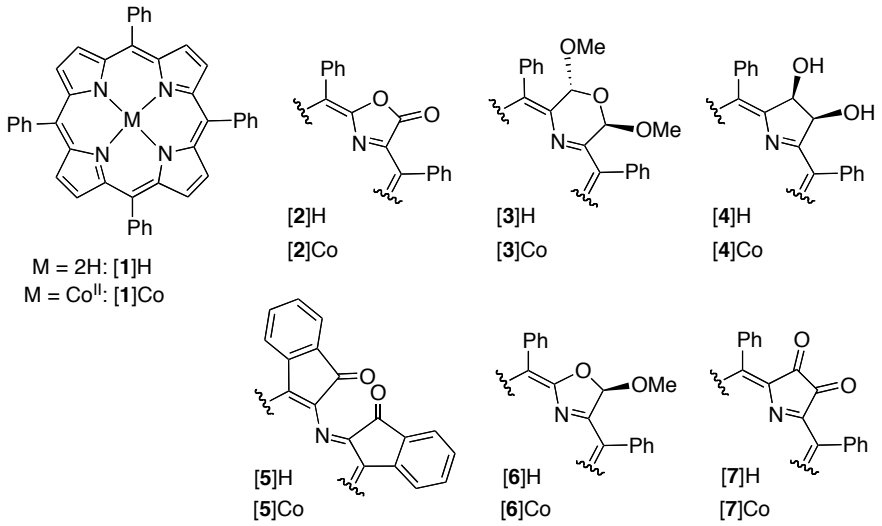

Compound	Molecular Formula	Exact Mass
[**1**]H	$C_{44}H_{30}N_4$	614.25
[**1**]Co	$C_{44}H_{28}CoN_4$	671.16
[**2**]H	$C_{43}H_{28}N_4O_2$	632.22
[**2**]Co	$C_{43}H_{26}CoN_4O_2$	689.14
[**3**]H	$C_{46}H_{36}N_4O_3$	692.28
[**3**]Co	$C_{46}H_{34}CoN_4O_3$	749.20
[**4**]H	$C_{44}H_{32}N_4O_2$	648.25
[**4**]Co	$C_{44}H_{30}CoN_4O_2$	705.17
[**5**]H	$C_{44}H_{26}N_4O_2$	642.21
[**5**]Co	$C_{44}H_{24}CoN_4O_2$	699.12
[**6**]H	$C_{44}H_{30}CoN_4O_2$	648.25
[**6**]Co	$C_{44}H_{32}N_4O_2$	705.17
[**7**]H	$C_{44}H_{28}N_4O_2$	644.22
[**7**]Co	$C_{44}H_{26}CoN_4O_2$	701.14

Figure 5-6. Structures and exact masses of the free base *meso*-tetraphenylporphyrinoids **1**-**7** and their cobalt(II) complexes **1Co**-**7Co** investigated.

Thus, we are reporting a comparison of the fragmentation patterns observed for six free base *meso*-tetraphenyl-substituted porphyrinoids and their Co(II) complexes (Figure 5-6) with each other and against the benchmark porphyrin **1** (as free base and cobalt complex) when subjected to +ESI tandem mass spectrometry conditions. All members of the investigated group are well described by spectroscopic or structural methods.[10,12-14,40] Therefore, the aim of this study is not on their structural characterization. Instead, focus is on the identification of

diagnostic fragmentations for the porphyrinoid classes studied. Perhaps some of these fragmentation patterns illustrate general reactivity trends for other pyrrole-modified porphyrins. Further, some fragmentation may reveal low energy pathway reactions that are suggestive of novel bulk transformations for this class of porphyrinoids.

5.2.1. Results and Discussion

The ESI CID spectra of all free base porphyrinoids and their cobalt(II) complexes investigated were recorded in the positive ion mode. Representative MS^2 fragmentation spectra are shown, while all other spectra are not shown. The free base porphyrinoids are ionized by protonation (forming $[MH]^+$), while the Co(II) complexes are ionized to the singly charged Co(III) porphyrin cations by electrochemical oxidation during the electrospray process (forming $[M]^+$).[21] Thus, the free base and cobalt complexes can reveal the macrocycle fragmentations induced by two different ionization mechanisms. Moreover, the templating effect of the metal is likely also having an effect on the fragmentation of the macrocycles.

*MS-MS Fragmentation Patterns Observed for meso-Tetraphenyl-substituted Porphyrinoids **2** through **7** and their Respective Cobalt Complexes **2Co** through **7Co***

The MS/MS of our benchmark free base compound **1**, i.e., its monoprotonated form $[\mathbf{1H}]^+$ shows, as described before, a simple fragmentation pattern which shows primarily the characteristic loss of one (major path) and two (minor path) phenyl groups.[47] While some loss of single hydrogen atoms is also detectable, no appreciable loss of carbon fragments that would indicate the fragmentation of the ring are observed. The MS/MS spectrum of the corresponding benchmark metalloporphyrin $[\mathbf{1Co}]^+$ shows exclusively the loss of one and two phenyl radicals, respectively (Scheme 5-2). These fragmentation patterns illustrate the general high stability of

the free base porphyrin macrocycle that is even further increased by coordination to cobalt(III) (or, any other metal forming stable porphyrin complexes).[47,48]

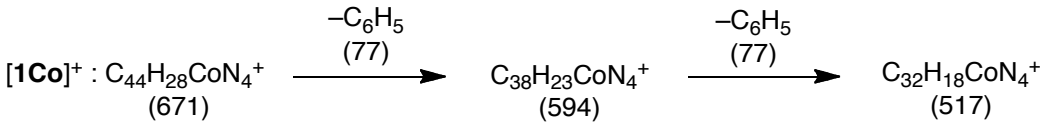

Scheme 5-2. Interpretation of the ESI+ CID spectra of [**1Co**]$^+$.

A chlorin is a 2,3-dihydroporphyrin. The presence of the reduced β,β'-double bond and the diol functionality in dihydroxychlorin **4** are directly reflected in its ESI MS/MS spectra, whereby the free base and cobalt complex show different patterns. The main fragmentation of the protonated free base chlorin [**4H**]$^+$ is the loss of H_2O, followed by the loss of two H_2O, the loss of one H_2O and one CO, or one H_2O, one CO, and one CH_2 group (Figure 5-7). These fragmentations can be readily rationalized by considering the fragmentation of the 2,3-dihydroxypyrrolin moiety only, whereby solution phase precedents for most of the hypothesized intermediate structures exist (Scheme 5-3).

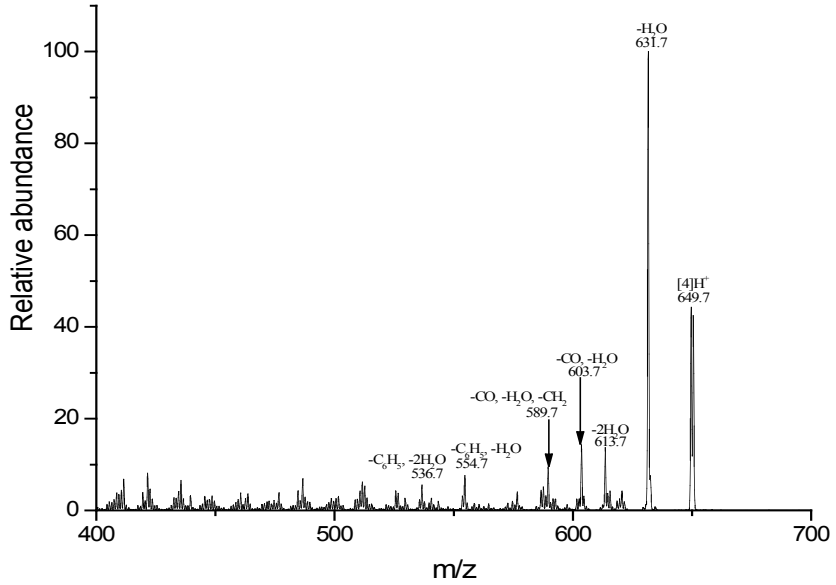

Figure 5-7. ESI(+) MS/MS spectrum of [**4H**]$^+$.

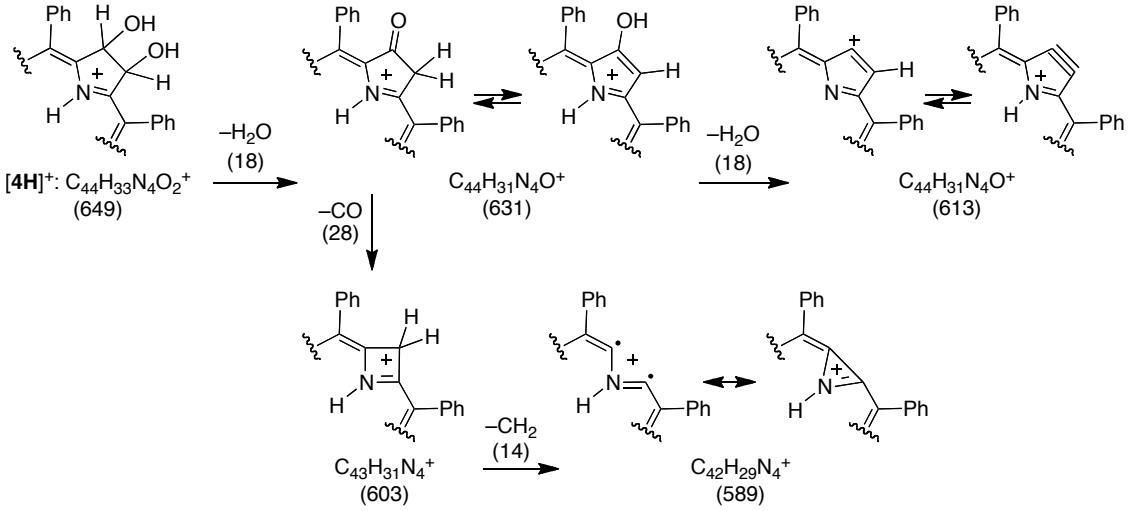

Scheme 5-3. Interpretation of the ESI+ CID spectra of [**4H**]$^+$. See Figure 5-7 for a reproduction of the MS/MS spectrum of [**4H**]$^+$.

The loss of H_2O leads to the formation of a well-known oxochlorin.[49] It can made in the bulk phase along an analogous route: the acid-induced dehydration of **4**.[50] This species, accessible also via alternative routes, can exists in two tautomeric forms.[51-53] Further loss of H_2O

leads to the formation of a cationic species that may possess benzyne-type character. Loss of CO from the oxochlorin-type intermediate can be understood as a typical carbonyl fragmentation, likely leading to the formation of an azeteochlorin structure. The presence of a four-membered ring in a porphyrin-like ring structure was previously shown not to distort the conformation of the idealized planar macrocycle.[19,54] The azete ring further fragments by losing a CH_2 fragment, leading to either the formation of a resonance-stabilized diradical or an azirene-substituted pyrrole-modified ring. We conclude that the CH_2 fragment originated in the azete moiety as this is the only likely source of a methylene fragment. Porphyrin analogue in which a pyrrole was reduced to an imide linkage, are known (these compounds are known as chlorophins)[55-58], but azirene-substituted pyrrole-modified are as yet unknown. As the fragmentations of a number of chromophores detailed below will show, the occurrence of the putative four- and three-membered ring analogues are commonly observed fragment ions for the pyrrole-modified porphyrins.

The fragmentation spectrum of the dihydroxychlorin cobalt complex $[\mathbf{4Co}]^+$ is different from that of its free base (Figure 5-8, Scheme 5-4). As the primary fragmentation channel, the loss of one or two $OH^{\cdot}$ radicals is observed. The loss of one hydroxyl radical generates a radical that is in a benzylic position with respect to the porphyrin π-system and, thus, well stabilized. The loss of two hydroxyl radicals reconstitutes the parent metalloporphyrin cation $[\mathbf{1Co}]^+$. It therefore does not surprise that the loss of a phenyl group is a subsequent fragmentation.

In addition, the loss of a 56 Da species from $[\mathbf{4Co}]^+$, followed by a hydroxyl radical, combining to a total loss of a 73 Da, is observed. HR-MS indicated this fragment possessed the composition $C_2H_3NO_2$. A continuous fragment of the required composition is highlighted in bold in the structure of $[\mathbf{4Co}]^+$ (Scheme 5-4). However, the loss of this fragment would be all together

unusual as the loss of a nitrogen and inner ring carbons are hard to understand without being able to invoke as a product a highly stable–likely even aromatic–species that also coordinatively saturates the central metal ion. In fact, the 632 Da species must be particularly stable as only comparably little subsequent fragmentations are observed. Importantly also, this fragmentation is not specific to the cobalt complex: the corresponding iron(III) complex displays it too (Figure not shown). Alas, the exact nature of the fragment metal complex structure must for now remain enigmatic.

(a)

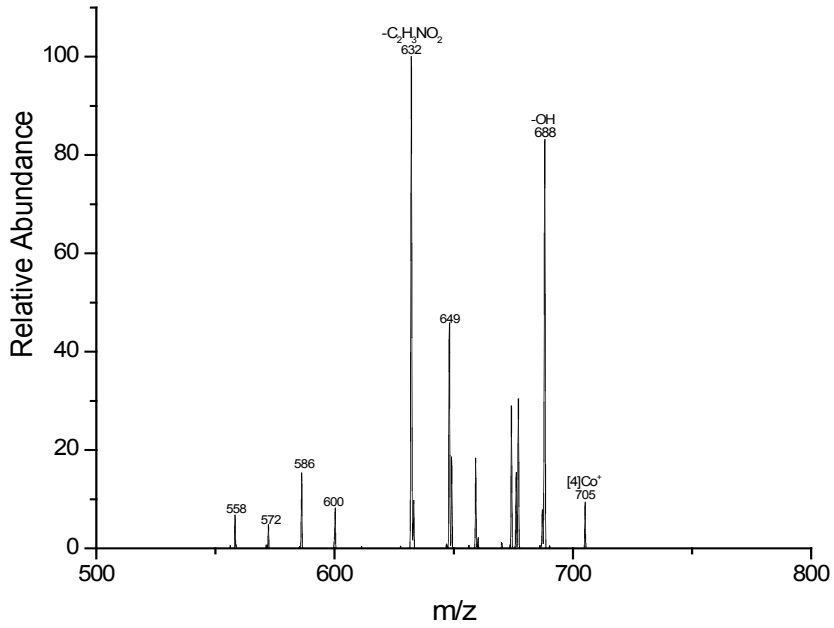

(b)

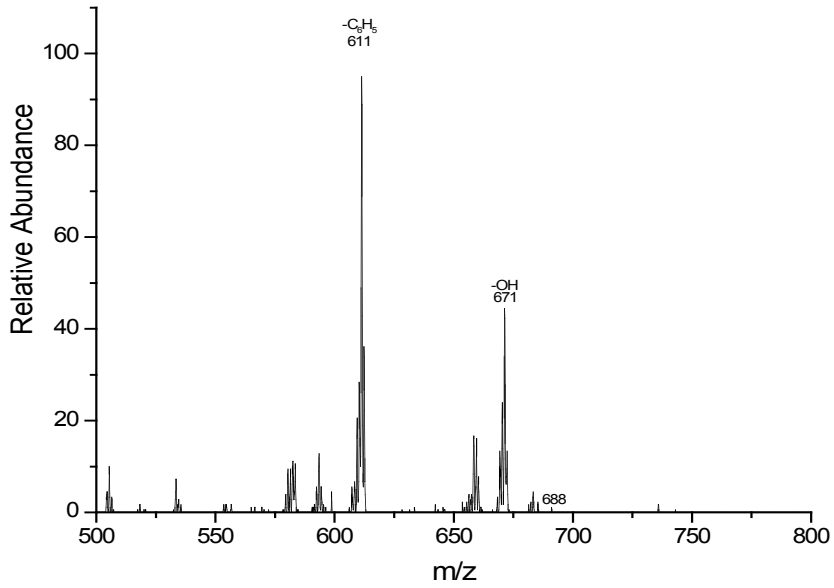

Figure 5-8. ESI(+) MS/MS spectrum of [**4Co**]$^+$ (a) and and MS^3 spectrum of m/z 688 (b).

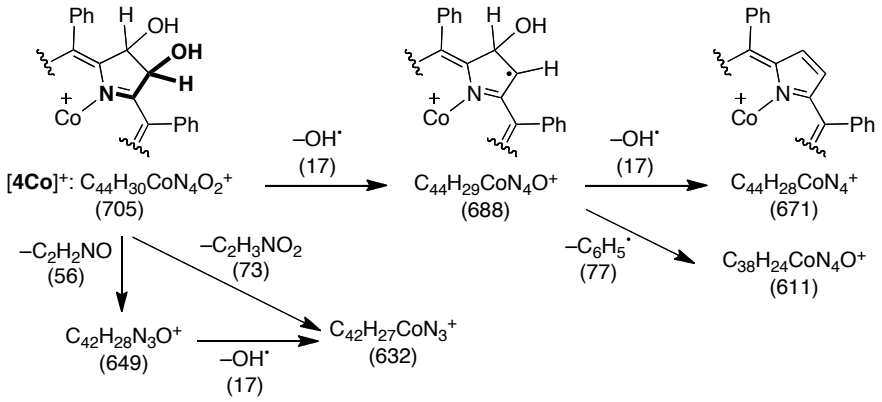

Scheme 5-4. Interpretation of the ESI+ CID spectra of [**4Co**]$^+$. See Figure 5-8 for a reproduction of the MS/MS spectrum of [**4Co**]$^+$.

In both the diol chlorin free base **4** and its cobalt complex **4Co**, only in advanced stages of the fragmentations are low intensity fragments visible in which the loss of a phenyl radical is superposed onto the other fragmentations; the sole loss of a phenyl group in the absence of other fragmentations is not observed. In comparison to the fragmentation pattern of porphyrin **1**, this serves to highlight the degree of activation toward ring fragmentations the dihydroxylation/pyrrole reduction introduces. This finding further allows the hypothesis to be made that the fragmentations of the other pyrrole-modified porphyrins will also be determined by the fragmentations of the non-pyrrolic heterocycle. This hypothesis will be shown to be accurate.

The ESI MS/MS spectrum of metallodioxoporphyrin [**7Co**]$^+$ is exceedingly simple (Figure 5-9). The overwhelmingly prominent fragmentation shows the loss of one molecule of CO, presumably forming the four-membered azeteone-containing porphyrinoid shown (Scheme 5-5). This fragment structure corresponds to a known molecule.[17,57,59,60] It is in the same redox relationship to the azete-substituted fragment derived from the dihydroxychlorin (Scheme 5-4), as the parent porphyrin dione and diol chlorin are to each other. Much less prominent is the loss of one molecule of CO_2, perhaps forming an azeteoporphyrin (triplet) carbene. In solution state,

triplet state carbenes have been shown to be greatly stabilized by being in a benzylic position with respect to aromatic systems.[61] No equivalent porphyrin-based derivative has been described in solution. In the MS^3 spectrum of the peak at *m/z* 673, the putative azeteone structure, the loss of a second CO molecule is recorded, forming either a secochlorin diradical or, more likely, the azireneporphyrin species of *m/z* 645 shown. Even though no azirene-containing pyrrole-modified porphyrins have been described in the solution phase to date, the latter fragment ion structure is evidently relatively stable as the peak corresponding to the loss of one *meso*-phenyl substituent is similarly intense as the peak assumed to correspond to a ring-degraded product (at *m/z* 502).

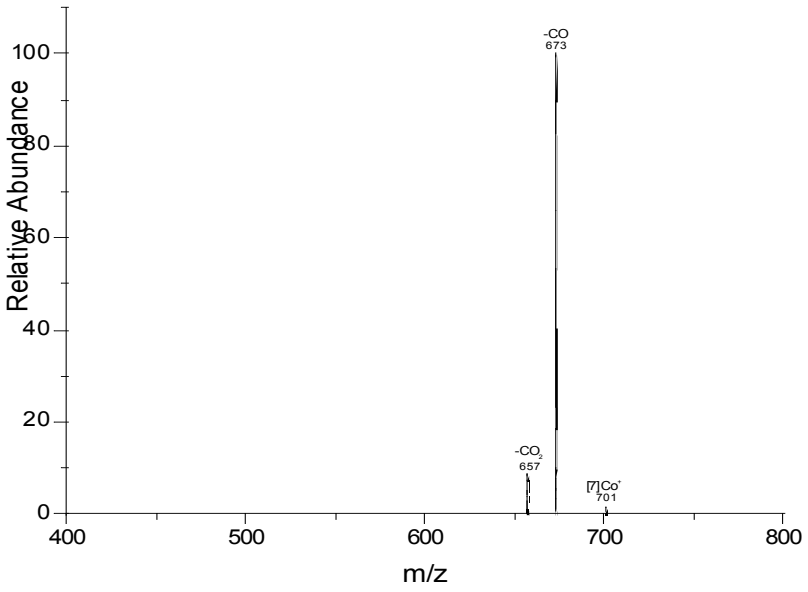

Figure 5-9. ESI(+) MS/MS spectrum of [**7Co**]$^+$.

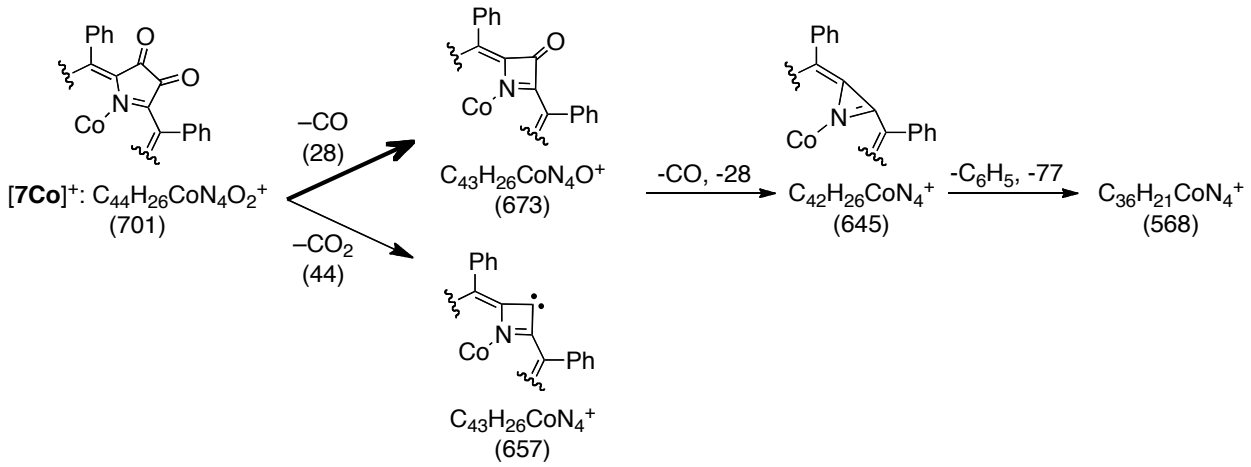

Scheme 5-5. Interpretation of the ESI+ CID spectra of [**7Co**]$^+$. See Figure 5-9 for a reproduction of the MS/MS spectrum of [**7Co**]$^+$.

Free base porphyrin dione [**7H**]$^+$ shows a comparable fragmentation pattern to the metallated form, except that the loss of CO_2 is not observed (Figure 5-10, Scheme 5-6). In other words, the CID spectrum of [**7H**]$^+$ suggests that the corresponding free base carbene is not formed. However, the molecular mechanism of the stabilization of the putative carbene by the central metal is unclear. Again, the similarity of the fragmentations in both cases and the parallels to the fragmentations of a number of other porphyrinoids studied here lend further credence to the proposition of the formation of the azeteone- and azirene-based semi-stable fragment structures.

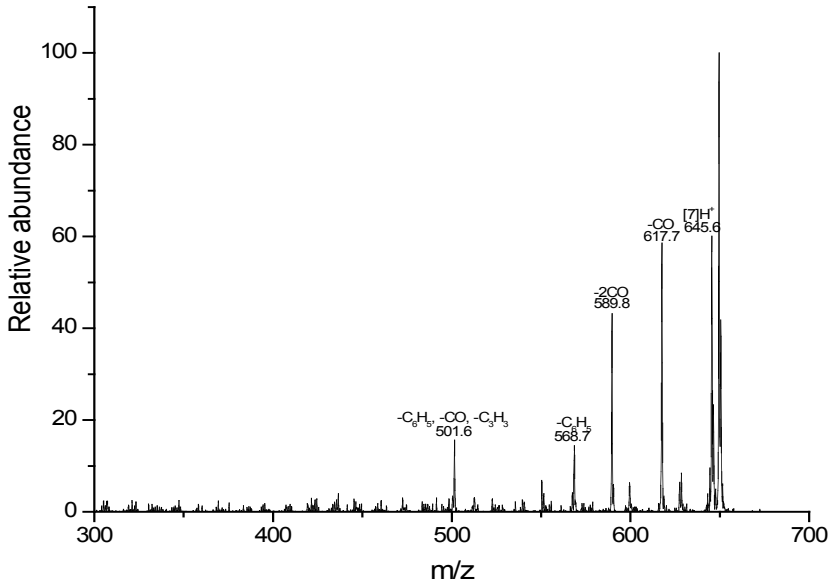

Figure 5-10. ESI(+) MS/MS spectrum of [**7H**]$^+$.

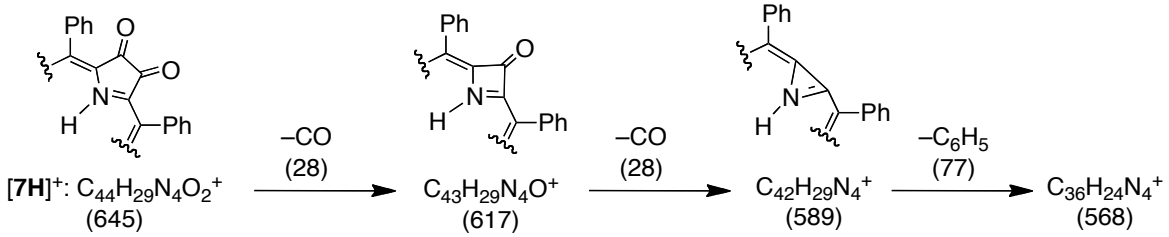

Scheme 5-6. Interpretation of the ESI+ CID spectra of [**7H**]$^+$. See Figure 5-10 for a reproduction of the spectrum [**7H**]$^+$.

In porpholactones, a β,β'-bond of a regular porphyrin was replaced by a lactone moiety.[13] Electronically, this difference is barely noticeable as judged by the very similar optical spectra of free base porpholactones and porphyrins.[13,62] Unlike porphyrin/metalloporphyrin **1**/**1Co**, however, the MS-MS spectra of free base porpholactone [**2H**]$^+$ and its cobalt complex species [**2Co**]$^+$ exhibit similar simple and prominent chromophore fragmentation pathways (Figure 5-11, Scheme 5-7).

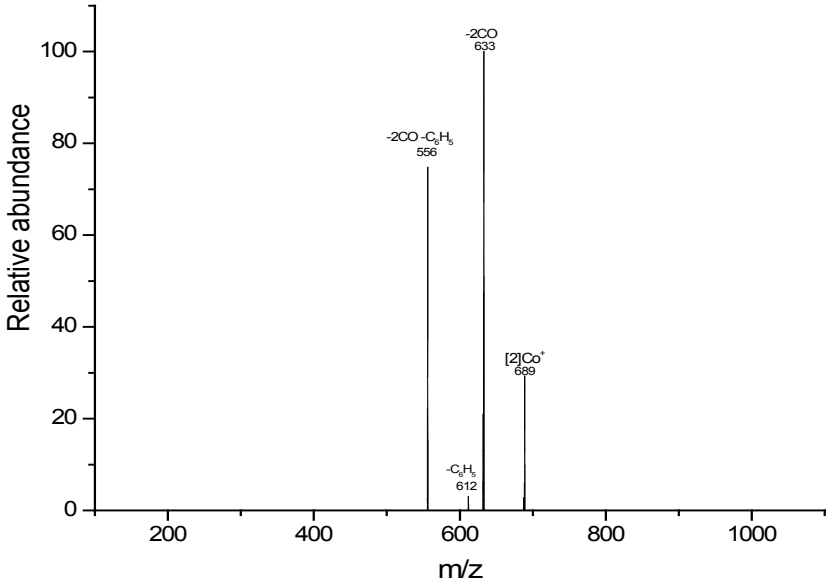

Figure 5-11. ESI(+) MS/MS spectrum of $[\mathbf{2Co}]^+$.

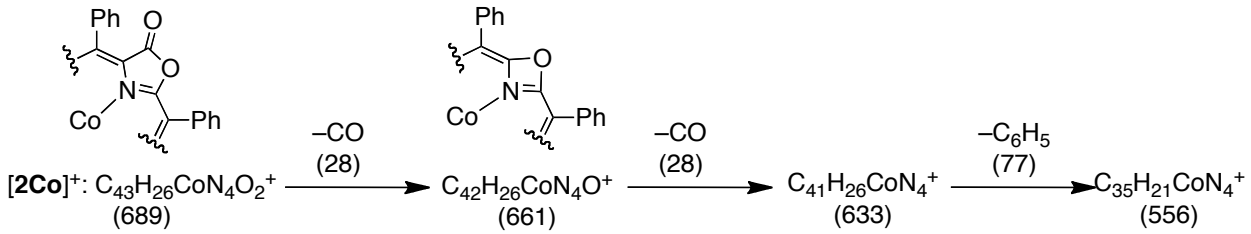

Scheme 5-7. Interpretation of the ESI+ CID spectra of $[\mathbf{2Co}]^+$. See Figure 5-11 for a reproduction of the ES/ES spectrum of $[\mathbf{2Co}]^+$.

The extrusion of a single CO from $[\mathbf{2Co}]^+$ (and $[\mathbf{2H}]^+$) likely resulted in the formation of an oxazete-containing pyrrole-modified porphyrin. While the contraction of a porphyrin to generate a pyrrole-modified porphyrin containing a four-membered azete and azetone ring was reported to occur under a number of thermal and light-driven reaction conditions[17,57,59,60,63] (see also above) oxazete-derived pyrrole-modified have not been reported. This makes this class of pyrrole-modified porphyrins an interesting synthetic target, particularly since we were able to show for the five-membered analogues that the replacement of a ring carbon by an oxygen can

be credited for imparting favorable electronic properties for a range of key applications onto these chromophores.[13,23,64]

The second fragmentation observed for both $[\mathbf{2Co}]^+$ and $[\mathbf{2H}]^+$ is another loss of CO (Scheme 5-7; confirmed by high resolution mass spectrometry). Making the likely assumption that the carbon lost in the CO was also previously attached to the oxygen in the macrocycle, the loss of this second molecule of CO from the presumed oxazete-based macrocycle implies that either the macrocycle is broken up or, perhaps more likely in the absence of further major fragmentations, that a rearrangement to a relatively stable species had taken place. Remarkably, the formation of the $[M–2\ CO]^+$ ion is independent whether the central metal was present, or not. However, while the second loss of CO is the 'terminal' fragmentation for the free base (i.e. before it fragments non-specifically into a large number of smaller fragments at higher collision energies), its Co complex also exhibits the loss of a phenyl group. Again, this phenyl loss in the absence of any further fragmentations we take as an indication that this fragment ion is a stable, perhaps even aromatic, species. At this time we cannot offer a possible structure for the $[M–2\ CO]^+$ species. We are currently studying this fragmentation in further detail and will report on this intriguing species in due time.

Oxazolochlorins **6**/**6Co** are related to the porpholactones **2**/**2Co** in that both contain an oxazole moiety as non-pyrrolic building block. However, the oxazole in **6**/**6Co** is in a lower oxidation state and an acetal moiety is formally replacing a pyrrolic double bond. Oxazolochlorins can be prepared from porpholactones by reduction (and subsequent acetalization)[13,21,65] but other pathways toward these chromophores are also available.[22,23] Porpholactones and oxazolochlorins are in the same redox relationship to each other as are porphyrins to chlorins.

The structural difference between porpholactones and oxazolochlorins is also reflected in their fragmentation patterns (Figure 5-12, Scheme 5-8). Expectedly, the acetal functionality breaks up (i.e. loss of $CH_3O^{\cdot}$ to form a resonance-stabilized benzylic radical). The subsequent losses of CO suggest the collapse of the oxazole moiety. This fragmentation is concomitant with a loss of a phenyl radical, perhaps thereby permitting the azirene formation shown. This fragmentation has the same net results as the fragmentations observed for $[\mathbf{4H}]^+$ and $[\mathbf{7H}]^+$ (not shown) (cf. Figure 5-7), thus it begins to sketch a general trend for the fragmentation of pyrrole-modified porphyrins. The loss of a methyl group and of CO_2 generate a fragment of *m/z* 646 that is suggestive of the formation of a (stable) chlorophin radical. An additional loss of a phenyl group either generates a diradical or, after H· migration, the azirene structure, a seemingly meta-stable fragment. Again, this fragment structure was proposed to also occur during fragmentation of $[\mathbf{4H}]^+$ and $[\mathbf{7H}]^+$/$[\mathbf{7Co}]^+$ (cf. Schemes 5-3, 5-5 and 5-6, respectively).

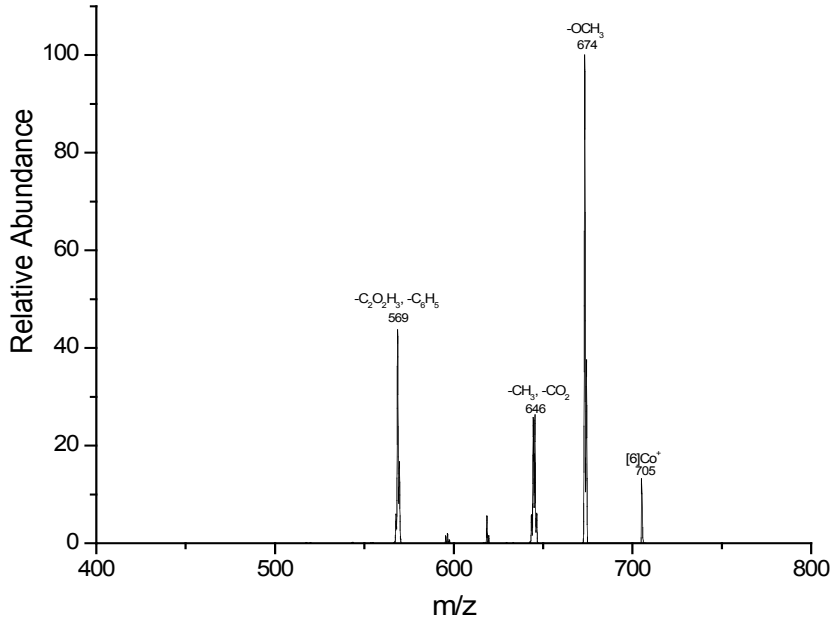

Figure 5-12. ESI(+) MS/MS spectrum of $[\mathbf{6Co}]^+$.

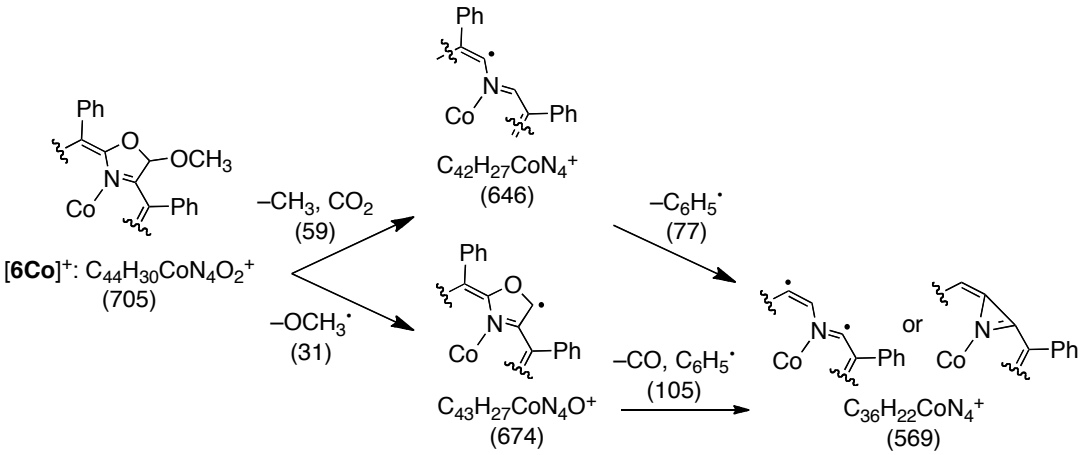

Scheme 5-8. Interpretation of the ESI+ CID spectra of [**6Co**]$^+$. See Figure 5-12 for a reproduction of the MS-MS spectrum of [**6Co**]$^+$.

The fragmentations observed in the MS/MS of free base oxazolochlorin **6** are much more rich than in the corresponding metal complex (Figure not shown) but are principally also due to the fragmentation of the acetal moiety (losses of CH_3, OCH_3, OCH_3+H, CO+CH_3) combined with ring oxygen losses (such as loss of CO), followed by extensive fragmentations of the tetrapyrrole ring. Again, this demonstrates the stabilizing effect of the central metal ion.

In the morpholinochlorins **3** and **3Co**, a porphyrin pyrrole was replaced by a morpholine functionality substituted by two alkoxy chains, forming double acetal functionalities.[8-10] As perhaps expected, the fragmentation of the double-acetal moiety dominates the MS/MS spectra of complex [**3Co**]$^+$. It shows loss of the substituents of the morpholine moiety and a break-up of the morpholine ring (Figure 5-13). Fragment ions with compositions suggestive of a number of know pyrrole-modified porphyrin framework structures (such as the monoformylchlorophin[56,57], *m/z* 675, and the azeteochlorin[63], *m/z* 659) form (Scheme 5-9). Again highlighting the stability of these fragment ion structures, CID of these ions results in the loss of one or more *meso*-phenyl groups, presumably under retention of the macrocycle structure.

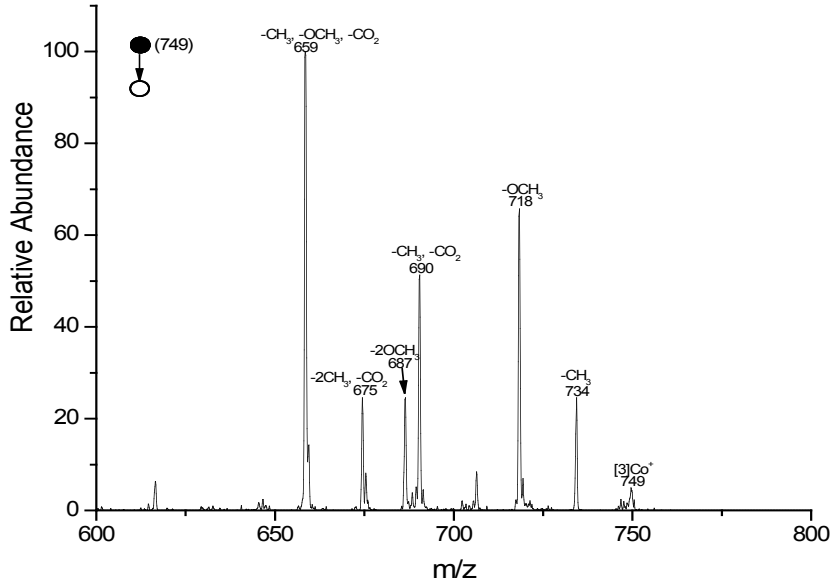

Figure 5-13. ESI(+) MS/MS spectrum of **[3Co]$^+$.**

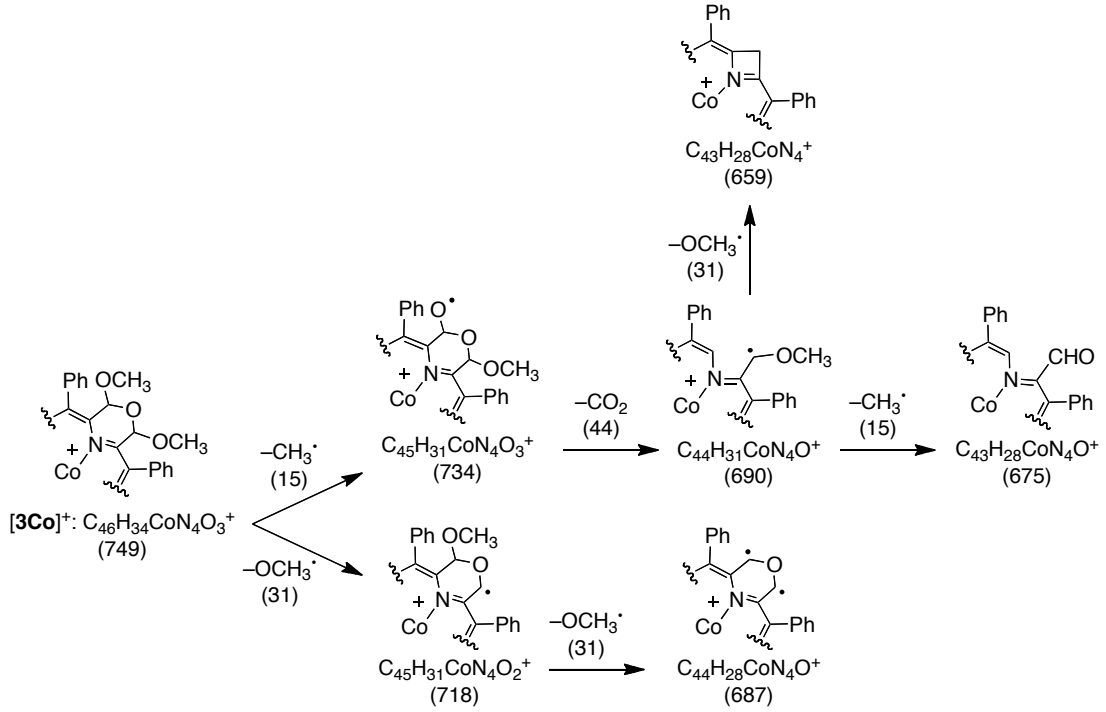

Scheme 5-9. Interpretation of the ESI+ CID spectra of **[3Co]$^+$.** See Figure 15-3 for a reproduction of the MS-MS spectrum of **[3Co]**$^+$.

The MS/MS spectrum of free base morpholinochlorin $[\mathbf{3H}]^+$ shows the fragmentation of the morpholine moiety similar to those observed for its cobalt complex $[\mathbf{3Co}]^+$, except that losses of H_2O were also observed (Scheme 5-10, Figure not shown). Moreover, the cumulative losses are suggestive of the formation of a azete carbene (or its open-chain, diradical resonance form) that was also proposed to form in the fragmentation of the dione cobalt complex $[\mathbf{7Co}]^+$ (cf. Scheme 5-5) is noted.

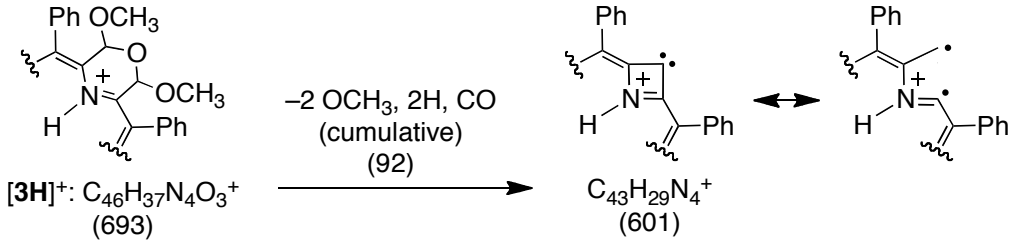

$[\mathbf{3H}]^+$: $C_{46}H_{37}N_4O_3^+$
(693)

$C_{43}H_{29}N_4^+$
(601)

Scheme 5-10. Abbreviated interpretation of the ESI+ MS/MS spectra of $[\mathbf{3H}]^+$.

In indaphyrins, the β,β'-bond of a porphyrin is oxidatively cleaved and the oxo-substituted β-carbons are tethered to the *o*-position of the flanking *meso*-phenyl groups. The fragmentation patterns observed for the indaphyrin cobalt complex $[\mathbf{5Co}]^+$ are simple and well-defined (Figure 5-14). The loss of CO is as expected for an indanone. The loss of a phenyl group constitutes another major fragmentation path, and the combined losses of one phenyl radical and a single CO molecule.

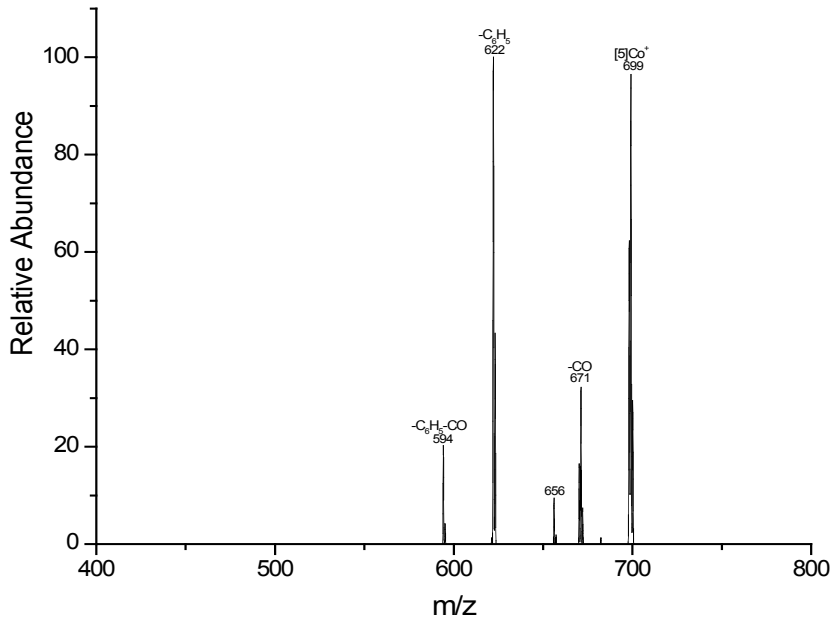

Figure 5-14. ESI(+) MS/MS spectrum of [**5Co**]$^+$.

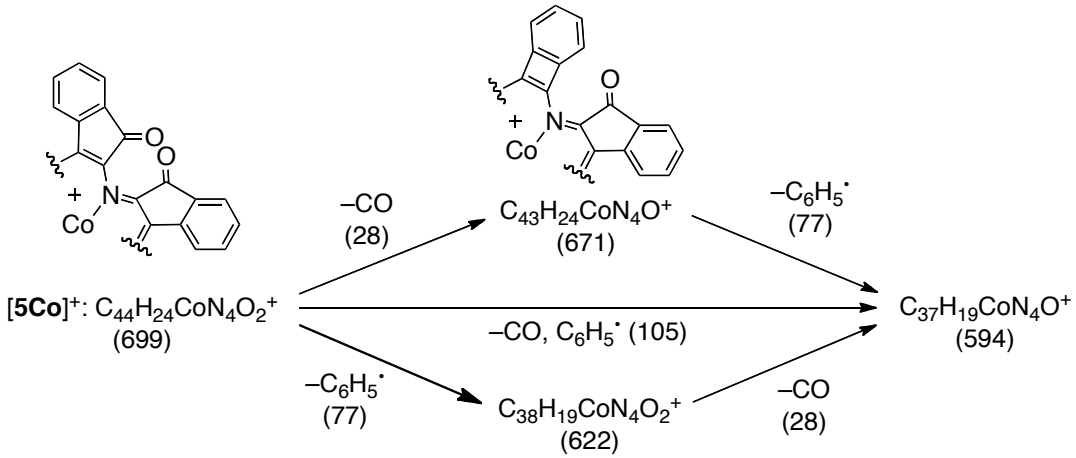

Scheme 5-11. Interpretation of the ESI+ MS/MS spectra of [5Co]$^+$. See Figure 5-14 for a reproduction of the MS-MS spectrum of [5Co]$^+$.

The interpretation of the fragmentation is straight forward (Scheme 5-11). The loss of CO likely forms the phenylene-annulated system shown. While phenyl-to-β-linkages are frequently observed in *meso*-arylporphyrins, the proposed phenyl-to-α-linkage in the [M-CO]$^+$ products is a novel motif.[48,66] Somewhat surprising is the fact that only one carbonyl loss is observed for this

bis-indanone-bearing molecule. Perhaps the annulation of two phenylenes is sterically too demanding to take place. A low intensity loss of a 43 Da fragment could not be assigned.

The fragmentation for the free base indaphyrin [**5H**]$^+$ is similar to that of its cobalt complex but again shows that the free base chromophore and its fragments are much more fragile. Thus, super-positioned over the major losses of CO and one and two phenyl groups are the sequential losses of single heavy atom fragments, indicative of a break-up of the macrocycle.

5.2.2. Conclusions

Multi-stage tandem mass spectrometry was used to study the fragmentation patterns of free base and cobalt *meso*-arylporphyrinoids containing *meso*-phenyl groups and a non-pyrrolic heterocycle in the porphyrinoid ring. A stark contrast in the fragmentation of the porphyrinoids with and without intact $C_{20}N_4$ macrocycles could also be detected: those complexes with intact macrocycles showed primarily – or even exclusively – the loss or fragmentation of *meso*-substituents, while those with altered macrocycles showed primarily fragmentations of the macrocycle. However, they do not fragment indiscriminately but tend to loose diagnostic fragments that lead to the formation pyrrole-modified systems containing four- and three-membered heterocycles, some of which are also known to exist in the condensed phase. Alas, not all fragmentations could be assigned. Nonetheless, the predominant fragmentation patterns that could be identified, such as the formation of ring-contracted porphyrinoids or a porphyrin analogues lacking any β-carbons, are deemed to be fairly and are predicted to also be observed for a number of other pyrrole-modified porphyrins. The cobalt(III) complexes investigated appear to be overall stabilized but they rarely show different fragmentation patterns than their corresponding free bases; they simply show fewer fragmentations.

This study contributes to the understanding of the chemistry of porphyrin and chlorin analogues. It further helps to establish ESI-MS as a premier technique not only to characterize porphyrinoids but to also probe their chemical properties.

5.3. MS/MS Fragmentation Behavior Study of *meso*-Thienyl-substituted Porphyrins

The most popular synthetic porphyrins are, owing to the ease of their synthesis and versatility, *meso*-tetraarylporphyrins with the aryl being a (substituted) phenyl group.[67,68] However, other *meso*-arylporphyrins were also reported. Among them, *meso*-thienyl-substituted porphyrins, such as **10**, **11**, and **12**, have become particularly prominent.[69-74] They have been used in the design of light harvesting and energy-transfer molecules,[75-77] the realization of organic semiconductor devices,[78] supramolecular architectures with extended electronic states[79] and the study of rotational barriers in peripherally crowded porphyrins.[80] Some *meso*-tetrathienyl substituted core-modified porphyrins proved to be potent phototoxins.[81] Thienyl-substituted porphyrins can be (electro)-polymerized,[82] furnishing, inter alia, ultrathin films of quasi two-dimensional porphyrin polymers.[83] Electro-polymerized (metallo)thienylporphyrins were utilized in electrodes possesses electrocatalytic properties, in an electrochemical glucose sensors, or in a novel TNT sensor. *meso*-Thienyl-substituted corroles[84] and pyrrole-modified porphyrins[85] were also reported. One aspect of the utility of the *meso*-thienyl groups is that they are much more tightly conjugated with the porphyrin chromophore that the larger phenyl groups, giving rise to red-shifted optical spectra when compared to the phenyl analogues.[45,85] The reactivity of the thienyl group can also be used to oligo- or polymerize the porphyrin.[82,83,86-88] For instance, the modified electrode surfaces resulting from the electropolymerization of **11Co** possess excellent catalytic properties for the four-electron reduction of dioxygen.[86]

Here we describe the fragmentation observed for three *meso*-thienylporphyrins and their cobalt(II) complexes (Figure 5-15). Again, the fragmentations are aimed at revealing diagnostic fragmentation patterns and at getting a general understanding of the chemistry of the *meso*-thienyl groups in the gas phase.

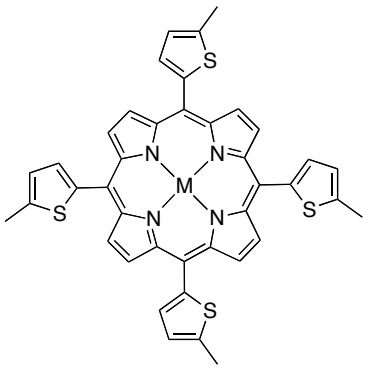

M = 2H, **10**
M = Co, **10Co**

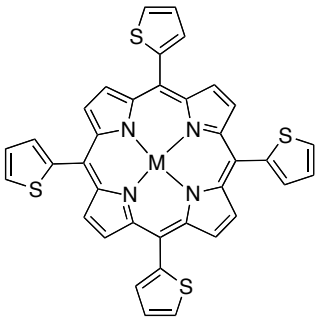

M = 2H, **11**
M = Co, **11Co**

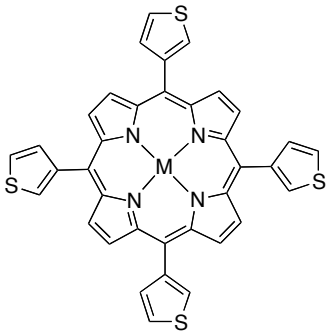

M = 2H, **12**
M = Co, **12Co**

Compound	Molecular Formula	Exact Mass
10	$C_{40}H_{30}N_4S_4$	694.14
10Co	$C_{40}H_{28}CoN_4S_4$	751.05
11	$C_{36}H_{22}N_4S_4$	638.07
11Co	$C_{36}H_{20}CoN_4S_4$	694.99
12	$C_{36}H_{22}N_4S_4$	638.07
12Co	$C_{36}H_{20}CoN_4S_4$	694.99

Figure 5-15. Structures and exact masses of the free base *meso*-thienylporphyrins **10**-**12** and their cobalt(II) complexes.

5.3.1. Results and Discussion

The replacement of the phenyl groups by thienyl groups fundamentally shifts the fragmentation pattern of the porphyrins as the *meso*-thienyl substituents become susceptible to ring-openings. Whereas this fragmentation type was not at all observed in the *meso*-phenylporphyrins, it dominates the CID spectra of the *meso*-thienylporphyrins.

For instance, the thien-2-yl-derivatized species $[\mathbf{11Co}]^+$ shows major fragmentations of the thienyl group in the form of losses of H_2S and $HCS^{\cdot}$ (Figure 5-16). The subsequent MS^n spectra allow little interpretation as to the structure of the porphyrin fragment ions but it is tempting to propose the formation of the alkynyl species shown (Scheme 5-12). *meso*-Alkynyl-substituted porphyrins are well known and stable.[89,90] The loss of two sulfur-containing fragments (H_2S and $HCS^{\cdot}$) indicates that the fragmentation is taking place at more than one *meso*-substituent, again an indication for the stability of the resulting species. The loss of an intact *meso*-substituent observed to only a minor degree. The fragmentation of free base $[\mathbf{10H}]^+$ is similar to that of its cobalt complex except that, as generally was observed for the free base compounds, more extensive fragmentations are observed (Figure not shown).

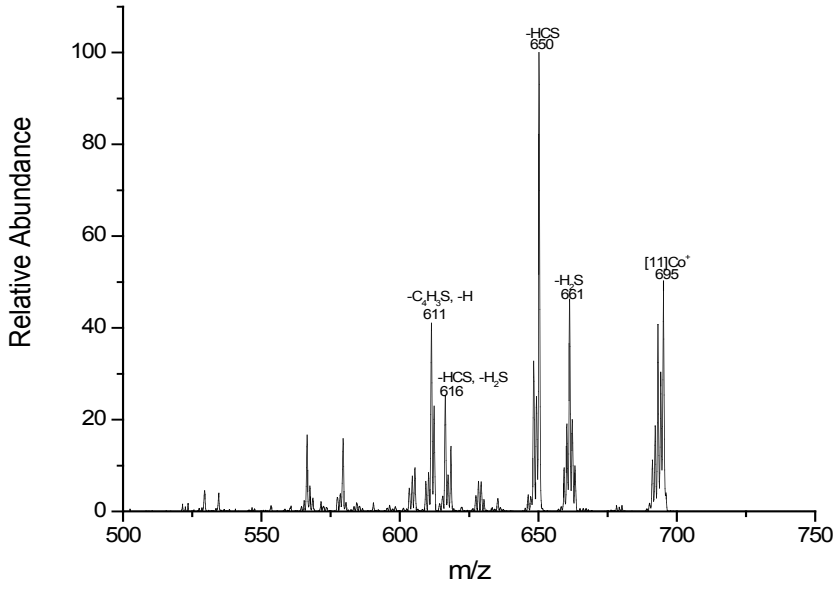

Figure 5-16. ESI(+) MS/MS spectrum of $[\mathbf{11Co}]^+$.

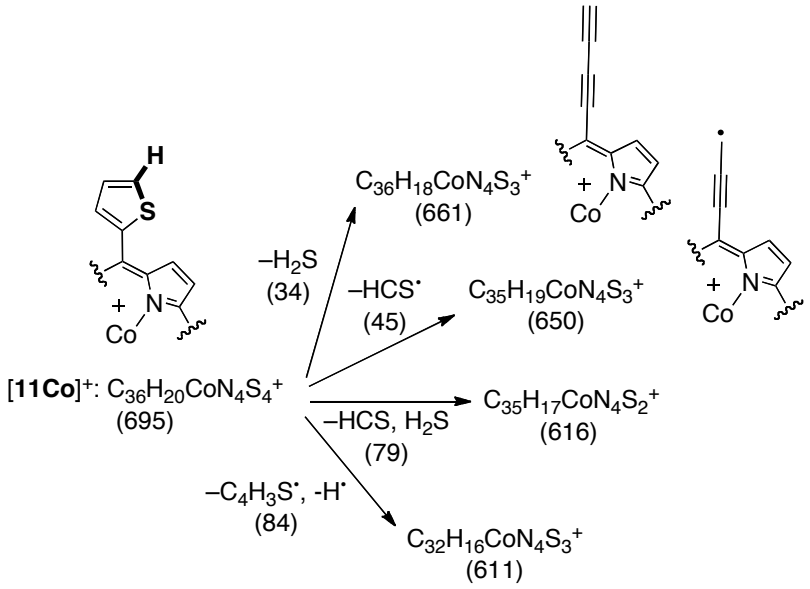

Scheme 5-12. Interpretation of the ESI+ CID spectra of [**11Co**]$^+$. See Figure 5-16 for a reproduction of the MS-MS spectrum of [**11Co**]$^+$.

The fragmentation seen in the MS-MS spectrum for the thien-2-yl-substituted porphyrins is somewhat independent from the attachment point of the thienyl group. Thus, the isomer to [**11Co**]$^+$, thien-3-ylporphyrin cobalt complex [**12Co**]$^+$, also shows the loss of H_2S and HCS, indicative of a breakup of the thienyl group and (Figure 5-17), perhaps, forming the same mono- and bis-alkynyl (after a rearrangement) species shown (Scheme 5-14), and the loss of an entire thienyl group. The loss of the entire thienyl group is more prominent in the 3-yl-isomer than in the 2-yl-isomer. This may be rationalized by the fact that the 3-thienyl radical can be estimated to be more stable the 2-thienyl radical. MS^3 spectra again show a repeat of this pattern (Figure 5-16).

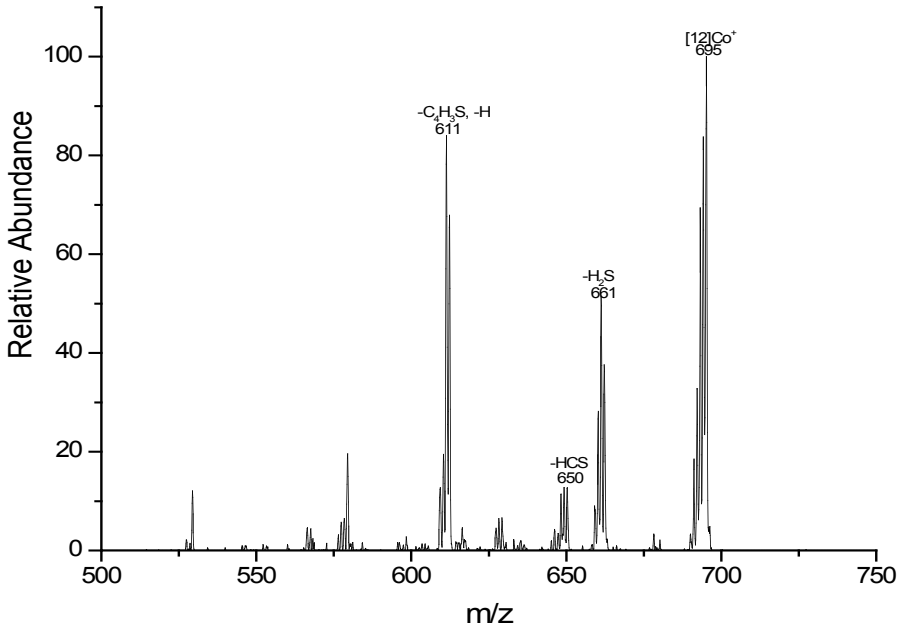

Figure 5-17. ESI(+) MS/MS spectrum of [**12Co**]$^+$.

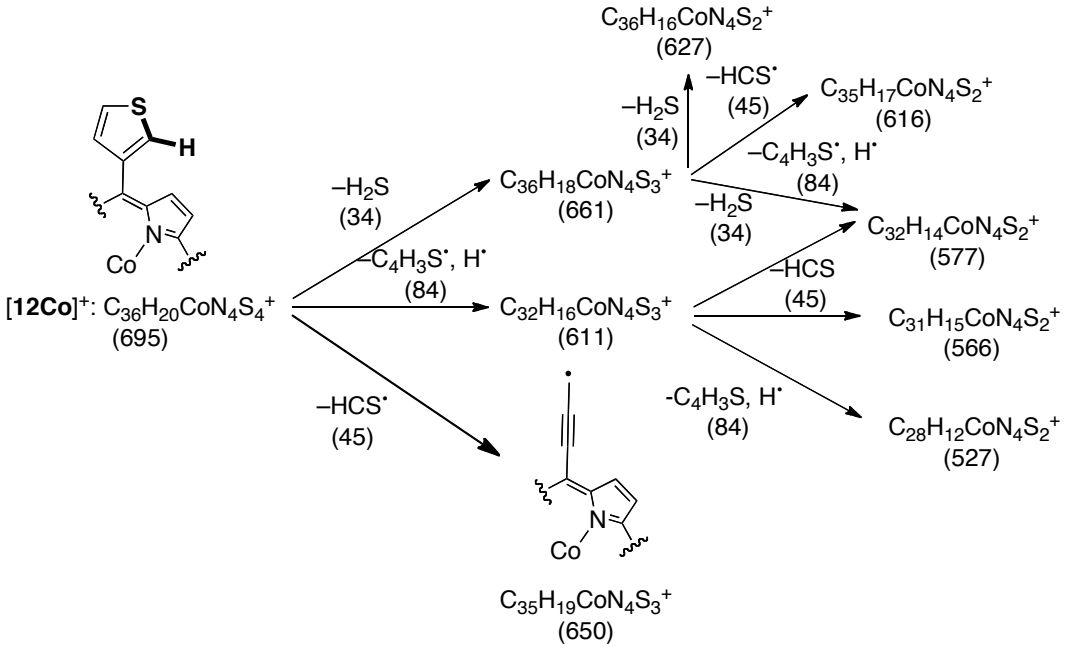

Scheme 5-13. Interpretation of the ESI+ CID spectra of [**12Co**]$^+$. See Figure 5-17 for a reproduction of the MS-MS spectrum of [**12Co**]$^+$.

The fragmentation pattern observed for the 5-methyl-thien-2-yl group in $[\mathbf{10Co}]^+$ (Figure 17) is analogous to the patterns established for $[\mathbf{11Co}]^+$ and $[\mathbf{12Co}]^+$. Interestingly, the loss of $CH_3CS\cdot$ from the methyl-thienyl group in $[\mathbf{10Co}]^+$ likely leads to equivalent stable *meso*-propargyl radical as the loss of $HCS\cdot$ from $[\mathbf{11Co}]^+$ and $[\mathbf{12Co}]^+$ (Scheme 5-15; cf. Schemes 5-13, 5-14), lending further support to its proposed structure. Also as before, the free base fragmentations are principally similar to those observed in the cobalt complex (Figures not shown).

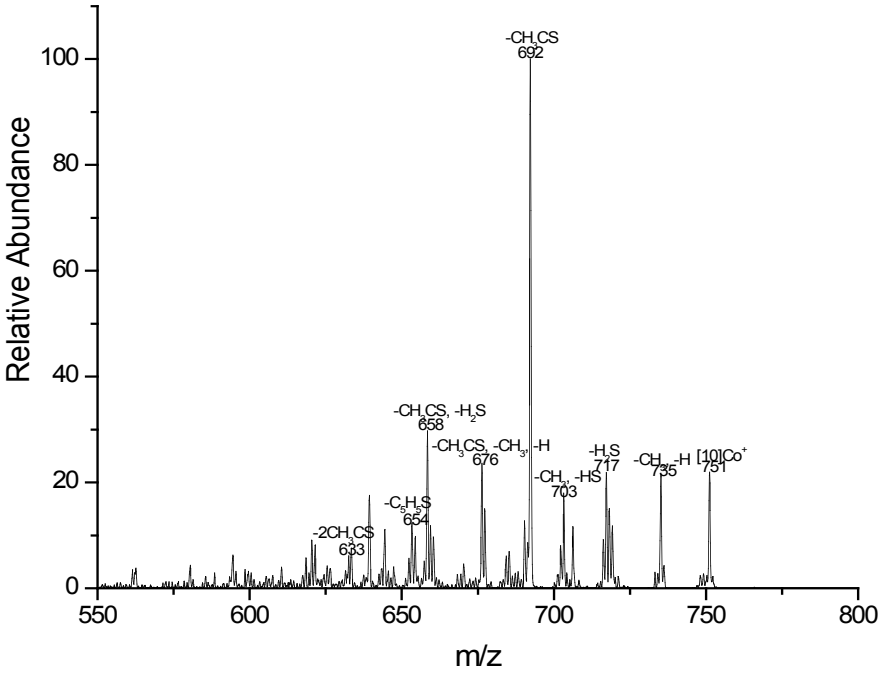

Figure 5-18. ESI(+) MS/MS spectrum of $[\mathbf{10Co}]^+$

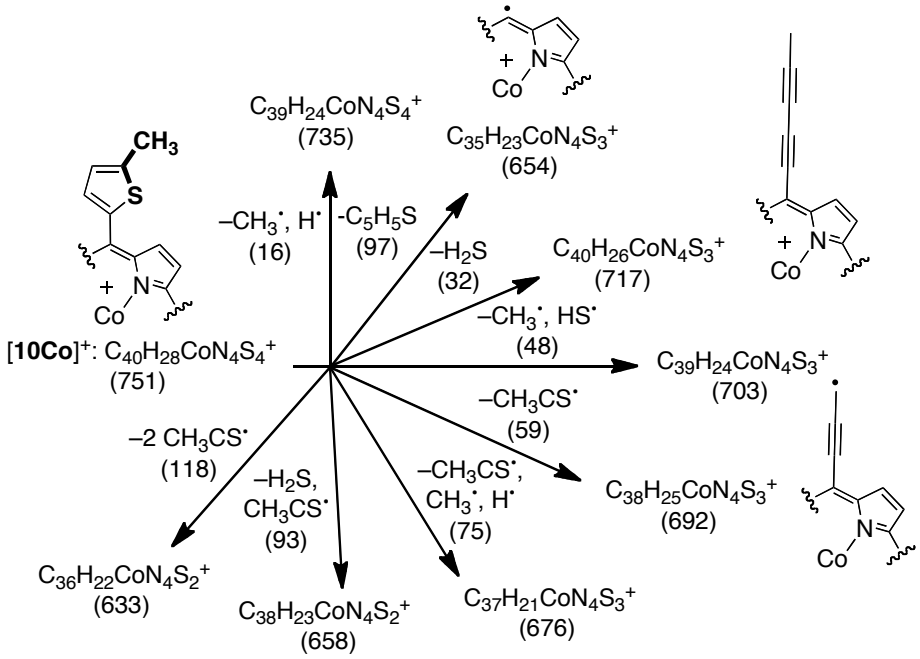

Scheme 5-14. Interpretation of the ESI+ CID spectra of [**10Co**]$^+$. See Figure 5-17 for a reproduction of the MS-MS spectrum of [**10Co**]$^+$

5.3.2. Conclusions

Multi-stage tandem mass spectrometry was used to study the fragmentation patterns *meso*-thienyl groups on a porphyrin macrocycle. While only the loss of an entire *meso*-phenyl groups is observed in *meso*-tetraphenylporphyrins, the corresponding *meso*-thienyl derivatives also exhibit major but diagnostic fragmentation of the *meso*-substituents. The cobalt(III) complexes investigated appear to be overall stabilized but they rarely show different fragmentation patterns than their corresponding free bases; they simply show fewer fragmentations.

5.4. Experimental

Porphyrin Syntheses

The Co(II) complexes **1Co** through **12Co** were synthesized using classic metal ion insertions into the corresponding known free bases that were all prepared along literature procedures: The free base porphyrins **1** and **9** were made according to the method of Adler[91], as were the free base thienylporphyrins **10** through **12** [45]. Free base diolchlorins **4** and **8** were prepared by OsO_4-mediated dihydroxylation of the corresponding porphyrins.[45,76] Free bases of porpholactones **2**[9], dioxoporphyrin **7**[14], indaphyrin **5**[12], and morpholinochlorin **3**[9] were made by oxidation/derivatization of free base *meso*-tetraphenyl-2,3-diolchlorin **4**. Free base oxazolochlorin **6** was obtained by reduction and acetalization of the corresponding porpholactones.[64,92]

Mass Spectrometry – General

The mass spectrometric analysis of the compound was performed at Northern Illinois State University, Dekalb, IL by Ekta Mishra in the group of Professor Victor Ryzhov. The details to the CID analyses are included in her thesis and the joint publication.[93] Experiments were performed on a quadrupole ion trap mass spectrometer equipped with an ESI source. The mass spectrometer was operated in the positive ion mode.

Mass Spectrometry – Axial Imidazole Binding Strenght Studies

In short, for the binding energy studies, the imidazole complexes of the Co(II) porphyrinoids **1** through **12** were generated in the solution phase by mixing 0.1 M solutions of porphyrins and imidazole in acetonitrile. The solutions were diluted to ~10^{-4} M with acetonitrile for the infusion into the mass spectrometer. For the binding energy studies, the porphyrin-imidazole complexes were infused by syringe pump at a flow rate of 5 μL/min. The singly

charged cobalt(III) porphyrin cationic complexes with one or two imidazoles ($[(Por)(Imi)]Co^{III}]^+$ and $[(Por)(Imi)_2]Co^{III}]^+$) were formed by (electrochemical) oxidation of the neutral cobalt(II) porphyrinoid complexes during the electrospray process. These ions were isolated in the ion trap and subjected to CID. Energy-variable CID experiments were performed by ramping the resonance excitation voltages from 0 V to the value corresponding to the total dissociation of the complex. Plots of the relative abundance of the parent ion versus applied normalized collisional energy were generated to determine $E_{1/2}$ values.[44] $E_{1/2}$ voltages were taken at resonance excitation voltage values at which the intensity of the porphyrin-imidazole complex and porphyrin ions were equal. The normalized collision energy (NCE%) was then converted to the amplitude in volts. The $E_{1/2}$ values obtained were corrected for the number of degrees of vibrational freedom (DOF).[44]

Mass Spectrometry – Fragmentation Studies

For the fragmentation studies, 0.1 M solutions of the porphyrinoids **1** through **12** and **1Co** through **12Co** were prepared in acetonitrile. The solutions were then diluted with acetonitrile to a final concentration of 10^{-4} M. The ESI source conditions were optimized to maximize the yield of ions of interest. These ions were isolated in the ion trap and subjected to CID in the trap with an excitation voltage high enough to induce fragmentation, but to still also retain some precursor ions. In select cases, MS^3 and MS^4 experiments or high resolution analyses were performed on the major fragment ions.

5.5. References

(1) Lash, T. D. In *The Porphyrin Handbook*; Kadish, K. M., Smith, K. M., Guilard, R., Eds.; Academic Press: San Diego, 2000; Vol. 2 - Heteroporphyrins, Expanded Porphyrins and Related Macrocycles, p 125-200.

(2) Latos-Grazynski, L. In *The Porphyrin Handbook*; Kadish, K. M., Smith, K. M., Guilard, R., Eds.; Academic Press: San Diego, 2000; Vol. Vol. 2 - Heteroporphyrins, Expanded Porphyrins and Related Macrocycles, p 361-416.

(3) Pawlicki, M.; Latos-Grazynski, L. In *Handbook of Porphyrin Science*; Kadish, K. M., Smith, K. M., Guilard, R., Eds.; World Scientific: Singapore, 2010; Vol. 2, p 103-192.

(4) Lash, T. D. In *Handbook of Porphyrin Science*; Kadish, K. M., Smith, K. M., Guilard, R., Eds.; World Scientific: Singapore, 2010; Vol. 16, p 1–330.

(5) Toganoh, M.; Furuta, H. In *Handbook of Porphyrin Science*; Kadish, K. M., Smith, K. M., Guilard, R., Eds.; World Scientific: Singapore, 2010; Vol. 2, p 295-367.

(6) Upmacis, R. K.; Hajjar, D. P.; Chait, B. T.; Mirza, U. A. *J. Am. Chem. Soc.* **1997**, *119*, 10424-10429.

(7) Chen, Y. L.; Campbell, J. M.; Collins, B. A.; Konermann, L.; Douglas, D. J. *Rapid Commun. Mass Spectrom.* **1998**, *12*, 1003-1010.

(8) Brückner, C.; Rettig, S. J.; Dolphin, D. *J. Org. Chem.* **1998**, *63*, 2094-2098.

(9) McCarthy, J. R.; Jenkins, H. A.; Brückner, C. *Org. Lett.* **2003**, *5*, 19-22.

(10) Brückner, C.; Götz, D. C. G.; Fox, S. P.; Ryppa, C.; McCarthy, J. R.; Bruhn, T.; Akhigbe, J.; Banerjee, S.; Daddario, P.; Daniell, H. W.; Zeller, M.; Boyle, R. W.; Bringmann, G. *J. Am. Chem. Soc.* **2011**, *133*, 8740–8752.

(11) McCarthy, J. R.; Hyland, M. A.; Brückner, C. *Chem. Commun.* **2003**, 1738-1739.

(12) McCarthy, J. R.; Hyland, M. A.; Brückner, C. *Org. Biomol. Chem.* **2004**, *2*, 1484-1491.

(13) Brückner, C.; Ogikubo, J.; McCarthy, J. R.; Akhigbe, J.; Hyland, M. A.; Daddario, P.; Worlinsky, J. L.; Zeller, M.; Engle, J. T.; Ziegler, C. J.; Ranaghan, M. J.; Sandberg, M. N.; Birge, R. R. *J. Org. Chem.* **2012**, *77*, 6480–6494.

(14) Daniell, H. W.; Williams, S. C.; Jenkins, H. A.; Brückner, C. *Tetrahedron Lett.* **2003**, *44*, 4045-4049.

(15) Akhigbe, J.; Haskoor, J.; Zeller, M.; Brückner, C. *Chem. Commun.* **2011**, *47*, 8599–8601.

(16) Akhigbe, J.; Haskoor, J. P.; Krause, J. A.; Zeller, M.; Brückner, C. *Org. Biomol. Chem.* **2013**, *11*, 3616–3628.

(17) Crossley, M. J.; King, L. G. *J. Chem. Soc., Chem, Commun.* **1984**, 920-922.

(18) Jayaraj, K.; Gold, A.; Austin, R. N.; Ball, L. M.; Terner, J.; Mandon, D.; Weiss, R.; Fischer, J.; DeCian, A.; Bill, E.; Müther, M.; Schünemann, V.; Trautwein, A. X. *Inorg. Chem.* **1997**, *36*, 4555-4566.

(19) Köpke, T.; Pink, M.; Zaleski, J. M. *Chem. Commun.* **2006**, 4940-4942.

(20) Yu, Y.; Lv, H.; Ke, X.; Yang, B.; Zhang, J.L. *Adv. Synth. Catal.* **2012**, *354*, 3509–3516.

(21) McCarthy, J. R.; Melfi, P. J.; Capetta, S. H.; Brückner, C. *Tetrahedron* **2003**, *59*, 9137-9146.

(22) Akhigbe, J.; Ryppa, C.; Zeller, M.; Brückner, C. *J. Org. Chem.* **2009**, *74*, 4927-4933.

(23) Ogikubo, J.; Worlinsky, J. L.; Fu, Y.-J.; Brückner, C. *Tetrahedron Lett.* **2013**, *54*, 1707–1710.

(24) Promarak, V.; Burn, P. L. *J. Chem. Soc., Perkin Trans. 1* **2001**, 14-20.

(25) Wicks, M. N.; Burn, P. L. *J. of Porphyrins and Phthalocyanines* **2005**, *9*, 444-450.

(26) Smith, K. M. *Porphyrins Metalloporphyrins* **1975**, 381-398.

(27) Antonini, E.; Brunori, M. *Hemoglobin and Myoglobin in Their Reactions with Ligands*; North-Holland Publication Co: Amsterdam, **1971**; Vol. 21.

(28) Scheidt, R. W. In *The Porphyrin Handbook*; Kadish, K. M., Smith, K. M., Guilard, R., Eds.; Academic Press: San Diego, **2000**; Vol. 3, p 49-112.

(29) Walker, F. A.; Benson, M. *J. Am. Chem. Soc.* **1980**, *102*, 5530-5538.

(30) Pasternack, R. F.; Gillies, B. S.; Stahlbush, J. R. *J. Am. Chem. Soc.* **1978**, *100*, 2613-2619.

(31) Cooks, R. G. *J. Mass Spectrom.* **1995**, 1215-1221.

(32) Hart, K. J.; McLuckey, S. A. *J. Am. Soc. Mass Spectrom.* **1994**, *5*, 250-259.

(33) Colorado, A.; Brodbelt, J. *J. Am. Soc. Mass Spectrom.* **1996**, *7*, 1116-1125.

(34) Vinokur, N.; Ryzhov, V. *J. Mass Spectrom.* **2004**, *39*, 1268-1274.

(35) Hayes, L. A.; Chappell, A. M.; Jellen, E. E.; Ryzhov, V. *Int. J. Mass Spectrom.* **2003**, *227*, 111-120.

(36) Jellen, E. E.; Ryzhov, V. *Eur. J. Mass Spectrom.* **2005**, *11*, 65-72.

(37) Jellen, E. E.; Chappell, A. M.; Ryzhov, V. *Rapid Commun. Mass Spectrom.* **2002**, *16*, 1-6.

(38) Liao, M.-S.; Scheiner, S. *J. Chem. Phys.* **2002**, *117*, 205-219.

(39) Whitlock Jr., H. W.; Hanauer, R.; Oester, M. Y.; Bower, B. K. *J. Am. Chem. Soc.* **1969**, *91*, 7485-7489.

(40) Samankumara, L. P.; Zeller, M.; Krause, J. A.; Brückner, C. *Org. Biomol. Chem.* **2010**, *8*, 1951-1965.

(41) Gouterman, M.; Hall, R. J.; Khalil, G. E.; Martin, P. C.; Shankland, E. G.; Cerny, R. L. *J. Am. Chem. Soc.* **1989**, *111*, 3702-3707.

(42) Fajer, J. *Chem. Ind.* **1991**, 869-873.

(43) Campbell, C. J.; Rusling, J. F.; Brückner, C. *J. Am. Chem. Soc.* **2000**, *122*, 6679-6685.

(44) David, W. M.; Brodbelt, J. S. *J. Am. Soc. Mass Spectrom.* **2003**, *14*, 383-392.

(45) Brückner, C.; Foss, P. C. D.; Sullivan, J. O.; Pelto, R.; Zeller, M.; Birge, R. R.; Crundwell, G. *Phys. Chem. Chem. Phys.* **2006**, *8*, 2402-2412.

(46) Bhyrappa, P.; Bhavana, P. *Chem. Phys. Lett.* **2001**, *349*, 399-404.

(47) Gozet, T.; Huynh, L.; Bohme, D. K. *Int. J. Mass Spectrom.* **2009**, *279*, 113-118.

(48) Lau, K. S. F.; Sadilek, M.; Khalil, G. E.; Gouterman, M.; Brückner, C. *J. Am. Soc. Mass Spectrom.* **2006**, *17*, 1306-1314.

(49) Crossley, M. J.; King, L. G.; Pyke, S. M. *Tetrahedron* **1987**, *43*, 4569-4577.

(50) Brückner, C.; Dolphin, D. *Tetrahedron Lett.* **1995**, *36*, 3295-3298.

(51) Callot, H. J. *Bull. Chem. Soc. Chim. Fr.* **1974**, 1492-1496.

(52) DiMagno, S. G.; Lin, V. S.Y.; Therien, M. J. *J. Org. Chem.* **1993**, *58*, 5983-5993.

(53) Crossley, M. J.; Field, L. D.; Harding, M. M.; Sternhell, S. *J. Am. Chem. Soc.* **1987**, *109*, 2335-2341.

(54) Köpke, T.; Pink, M.; Zaleski, J. M. *Org. Biomol. Chem.* **2006**, *4*, 4059-4062.

(55) Bohusch, M.; Flitsch, W.; Kneip, H.-G. *Liebigs Annalen der Chemie* **1991**, 67-70.

(56) Brückner, C.; Sternberg, E. D.; MacAlpine, J. K.; Rettig, S. J.; Dolphin, D. *J. Am. Chem. Soc.* **1999**, *121*, 2609-2610.

(57) Brückner, C.; Hyland, M. A.; Sternberg, E. D.; MacAlpine, J.; Rettig, S. J.; Patrick, B. O.; Dolphin, D. *Inorg. Chim. Acta* **2005**, *358*, 2943-2953.

(58) Li, K.L.; Guo, C.C.; Chen, Q.Y. *Org. Lett.* **2010**, *11*, 2724-2727.

(59) Köpke, T.; Pink, M.; Zaleski, J. M. *Chem. Commun.* **2006**, 4940–4942.

(60) Köpke, T.; Pink, M.; Zaleski, J. M. *Org. Biomol. Chem.* **2006**, *4*, 4059–4062.

(61) Tomioka, H; Iwamoto, E; Itakura, H; Hirai, K. *Nature*, **2010**, 626–628.

(62) Gouterman, M.; Hall, R. J.; Khalil, G. E.; Martin, P. C.; Shankland, E. G.; Cerny, R. L. *J. Am. Chem. Soc.* **1989**, *111*, 3702-3707.

(63) Banerjee, S.; Hyland, M. A.; Brückner, C. *Tetrahedron Lett.* **2010**, *51*, 4505–4508.

(64) Ogikubo, J.; Meehan, E.; Engle, J. T.; Ziegler, C.; Brückner, C. *J. Org. Chem.* **2012**, *77*, 6199–6207.

(65) Brückner, C.; McCarthy, J. R.; Daniell, H. W.; Pendon, Z. D.; Ilagan, R. P.; Francis, T. M.; Ren, L.; Birge, R. R.; Frank, H. A. *Chem. Phys.* **2003**, *294*, 285-303.

(66) Fox, S.; Boyle, R. W. *Tetrahedron* **2006**, *62*, 10039-10054.

(67) Lindsey, J. S. In *The Porphyrin Handbook*; Kadish, K. M., Smith, K. M., Guilard, R., Eds.; Academic Press: San Diego, 2000; Vol. 1, p 45-118.

(68) Lindsey, J. S. *Acc. Chem. Res.* **2010**, *43*, 300-311.

(69) Diskin-Posner, Y.; Balasubramanian, S.; Kumar Patram, G.; Goldberg, I. *Acta Cryst.* **2001**, *E57*, m346-m348.

(70) Purushothaman, B.; Varghese, B.; Bhyrappa, P. *Acta Crystallogr., Sect. C: Cryst. Struct. Commun.* **2001**, *57*, 252-253.

(71) Ono, N.; Miyagawa, H.; Ueta, T.; Ogawa, T.; Tani, H. *J. Chem. Soc., Perkin Trans. 1* **1998**, 1595-1601.

(72) Gupta, I.; Hung, C.-H.; Ravikanth, M. *Eur. J. Org. Chem.* **2003**, 4392-4400.

(73) Shi, D.-F.; Wheelhouse, R. T. *Tetrahedron Lett.* **2002**, *43*, 9341-9342.

(74) Gupta, I.; Ravikant, M. *J. Photochem. Photobiol. A* **2005**, *177*, 156-163

(75) Collis, G. E.; Campbell, W. M.; Officer, D. L.; Burrell, A. K. *Org. Biomol. Chem.* **2005**, *3*, 2075-2084.

(76) Vollmer, M. S.; Würthner, F.; Effenberger, F.; Emele, P.; Meyer, D. U.; Stümpfig, T.; Port, H.; Wolf, H. C. *Chem. Eur. J.* **1998**, *4*, 260-269.

(77) Odobel, F.; Suresh, S.; Blart, E.; Nicolas, Y.; Quintard, J.P.; Janvier, P.; Le Questel, J.Y.; Illien, B.; Rondeau, D.; Richomme, P.; Häupl, T.; Wallin, S.; Hammarström, L. *Chem. Eur. J.* **2002**, *8*, 3027-3046.

(78) Shimidzu, T.; Segawa, H.; Wu, F.; Nakayama, N. *J. Photochem. Photobiol. A* **1995**, *92*, 121-127.

(79) Friedlein, R.; Kieseritzky, F. v.; Braun, S.; Linde, C.; Osikowicz, W.; Hellberg, J.; Salaneck, W. R. *Chem. Commun.* **2005**, *15*, 1974-1976.

(80) Medforth, C. J.; Haddad, R. E.; Muzzi, C. M.; Dooley, N. R.; Jaquinod, L.; Shyr, D. C.; Nurco, D. J.; Olmstead, M. M.; Smith, K. M.; Ma, J.G.; Shelnutt, J. A. *Inorg. Chem.* **2003**, *42*, 2227-2241.

(81) You, Y.; Gibson, S. L.; Hilf, R.; Ohulchanskyy, T. Y.; Detty, M. R. *Bioorg. Med. Chem.* **2005**, *13*, 2235-2251.

(82) Li, G.; Bhosale, S.; Tao, S.; Guo, R.; Bhosale, S.; Li, F.; Zhang, Y.; Wang, T. Y.; Fuhrhop, J.H. *Polymer* **2005**, *46*, 5299-5307.

(83) Maruyama, H.; Segawa, H.; Sodota, S.; Sato, T.; Kosai, N.; Sagisaka, S.; Shimidzu, T.; Tanaka, K. *Synth. Met.* **1998**, *96*, 141-149.

(84) Maiti, N.; Lee, J.; Kwon, S. J.; Juhyoun Kwak; Do, Y.; Churchill, D. G. *Polyhedron* **2006**, *25*, 1519–1530.

(85) Lau, K. S. F.; Zhao, S.; Ryppa, C.; Jockusch, S.; Turro, N. J.; Zeller, M.; Gouterman, M.; Khalil, G. E.; Brückner, C. *Inorg. Chem.* **2009**, *48*, 4067-4074.

(86) Chen, W.; Akhigbe, J.; Brückner, C.; Li, C. M.; Lei, Y. *J. Phys. Chem. C* **2010**, *114*, 8633-8638.

(87) Chen, W.; Ding, Y.; Akhigbe, J.; Brückner, C.; Li, C. M.; Lei, Y. *Biosens. Bioelectron.* **2010**, *26*, 504-510.

(88) Chen, W.; Wang, Y.; Brückner, C.; Li, C. M.; Lei, Y. *Sens. Actuators, B* **2010**, *147*, 191-197.

(89) Shediac, R.; Gray, M. H. B.; Uyeda, H. T.; Johnson, R. C.; Hupp, J. T.; Angiolillo, P. J.; Therien, M. J. *J. Am. Chem. Soc.* **2000**, *122*, 7017-7033.

(90) Reeve, J. E.; Collins, H. A.; De, M. K.; Kohl, M. M.; Thorley, K. J.; Paulsen, O.; Clays, K.; Anderson, H. L. *J. Am. Chem. Soc.* **2009**, *131*, 2758-2759.

(91) Adler, A. D.; Longo, F. R.; Finarelli, J. D.; Goldmacher, J.; Assour, J.; Korsakoff, L. *J. Org. Chem.* **1967**, *32*, 476.

(92) Ogikubo, J.; Meehan, E.; Engle, J. T.; Ziegler, C. J.; Brückner, C. *J. Org. Chem.* **2013**, *78*, 2840-2852.

(93) Mishra, E.; Worlinsky, J. L.; Gilbert, T. M.; Brückner, C.; Ryzhov, V. *J. Am. Soc. Mass. Spectrom.* **2012**, *23*, 1135–1147. Erratum (correction of systemic typesetting errors): *J. Am. Soc. Mass. Spectrom.* **2012**, *23*, 1428–1439.

6. Trends in the CO Stretching Frequency and Bond Distance in [Porphyrinoid]Ru(py)CO Complexes

6.1. Introduction

Porphyrins form square planar coordination sphere around a metal. One or two (or, in some cases, more) axial ligands may bind to the central metal, formatting square pyramidal or octahedral complexes, respectively (see also Chapters 4 and 5). The ability of the heme co-factor to reversibly form complexes with a range of substrates is the basis of their utility on small molecule activation or transport. Prime examples are hemoglobin/myoglobin (O_2 transport and storage, respectively), the cytochrome P450 family of mono-oxygenases (O_2 activation and transfer), or NO synthase (generation and coordination to NO). Also, the molecular origin of the toxicity of certain ions, such as CO and CN^-, is their ability to coordinate to (and thus deactivate) heme enzymes.[1,2] It thus does not surprise that the axial coordination chemistry of hemes and heme models was thoroughly studied.[3-5] In the fast majority of the studied systems, the metal was varied or the axial ligands were varied.[2-4,6-13] In much fewer systems, the porphyrinic chromophore was varied.

Carbon monoxide binds to transition metals through synergistic π-back-bonding, which is dictated by the electronic properties of the transition metals. The electronic structure of the metals in metalloporphyrins, in turn, are tuned by the tetrapyrrolic ligand (and the second axial ligand, if present). Therefore, altering the porphyrin structure increases or decreases the strength of the M–CO bond, which is inversely correlated to the strength of the C–O triple bond.[1,2,5] The latter is conveniently assessed by either recording the ν_{C-O} stretching frequency of the complex

(in the IR or resonance Raman spectrum of the compound), or directly by measuring the C–O bond distance by single crystal X-ray diffractometry.[1,6,11,12,14]

Although carbonyl complexes of iron(II) porphyrins have been reported, these complexes are stable only in presence of excess CO or in solid state.[11] Iron porphyrins also tend to readily switch oxidation states depending on the ligand environment. The corresponding ruthenium(II) porphyrins form well-defined pseudo-octahedral low-spin diamagnetic complexes, M(CO)(L)(Por) that are much more chemically stable and kinetically more inert.[4,10]

To learn more about the electronic properties of the pyrrole-modified porphyrins, we decided to form their novel [pyrrole-modified porphyrinato]Ru(II)(pyridine)(CO) and to perform a comparative study of the carbonyl stretching frequencies. As the well-investigated benchmark complex, [*meso*-tetraphenylporphyrinato]Ru(py)(CO) **1Ru** was chosen (Scheme 6-1).

6.2. Results and Discussion

6.2.1. Synthesis of Ru(Por)(CO)(py) Complexes 1Ru-6Ru

The chlorin species, 2,3-dimethoxychlorin **2** and 2,2-dimethyloxazolochlorin **3** are considered to be more electron-rich than the benchmark porphyrin, while porpholactone **4** and 2,3-dioxoporphyrin **5** are considered to be porphyrin-like, yet they are less electron-rich than the benchmark porphyrin (as per computations).[15] The incorporation of a six-membered ring in the macrocycle structure form the chlorin-like morpholinochlorin **6** that, however, possesses an increased conformational flexibility than the parent porphyrin (or chlorin **2**).[16] All these ligands are, like a porphyrin, dianionic N_4-ligands that can coordinate to the metal in a square planar fashion.

The novel ruthenium carbonyl complexes **2Ru-6Ru** were synthesized by metalation of the free base chromophores **2-6** using $Ru_3(CO)_{12}$ as the ruthenium source and using microwave heating along a standard procedure for the insertion of ruthenium (Scheme 6-1). The *trans* axial pyridine ligand complexes were isolated from the ethanol adduct.

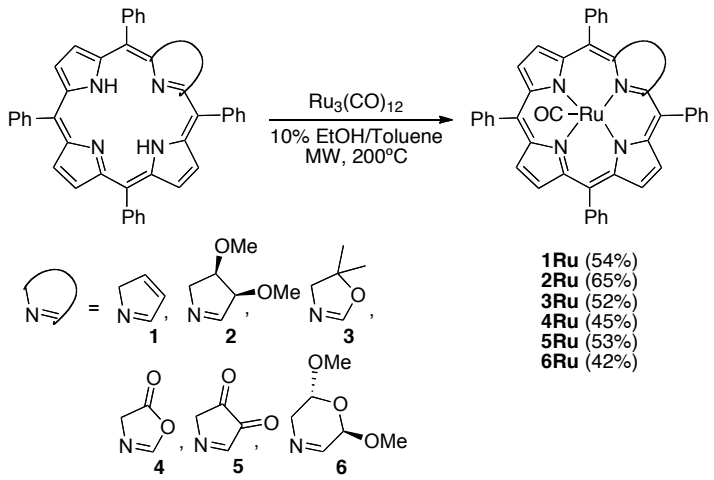

Scheme 6-1. Synthesis of Ru(Por)(CO)(py) complexes **1Ru-6Ru**.

All spectroscopic and analytical data confirmed the formation of the target complexes. For instance, the coordination of the pyridine groups to the central metal in **4Ru** can be readily seen in the ^{1}H NMR spectrum of the compound (Figure 6-1). The resonances corresponding to the axial pyridine are upfield-shifted through the anisotropic ring current effect of the porphyrin macrocycle.[11]

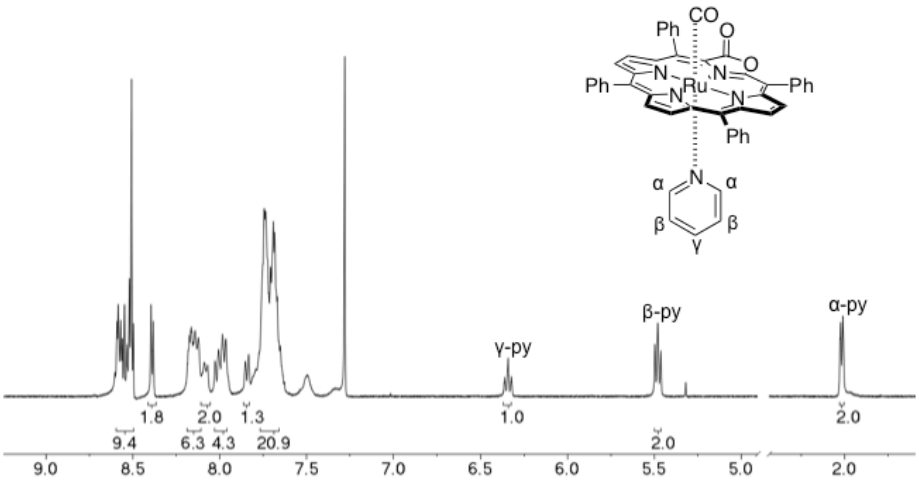

Figure 6-1. ^{1}H NMR spectrum (400 MHz, $CDCl_3$) of **4Ru**.

6.2.2. Comparison of the crystal structures of 1Ru* and 4Ru

We were able to obtain the crystal structure for **4Ru** (Figure 6-2). Thus, we can make some comparisons to the known structure of Ru(TPP)(CO)(py) **1Ru***.[4] In Table 6-1, we compare some of the pertinent bond distances and angles reported for **1Ru*** with those found for **4Ru**.

Table 6-1. Bond distances (Å) and angles (°) of **1Ru***[4] and **4Ru**.

	Ru(TPP)(CO)(py)	Ru(TPL)(CO)(py)
Bond distances (Å)		
Ru — N5	2.193 (4)	2.183 (2)
Ru — C	1.838 (9)	1.835 (3)
C — O	1.141 (10)	1.153 (3)
Bond Angles (°)		
Ru — C — O	178.4	175.9
C — Ru — N5	178.9	177.1

The axial Ru-N(pyridine) bond distance of 2.183 (2) Å observed for **4Ru** is slightly smaller the bond distance of 2.193 (4) Å for the **1Ru***. This long ruthenium-pyridine bond length in both complexes is consistent with the kinetic lability of the axial ligand as observed by Eaton,

et al.[17] Although, the Ru-C bond distances are nearly identical for **1Ru*** and **4Ru** complexes, the corresponding C-O bond distances, 1.141 (10) Å and 1.153 (3) Å are fairly different.

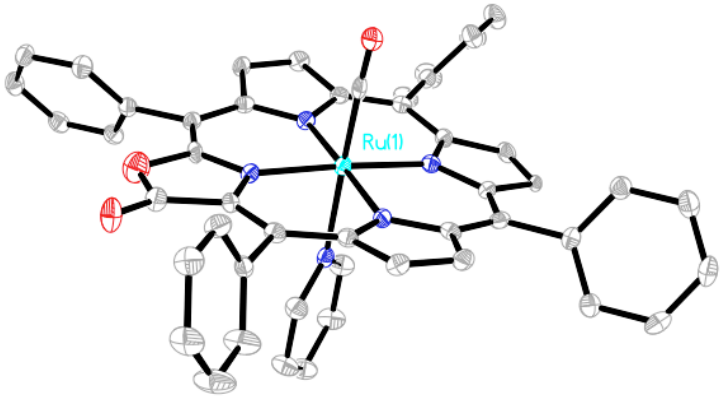

Figure 6-2. ORTEP representation of the crystal structure of **4Ru**.

6.2.3. Carbonyl Stretching Frequencies of 1Ru-6Ru

The CO stretching frequency of the **1Ru*** was determined be 1939 cm^{-1} (in tetrachloroethane).[4] The CO stretching frequencies of **1Ru-6Ru** were measured in solid state (ATR). The υ_{CO} data obtained for these complexes are compiled in Table 6-2. The canonical structures involved in the binding of CO to ruthenium are shown in Figure 6-3.

Table 6-2. Carbonyl stretching frequencies measured for the Ru(Por)(CO)(py) complexes (solid state, ATR).

Compound	ν_{CO} (cm^{-1})
1Ru	1948
2Ru	1957
3Ru	1950
4Ru	1959
5Ru	1958
6Ru	1940

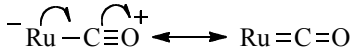

Figure 6-3. Limiting resonance structures of a ruthenium-carbonyl bond.

The ν_{CO} for the benchmark porphyrin **1Ru** was 1948 cm^{-1}. The higher π-acidity of lactone **4Ru** (that was also shown to possess a much reduced Brønsted acidity)[16] and dione **5Ru** compared to **1Ru** is apparent in the ν_{CO}, of 1959 and 1958 cm^{-1}, respectively. The reduced donor ability of the N_4-ligand (compared to that of **1Ru**) reduces the electron density of the ruthenium. This results in a diminished Ru-CO back-bonding, thereby strengthening the C-O bond; it will vibrate at a higher frequency.

Following this π-acidity argument, the higher υ_{CO} frequencies of 1957 and 1950 cm^{-1} measured for the dimethoxychlorin complex **2Ru** and oxazolochlorin complex **3Ru**, respectively, also suggest that these macrocycles are less electron-donating than a porphyrin. And indeed, *meso*-tetraphenylchlorin was shown to be less Brønsted basic than a porphyrin.[18] The difference in their ν_{CO} frequencies is also reflected in their UV-vis spectra. The UV-vis spectrum of **2Ru** resembles a metalloporphyrin-like spectrum while **3Ru** has a metallochlorin-like spectrum (Figure 6-4). The ν_{CO} for **2Ru** is extremely close to that of **5Ru**, which also has a metalloporphyrin-like UV-vis spectra (See experimental, Figure 6-16).

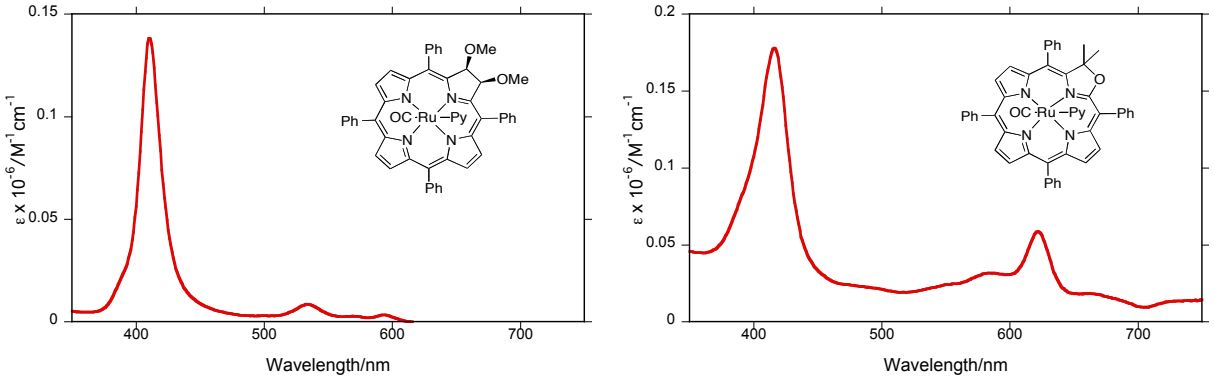

Figure 6-4. Comparison of the UV-Vis Spectra of **2Ru** and **3Ru**.

The lowest CO stretching frequency of 1940 cm^{-1} is observed for the morpholino complex **6Ru**. This indicates that this ligand possess the highest degree of electron donation to the central metal. Morpholins are conformationally very flexible and we thus surmise that this chlorin-like ligand can arrange itself around the metal to assume ideal N–Ru bond distances and therefore bonding interactions. In the absence of a crystal structure, however, this supposition cannot be further substantiated.

6.3. Conclusions

Five new carbonyl complexes of ruthenium porphyrinoids have been prepared and characterized. This permits a comparison of the carbonyl stretching frequencies with pyridine as a *trans* axial ligand to the previously studied Ru(TPP)(CO)(py). The crystal structure obtained for **4Ru** made for a good comparison to the crystal structure known for Ru(TPP)(CO)(py) and we can deduce that the Ru-C bond length of both complexes is nearly identical. Only small changes in the carbonyl stretching frequencies were observed for the five complexes in comparison to the benchmark porphyrin. However, we can attribute these changes to the π-

acidity of these ruthenium complexes, which can be altered by pyrrole modification of the porphyrin macrocycles.

6.4. Experimental

Materials and instruments. All solvents and reagents (Aldrich, Acros) were used as received. Analytical (aluminum backed, silica gel 60, 250 μm thickness), preparative (20 × 20 cm, glass backed, silica gel, 60, 500 or 1000 μm thickness) TLC plates, and the flash column silica gel (premium grade, 60 Å, 32-63 μm) used were provided by Sorbent Technologies, Atlanta, GA.

^{1}H and ^{13}C NMR spectra were recorded on a Bruker DRX400 spectrometer in the solvents indicated. IR spectra were recorded on a Thermo Nicolet Nexus 670 FTIR spectrometer using an ATR attachment. UV-vis spectra were recorded on a Cary 50 (Varian) spectrometer.

The free base porphyrin **1** was prepared according to the method of Adler.[19] Free base oxazolochlorin of complex **3** was obtained by reduction and acetalization of the corresponding porpholactone.[20] Free bases of dimethoxy chlorin **2,** porpholactone **4**, dioxoporphyrin **5**, and morpholinochlorin **6** were synthesized by oxidation/derivatization of free base *meso*-tetraphenyl diolchlorin.[16,21,22]

Carbonyl-pyridine-[*meso*-tetraphenylporphyrinato)ruthenium(II) 1Ru. In a 10 mL thick-walled tube containing a stir bar were placed **1** (50 mg, 8.14×10^{-5} mol), $Ru_3(CO)_{12}$ (52 mg, 1 equiv) and 10% toluene/EtOH (5 mL). The vessel was sealed with a septum and placed in the microwave cavity. Using an initial microwave power of 200 W, the reaction mixture was heated from room temperature to 250°C and held at the temperature for 30 min. Upon completion the reaction was cooled to room temperature and evaporated to dryness using

rotary evaporation. The resulting residue was separated on a preparative plate (silica, 60% hexanes/39% CH_2Cl_2/1% pyridine) to give 36 mg (54% yield); R_f (silica, 60% hexanes/39% CH_2Cl_2/1% pyridine) = 0.33; UV-vis ($CHCl_2$) λ_{max} (log ε): 412 (5.44), 532 (4.44), 565 (4.10) nm; ^{1}H NMR (400 MHz $CDCl_3$, δ): 8.72-8.58 (m, 8H), 8.30-8.21 (m, 4H); 8.12-8.03 (m, 4H), 7.81-7.66 (m, 12H), 6.16-6.07 (m, 1H), 5.27-5.18 (m, 2H), 1.57-1.54 (m, 2H) ppm; ^{13}C NMR (400 MHz, $CDCl_3$, δ): 144.20, 143.83, 142.88, 134.56, 134.23, 131.99, 127.48, 126.81, 121.81, 121.73 ppm; IR: υ = 1947.67 cm^{-1} (C=O). This data is identical to the reported. Included here for comparison.[23]

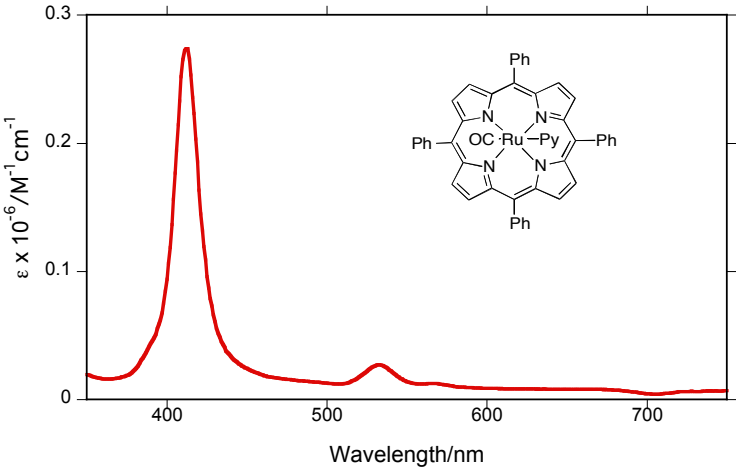

Figure 6-5. UV-vis spectrum (CH_2Cl_2) of **1Ru**.

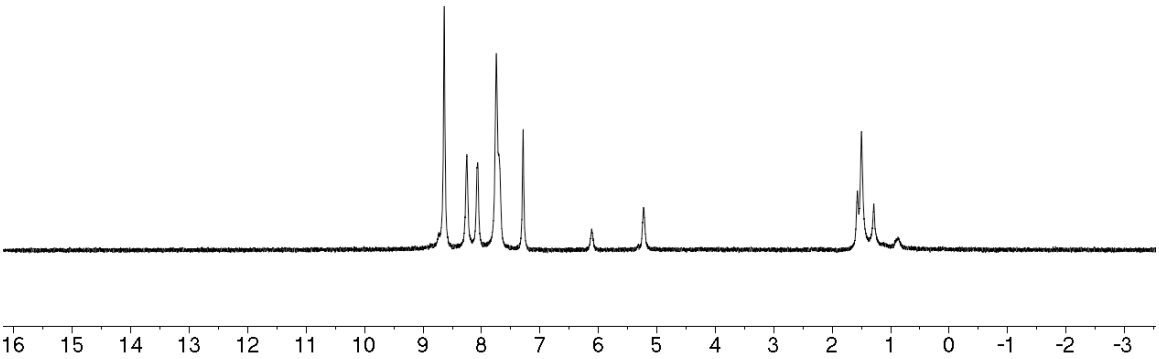

Figure 6-6. ^{1}H NMR spectrum (400 MHz, $CDCl_3$) of **1Ru**.

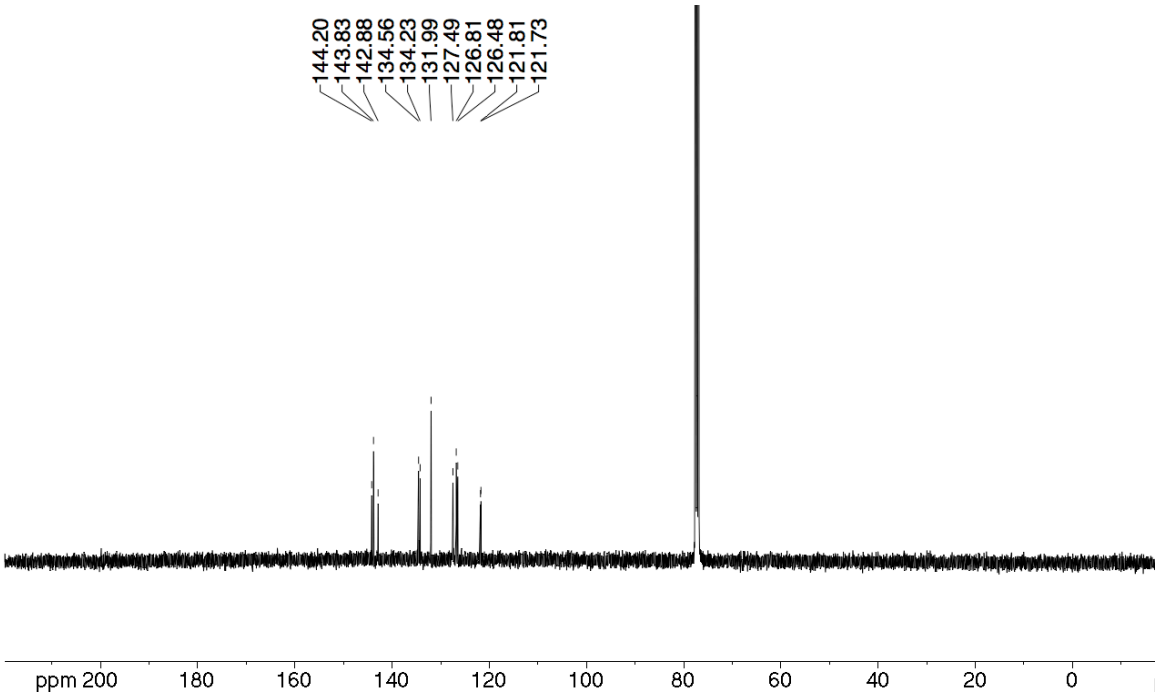

Figure 6-7. ^{13}C NMR spectrum (400 MHz, $CDCl_3$) of **1Ru.**

Carbonyl-pyridine-[*meso*-tetraphenyl-2,3-dimethoxychlorinato]ruthenium(II) 2Ru.

This complex was prepared from **2** (50 mg, 7.39×10^{-5} mol) according to the procedure described for the synthesis of **1Ru**. Product **2Ru** was isolated by column chromatography (silica, 30% hexanes/69% CH_2Cl_2/1% pyridine) and recrystallized by solvent exchange with $CHCl_3$/EtOH to give 42 mg (65% yield); R_f (silica, 30% hexanes/69% CH_2Cl_2/1% pyridine) = 0.69; UV-vis (CH_2Cl_2) λ_{max} (log ε): 410 (5.14), 534 (3.93), 569 (3.44), 593 (3.93) nm; ^{1}H NMR (400 MHz $CDCl_3$, δ): 8.67-8.61 (m, 10H), 8.58 (dd, J = 14.8, 5.8 Hz, 3H), 8.51 (d, J = 4.4 Hz, 2H) 8.23 (s, 6H), 8.08 (s, 9H), 7.97-7.91 (m, 4H), 6.13-6.07 (m, 2H), 5.27-5.21 (m, 4H), 7.75 (s, 12H), 7.68 (s, 15H) 1.66 (d, J = 4.83 Hz, 2H) ppm; ^{13}C NMR (400 MHz, $CDCl_3$, δ): 180.90, 164.16, 145.31, 144.71, 144.32, 144.21, 144.12, 143.78, 143.46, 143.38, 143.08, 142.91, 142.88,

142.78, 142.74, 142.70, 142.60, 134.49, 134.45, 134.39, 134.33, 134.22, 134.17, 134.13, 134.08, 133.93, 133.13, 132.73, 132.09, 131.93, 131.57, 131.37, 131.31, 127.43, 127. 39, 127.32, 126.88, 126.86, 126.74, 126.69, 126.68, 126.54, 126.37, 126.03, 122.51, 122.14, 121.78, 121.63, 119.88, 119.41, 105.88, 58.38 ppm; IR: υ = 1957.5 cm^{-1} (C=O).

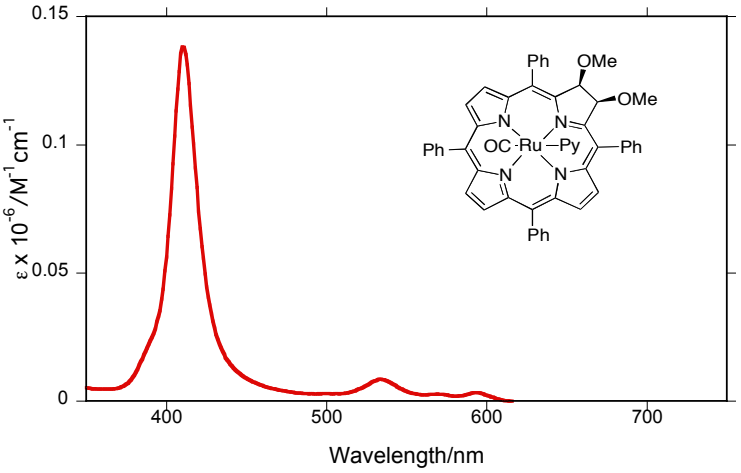

Figure 6-8. UV-vis spectrum (CH_2Cl_2) of **2Ru**.

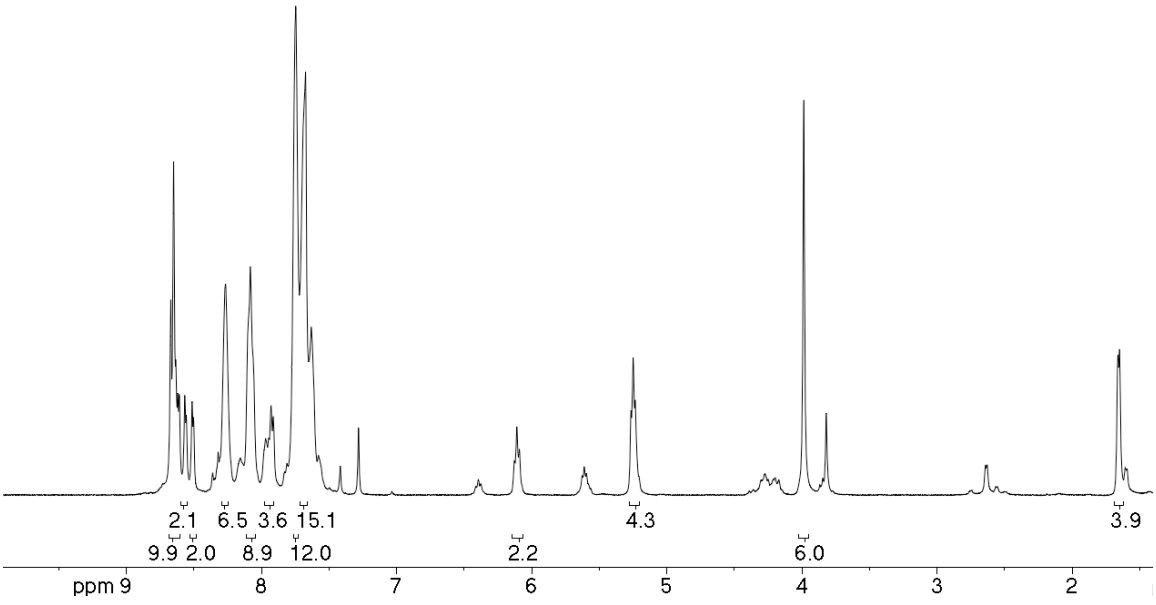

Figure 6-9. ^{1}H NMR spectrum (400 MHz, $CDCl_3$) of **2Ru**.

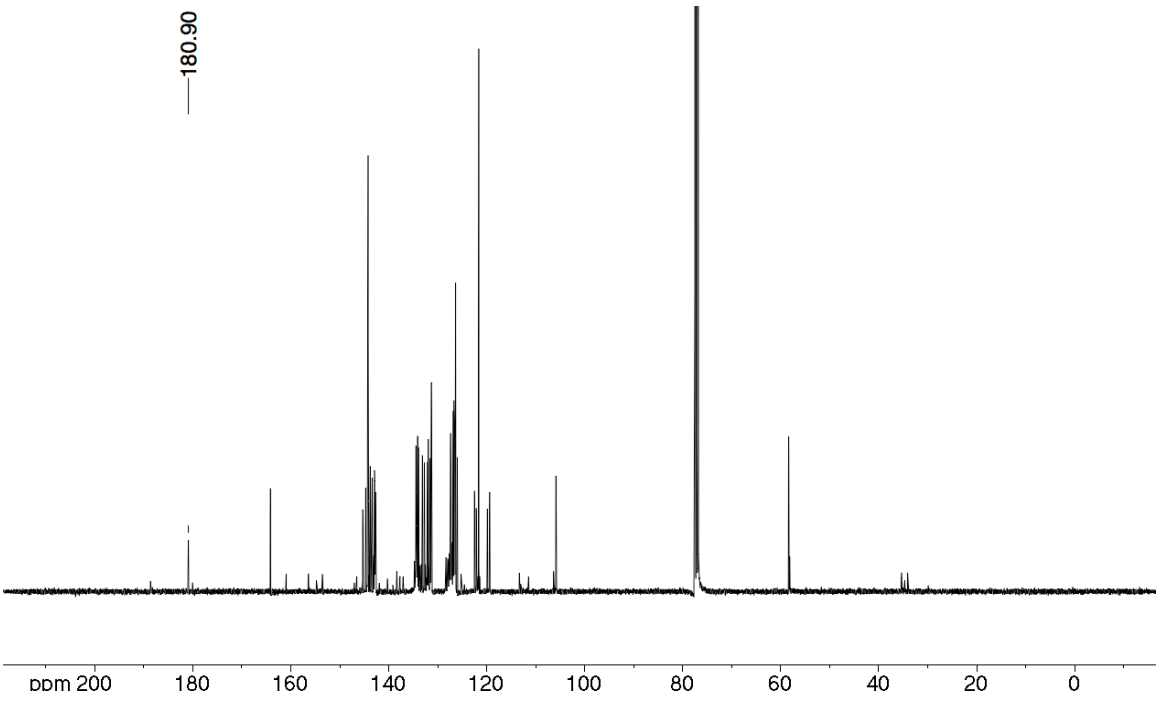

Figure 6-10. ^{13}C NMR spectrum (400 MHz, $CDCl_3$) of **2Ru**.

Carbonyl-pyridine-(*meso*-tetraphenyl-2-dimethyl-3oxachlorinato)ruthenium(II)

3Ru. This complex was prepared from **3** (23 mg, 7.39×10^{-5} mol) according to the procedure described for the synthesis of **1Ru**. Product **3Ru** was separated on a preparative plate (silica, 60% hexanes/39% CH_2Cl_2/1% pyridine) to give 15 mg (52% yield); R_f (silica, 30 hexanes/1% pyridine/CH_2Cl_2) = 0.66; UV-vis (CH_2Cl_2) λ_{max} (log ε): 416 (5.25), 517 (4.29), 622 (4.77) nm; ^{1}H NMR (400 MHz $CDCl_3$, δ): 8.23-8.19 (m, 3H), 8.15-8.14 (m, 1H); 811-8.03 (m, 3H), 7.98-7.89 (m, 4H), 7.75 (t, J = 5.1 Hz, 1H), 7.69-7.54 (m, 15H), 6.52-6.48 (m, 1H), 5.73-5.69 (m, 2H), 2.91-2.90 (m, 2H), 1.93-1.92 (m, 3H), 1.77-1.75 (m, 3H) ppm; IR: υ = 1950.0 cm^{-1} (C=O).

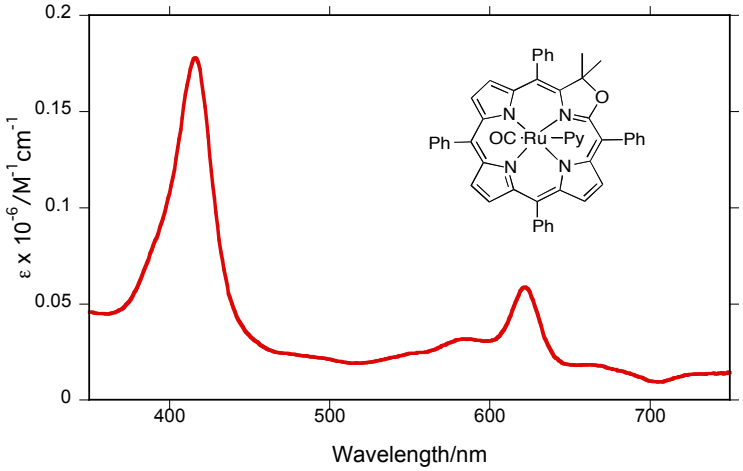

Figure 6-11. UV-vis spectrum (CH_2Cl_2) of **3Ru**.

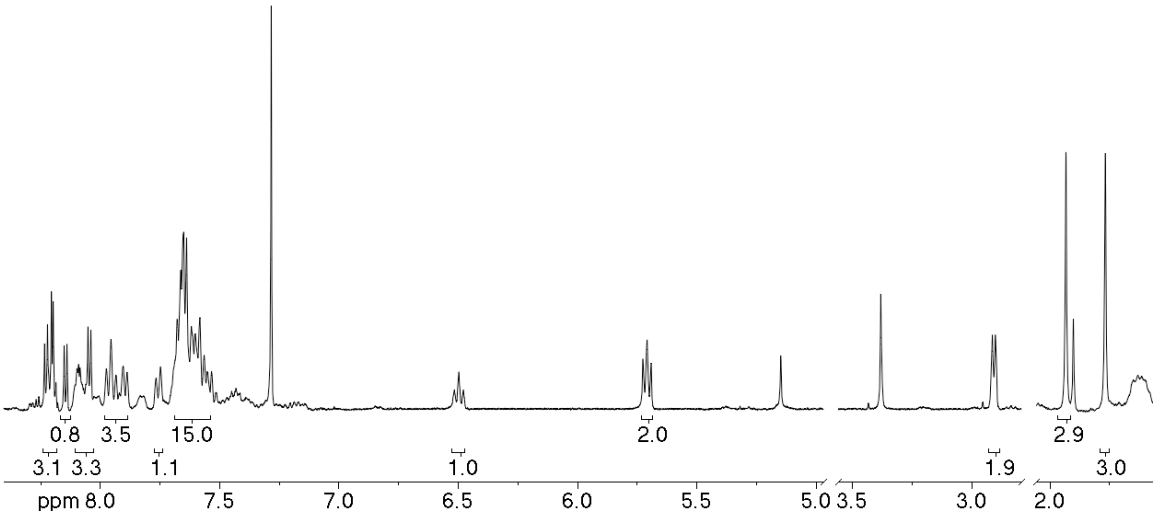

Figure 6-12. ^{1}H NMR spectrum (400 MHz, $CDCl_3$) of **3Ru**.

Carbonyl-pyridine-(*meso*-tetraphenyl-2-oxo-3-oxaporphyrinato)ruthenium(II) 4Ru. This complex was prepared from **4** (50 mg, 7.91×10^{-5} mol) according to the procedure described for the synthesis of **1Ru**. Product **4Ru** was separated on a preparative plate (silica, 30% hexanes/69% CH_2Cl_2/1% pyridine) to give 31 mg (45% yield); R_f (silica, CH_2Cl_2) = 0.62; UV-vis (CH_2Cl_2) λ_{max} (log ε): 414 (5.15), 539 (4.26), 579 (4.43) nm; ^{1}H NMR (400 MHz $CDCl_3$,

δ): 8.59-8.50 (m, 9H), 8.41-8.38 (m, 2H), 8.18-8.11 (m, 6H), 8.03-7.97 (m, 4H), 7.86-7.83 (m, 1H), 7.75-7.66 (m, 21H) 6.36-6.32 (m 1H) ppm; ^{13}C NMR (400 MHz, $CDCl_3$, δ): 182.79, 167.07, 166.79, 149.39, 148.75, 147.97, 147.63, 145.52, 145.05, 144.95, 144.53, 144.37, 143.07, 142.93, 142.72, 142.58, 142.49, 141.97, 141.88, 141.81, 139.07, 138.94, 138.01, 137.93, 135.41, 134.39, 134.29, 134.14, 134.12, 134.00, 133.95, 133.79, 132.76, 132.43, 132.21, 132.07, 131.48, 131.45, 131.36, 131.24, 131.18, 130.69, 130.51, 128.11, 128.05, 127.94, 127.86, 127.58, 127.24, 127.07, 127.04, 126.90, 126.76, 126.74, 126.54, 123.93, 123.80, 122.53, 121.66, 121.28, 120.31, 119.92, 103.54, 103.19; IR: υ = 1959.1 cm^{-1} (C=O).

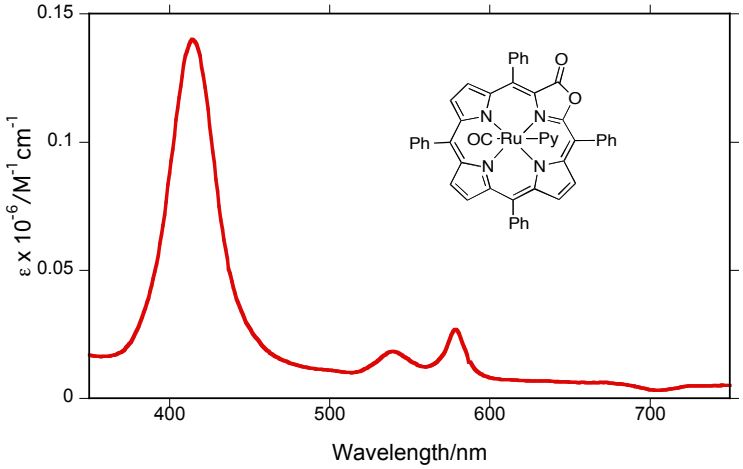

Figure 6-13. UV-vis spectrum (CH_2Cl_2) of **4Ru**.

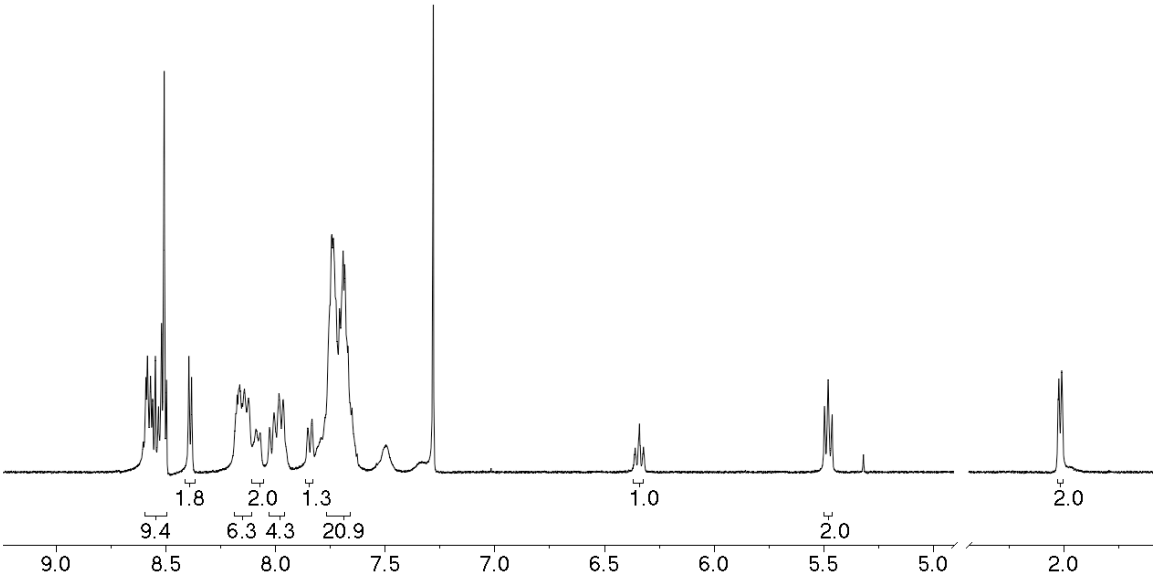

Figure 6-14. ^{1}H NMR spectrum (400 MHz, $CDCl_3$) of **4Ru**.

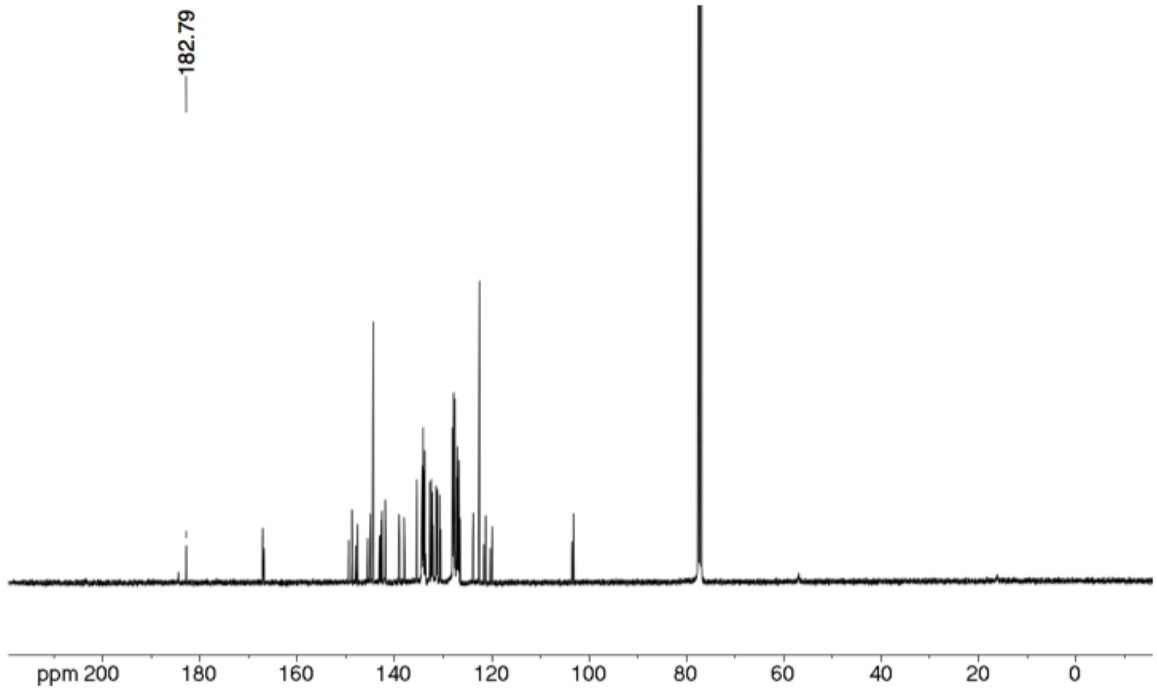

Figure 6-15. ^{13}C NMR spectrum (400 MHz, $CDCl_3$) of **4Ru**.

Carbonyl-pyridine-(*meso*-tetraphenyl-2,3-dioxochlorinato)ruthenium(II) 5Ru. This complex was prepared from **5** (32 mg, 4.96×10^{-5} mol) according to the procedure described for the synthesis of **1Ru**. Product **5Ru** was separated on a preparative plate (silica, 30% hexanes/69% CH_2Cl_2/1% pyridine) to give 23 mg (53% yield); R_f (silica, 30% hexanes/69% CH_2Cl_2/1% pyridine) = 0.30; UV-vis (CH_2Cl_2) λ_{max}: 397 (4.99), 488 (4.05), 681 (3.49) nm; ^{1}H NMR (400 MHz $CDCl_3$, δ): 8.53 (s, 2H), 8.41 (d, *J* = 4.9, 2H); 8.26 (d, *J* = 4.89, 2H), 8.14-8.12 (m, 2H), 7.96 (d, *J* = 7.4, 2H), 7.91 (d, *J* = 6.91, 2H), 7.74-7.61 (m, 14H), 6.47 (t, *J* = 7.6, 1H), 5.63 (t, *J* = 6.8, 2H), 2.64 (d, *J* = 5.3, 2H) ppm. ^{13}C NMR (400 MHz, $CDCl_3$, δ): 185.88, 184.92, 145.26, 144.84, 143.92, 141.94, 141.61, 140.15, 135.85, 134.64, 133.86, 133.61, 133.57, 132.48, 132.16, 131.01, 130.96, 128.11, 127.88, 127.46, 127.23, 127.16, 126.92, 126.57, 122.88, 117.80 ppm; IR: υ = 1957.65 cm^{-1} (C=O).

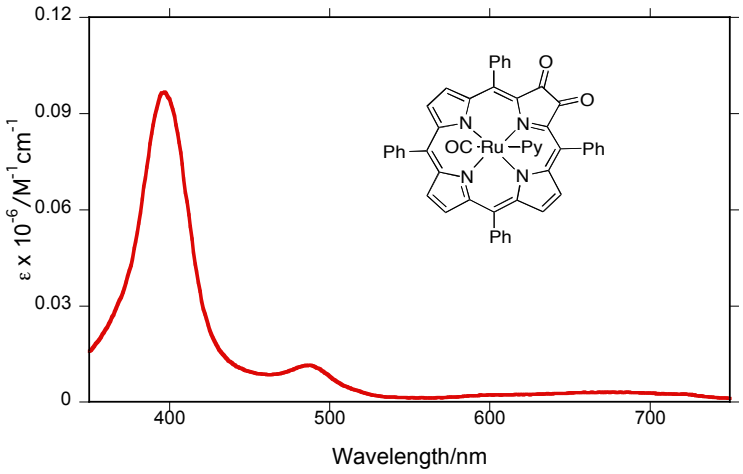

Figure 6-16. UV-vis spectrum (CH_2Cl_2) of **5Ru**.

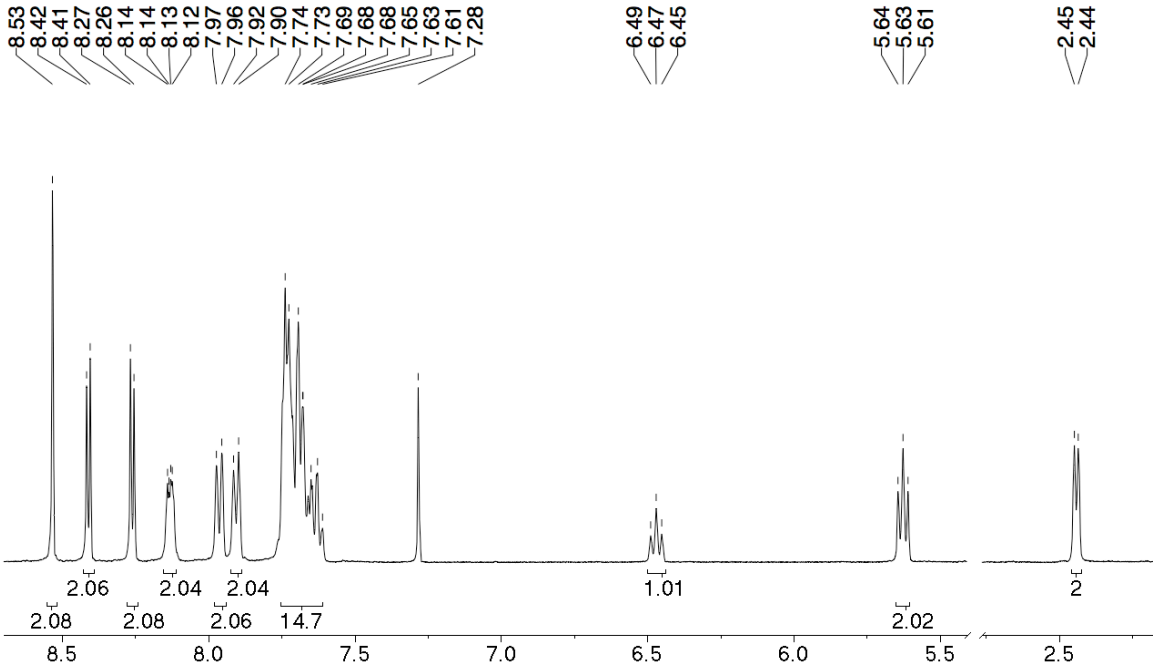

Figure 6-17. ^{1}H NMR spectrum (400 MHz, $CDCl_3$) of **5Ru**.

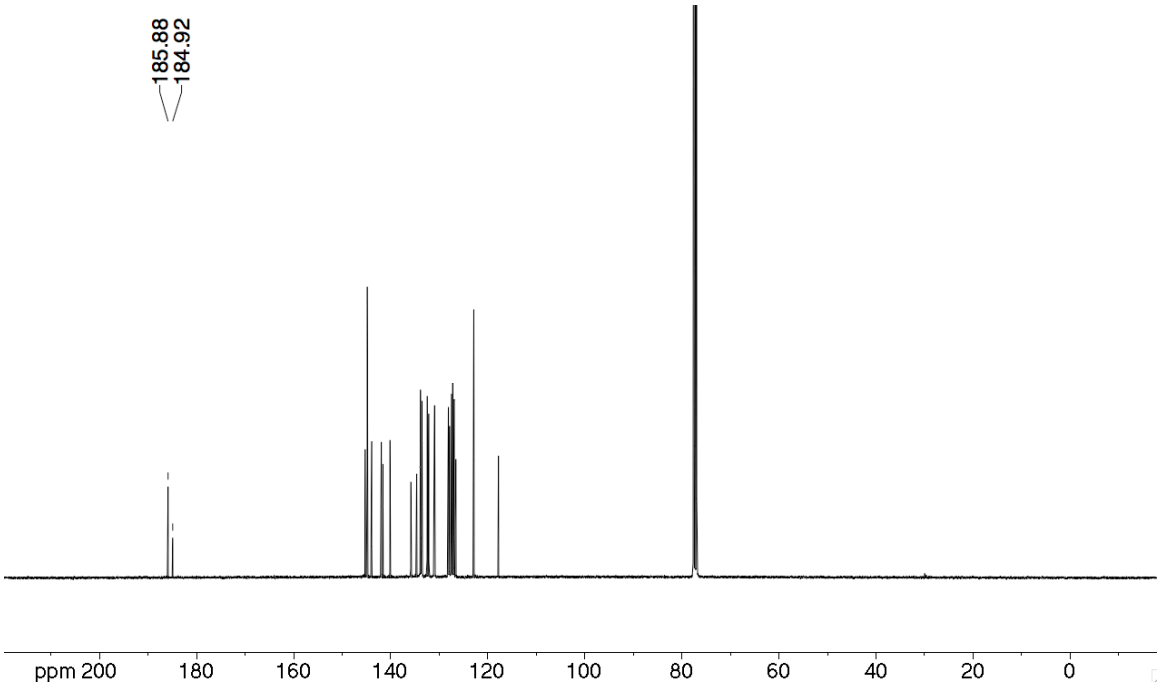

Figure 6-18. ^{13}C NMR spectrum (400 MHz, $CDCl_3$) of **5Ru**.

Carbonyl-pyridine-(*meso*-Tetraphenylmorpholinochlorinato)Ru(II) 6Ru. This was prepared from **6** (67 mg, 9.26×10^{-5} mol) according to the procedure described for the synthesis of **1Ru**. Product **6Ru** was separated on a preparative plate (silica, 30% hexanes/69% CH_2Cl_2/1% pyridine) to give 38 mg (42% yield); R_f (silica, CH_2Cl_2) = 0.80; UV-vis (CH_2Cl_2) λ_{max} (rel. int.): 383 (0.409), 441 (1.00), 614 (0.0258) nm; ^{1}H NMR (300 MHz $CDCl_3$, δ): 8.99-8.96 (m, 2H), 8.51-8.48 (m, 2H), 8.28-8.25 (m, 2H), 8.21-8.04 (m, 16H), 8.01-7.95 (m, 4H), 7.91-7.87 (m, 2H), 7.74-7.63 (m, 22H), 7.11-7.04 (m, 2H), 6.98-6.92 (m, 2H), 6.42-6.36 (m, 2H), 5.62-5.55 (m, 4H), 2.74-2.70 (m, 4H), 1.34-1.29 (m, 6H) ppm. IR: υ = 1940.00 cm^{-1} (C=O).

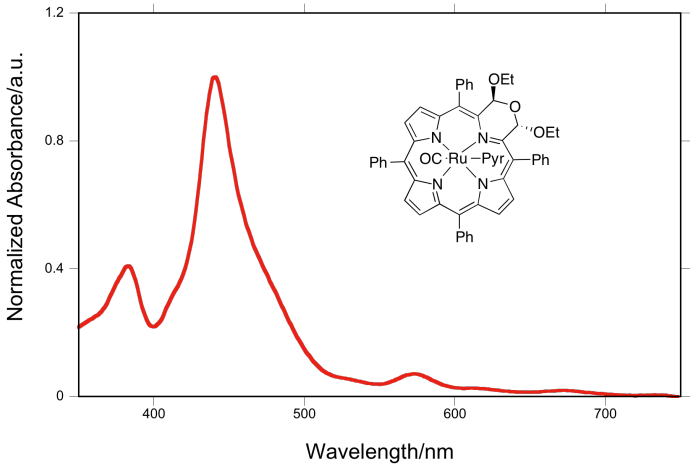

Figure 6-19. UV-vis spectrum (CH_2Cl_2) of **6Ru**.

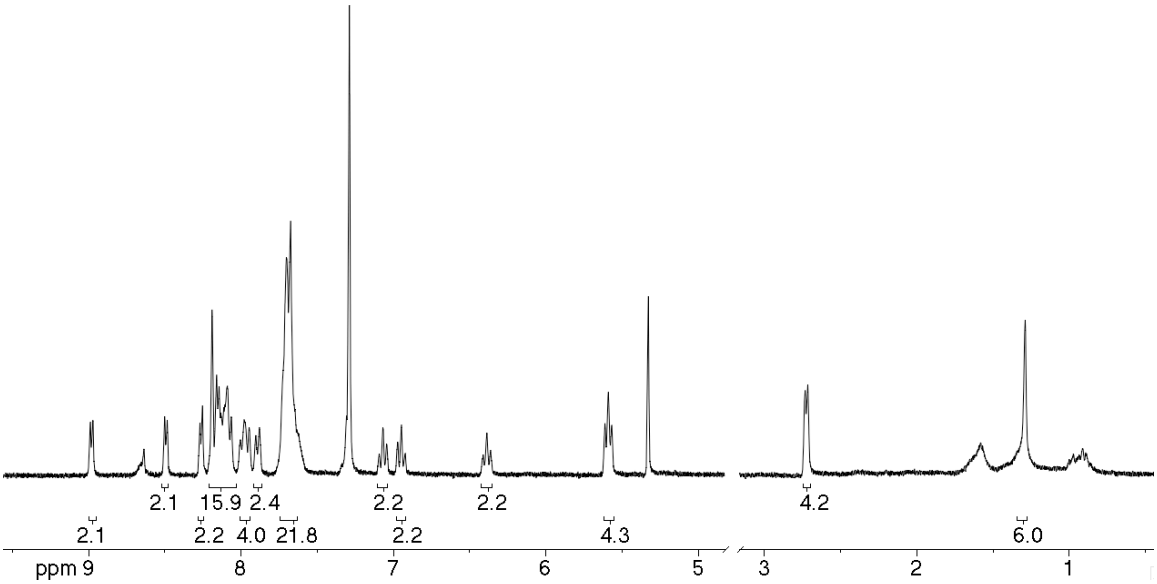

Figure 6-20. ^{1}H NMR spectrum (400 MHz, $CDCl_3$) of **6Ru**.

6.5. References

(1) Li, T.; Quillin, M. L.; Phillips, G. N.; Olson, J. S. *Biochem.* **1994**, *33*, 1433-1446.

(2) Silvernail, N. J.; Roth, A.; Noll, B. C.; Scheidt, W. R. *J. Am. Chem. Soc.* **2005**, *127*, 14422-14433.

(3) Salzmann, R.; Ziegler, C. J.; Godbout, N.; McMahon, M. T.; Suslick, K. S.; Oldfield, E. *J. Am. Chem. Soc.* **1998**, *120*, 11323-11334.

(4) Little, R. G.; Ibers, J. A. *J. Am. Chem. Soc.* **1973**, *95*, 8583-8590.

(5) Spiro, T. G.; Soldatova, A. V.; Balakrishnan, G. *Coord. Chem. Rev.* **2013**, *257*, 511-527.

(6) Wayland, B. B.; Mehne, L. F.; Swartz, J. *J. Am. Chem. Soc.***1978**, *100*, 2379-2383.

(7) Silvernail, N. J.; Noll, B. C.; Schulz, C. E.; Scheidt, W. R. *Inorg. Chem.* **2006**, *45*, 7050-7052.

(8) Seufert, K.; Bocquet, M.-L.; Auwarter, W.; Weber-Bargioni, A.; Reichert, J.; Lorente, N.; Barth, J. V. *Nature Chem.* **2011**, *3*, 114-119.

(9) Kadish, K. M.; Leggett, D. J.; Chang, D. *Inorg. Chem.* **1982**, *21*, 3618-3622.

(10) Barley, M.; Dolphin, D.; James, B. R.; Kirmaier, C.; Holten, D. *J. Am. Chem. Soc.* **1984**, *106*, 3937-3943.

(11) Cheng, R.-J.; Lin, S.-H.; Mo, H.-M. *Organometallics* **1997** *16*, 2121-2126.

(12) Kim, D.; Su, Y. O.; Spiro, T. G. *Inorg. Chem.***1986**, *25*, 3993-3997.

(13) Tait, C. D.; Holten, D.; Barley, M.; Dolphin, D.; James, B. R. *J. Am. Chem. Soc.* **1985**, *107*, 1930-1934.

(14) Caughey, W. S.; Eberspaecher, H.; Fuchsman, W. H.; McCoy, S.; Alben, J. O. *Annals of the New York Academy of Sciences* **1969**, *153*, 722-737.

(15) Mishra, E.; Worlinsky, J. L.; Gilbert, T. M.; Brückner, C.; Ryzhov, V. *J. Am. Soc. Mass. Spectrom.* **2012**, *23*, 1135–1147. Erratum (correction of systemic typesetting errors): *J. Am. Soc. Mass. Spectrom.* 2012, 23, 1428–1439.

(16) McCarthy, J. R.; Jenkins, H. A.; Brückner, C. *Org. Lett.* **2003**, *5*, 19-22.

(17) Eaton, S. S.; Eaton, G. R.; Holm, R. H. *J. Organom. Chem.***1972**, *39*, 179-195.

(18) Whitlock Jr., H. W.; Hanauer, R.; Oester, M. Y.; Bower, B. K. *J. Am. Chem. Soc.* **1969**, *91*, 7485-7489.

(19) Adler, A. D.; Longo, F. R.; Finarelli, J. D.; Goldmacher, J.; Assour, J.; Korsakoff, L. *J. Org. Chem.* **1967**, *32*, 476.

(20) Ogikubo, J.; Meehan, E.; Engle, J. T.; Ziegler, C.; Brückner, C. *J. Org. Chem.* **2012**, *77*, 6199–6207.

(21) Samankumara, L. P.; Zeller, M.; Krause, J. A.; Brückner, C. *Org. Biomol. Chem.* **2010**, *8*, 1951-1965.

(22) Daniell, H. W.; Williams, S. C.; Jenkins, H. A.; Brückner, C. *Tetrahedron Lett.* **2003**, *44*, 4045-4049.

(23) Bonnet, J. J.; Eaton, S. S.; Eaton, G. R.; Holm, R. H.; Ibers, J. A. *J. Am. Chem. Soc.* **1973**, *95*, 2141-2149.